Computational & Multiscale Mechanics of Materials

CM3

www.ltas-cm3.ulg.ac.be

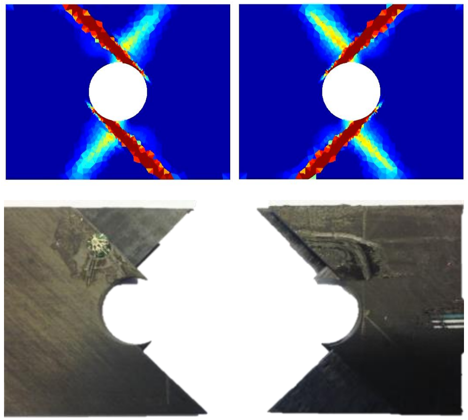

Non-local damage mean-field-homogenization

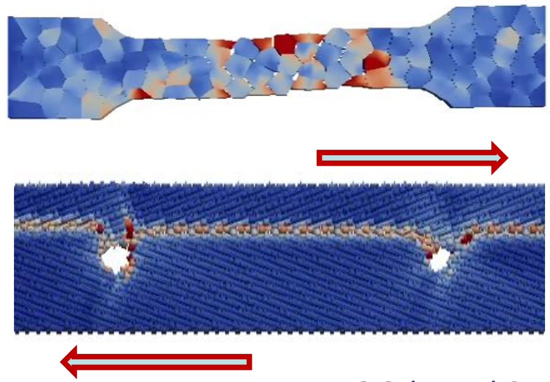

QC-based 2-scale method

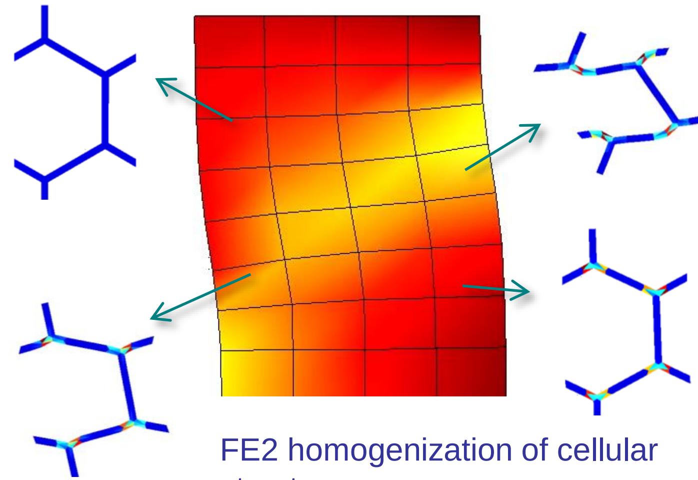

FE2 homogenization of cellular structures

Stochastic multi-scale methods

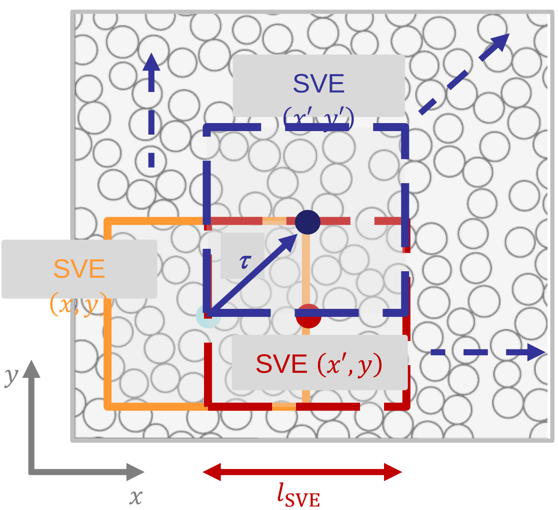

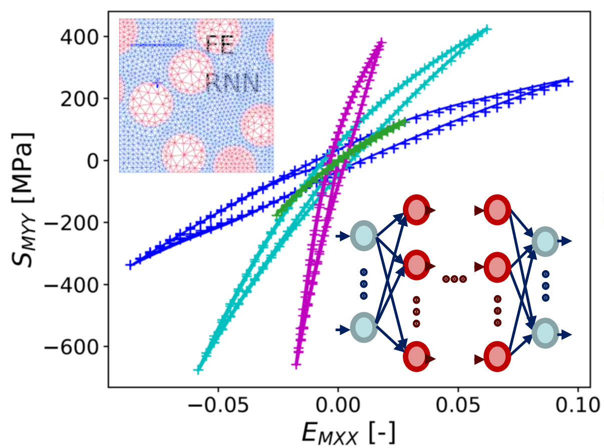

Data-driven multi-scale simulations

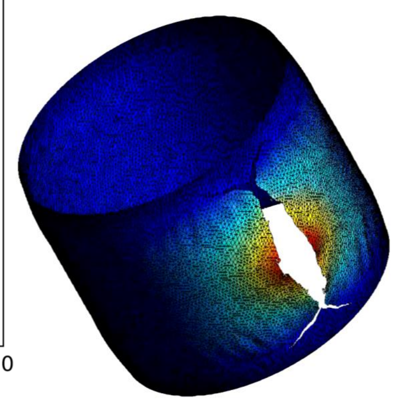

DG-based fracture

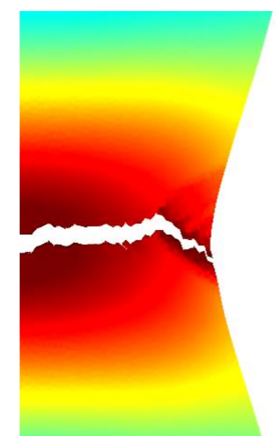

Nonlocal Gurson to crack transition

July 2020 - CM3 research projects

LIÈGE université

Direct links

- Data-driven approaches
  - Recurrent Neural Network-accelerated multi-scale simulations in elasto-plasticity
  - Bayesian identification of stochastic MFH model parameters
- Complex constitutive models for failure prediction under complex loading states
  - Shear and necking coalescence model for porous materials
  - Damage-enhanced viscoelastic-viscoplastic finite strain model for crosslinked resin
- Homogenization & Multi-Scale methods
  - Mean-Field-Homogenization for Elasto-Visco-Plastic Composites
  - Micro-structural simulation of fiber-reinforced highly crosslinked epoxy
  - Non-Local Damage Mean-Field-Homogenization
  - Stochastic Homogenization of Composite Materials
  - Stochastic 3-Scale Models for Polycrystalline Materials
  - Computational Homogenization For Cellular Materials
  - Boundary conditions and tangent operator in multi-physics FE^2
  - Stochastic Multi-Scale Model to Predict MEMS Stiction
  - Multi-Scale Modeling of Nano-Crystal Grain Boundary Sliding
- Fracture Mechanics
  - DG-Based Multi-Scale Fracture, DG-Based Dynamic Fracture
  - DG-Based Damage elastic damage to crack transition
  - Non-local Gurson damage model to crack transition
  - Stochastic Multi-Scale Fracture of Polycrystalline Films
- Smart Composite Materials – Shape Memory Effects

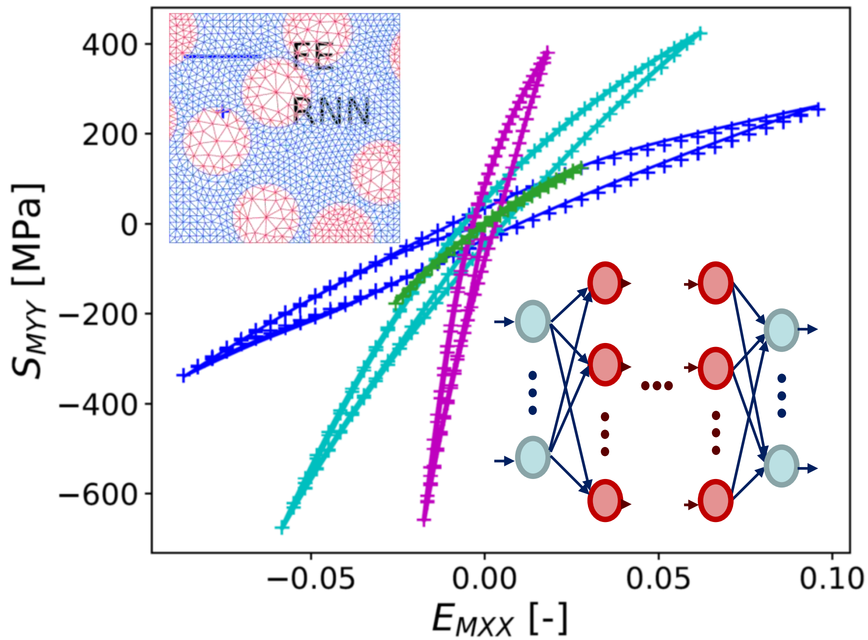

Recurrent Neural Network-accelerated multi-scale simulations in elasto-plasticity

European Commission

MOAMMM project has received funding from the European Union's Horizon 2020 research and innovation programme under grant agreement No 862015 for the project Multi-scale Optimisation for Additive Manufacturing of fatigue resistant shock-absorbing MetaMaterials (MOAMMM) of the H2020-EU.1.2.1. - FET Open Programme

MOAMMM

Recurrent Neural Network-accelerated multi-scale simulations

- Introduction to non-linear multi-scale simulations
  - FE multi-scale simulations
    - Problems to be solved at two scales
    - Requires Newton-Raphson iterations at both scales
  - Use of surrogate models
    - Train a meso-scale surrogate model (off-line)
      - Requires extensive data
      - Obtained from RVE simulations
    - Use the trained surrogate model during analyses (on-line)
      - Surrogate acts as a homogenised constitutive law
      - Expected speed-up of several orders

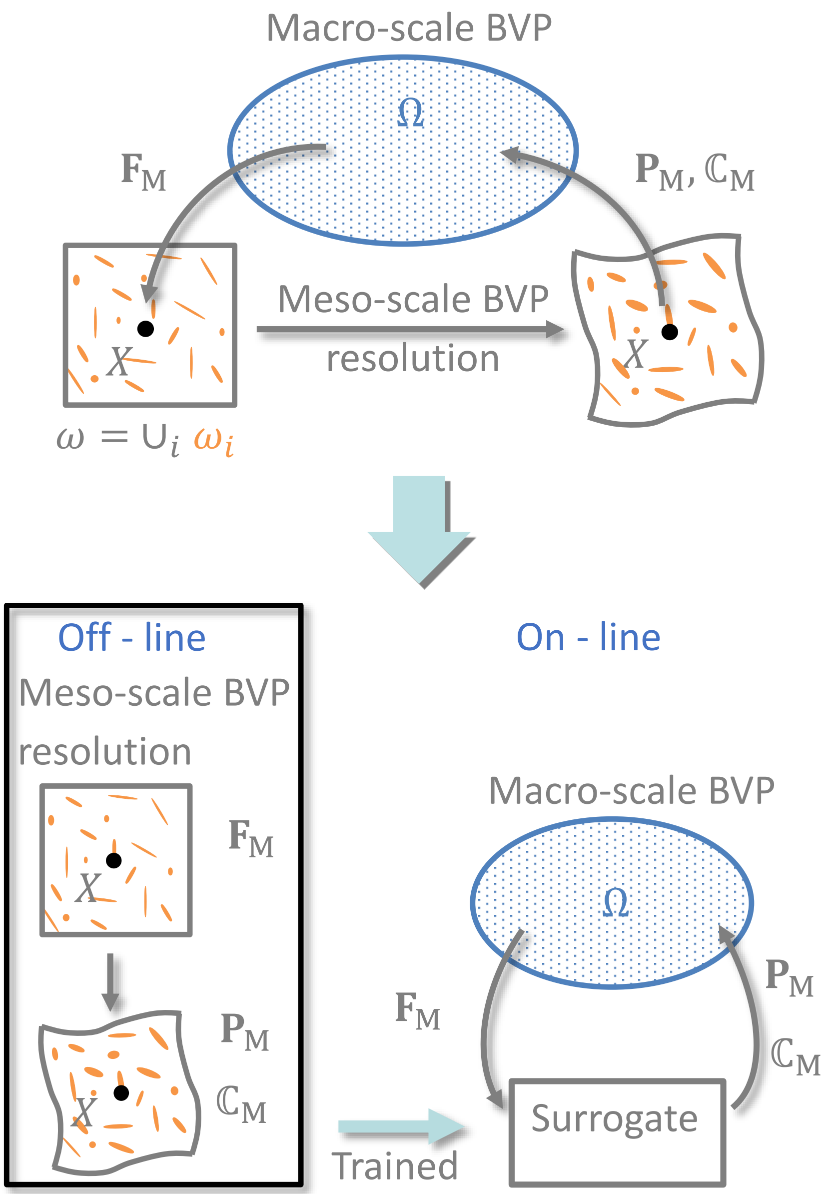

- Definition of the surrogate model: Artificial Neural Network
  - Artificial neuron
    - Non-linear function on n_0 inputs u_k
    - Requires evaluation of weights w_k
    - Requires definition of activation function f

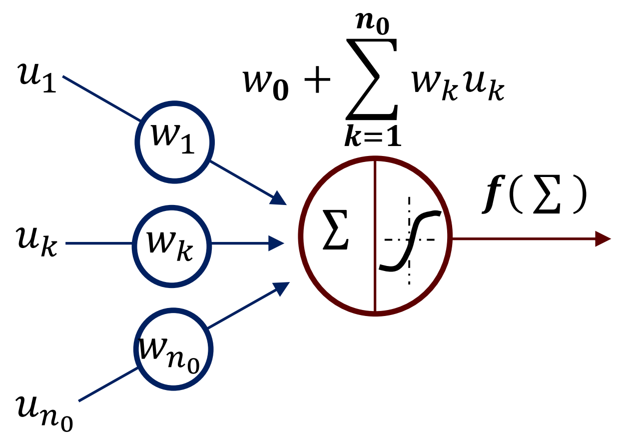

  - Feed-Forward Neuron Network
    - Simplest architecture
    - Layers of neurons
      - Input layer
      - $N-1$ hidden layers
      - Output layers
    - Mapping $\Re^{n_0} \rightarrow \Re^{n_N}$: $\boldsymbol{v} = \boldsymbol{g}(\boldsymbol{u})$

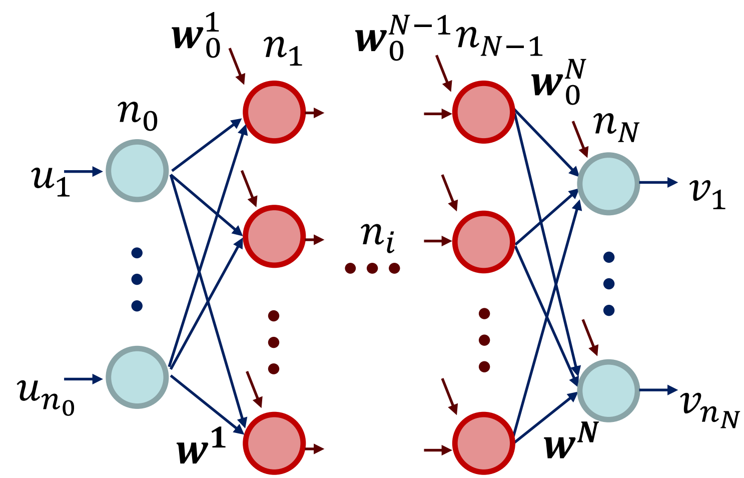

Recurrent Neural Network-accelerated multi-scale simulations

- Elasto-plastic material behaviour
  - No bijective strain-stress relation
    - Feed-forward NNW cannot be used
    - History should be accounted for
- Recurrent neural network
  - Allows a history dependent relation
    - Input $\boldsymbol{u}_t$
    - Output $\boldsymbol{v}_t = \boldsymbol{g}(\boldsymbol{u}_t, \boldsymbol{h}_{t-1})$
    - Internal variable $\boldsymbol{h}_t = \boldsymbol{g}(\boldsymbol{u}_t, \boldsymbol{h}_{t-1})$
  - Weights matrices $\mathbf{U}, \mathbf{W}, \mathbf{V}$
    - Trained using sequences
      - Inputs $\boldsymbol{u}_{t-n}^{(p)}, \ldots, \boldsymbol{u}_t^{(p)}$
      - Output $\boldsymbol{v}_{t-n}^{(p)}, \ldots, \boldsymbol{v}_t^{(p)}$

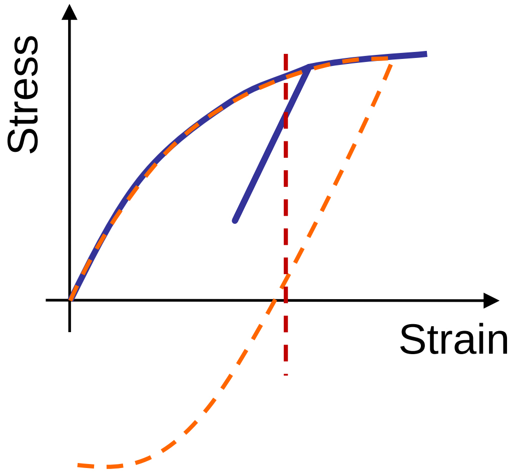

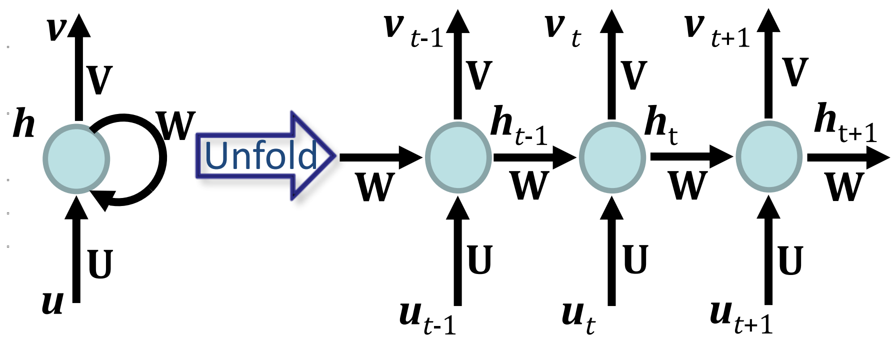

Recurrent Neural Network-accelerated multi-scale simulations

- Recurrent neural network design
  - 1 Gated Recurrent Unit (GRU)
    - Rest gate: select past information to be forgotten
    - Update gate: select past information to be passed along
  - 2 feed-forward NNWs
    - NNW_I to treat inputs $\boldsymbol{u_t}$
    - NNW_O to produce outputs $\boldsymbol{v_t}$
  - Details
    - $\boldsymbol{u_t}$: homogenised GL strain $\mathbf{E}_M$ (symmetric)
    - $\boldsymbol{v_t}$: homogenised 2nd PK stress $\mathbf{S}_M$ (symmetric)
    - 100 hidden variables $\boldsymbol{h_t}$
    - NNW_I one hidden layer of 60 neurons
    - NNW_O two hidden layers of 100 neurons

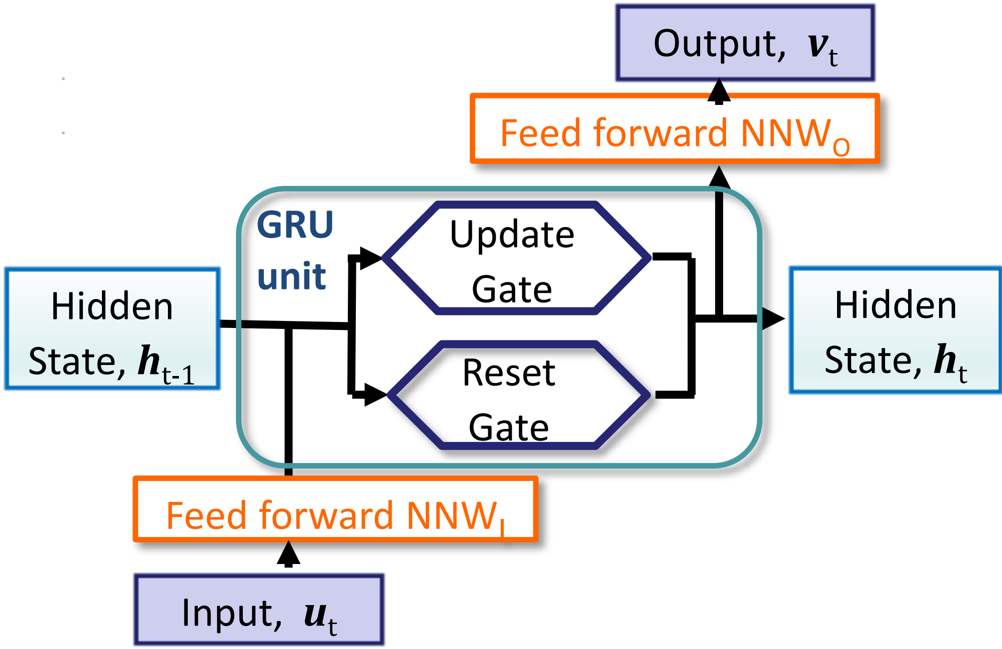

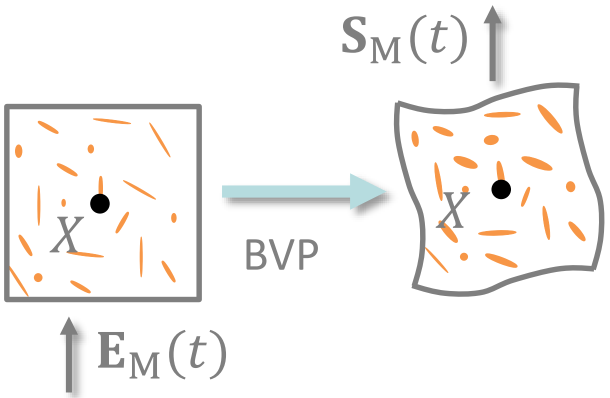

- Data generation
  - Elasto-plastic composite RVE
  - Training stage
    - Should cover full range of possible loading histories
    - Use random walking strategy (thousands)
    - Completes with random cyclic loading (tens)
    - Bounded by a sphere of 10% deformation

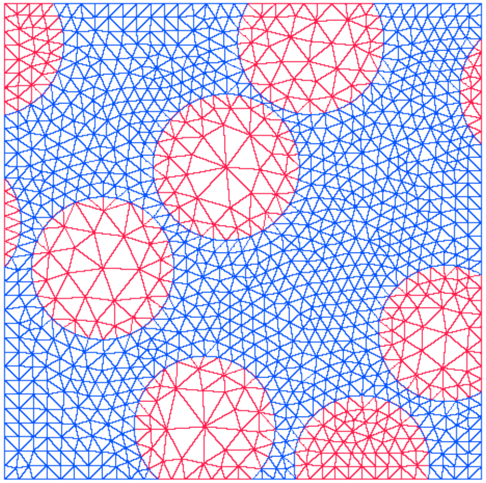

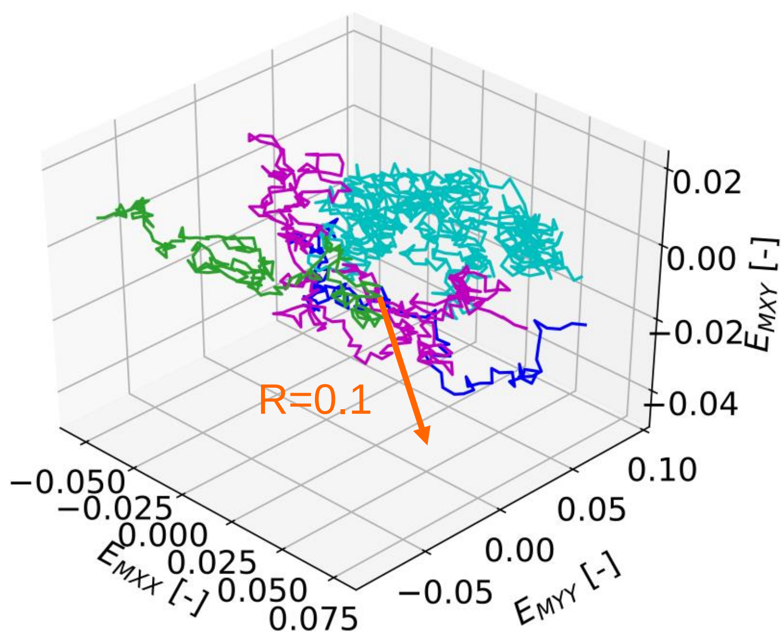

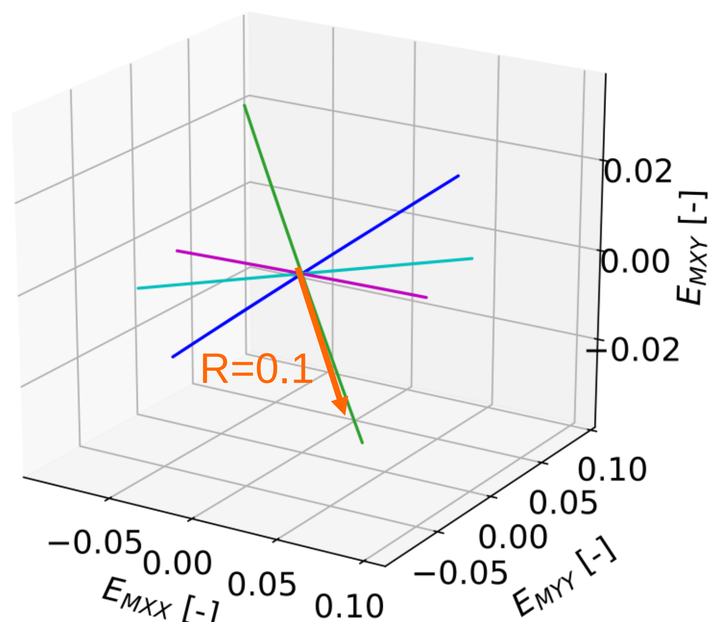

Recurrent Neural Network-accelerated multi-scale simulations

- Testing process (new data)
  - On random walk

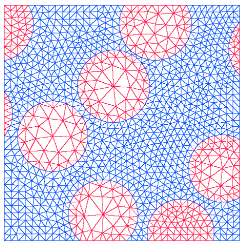

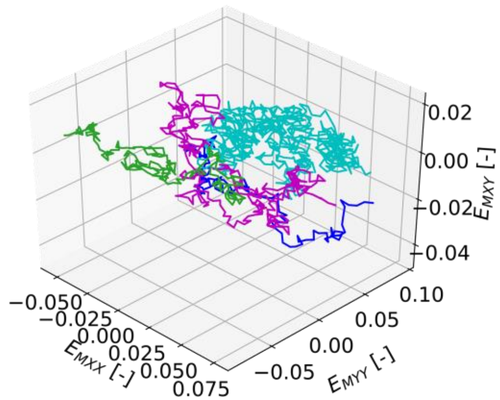

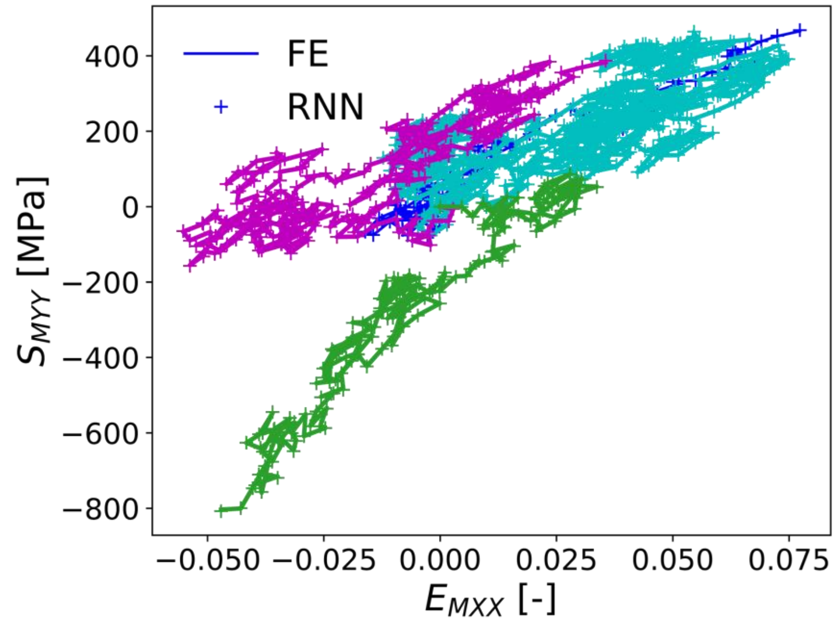

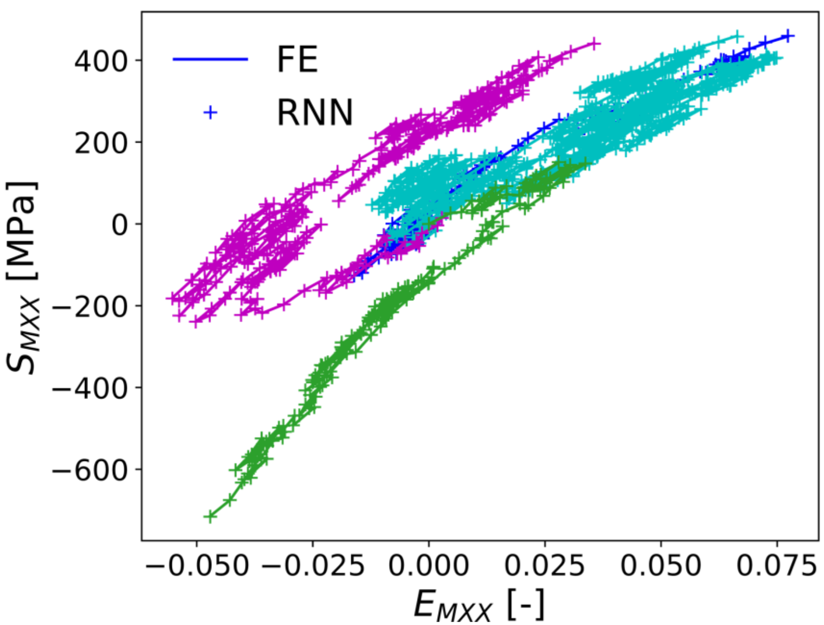

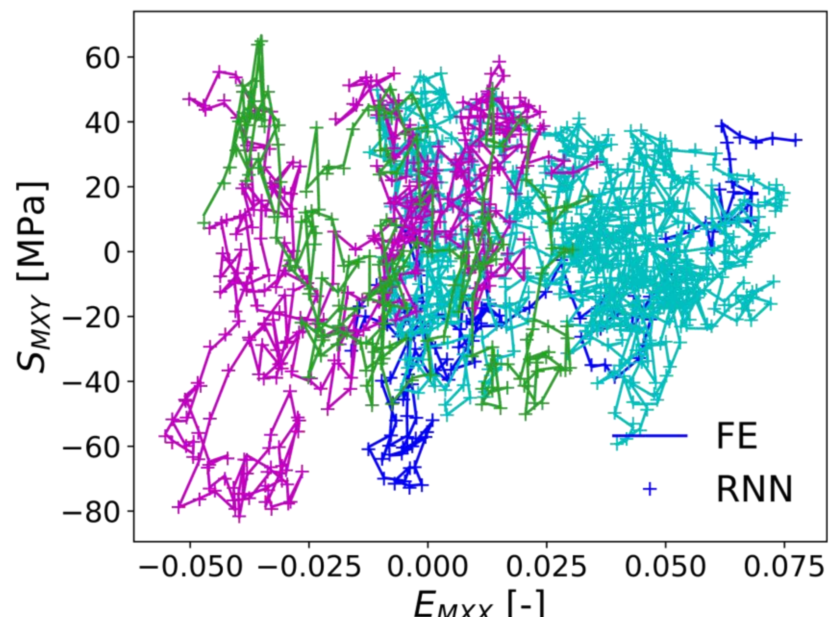

Recurrent Neural Network-accelerated multi-scale simulations

- Testing process (new data)
  - On cyclic loading

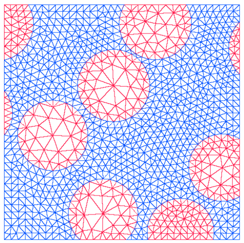

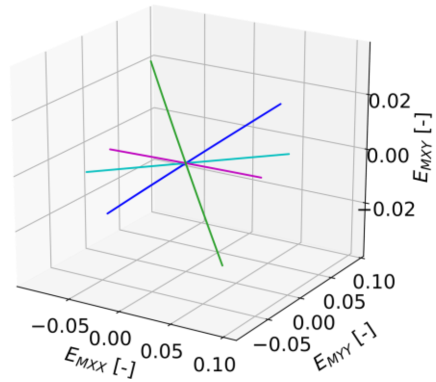

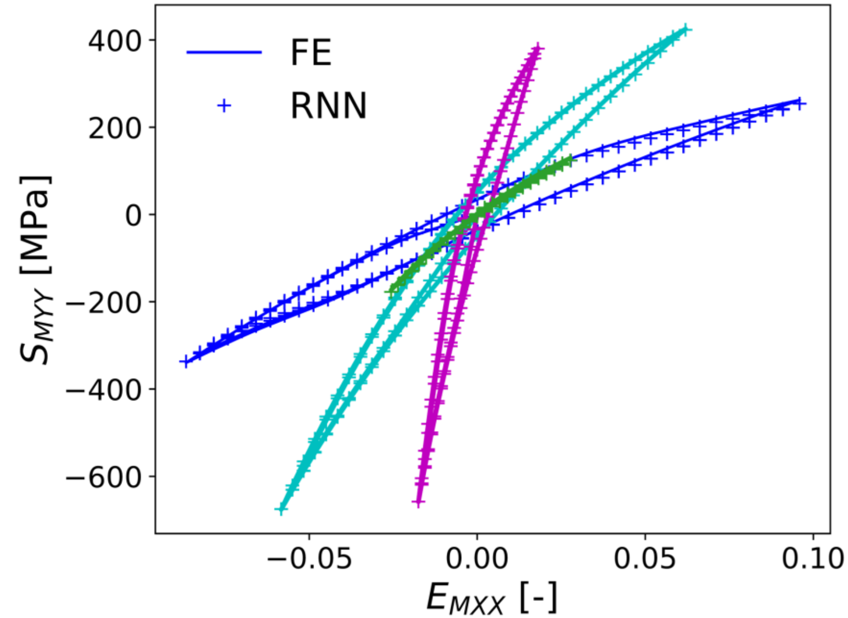

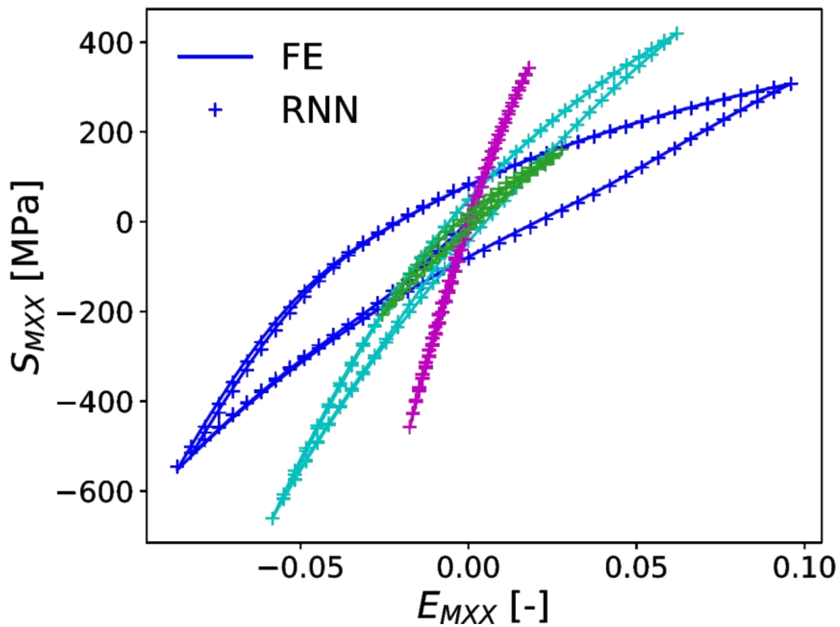

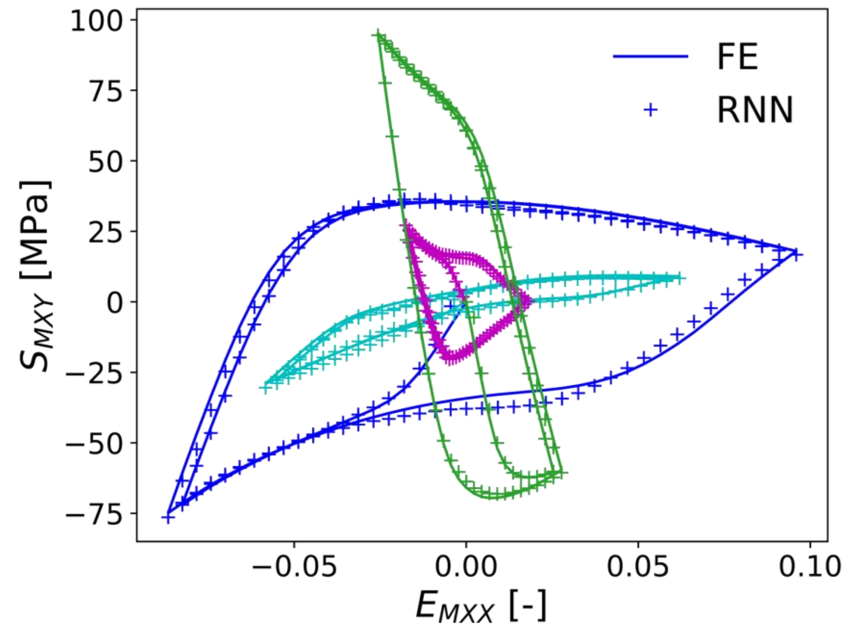

Recurrent Neural Network-accelerated multi-scale simulations

- Multiscale simulation
  - Elasto-plastic composite RVE
  - Comparison FE^2 vs. RNN-surrogate
  - Training data
    - Bounded at 10% deformation

Off-line	FE^2	FE-RNN
Data generation	-	9000 x 2 h-cpu
Training	-	3 day-cpu
On-line	**FE^2**	**FE-RNN**
Simulation	18000 h-cpu	0.5 h-cpu

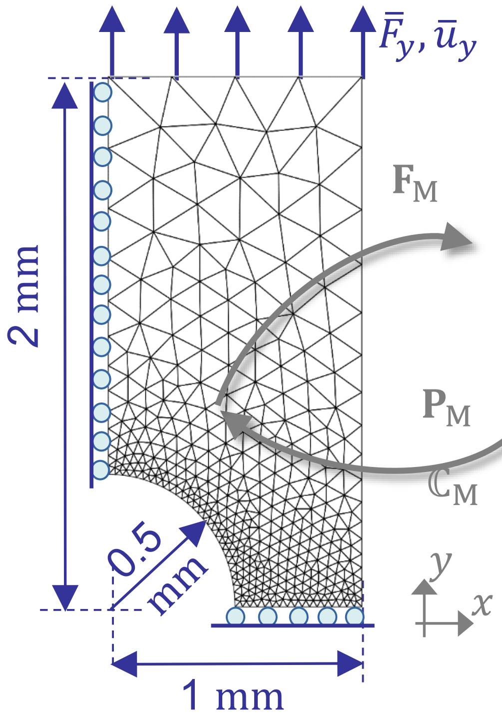

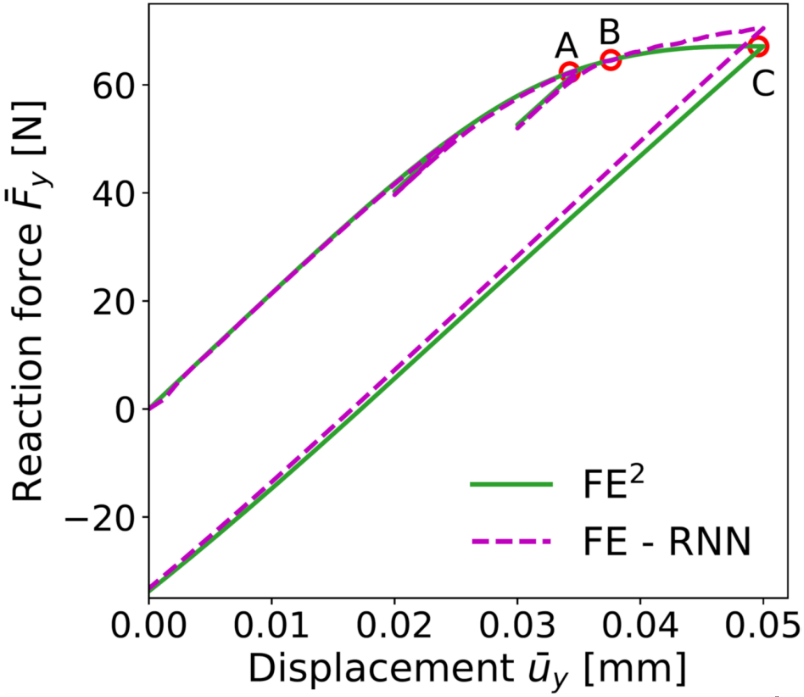

Recurrent Neural Network-accelerated multi-scale simulations

- Multiscale simulation
  - Stress-strain distribution at point A
  - Strain within the 10% training range

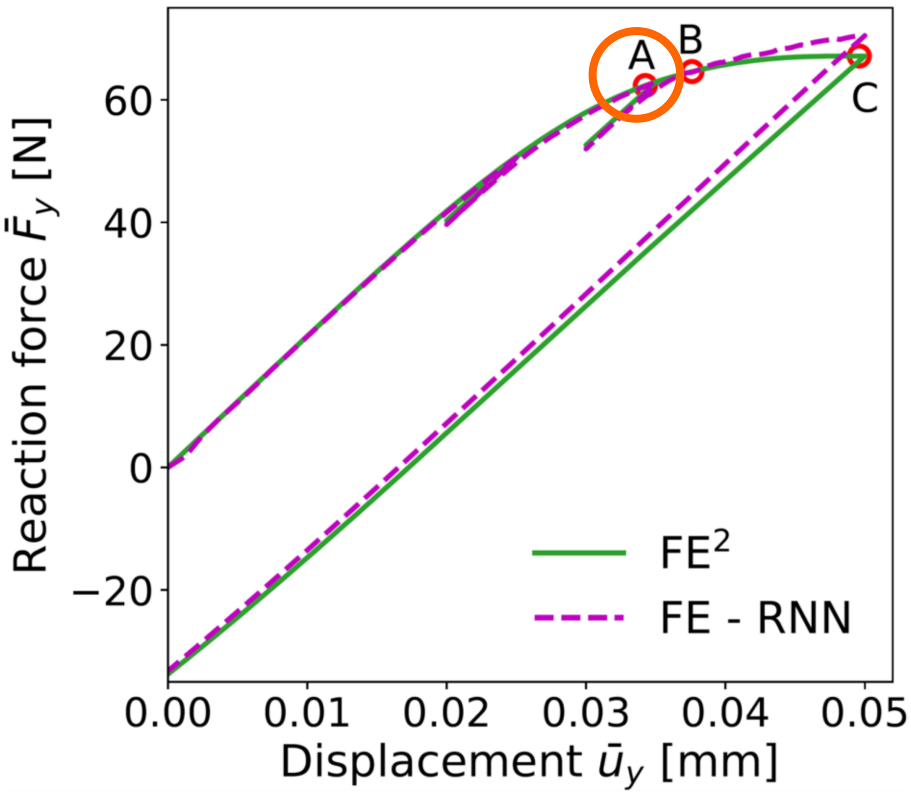

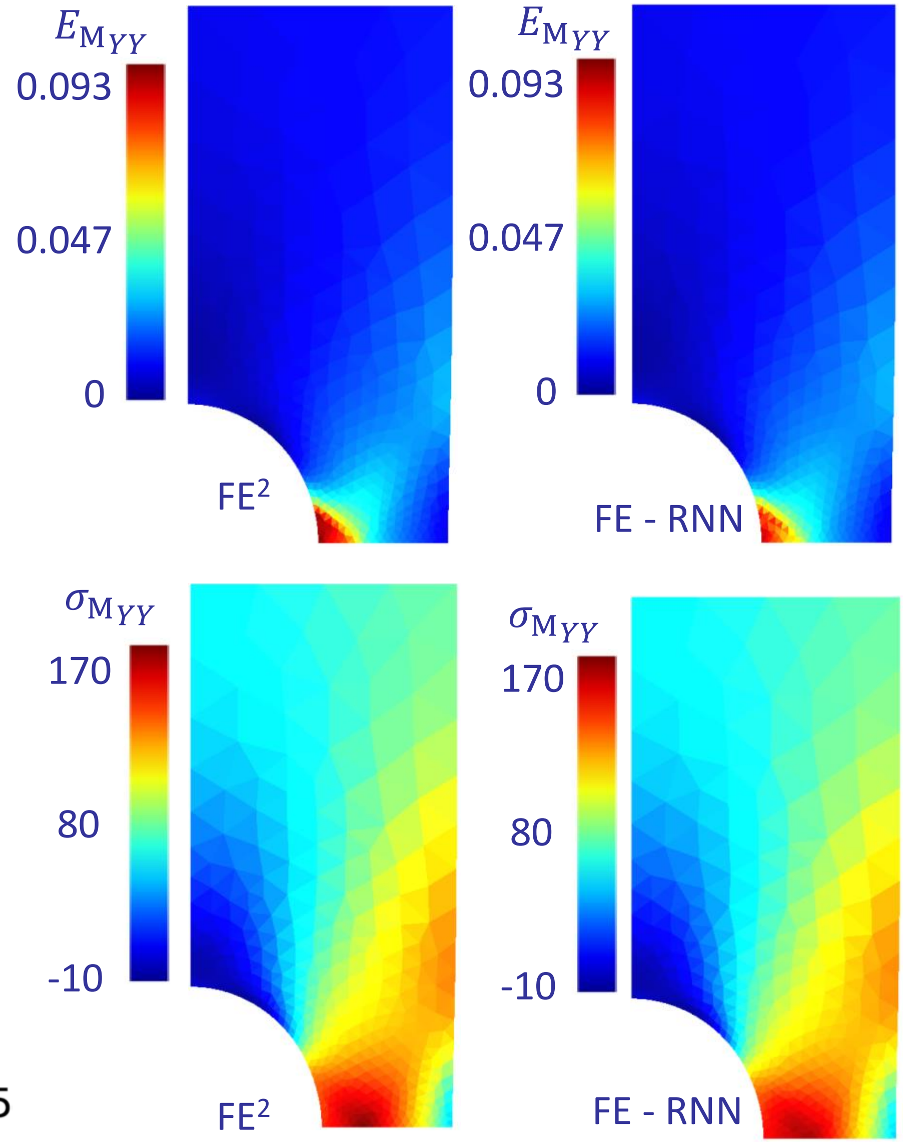

LIÈGE université

Recurrent Neural Network-accelerated multi-scale simulations

- Multiscale simulation
  - Stress-strain distribution at point B
  - Strain just at 10% training range

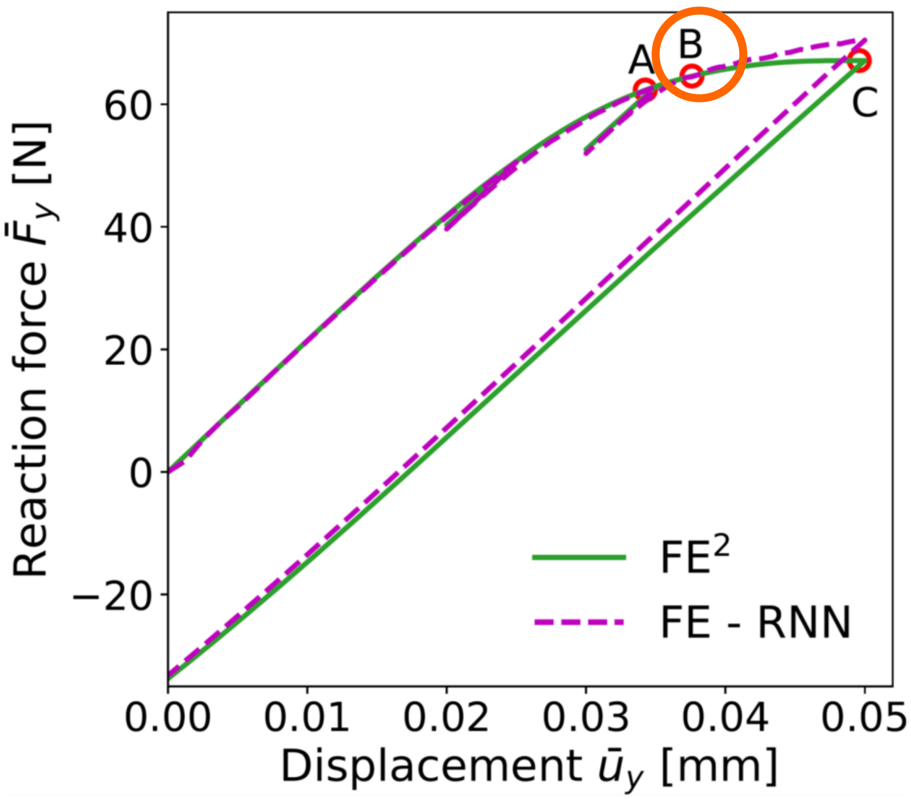

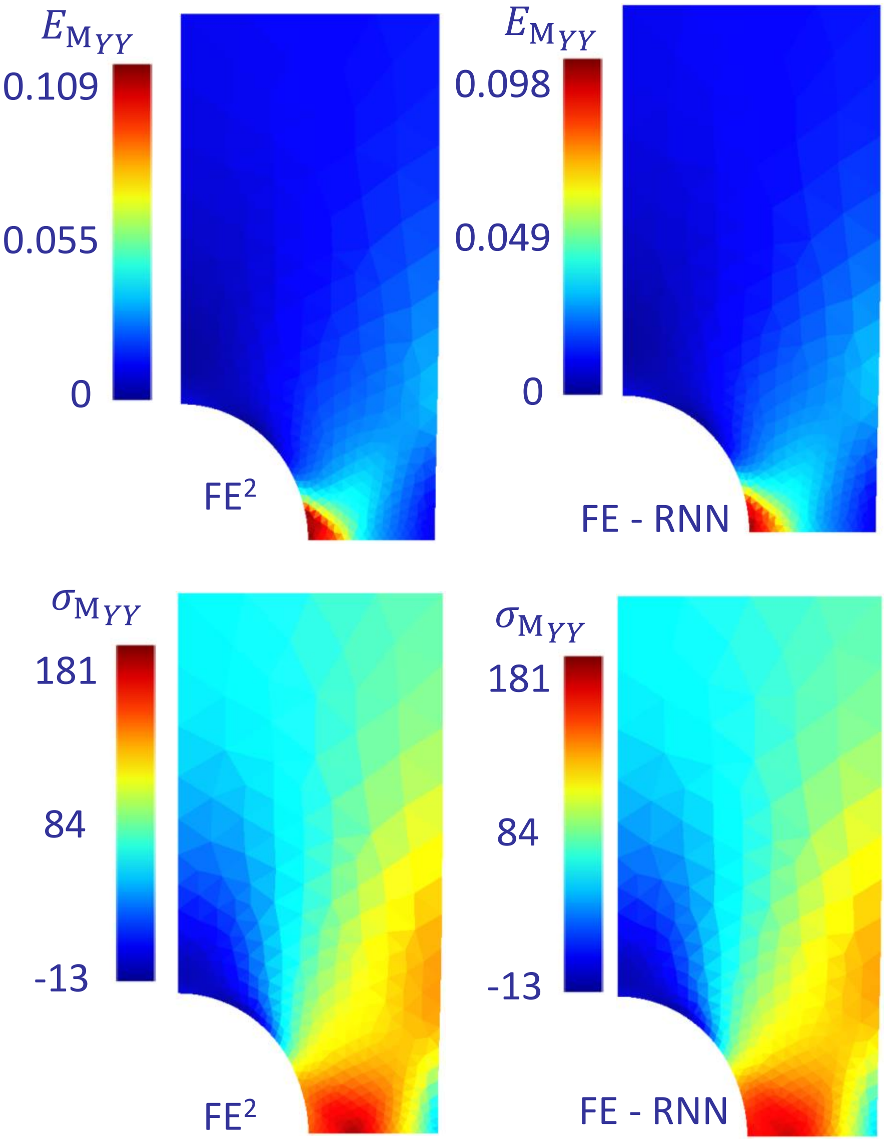

Recurrent Neural Network-accelerated multi-scale simulations

- Multiscale simulation
  - Stress-strain distribution at point C
  - Strain out of 10% training range

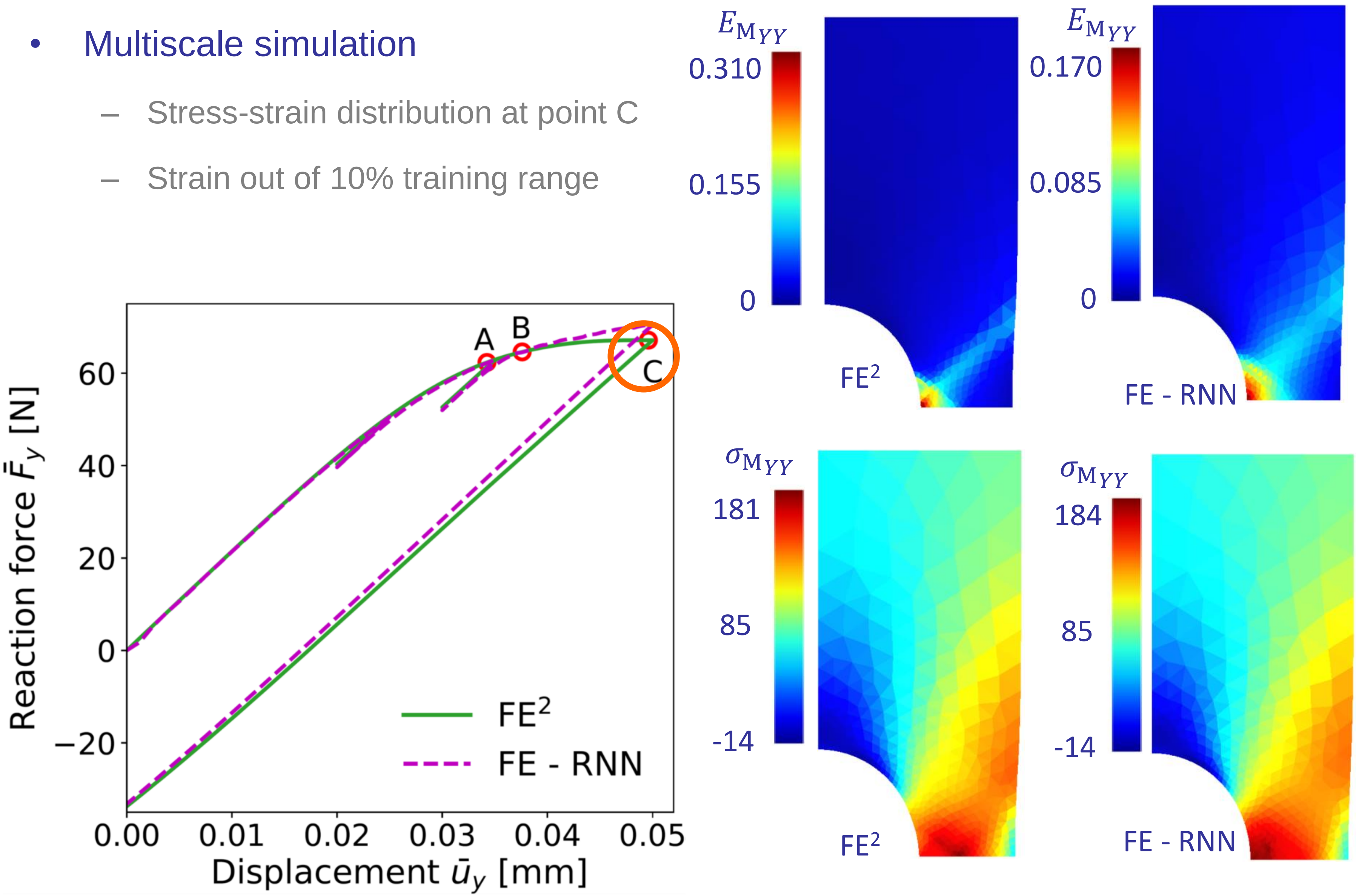

Recurrent Neural Network-accelerated multi-scale simulations

- MOAMMM FET-OPEN project (https://www.moammm.eu/)
  - ULiège, UCL (Belgium)
  - IMDEA Materials (Spain)
  - JKU (Austria)
  - cirp GmbH (Germany)

- Publications (doi)
  - 10.1016/j.cma.2020.113234
  - Data: 10.5281/zenodo.3902663

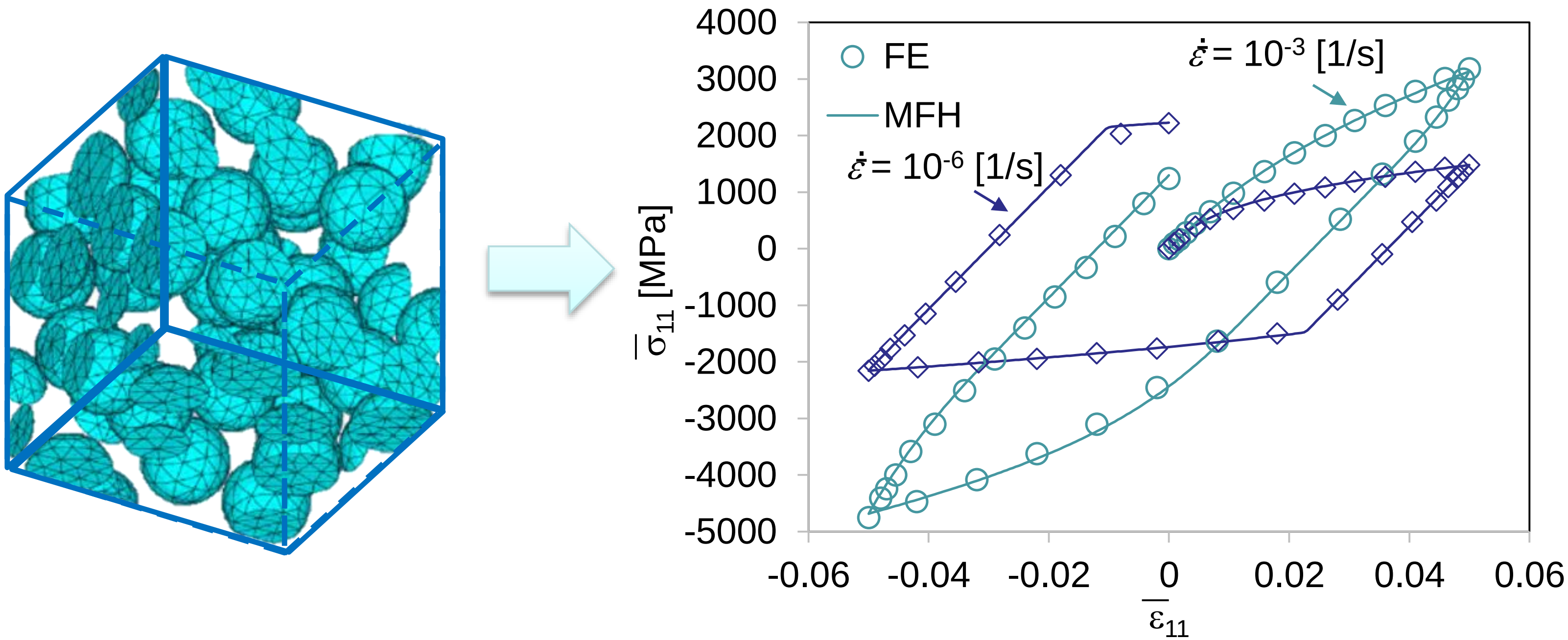

Mean-Field-Homogenization for Elasto-Visco-Plastic Composites

SIMUCOMP The research has been funded by the Walloon Region under the agreement no 1017232 (CT-EUC 2010-10-12) in the context of the ERA-NET +, Matera + framework.
The authors gratefully acknowledge the financial support from F.R.S-F.N.R.S. under the project number PDR T.1015.14
STOMMMAC The research has been funded by the Walloon Region under the agreement no 1410246-STOMMMAC (CT-INT 2013-03-28) in the context of M-ERA.NET Joint Call 2014.

Mean-Field-Homogenization for elasto-visco-plastic composites

- Multi-scale modeling
  - 2 problems are solved concurrently
    - The macro-scale problem
    - The meso-scale problem (on a meso-scale Volume Element)

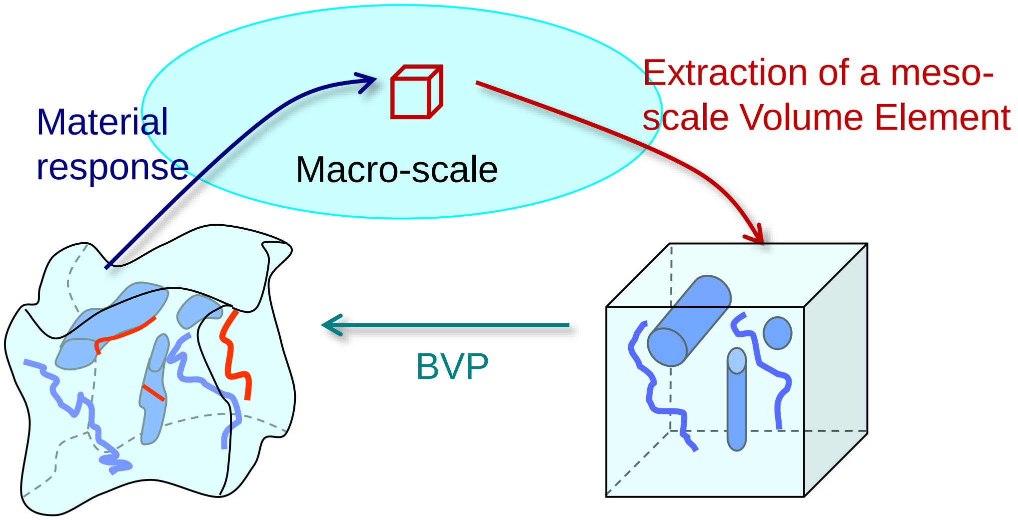

- Length-scales separation

$$L_{macro} >> L_{VE} >> L_{micro}$$

For accuracy: Size of the meso-scale volume element smaller than the characteristic length of the macro-scale loading

To be statistically representative: Size of the meso-scale volume element larger than the characteristic length of the micro-structure

Mean-Field-Homogenization for elasto-visco-plastic composites

- Incremental-secant mean-field-homogenization
  - Linear Comparison Composite material
    - Defined from unloaded state
  - Solve iteratively the system

$$\left\{\begin{array}{l}\Delta\bar{\boldsymbol{\varepsilon}}^{\mathrm{r}} = v_0\Delta\boldsymbol{\varepsilon}_0^{\mathrm{r}} + v_{\mathrm{I}}\Delta\boldsymbol{\varepsilon}_{\mathrm{I}}^{\mathrm{r}} \\ \Delta\boldsymbol{\varepsilon}_{\mathrm{I}}^{\mathrm{r}} = \Delta\boldsymbol{\varepsilon}_{\mathrm{I}} + \Delta\boldsymbol{\varepsilon}_{\mathrm{I}}^{\mathrm{unload}} \\ \Delta\boldsymbol{\varepsilon}_0^{\mathrm{r}} = \Delta\boldsymbol{\varepsilon}_0 + \Delta\boldsymbol{\varepsilon}_0^{\mathrm{unload}} \\ \Delta\boldsymbol{\varepsilon}_{\mathrm{I}}^{\mathrm{r}} = \mathbf{B}^{\varepsilon}\left(\mathrm{I}, \bar{\mathbf{C}}_0^{\mathrm{Sr}}, \bar{\mathbf{C}}_{\mathrm{I}}^{\mathrm{Sr}}\right) : \Delta\boldsymbol{\varepsilon}_0^{\mathrm{r}}\end{array}\right.$$

- With the stress tensors

$$\left\{\begin{array}{l}\bar{\boldsymbol{\sigma}} = v_0\boldsymbol{\sigma}_0 + v_{\mathrm{I}}\boldsymbol{\sigma}_{\mathrm{I}} \\ \boldsymbol{\sigma}_{\mathrm{I}} = \boldsymbol{\sigma}_{\mathrm{I}}^{\mathrm{res}} + \bar{\mathbf{C}}_{\mathrm{I}}^{\mathrm{Sr}} : \Delta\boldsymbol{\varepsilon}_{\mathrm{I}}^{\mathrm{r}} \\ \boldsymbol{\sigma}_0 = \boldsymbol{\sigma}_0^{\mathrm{res}} + \bar{\mathbf{C}}_0^{\mathrm{Sr}} : \Delta\boldsymbol{\varepsilon}_0^{\mathrm{r}}\end{array}\right.$$

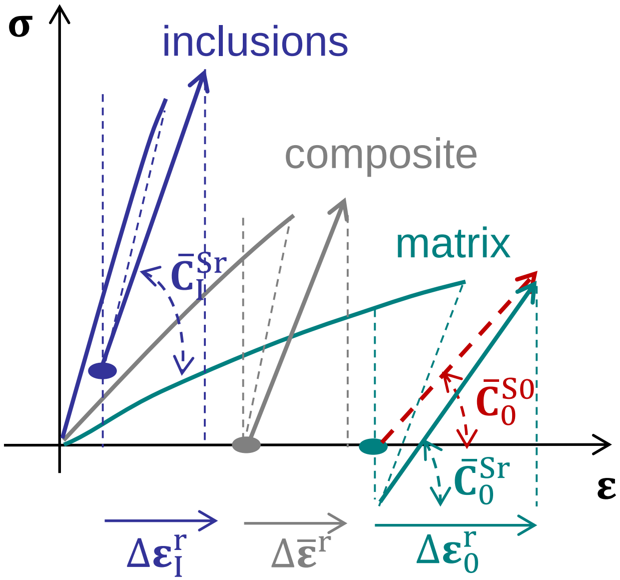

For elasto-plasticity: $f(\sigma^{\mathrm{eq}}, p) = 0$

&

For elasto-visco-plasticity: $\Delta p = g_v(\sigma^{\mathrm{eq}}, p)\Delta t$

  - For soft matrix response
    - Remove residual stress in matrix $\Delta\boldsymbol{\varepsilon}_{\mathrm{I}}^{\mathrm{r}} = \mathbf{B}^{\varepsilon}\left(\mathrm{I}, \bar{\mathbf{C}}_0^{\mathrm{S0}}, \bar{\mathbf{C}}_{\mathrm{I}}^{\mathrm{Sr}}\right) : \Delta\boldsymbol{\varepsilon}_0^{\mathrm{r}}$ & $\boldsymbol{\sigma}_0 = \bar{\mathbf{C}}_0^{\mathrm{S0}} : \Delta\boldsymbol{\varepsilon}_0^{\mathrm{r}}$
    - Or use second moment estimates

- Incremental-secant mean-field-homogenization
  - Stress tensor (2 forms)

$$\begin{cases} \boldsymbol{\sigma}_{\mathrm{I/0}} = \boldsymbol{\sigma}^{\mathrm{res}}_{\mathrm{I/0}} + \bar{\mathbf{C}}^{\mathrm{Sr}}_{\mathrm{I/0}} : \Delta\boldsymbol{\varepsilon}^{\mathrm{r}}_{\mathrm{I/0}} \\ \boldsymbol{\sigma}_{\mathrm{I/0}} = \bar{\mathbf{C}}^{\mathrm{S0}}_{\mathrm{I/0}} : \Delta\boldsymbol{\varepsilon}^{\mathrm{r}}_{\mathrm{I/0}} \end{cases}$$

  - Radial return direction toward residual stress
    - First order approximation in the strain increment (and not in the total strain)
    - Exact for the zero-incremental-secant method
  - The secant operators are naturally isotropic

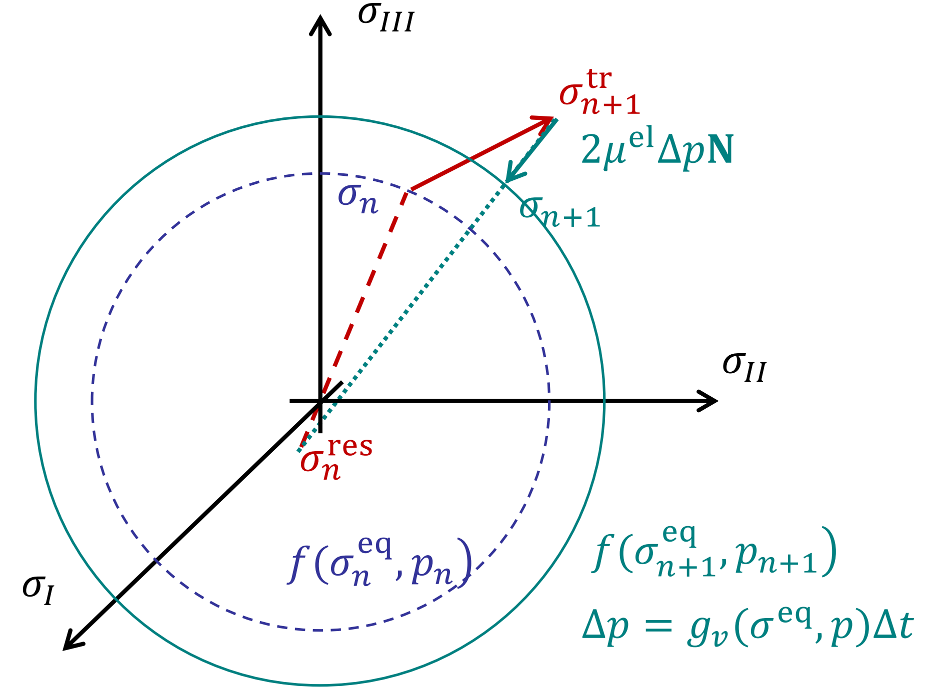

$$\begin{cases} \bar{\mathbf{C}}^{\mathrm{Sr}} = 3\kappa^{\mathrm{el}}\mathbf{I}^{\mathrm{vol}} + 2\left(\mu^{\mathrm{el}} - 3\dfrac{{\mu^{\mathrm{el}}}^2\Delta p}{\left(\boldsymbol{\sigma}_{n+1} - \boldsymbol{\sigma}^{\mathrm{res}}_n\right)^{\mathrm{eq}}}\right)\mathbf{I}^{\mathrm{vol}} \\ \bar{\mathbf{C}}^{\mathrm{S0}} = 3\kappa^{\mathrm{el}}\mathbf{I}^{\mathrm{vol}} + 2\left(\mu^{\mathrm{el}} - 3\dfrac{{\mu^{\mathrm{el}}}^2\Delta p}{\boldsymbol{\sigma}^{\mathrm{eq}}_{n+1}}\right)\mathbf{I}^{\mathrm{vol}} \end{cases}$$

- Incremental-secant mean-field-homogenization
  - Second-statistical moment estimation of the von Mises stress
    - First statistical moment (mean value) not fully representative

$$\bar{\sigma}^{\mathrm{eq}}_{\mathrm{I/0}} = \sqrt{\frac{3}{2}\bar{\boldsymbol{\sigma}}^{\mathrm{dev}}_{\mathrm{I/0}} : \bar{\boldsymbol{\sigma}}^{\mathrm{dev}}_{\mathrm{I/0}}}$$

    - Use second statistical moment estimations to define the yield surface

$$\hat{\hat{\sigma}}^{\mathrm{eq}}_{\mathrm{I/0}} = \sqrt{\frac{3}{2}\mathbf{I}^{\mathrm{dev}} :: \langle \boldsymbol{\sigma}_{\mathrm{I/0}} \otimes \boldsymbol{\sigma}_{\mathrm{I/0}} \rangle_{\omega_{\mathrm{I/0}}}} \geq \bar{\sigma}^{\mathrm{eq}}_{\mathrm{I/0}}$$

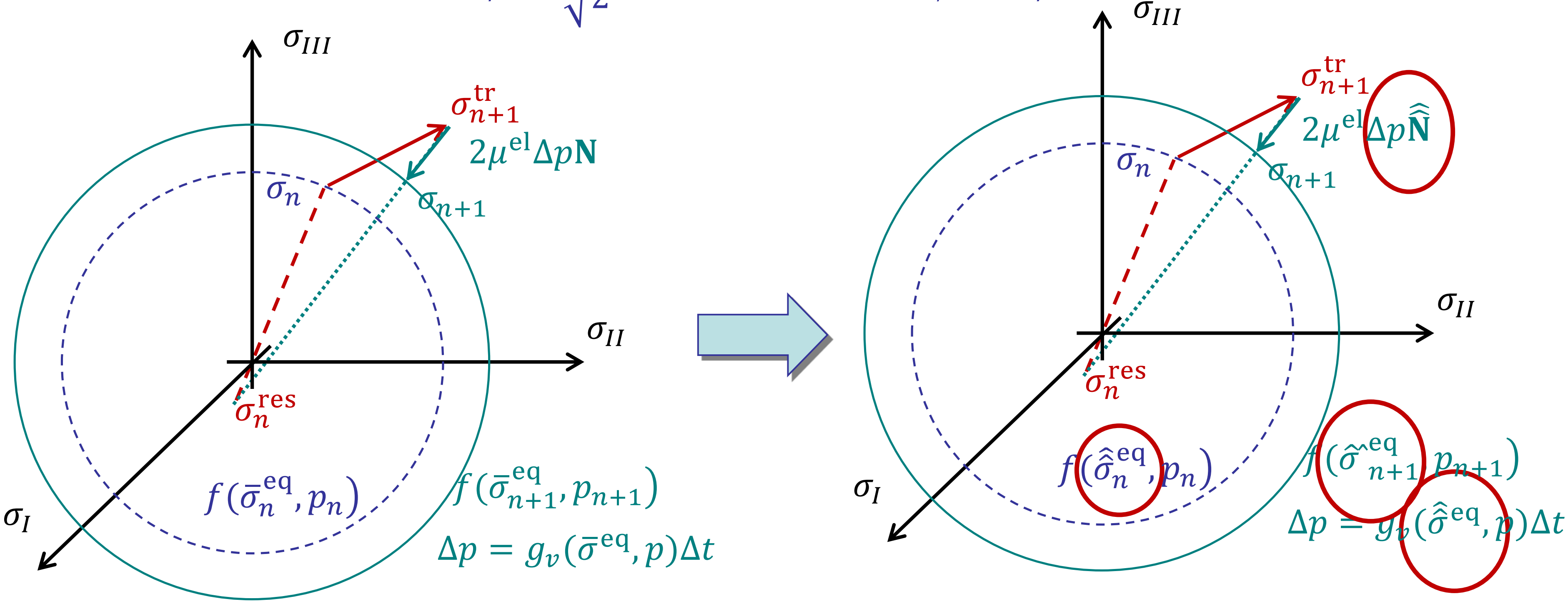

- Non-proportional loading
  - Spherical inclusions
    - 17 % volume fraction
    - Elastic
  - Elastic-perfectly-plastic matrix

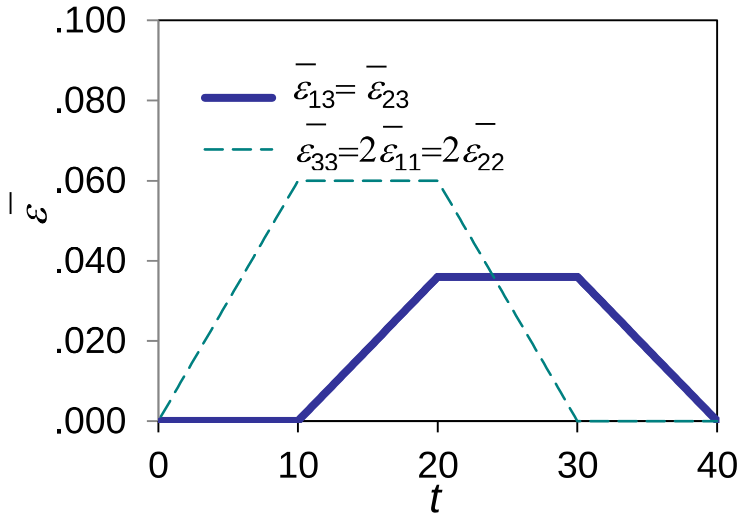

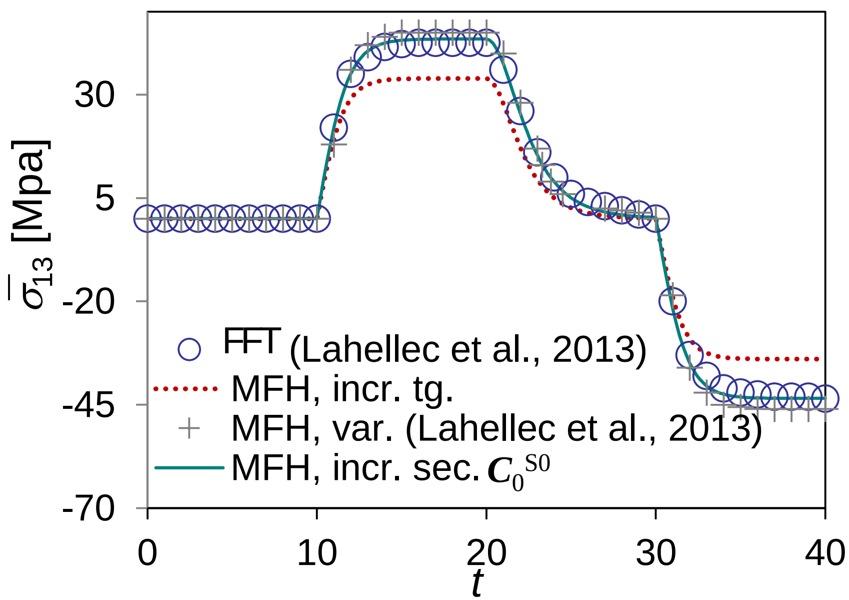

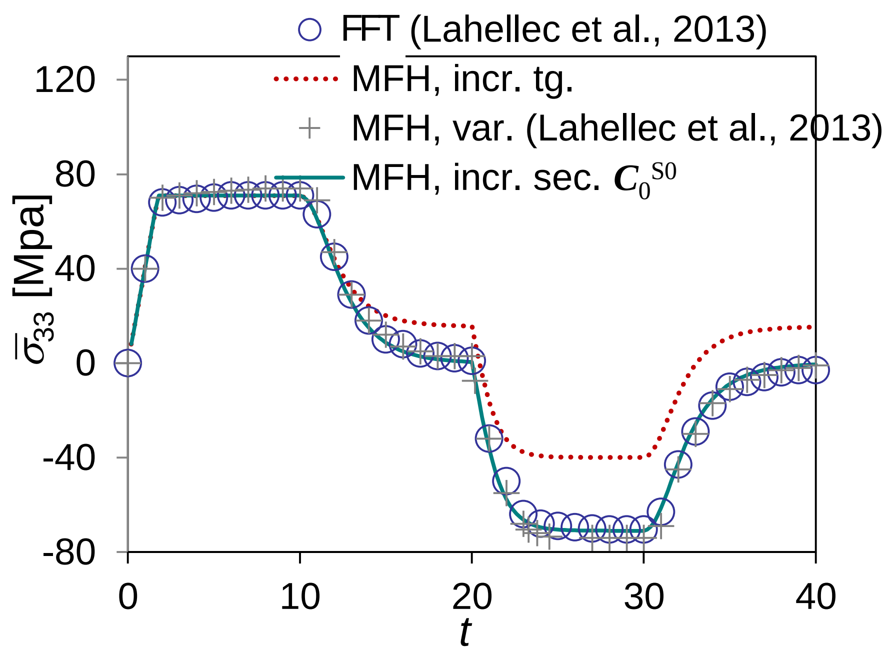

Mean-Field-Homogenization for elasto-visco-plastic composites

- Elasto-visco-plasticity
  - Elasto-visco-plastic short fibres
    - Spherical
    - 30 % volume fraction
  - Elasto-visco-plastic matrix

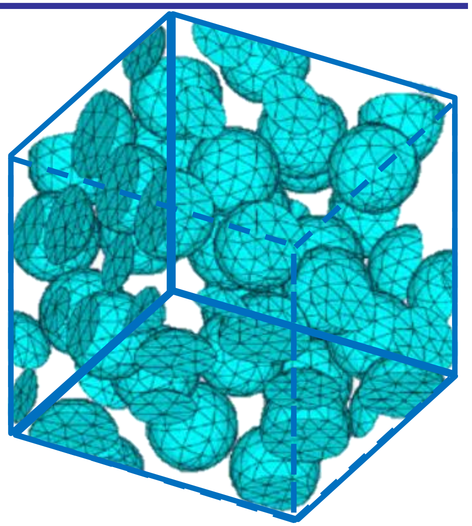

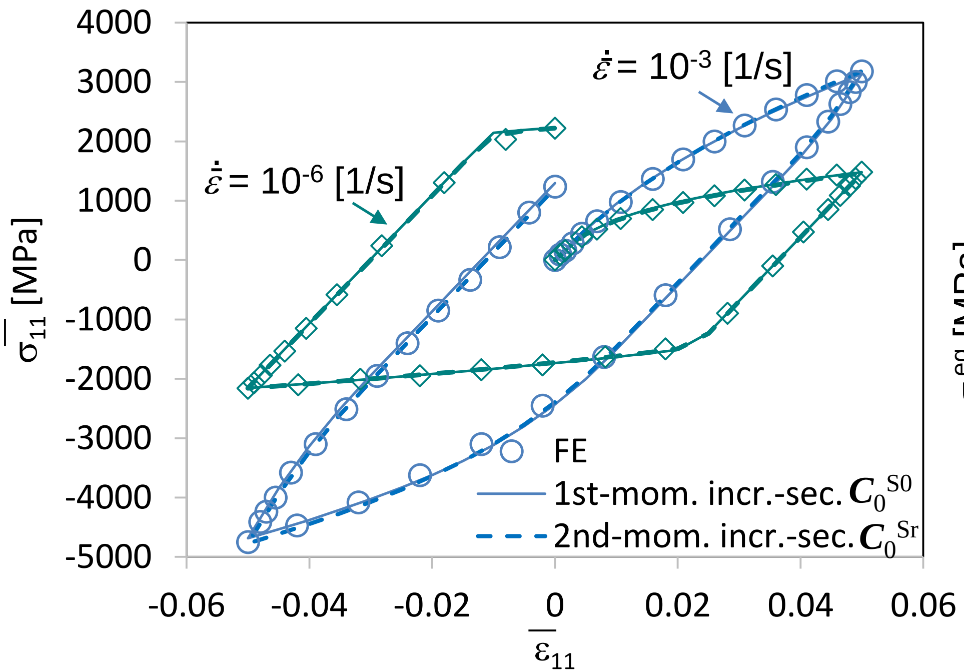

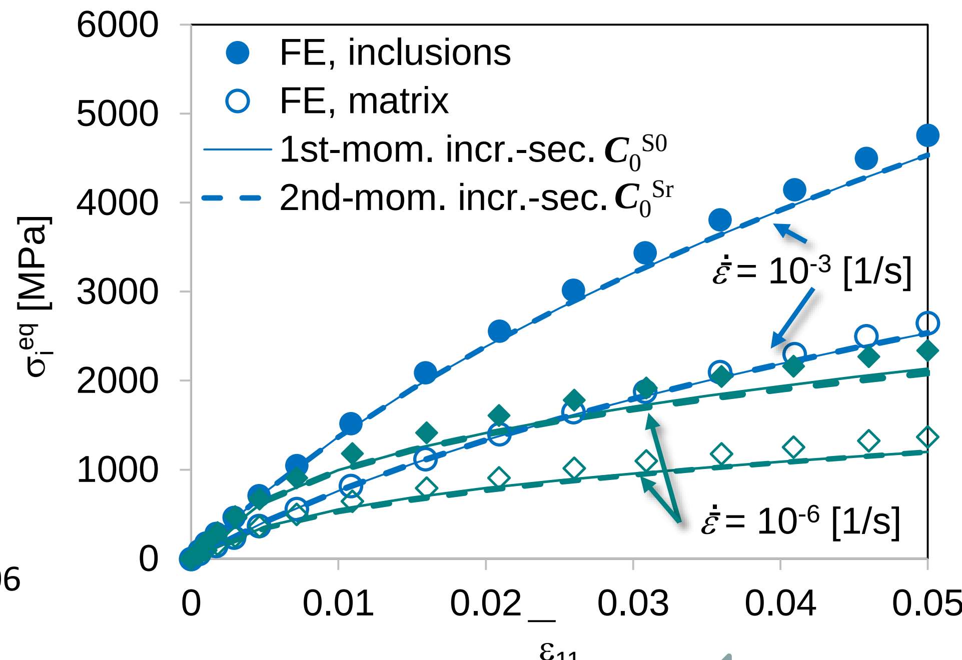

- Extension to finite deformations
  - Formulate everything in terms of elastic left Cauchy-Green tensor

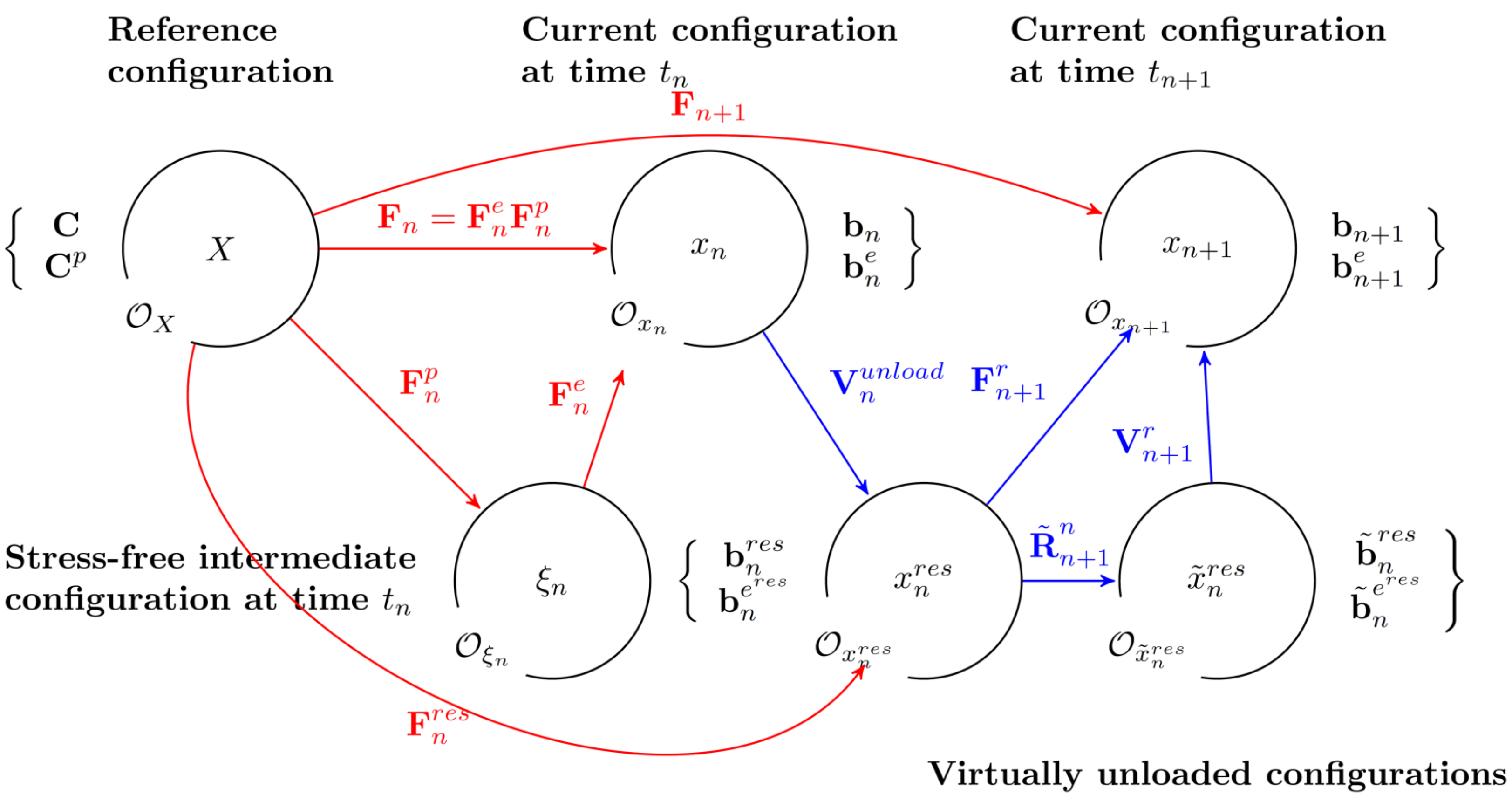

Mean-Field-Homogenization for elasto-visco-plastic composites

- Extension to finite deformations
  - Porous material: homogenized response

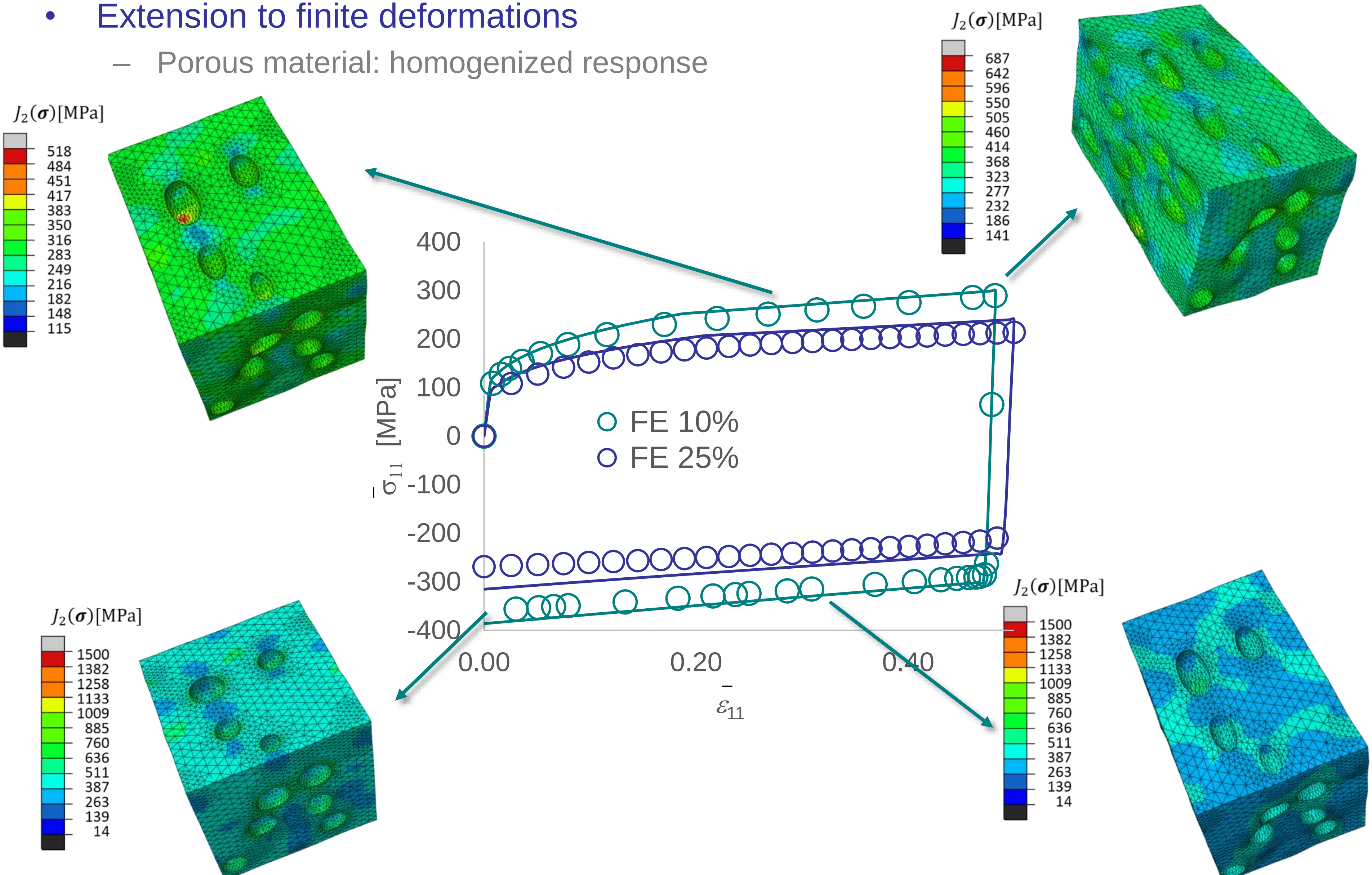

Beginning

- Extension to finite deformations
  - Porous material: micro-structure evolution

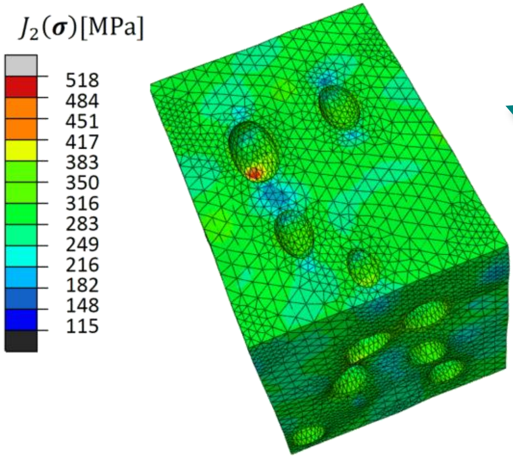

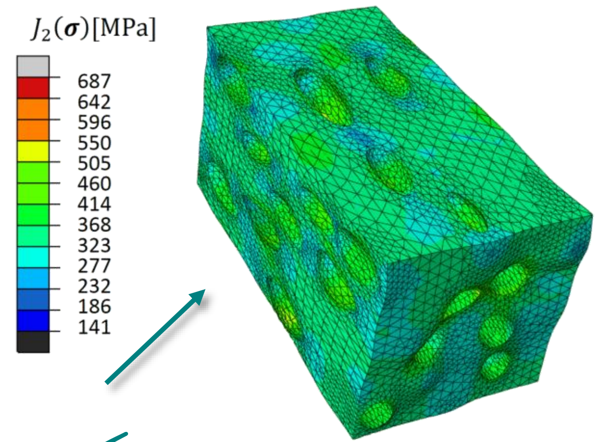

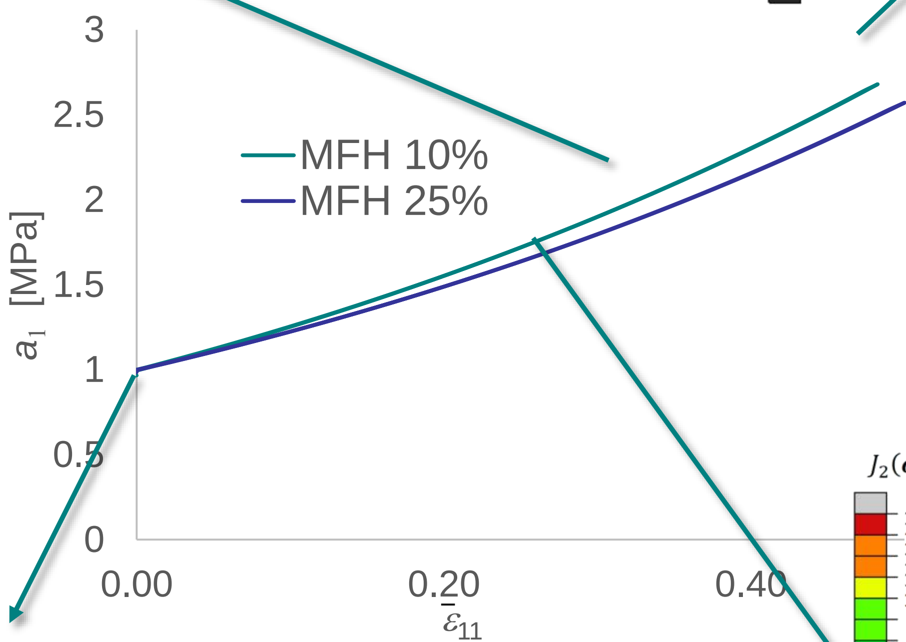

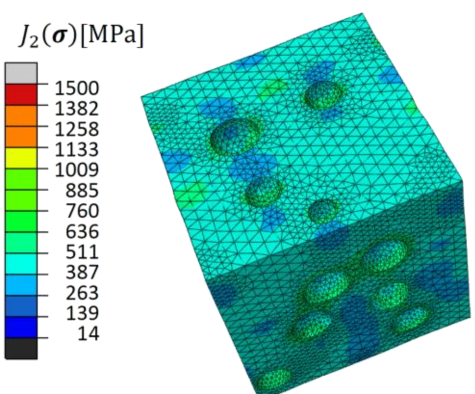

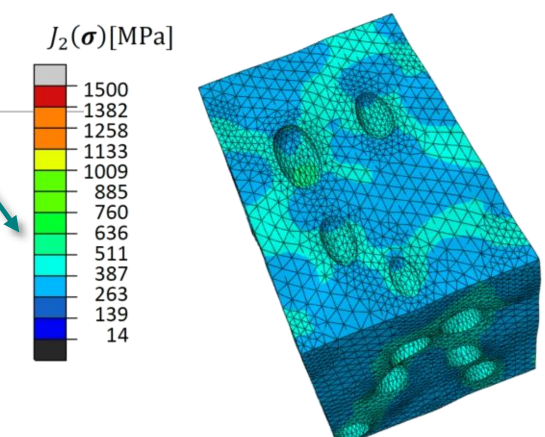

Mean-Field-Homogenization for elasto-visco-plastic composites

- SIMUCOMP ERA-NET project (incremental secant MFH)
  - e-Xstream, CENAERO, ULiège (Belgium)
  - IMDEA Materials (Spain)
  - CRP Henri-Tudor (Luxemburg)

- PDR T.1015.14 project (MFH with second-order moments)
  - ULiège, UCL (Belgium)

- STOMMMAC M.ERA-NET project (MFH for elasto-visco-plastic composites)
  - e-Xstream, ULiège (Belgium)
  - BATZ (Spain)
  - JKU, AC (Austria)
  - U Luxembourg (Luxemburg)

- Publications (doi)
  - 10.1016/j.mechmat.2017.08.006
  - 10.1080/14786435.2015.1087653
  - 10.1016/j.ijplas.2013.06.006
  - 10.1016/j.cma.2018.12.007

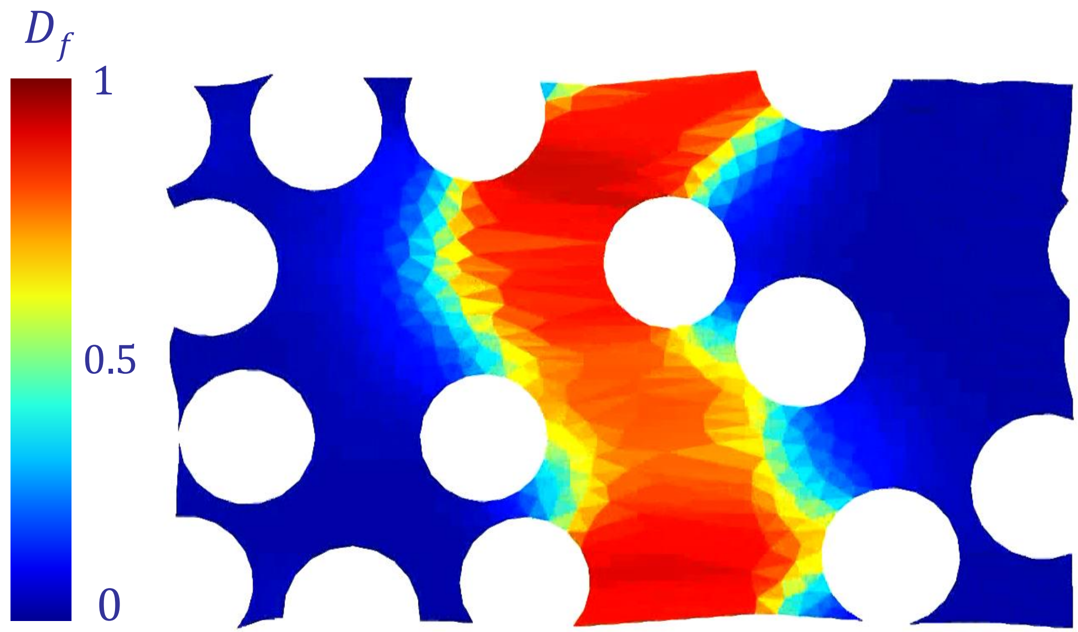

Micro-structural characterization and simulation of fiber-reinforced highly crosslinked epoxy

The authors gratefully acknowledge the nancial support from F.R.S-F.N.R.S. under the project number PDR T.1015.14

Micro-structural simulation of fiber-reinforced highly crosslinked epoxy

- Resin behavior (experiments UCL)
  - Viscoelasto-Viscoplaticity
  - Saturated softening
  - Asymmetry tension-compression
  - Pressure-dependent yield

- To used in micro-structural analysis
  - Behavior in composite is different
  - Introduce a length-scale effect

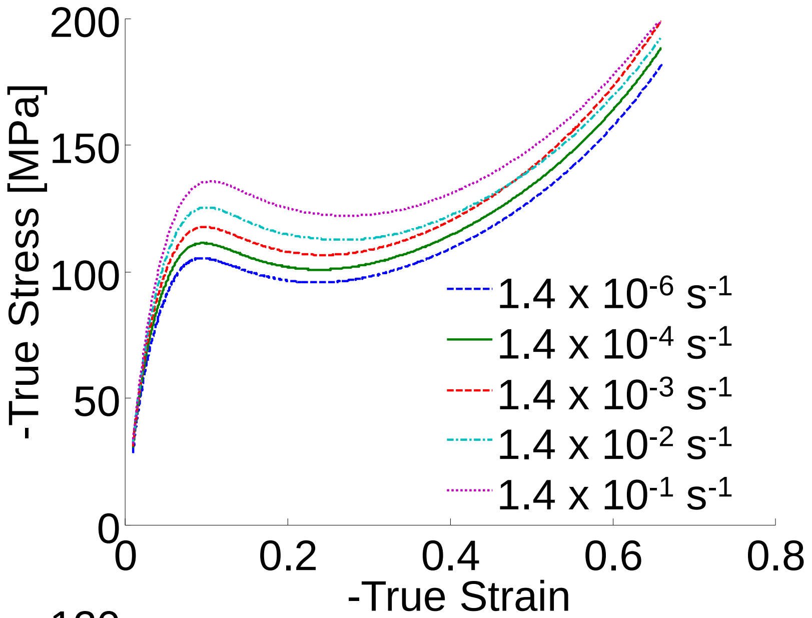

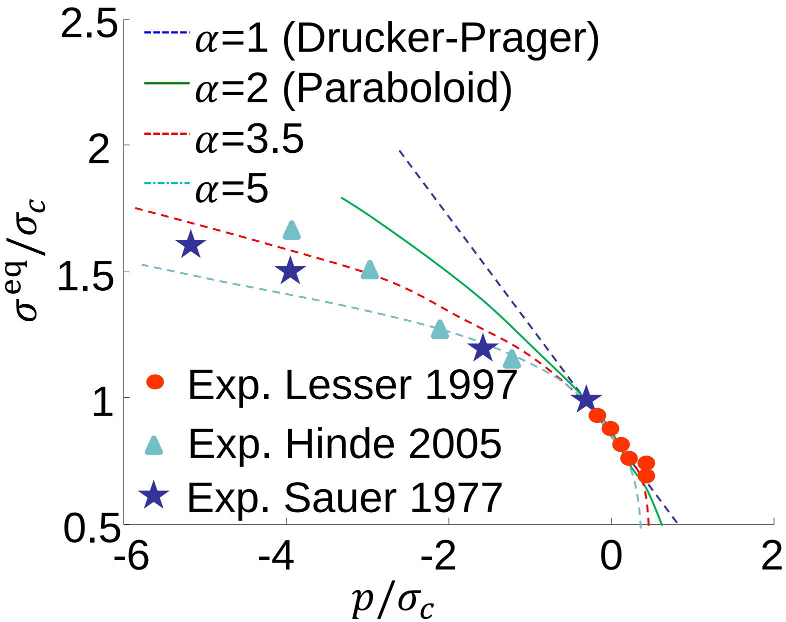

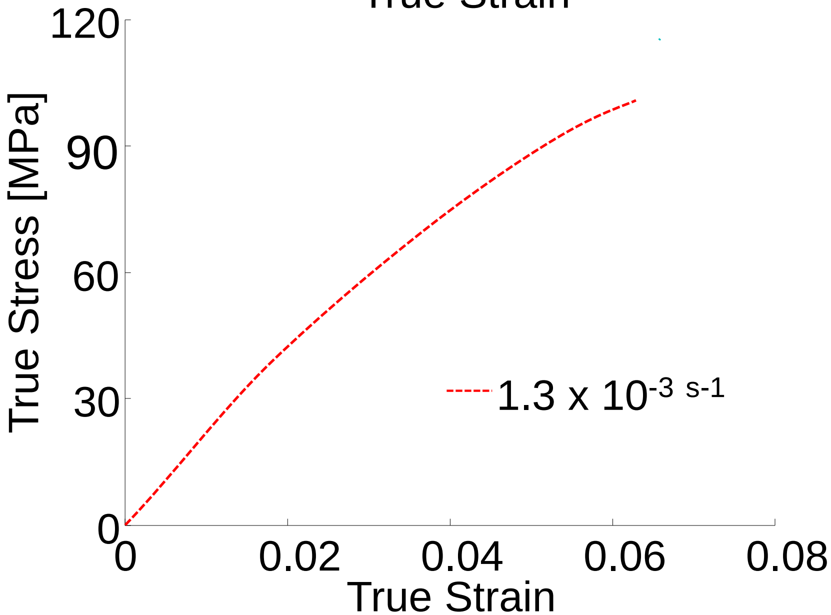

Micro-structural simulation of fiber-reinforced highly crosslinked epoxy

- Material changes represented via internal variables
  - Constitutive law $\mathbf{P}\left(\mathbf{F};\boldsymbol{Z}(t')\right)$
    - Internal variables $\boldsymbol{Z}(t')$
  - Multi-damage strategy

$$\mathbf{P} = (\mathbf{1} - D_s)(\mathbf{1} - D_f)\widehat{\mathbf{P}}$$

- Resin model implementation:
  - Requires non-local form [Bažant 1988]
    - Introduction of characteristic length l_c
    - Weighted average: $\tilde{Z}(\boldsymbol{x}) = \int_{V_C} W(\boldsymbol{y};\boldsymbol{x},l_c)\ Z(\mathbf{y})d\boldsymbol{y}$
  - Implicit form [Peerlings et al. 1998]
    - New degrees of freedom: $\tilde{Z}$
    - New Helmholtz-type equations: $\tilde{Z} - l_c^2\ \Delta\tilde{Z} = Z$
  - Damage evolution laws

$$\begin{cases} \dot{D}_{s/f} = D_{s/f}\left(D_{s/f},\mathbf{F}(t),\chi_{s/f}(t);Z(\tau),\tau\in[0\ t]\right)\dot{\chi}_{s/f} \\ \chi_{s/f}(t) = \max_{\tau}\left(\tilde{\gamma}_{s/f}(\tau)\right) \\ \tilde{\gamma}_{s/f} - l_{s/f}^2\ \Delta\tilde{\gamma}_{s/f} = \gamma_{s/f} \end{cases}$$

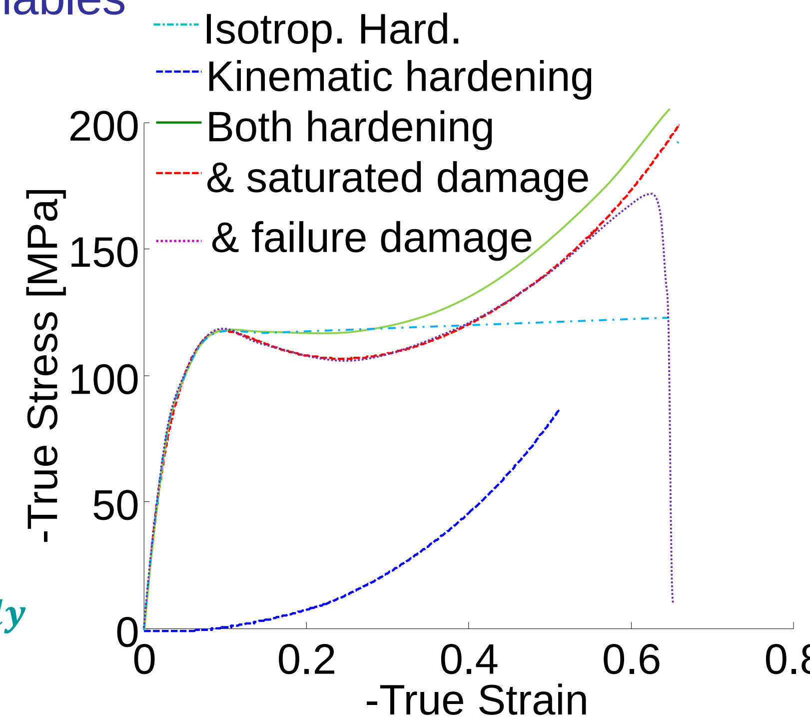

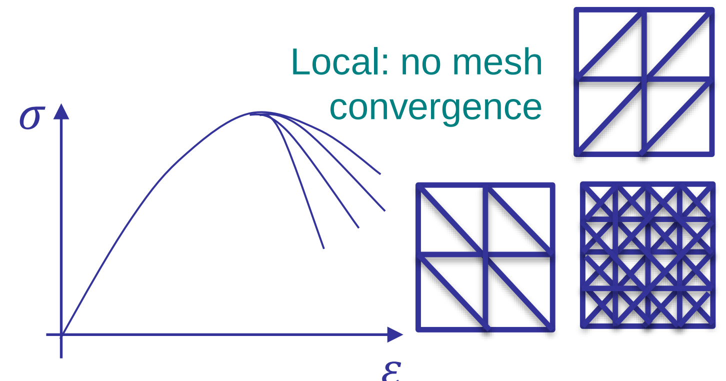

Micro-structural simulation of fiber-reinforced highly crosslinked epoxy

- Resin model: hyperelastic-based formulation
  - Multiplicative decomposition

    $\mathbf{F} = \mathbf{F}^{\mathrm{ve}} \cdot \mathbf{F}^{\mathrm{vp}}, \quad \mathbf{C}^{\mathrm{ve}} = \mathbf{F}^{\mathrm{ve}^T} \cdot \mathbf{F}^{\mathrm{ve}}, \quad J^{\mathrm{ve}} = \det(\mathbf{F}^{\mathrm{ve}})$
  - Undamaged stress tensor definition
    - Elastic potential $\psi(\mathbf{C}^{ve})$
    - Undamaged first Piola-Kirchhoff stress tensor

      $$\widehat{\mathbf{P}} = 2\mathbf{F}^{\mathrm{ve}} \cdot \frac{\partial \psi(\mathbf{C}^{\mathrm{ve}})}{\partial \mathbf{C}^{\mathrm{ve}}} \cdot \mathbf{F}^{\mathrm{vp}^{-T}}$$
    - Undamaged Kirchhoff stress tensors
      - In current configuration

        $$\widehat{\boldsymbol{\kappa}} = \widehat{\mathbf{P}} \cdot \mathbf{F}^T = 2\mathbf{F}^{\mathrm{ve}} \cdot \frac{\partial \psi(\mathbf{C}^{ve})}{\partial \mathbf{C}^{\mathrm{ve}}} \cdot \mathbf{F}^{\mathrm{ve}^T}$$
      - In co-rotational space

        $$\widehat{\boldsymbol{\tau}} = \mathbf{C}^{\mathrm{ve}} \cdot \mathbf{F}^{\mathrm{ve}^{-1}} \cdot \widehat{\boldsymbol{\kappa}} \cdot \mathbf{F}^{\mathrm{ve}^{-T}} = 2\mathbf{C}^{ve} \cdot \frac{\partial \psi(\mathbf{C}^{\mathrm{ve}})}{\partial \mathbf{C}^{\mathrm{ve}}}$$
  - Apparent stress tensor
    - Piola-Kirchhoff stress

      $$\mathbf{P} = (\mathbf{1} - D_s)(\mathbf{1} - D_f)\widehat{\mathbf{P}}$$

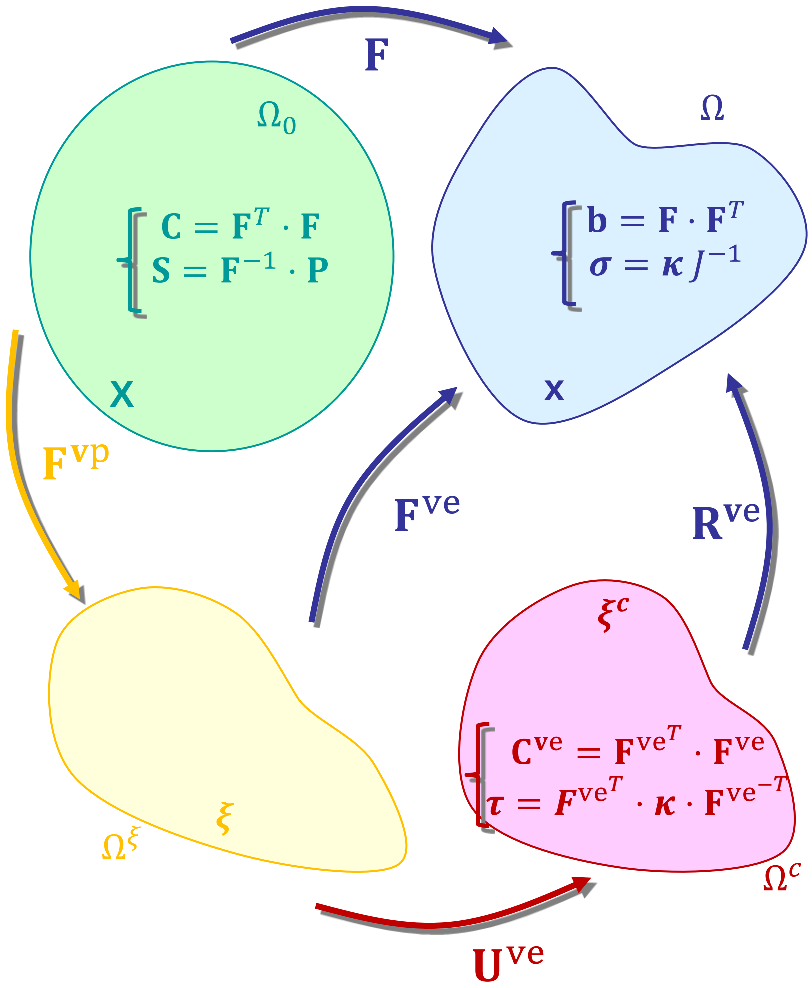

- Resin model: logarithmic visco-elasticity
  - Elastic potentials ψ_i:

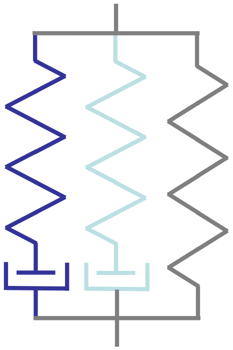

$$\psi_i(\mathbf{C}^{\mathrm{ve}}) = \frac{K_i}{2}\ln^2(J^{\mathrm{ve}}) + \frac{G_i}{4}(\ln(\mathbf{C}^{\mathrm{ve}}))^{\mathrm{dev}} : (\ln(\mathbf{C}^{\mathrm{ve}}))^{\mathrm{dev}}$$

  - Dissipative potentials Υ_i

$$\Upsilon_i(\mathbf{C}^{\mathrm{ve}}, \mathbf{q}_i) = -\mathbf{q}_i : \ln(\mathbf{C}^{\mathrm{ve}}) + \left[\frac{1}{18K_i}\mathrm{tr}^2(\mathbf{q}_i) + \frac{1}{4G_i}\mathbf{q}_i^{\mathrm{dev}} : \mathbf{q}_i^{\mathrm{dev}}\right]$$

$$\begin{cases} \dot{\mathbf{q}}_i^{\mathrm{dev}} = \dfrac{2G_i}{g_i}\,(\ln(\mathbf{C}^{\mathrm{ve}}))^{\mathrm{dev}} - \dfrac{1}{g_i}\mathbf{q}_i^{\mathrm{dev}} \\ \mathrm{tr}\,(\dot{\mathbf{q}}_i) = \dfrac{3K_i}{k_i}\,\ln^2(J^{\mathrm{ve}}) - \dfrac{1}{k_i}\mathrm{tr}\,(\mathbf{q}_i) \end{cases}$$

  - Total potential ψ:

$$\begin{cases} \psi(\mathbf{C}^{\mathrm{ve}}; \boldsymbol{q}_i) = \psi_\infty(\mathbf{C}^{\mathrm{ve}}) + \displaystyle\sum_i [\psi_i(\mathbf{C}^{\mathrm{ve}}) + \Upsilon_i(\mathbf{C}^{\mathrm{ve}}, \mathbf{q}_i)] \\ \widehat{\mathbf{P}} = 2\mathbf{F}^{\mathrm{ve}} \cdot \dfrac{\partial\psi(\mathbf{C}^{\mathrm{ve}})}{\partial\mathbf{C}^{\mathrm{ve}}} \cdot \mathbf{F}^{\mathrm{vp}^{-T}} \end{cases}$$

- Resin model: visco-plasticity
  - Stress, back-stress

    $\boldsymbol{\varphi} = \hat{\boldsymbol{\tau}} - \hat{\boldsymbol{b}}$
  - Perzina plastic flow rule

    $$\mathbf{D}^{\mathrm{vp}} = \dot{\mathbf{F}}^{\mathrm{v}p} \cdot \mathbf{F}^{\mathrm{v}p} = \frac{1}{\eta}\langle\phi\rangle^{\frac{1}{p}}\frac{\partial P}{\partial\hat{\boldsymbol{\tau}}}$$
  - Pressure dependent yield surface

    $$\begin{cases} \phi = \left(\dfrac{\varphi^{\mathrm{eq}}}{\sigma_c}\right)^{\alpha} - \dfrac{m^{\alpha}-1}{m+1}\dfrac{\mathrm{tr}\boldsymbol{\varphi}}{\sigma_c} - \dfrac{m^{\alpha}+m}{m+1} \leq 0 \\ m = \dfrac{\sigma_t}{\sigma_c} \end{cases}$$
  - Non-associated flow potential

    $$P = (\varphi^{\mathrm{eq}})^2 + \beta\left(\frac{\mathrm{tr}\boldsymbol{\varphi}}{3}\right)^2$$
  - Equivalent plastic strain rate:

    $$\begin{cases} \dot{\gamma} = \dfrac{\sqrt{\mathbf{D}^{\mathrm{vp}}:\mathbf{D}^{\mathrm{vp}}}}{\sqrt{\mathbf{1}+\mathbf{2}v_p^2}} \\ v_p = \dfrac{9-2\beta}{18+2\beta} \end{cases}$$

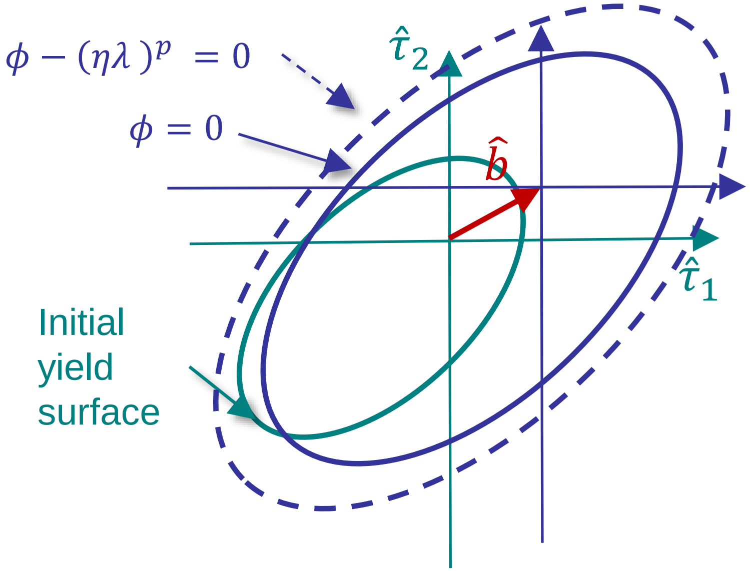

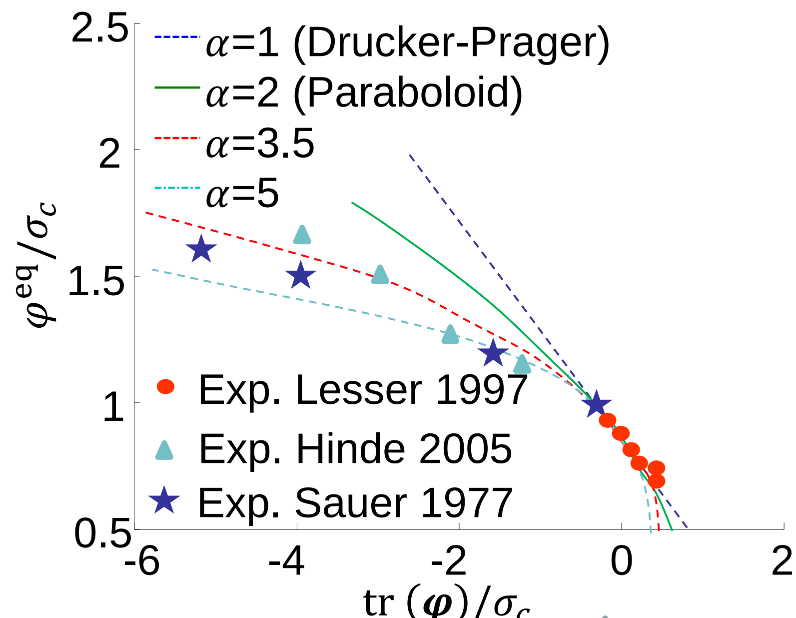

Micro-structural simulation of fiber-reinforced highly crosslinked epoxy

- Resin model: saturated softening
  - Damage evolution

$$\begin{cases} \dot{D}_s = H_s(\chi_s - \chi_{s0})^{\zeta_s}(D_{s\infty} - D_s)\dot{\chi}_s \\ \chi_s = \max_{\tau}\left(\chi_{s0}, \tilde{\gamma}_s(\tau)\right) \\ \tilde{\gamma}_s - l_s^2\,\Delta\tilde{\gamma}_s = \gamma \end{cases}$$

  - Calibration
    - Several hardening/softening combinations
    - Requires composite material tests
      - Length scale effect

$$l_s = 3\mu\text{m}\left(1 - \frac{D_s}{D_{s\infty}}\right)$$

      - Non-local BC at fiber interface $[\![\dot{\tilde{\gamma}}_s]\!] = 0$

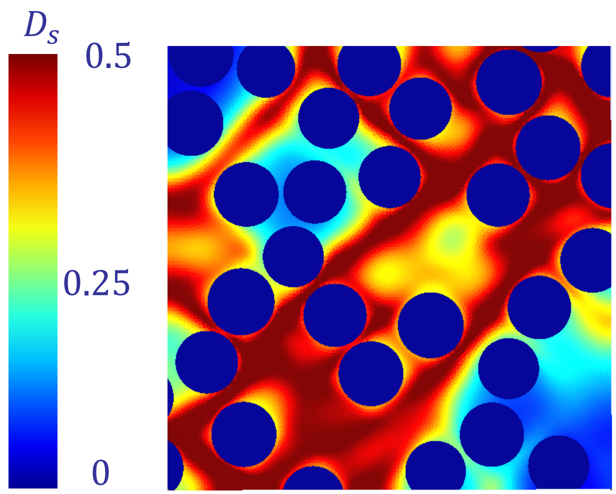

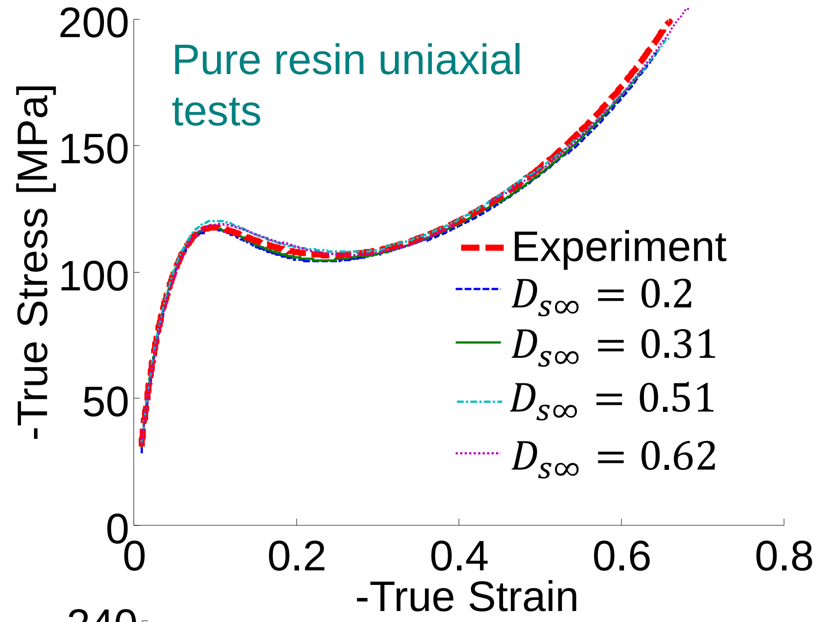

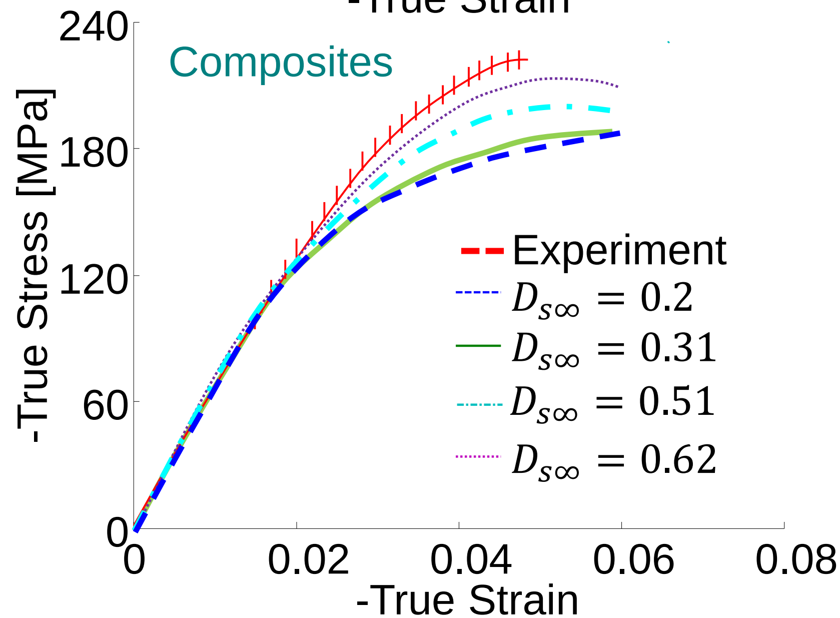

Micro-structural simulation of fiber-reinforced highly crosslinked epoxy

- Resin model: failure softening
  - Failure surface

$$\begin{cases} \phi_f = \gamma - a\exp\left(-b\frac{\mathrm{tr}(\hat{\boldsymbol{\tau}})}{3\hat{\tau}^{eq}}\right) - c \\ \phi_f - r \leq 0;\ \dot{r} \geq 0; \text{and } \dot{r}\left(\phi_f - r\right) = 0 \\ \dot{\gamma}_f = \dot{r} \end{cases}$$

  - Damage evolution

$$\begin{cases} \dot{D}_f = H_f\left(\chi_f\right)^{\zeta_f}\left(1 - D_f\right)^{-\zeta_d}\dot{\chi}_f \\ \chi_f = \max_{\tau}\left(\tilde{\gamma}_f(\tau)\right) \\ \tilde{\gamma}_f - l_f^2\,\Delta\tilde{\gamma}_f = \gamma_f \\ l_f = 3\ \mu\mathrm{m} \qquad \nabla_0\tilde{\gamma}_f \cdot \mathbf{N} = 0 \end{cases}$$

  - Affect ductility

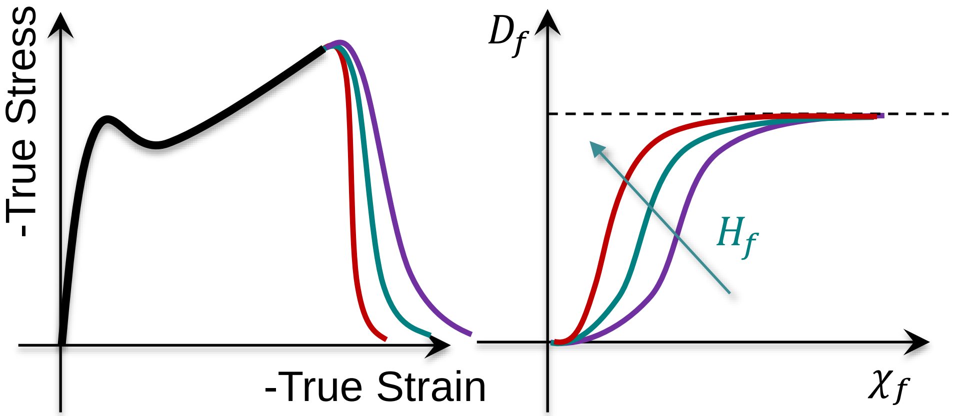

- Resin model: failure softening (2)
  - Damage evolution

$$\dot{D}_f = H_f(\chi_f)^{\zeta_f}(1-D_f)^{-\zeta_d}\,\dot{\chi}_f$$

$$\tilde{\gamma}_f - l_f^2\,\Delta\tilde{\gamma}_f = \gamma_f$$

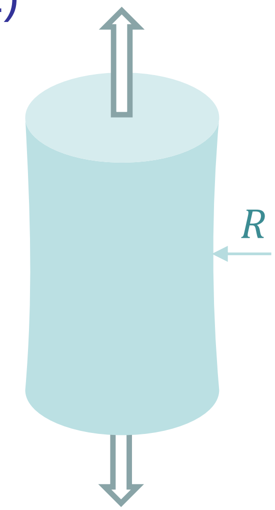

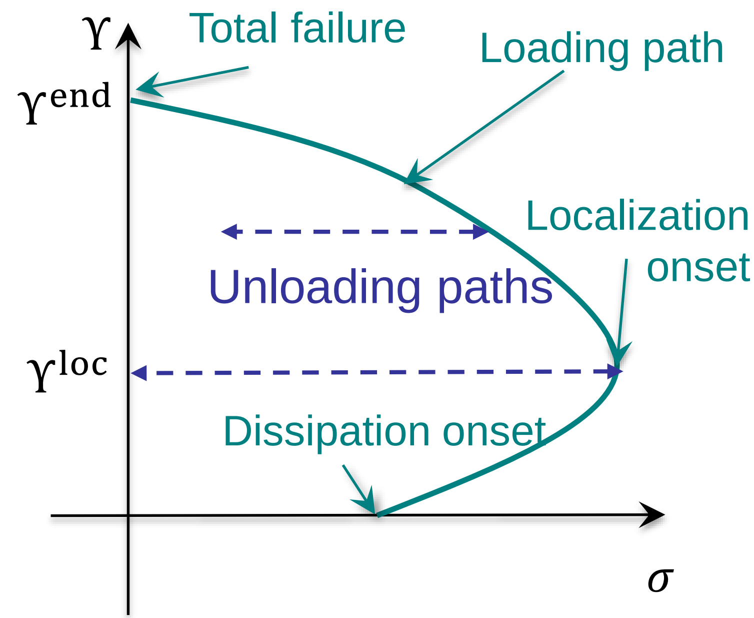

  - Calibration
    - Recover the epoxy G_c
    - From localization simulation

$$G_c A = \Upsilon^{\text{end}} - \Upsilon^{\text{loc}}$$

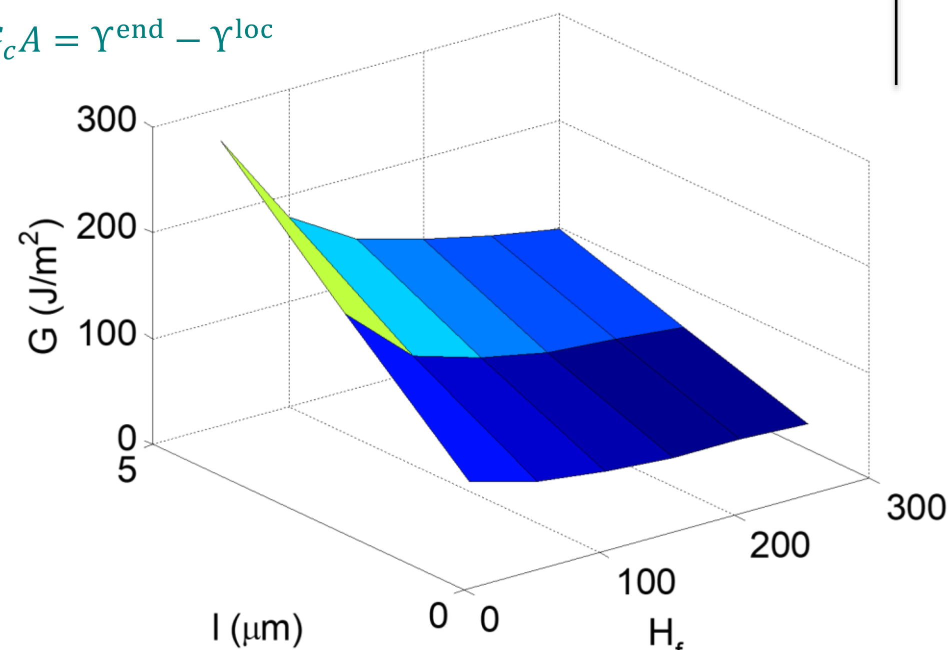

Micro-structural simulation of fiber-reinforced highly crosslinked epoxy

- Resin model: Validation
  - Compression without barrelling effect

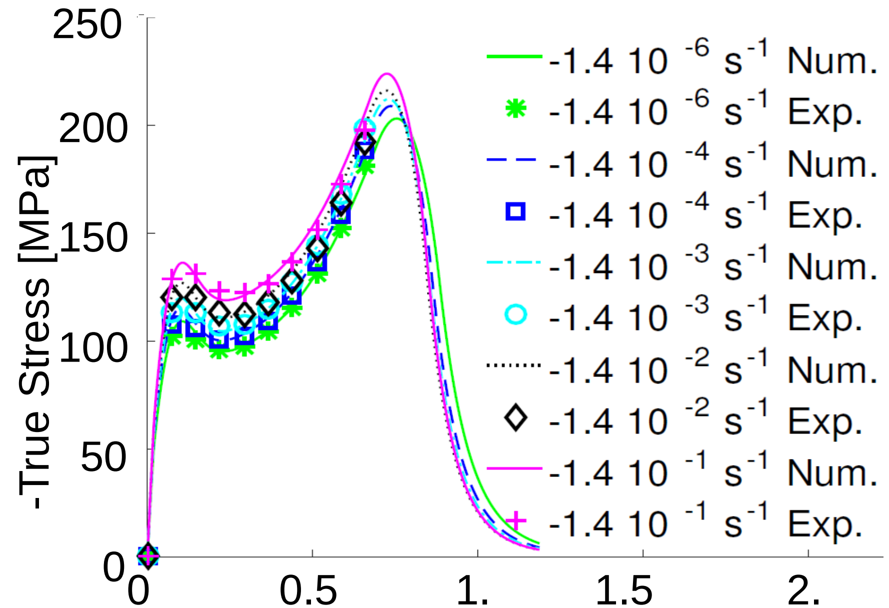

  - With barrelling effect

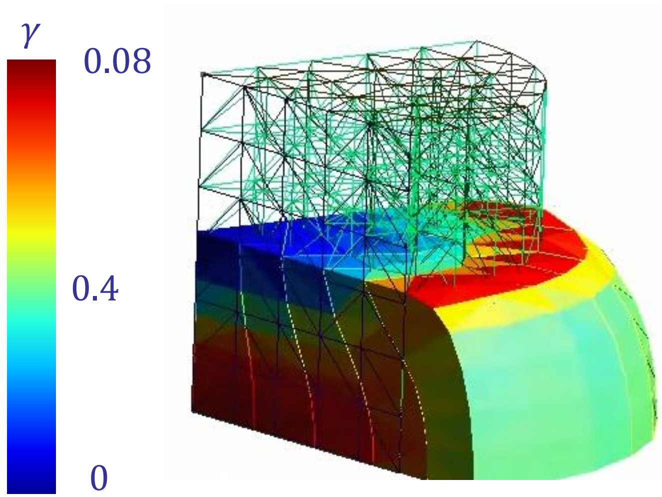

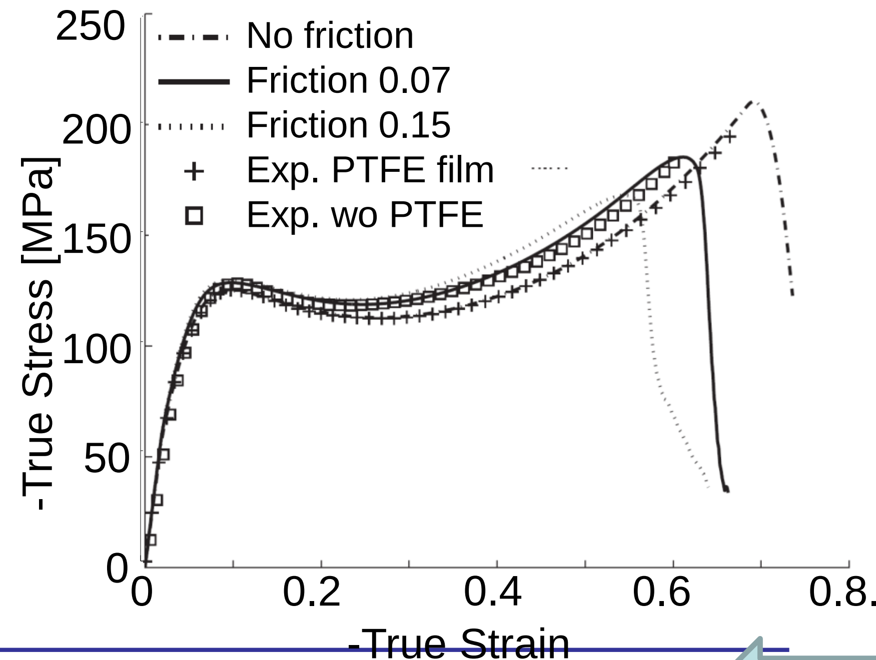

Micro-structural simulation of fiber-reinforced highly crosslinked epoxy

- Composite model: Extraction of G_c

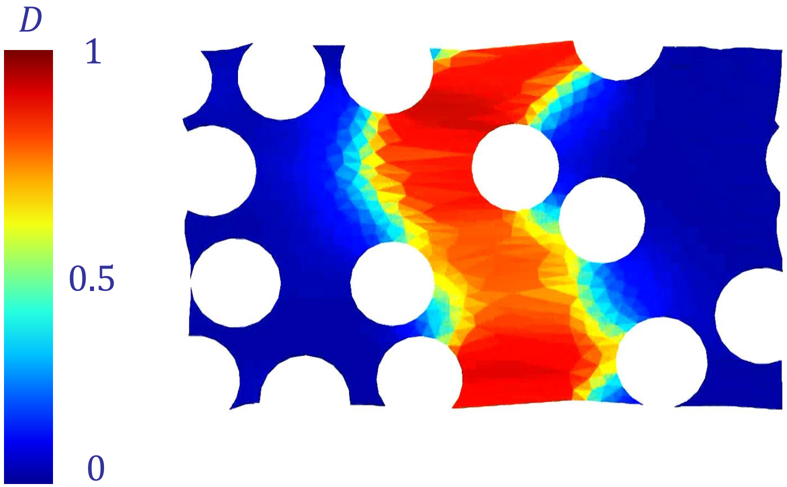

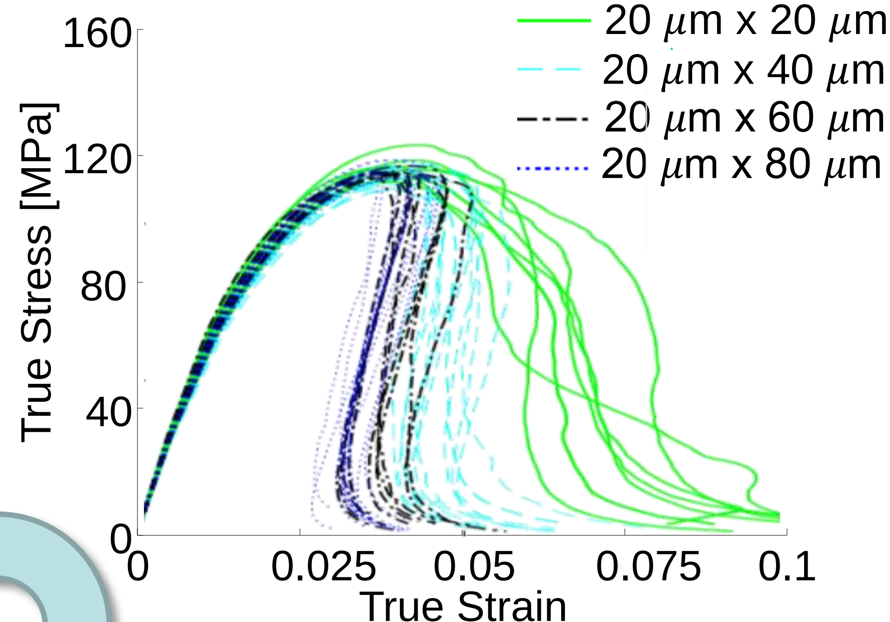

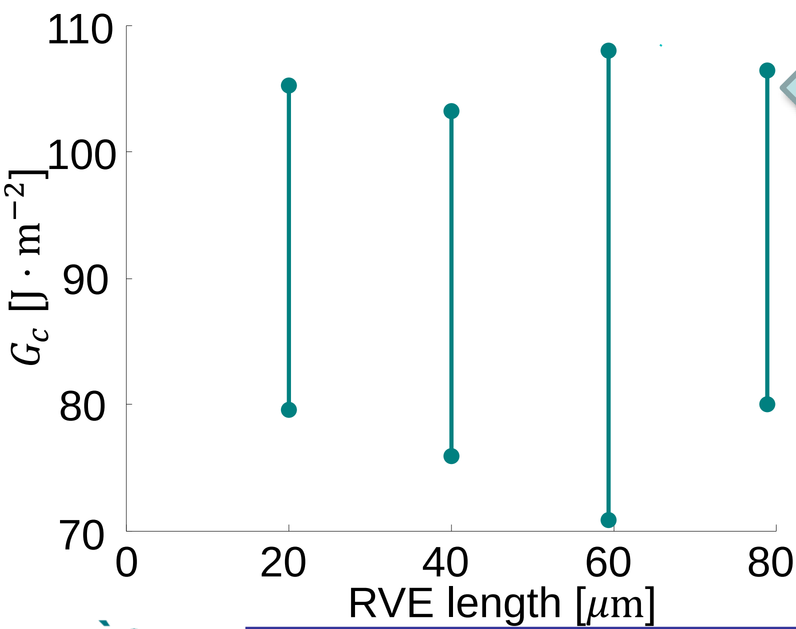

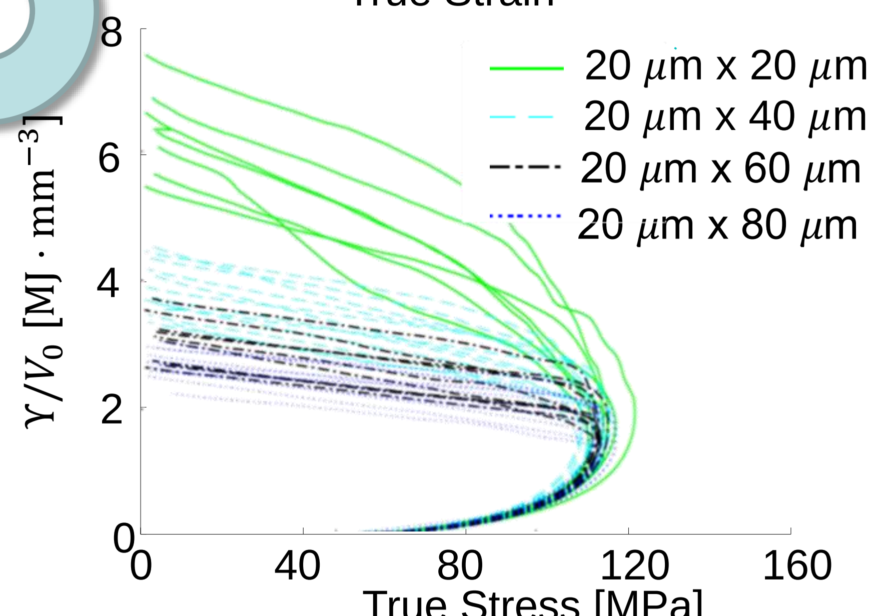

Micro-structural simulation of fiber-reinforced highly crosslinked epoxy

- Composite model: Validation
  - Compression test

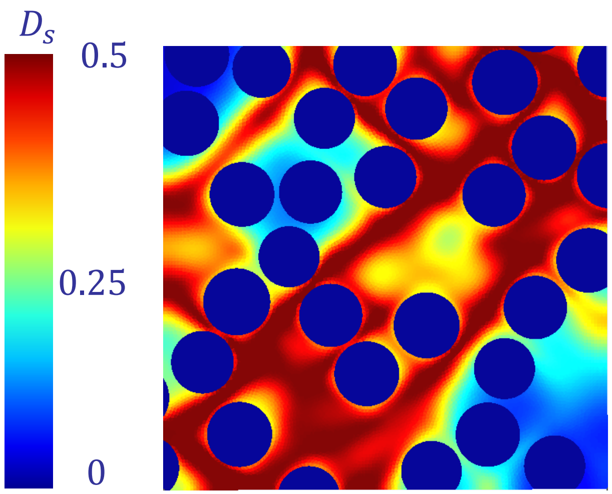

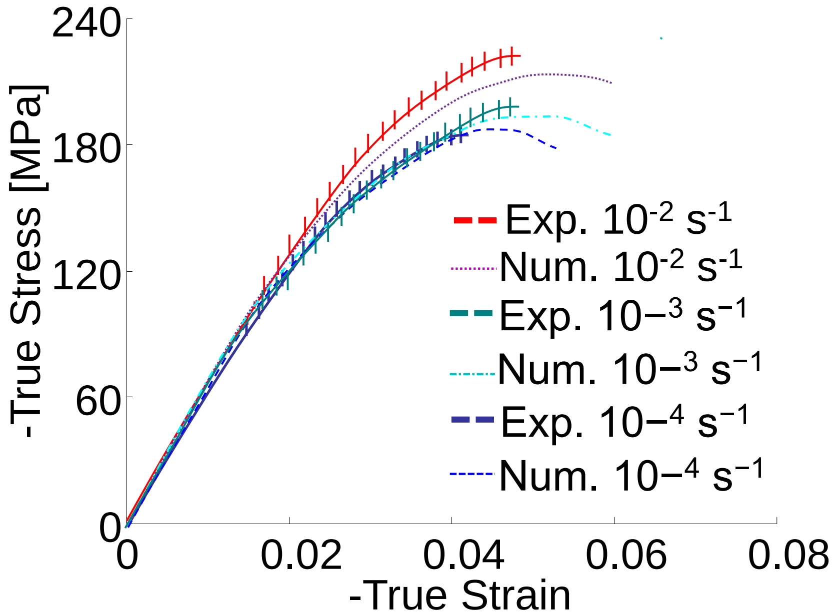

- PDR T.1015.14 project
  - ULiège, UCL (Belgium)

- Publications
  - 10.1016/j.ijsolstr.2016.06.008
  - 10.1016/j.mechmat.2019.02.017

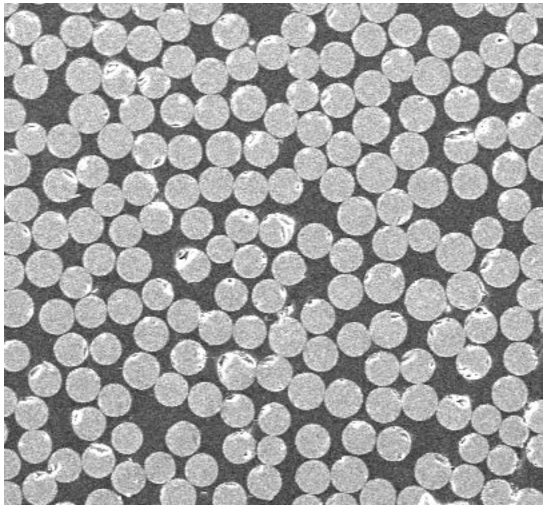

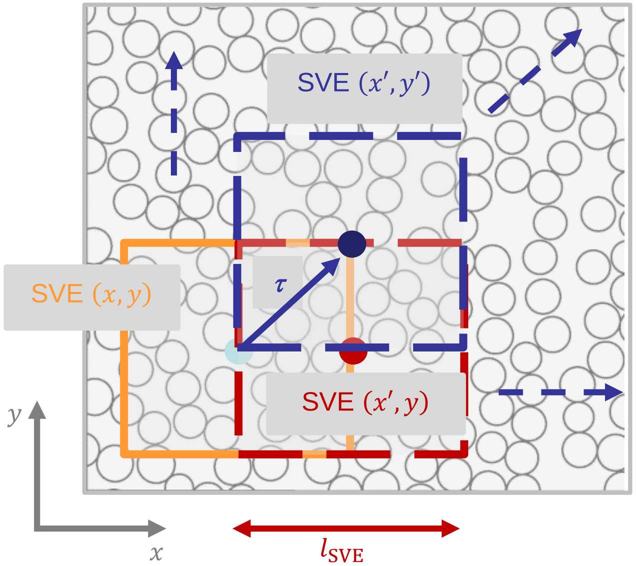

Stochastic Homogenization of Composite Materials

STOMMMAC The research has been funded by the Walloon Region under the agreement no 1410246-STOMMMAC (CT-INT 2013-03-28) in the context of M-ERA.NET Joint Call 2014.

- Multi-scale modeling
  - 2 problems are solved concurrently
    - The macro-scale problem
    - The meso-scale problem (on a meso-scale Volume Element)

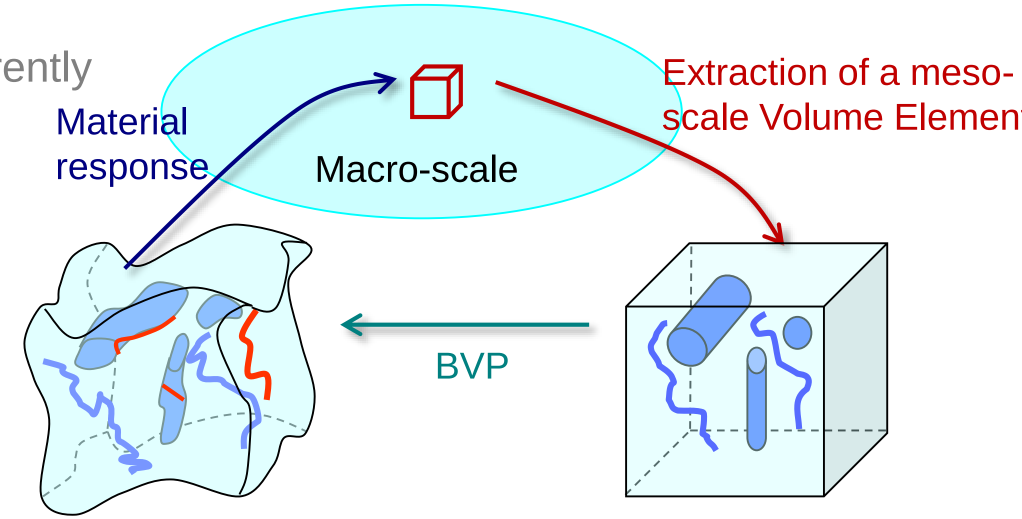

- For structures not several orders larger than the micro-structure size

$$L_{\mathrm{macro}} >> L_{\mathrm{VE}} >\sim L_{\mathrm{micro}}$$

For accuracy: Size of the meso-scale volume element smaller than the characteristic length of the macro-scale loading

Meso-scale volume element no longer statistically representative:
- **Stochastic Volume Elements**

- Material uncertainties affect structural behaviors

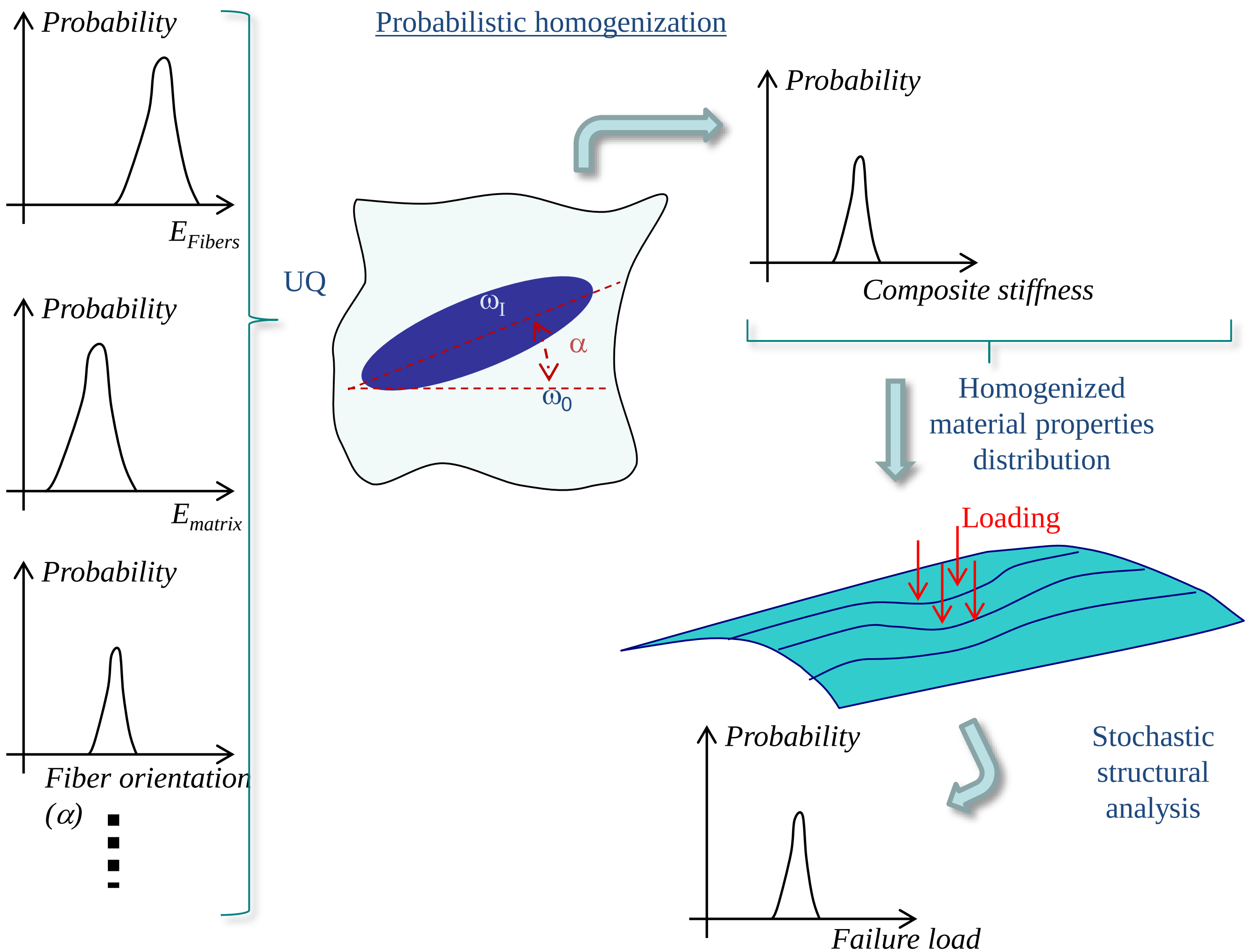

Stochastic Homogenization of Composite Materials

- Proposed methodology for material:
  - To develop a stochastic Mean Field Homogenization method able to predict the probabilistic distribution of material response at an intermediate scale from micro-structural constituents characterization

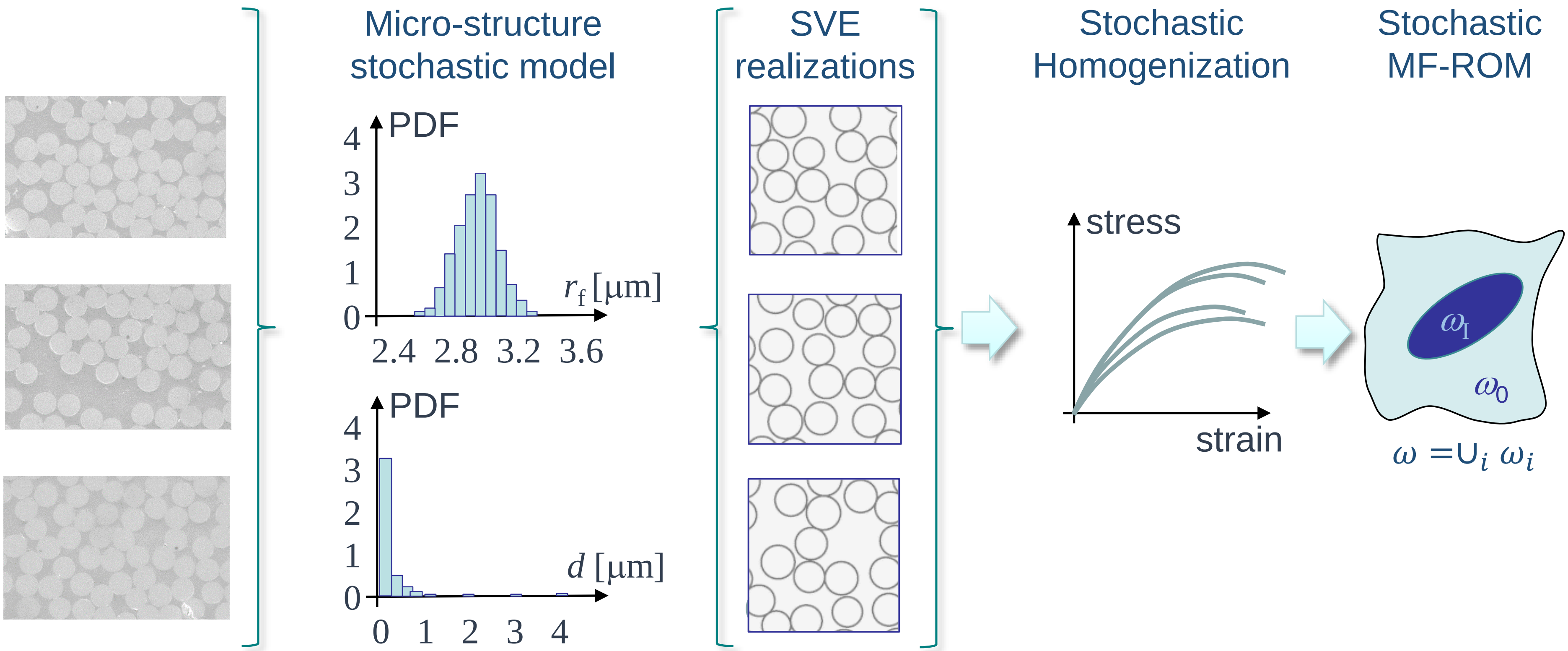

- Micro-structure stochastic model
  - 2000x and 3000x SEM images

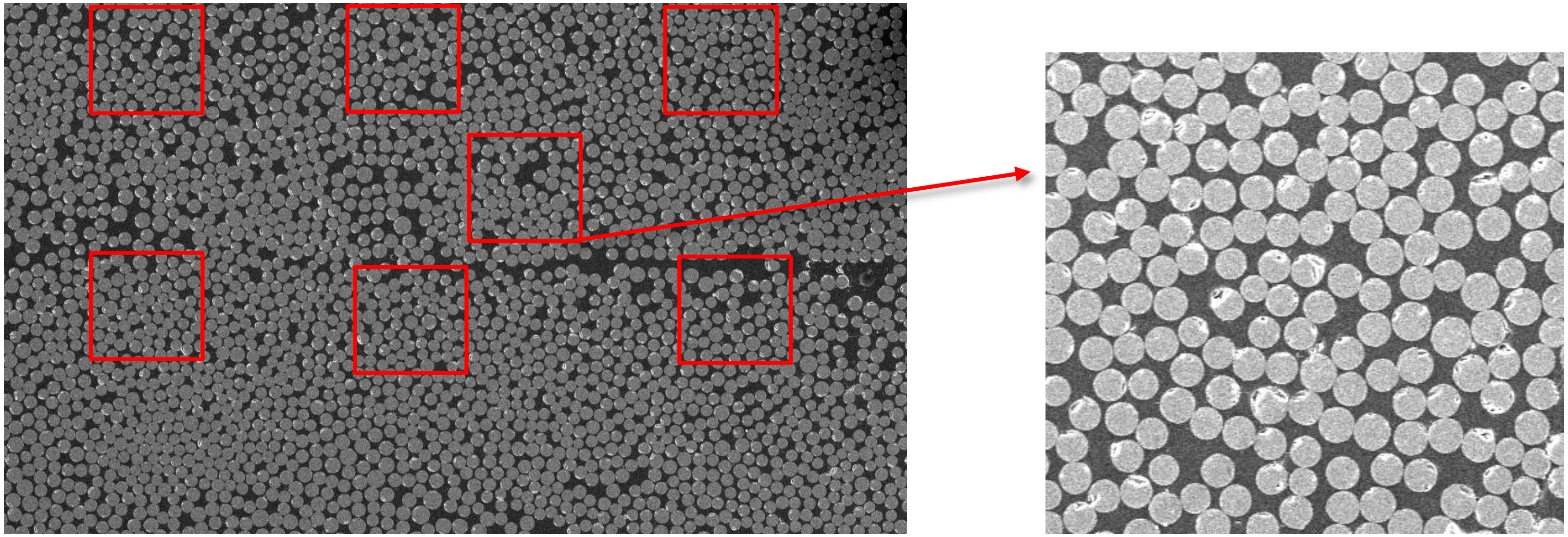

  - Fibers detection

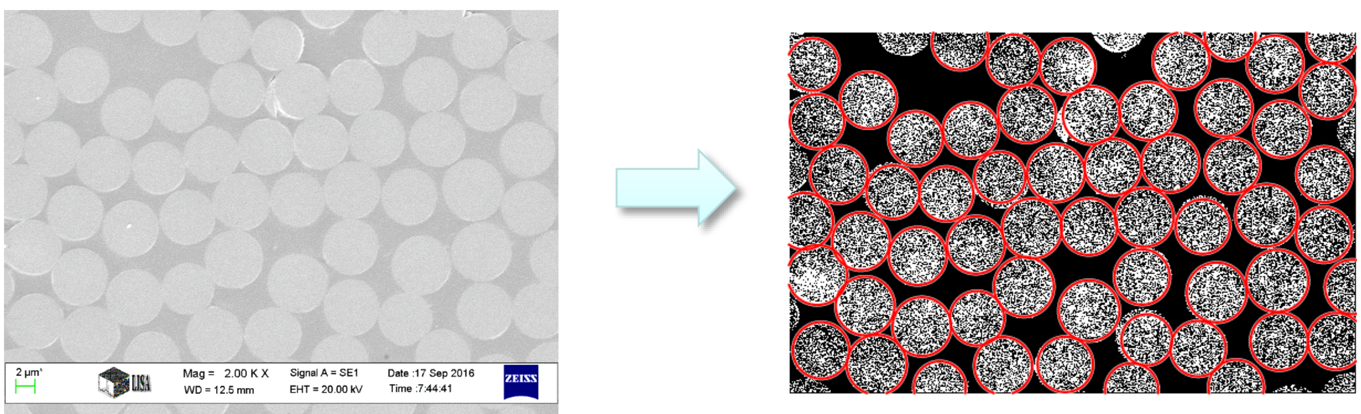

- Micro-structure stochastic model
  - Histograms of random micro-structures' descriptors

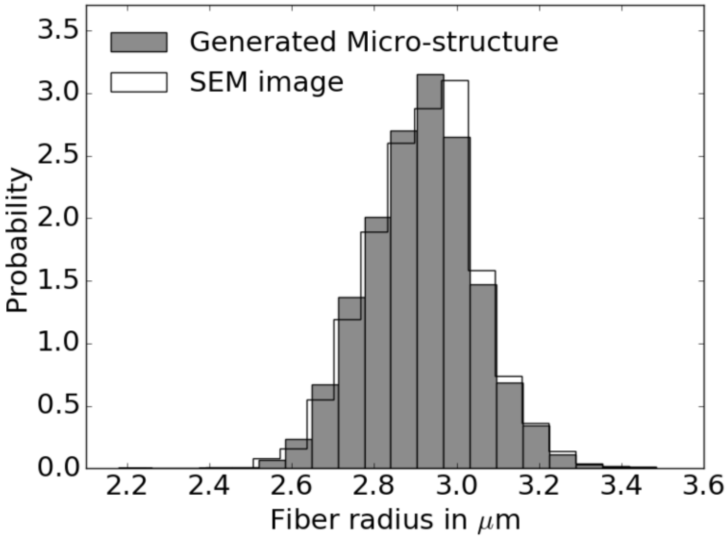

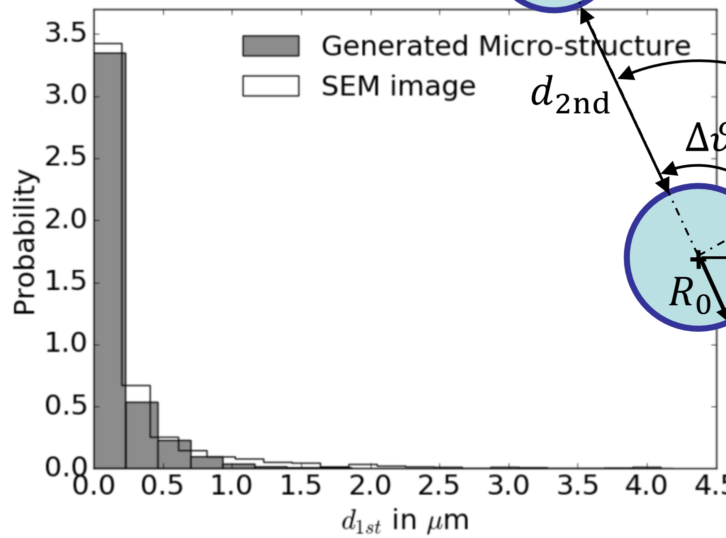

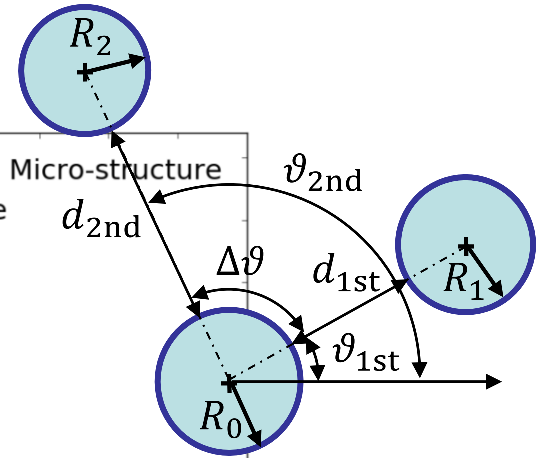

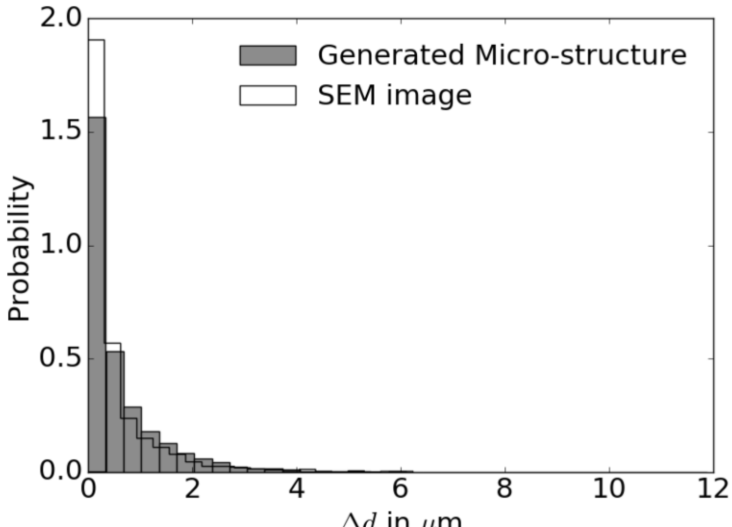

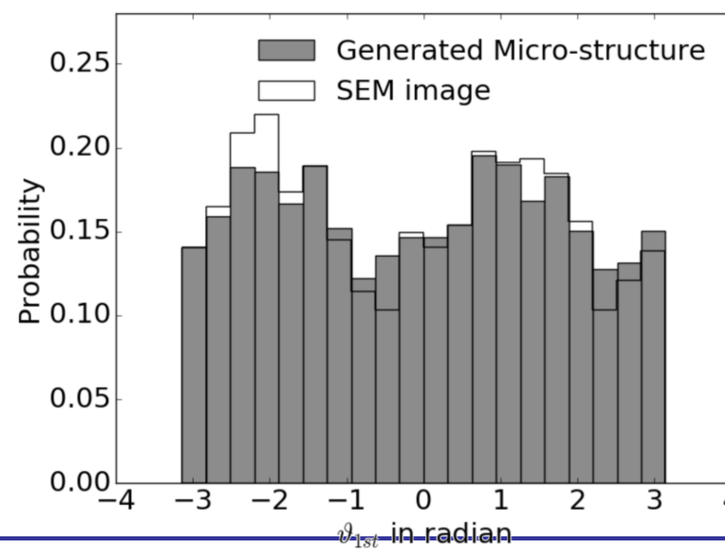

- Micro-structure stochastic model
  - Dependent variables generated using their empirical copula

SEM sample

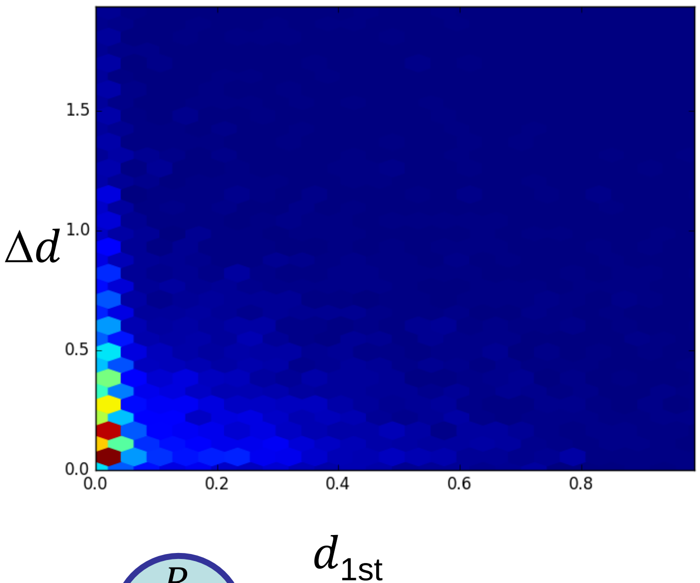

Generated sample

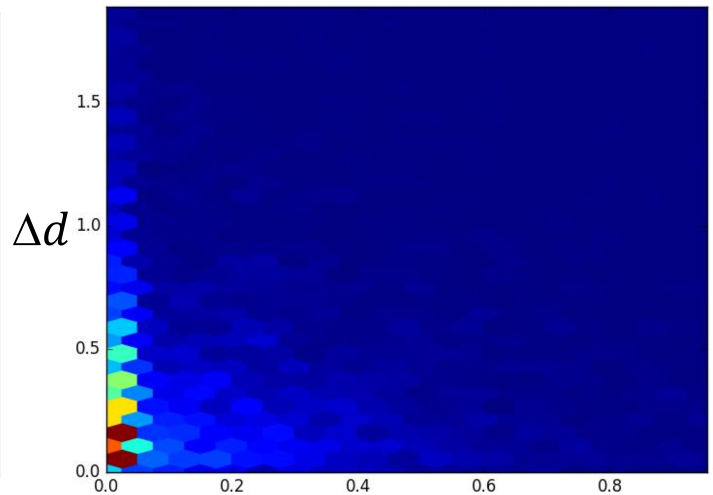

Directly from copula generator

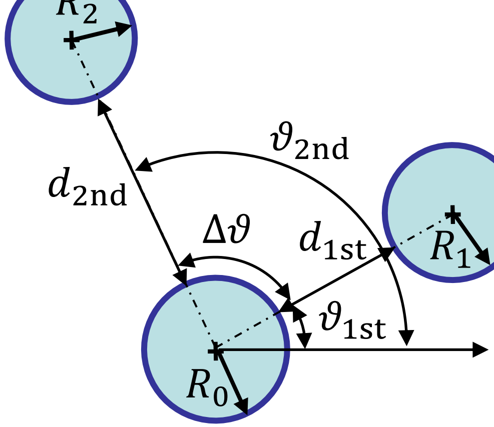

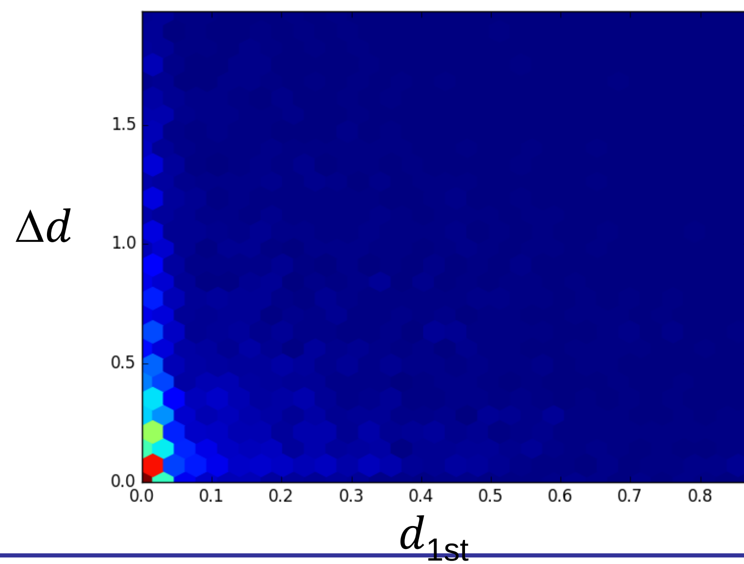

Statistic result from generated SVE

- Micro-structure stochastic model
  - Dependent variables generated using their empirical copula
  - Fiber additive process
    1) Define N seeds with first and second neighbors distances
    2) Generate first neighbor with its own first and second neighbors distances
    3) Generate second neighbor with its own first and second neighbors distances
    4) Change seeds & then change central fiber of the seeds

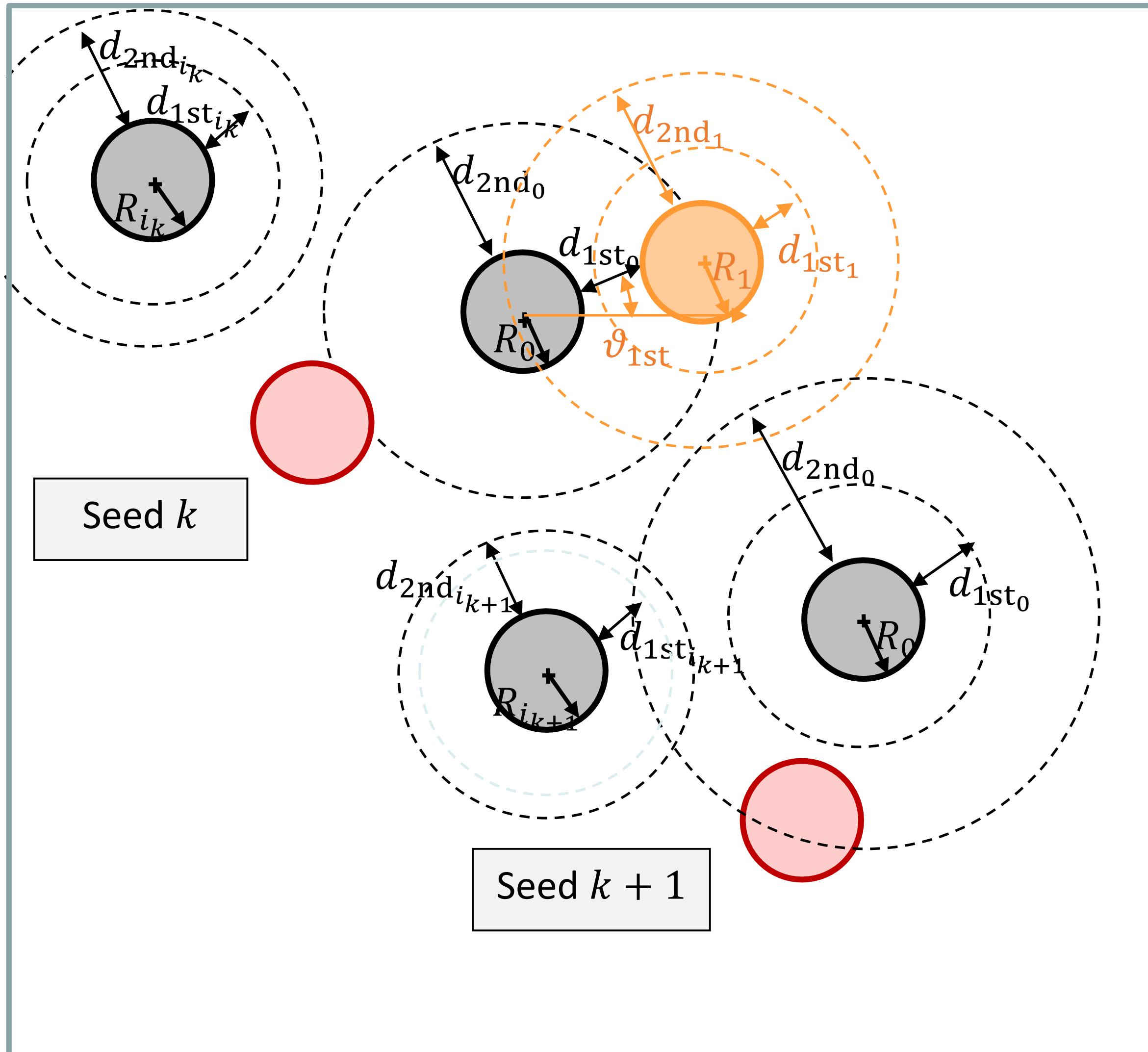

- Micro-structure stochastic model
  - Arbitrary size
  - Arbitrary number

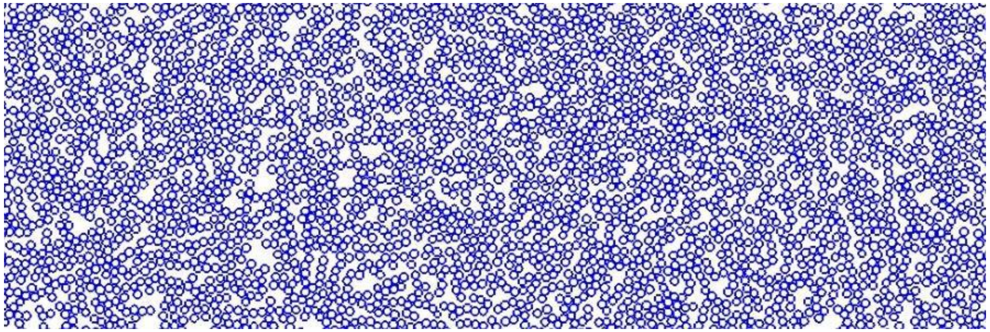

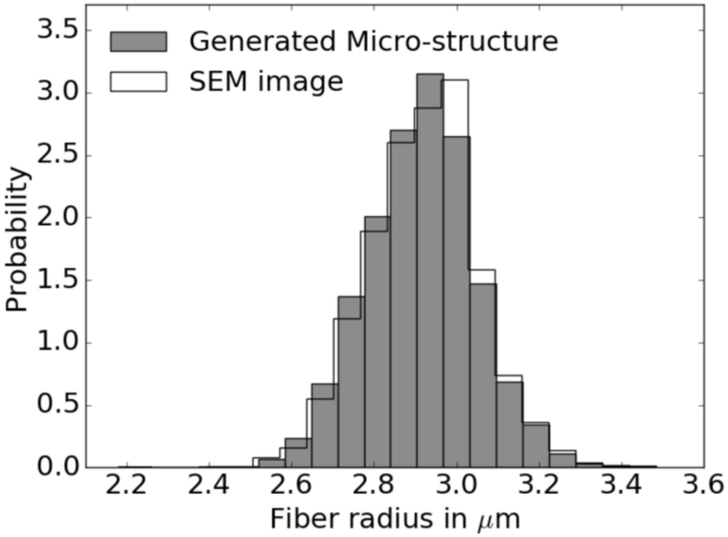

  - Possibility to generate non-homogenous distributions

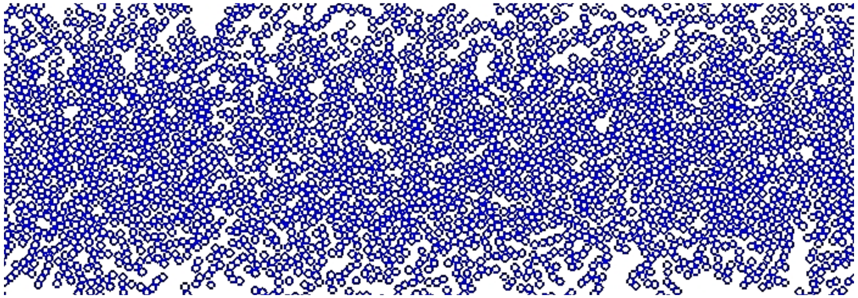

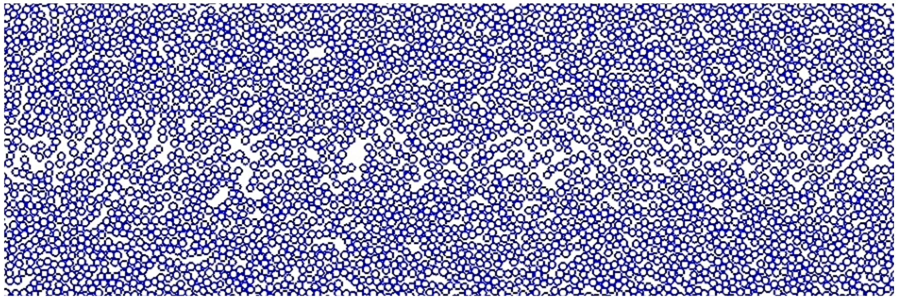

- Stochastic homogenization of SVEs
  - Extraction of Stochastic Volume Elements
    - 2 sizes considered: $l_{\mathrm{SVE}} = 10\ \mu m$ & $l_{\mathrm{SVE}} = 25\ \mu m$
    - Window technique to capture correlation

$$R_{\boldsymbol{rs}}(\boldsymbol{\tau}) = \frac{\mathbb{E}\left[\left(r(\boldsymbol{x}) - \mathbb{E}(r)\right)\left(s(\boldsymbol{x}+\boldsymbol{\tau}) - \mathbb{E}(s)\right)\right]}{\sqrt{\mathbb{E}\left[\left(r - \mathbb{E}(r)\right)^2\right]}\sqrt{\mathbb{E}\left[\left(s - \mathbb{E}(s)\right)^2\right]}}$$

  - For each SVE
    - Extract apparent homogenized material tensor $\mathbb{C}_{\mathrm{M}}$

$$\begin{cases} \boldsymbol{\varepsilon}_{\mathrm{M}} = \dfrac{1}{V(\omega)} \displaystyle\int_{\omega} \boldsymbol{\varepsilon}_{\mathrm{m}} d\omega \\ \boldsymbol{\sigma}_{\mathrm{M}} = \dfrac{1}{V(\omega)} \displaystyle\int_{\omega} \boldsymbol{\sigma}_{\mathrm{m}} d\omega \\ \mathbb{C}_{\mathrm{M}} = \dfrac{\partial \boldsymbol{\sigma}_{\mathrm{M}}}{\partial \boldsymbol{u}_{\mathrm{M}} \otimes \boldsymbol{\nabla}_{\mathrm{M}}} \end{cases}$$

    - Consistent boundary conditions:
      - Periodic (PBC)
      - Minimum kinematics (SUBC)
      - Kinematic (KUBC)

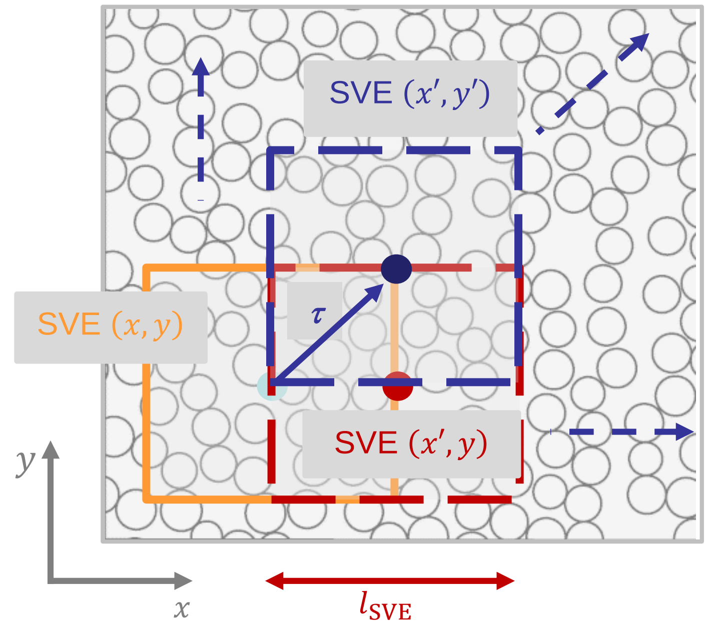

- Stochastic homogenization of SVEs
  - Apparent properties

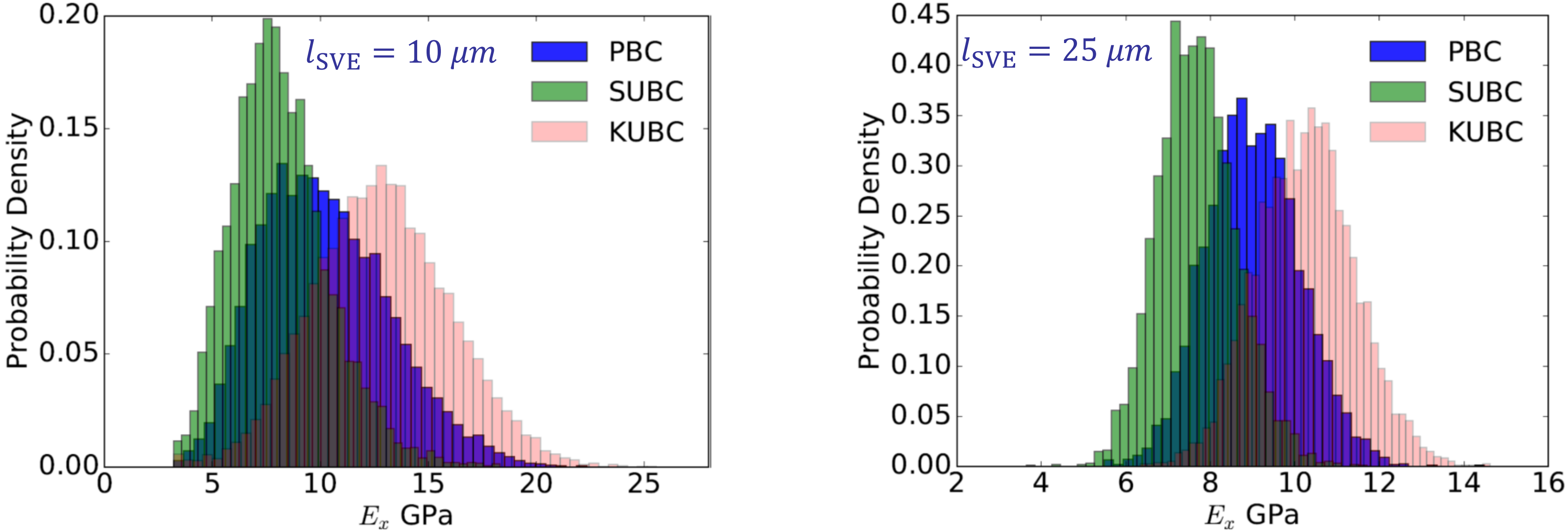

Increasing l_{SVE}

When l_{SVE} increases

- Average values for different BCs get closer (to PBC one)
- Distributions narrow
- Distributions get closer to normal

- Stochastic homogenization of SVEs
  - Correlation study

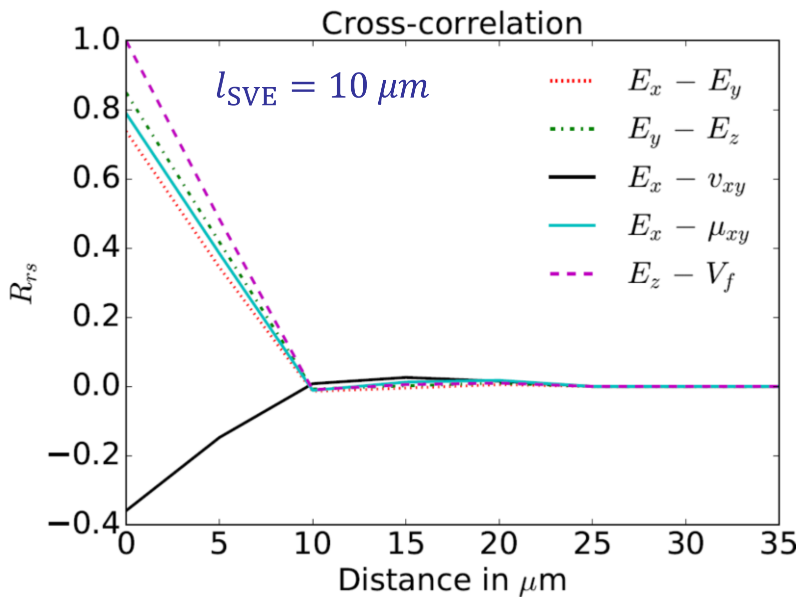

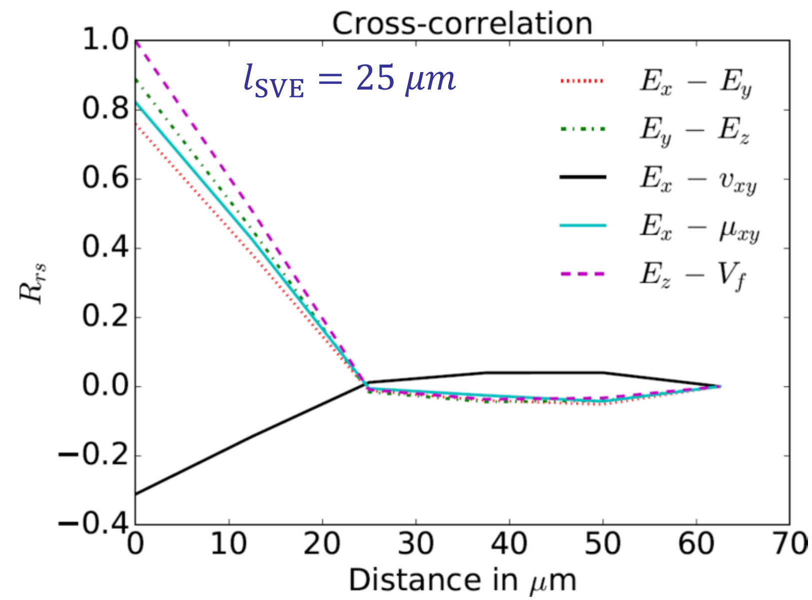

Increasing l_{SVE}

(1) Auto/cross correlation vanishes at $\tau = l_{\mathrm{SVE}}$
(2) When l_{SVE} increases, distributions get closer to normal

(1)+(2) Apparent properties are independent random variables
However the distribution depend on

- l_{SVE}
- The boundary conditions

Stochastic Homogenization of Composite Materials

- Mean-Field-homogenization (MFH)
  - Linear composites

$$
\begin{cases}
\boldsymbol{\sigma}_{\mathrm{M}} = \bar{\boldsymbol{\sigma}} = v_0 \boldsymbol{\sigma}_0 + v_{\mathrm{I}} \boldsymbol{\sigma}_{\mathrm{I}} \\
\boldsymbol{\varepsilon}_{\mathrm{M}} = \bar{\boldsymbol{\varepsilon}} = v_0 \boldsymbol{\varepsilon}_0 + v_{\mathrm{I}} \boldsymbol{\varepsilon}_{\mathrm{I}} \\
\boldsymbol{\varepsilon}_{\mathrm{I}} = \mathbb{B}^{\varepsilon}(\mathrm{I}, \mathbb{C}_0, \mathbb{C}_{\mathrm{I}}) : \boldsymbol{\varepsilon}_0
\end{cases}
$$

$$\Rightarrow \hat{\mathbb{C}}_{\mathrm{M}} = \hat{\mathbb{C}}_{\mathrm{M}}(\mathrm{I}, \mathbb{C}_0, \mathbb{C}_{\mathrm{I}}, v_{\mathrm{I}})$$

Defined as random variables

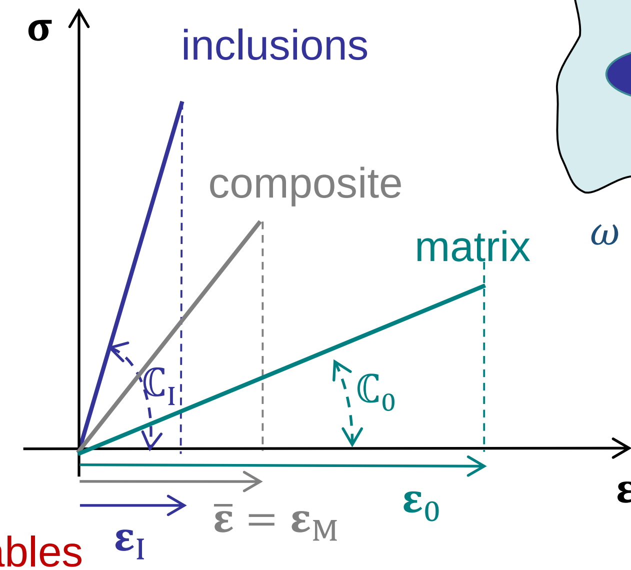

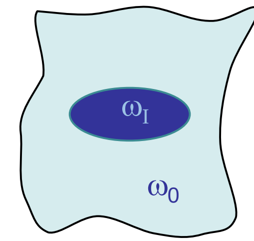

$\omega = \cup_i \omega_i$

- Consider an equivalent system
  - For each SVE realization i:
    - ⇒ $\mathbb{C}_{\mathrm{M}}$ and v_{I} known
  - Anisotropy from $\mathbb{C}^i_{\mathrm{M}}$
    - ⇒ θ is evaluated
  - Fiber behavior uniform
    - ⇒ $\hat{\mathbb{C}}_{\mathrm{I}}$ for one SVE

$$\mathbb{C}_{\mathrm{M}} \simeq \hat{\mathbb{C}}_{\mathrm{M}}(\hat{\mathrm{I}}, \hat{\mathbb{C}}_0, \hat{\mathbb{C}}_{\mathrm{I}}, v_{\mathrm{I}}, \theta)$$

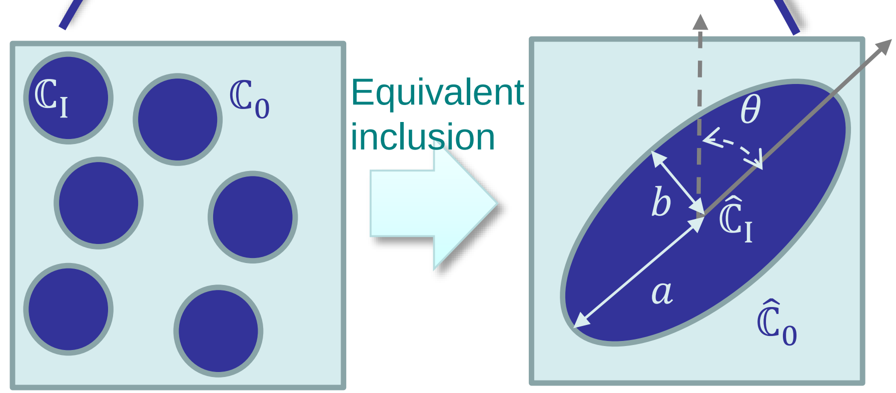

  - Remaining optimization problem:

$$\min_{\frac{a}{b}, \hat{E}_0, \hat{\nu}_0} \left\| \mathbb{C}_{\mathrm{M}} - \hat{\mathbb{C}}_{\mathrm{M}}\left(\frac{a}{b}, \hat{E}_0, \hat{\nu}_0 ; v_{\mathrm{I}}, \theta, \hat{\mathbb{C}}_{\mathrm{I}}\right) \right\|$$

- Inverse stochastic identification
  - Comparison of homogenized properties from SVE realizations and stochastic MFH

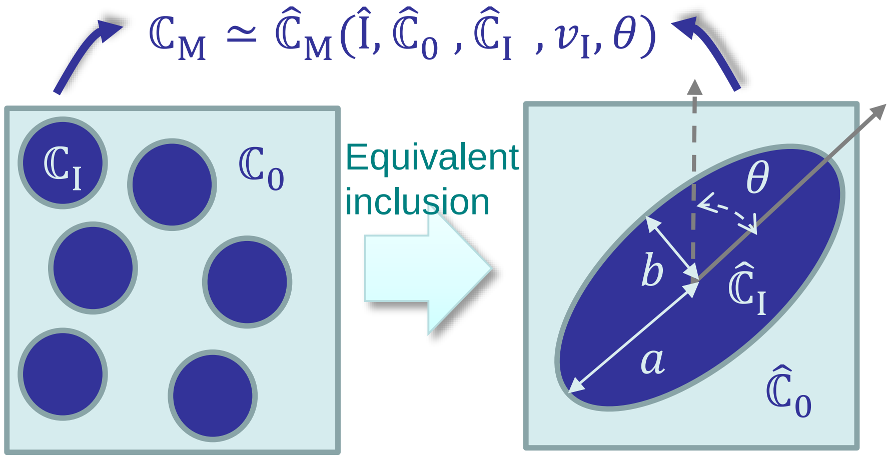

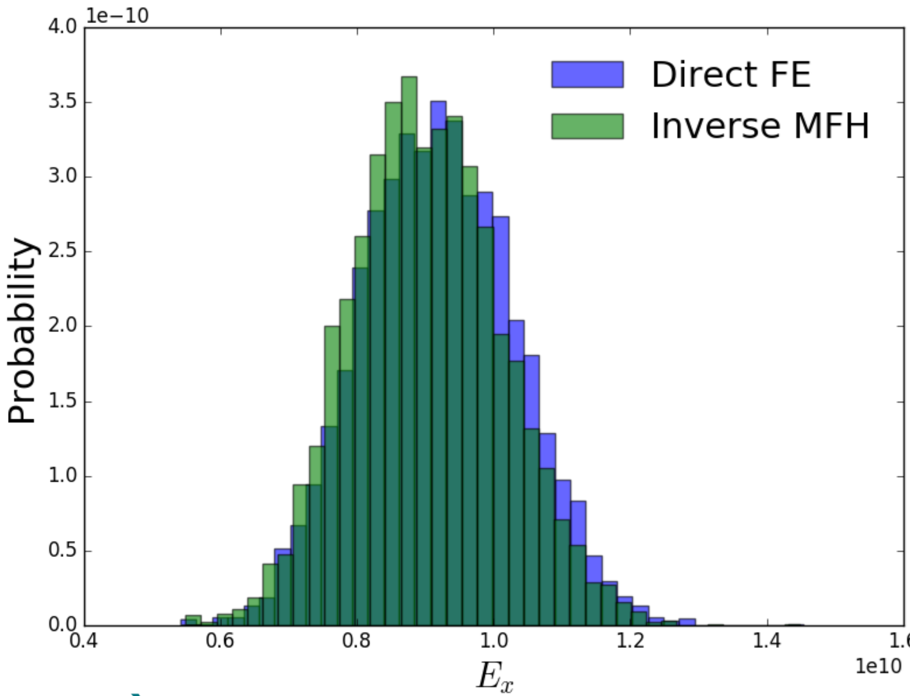

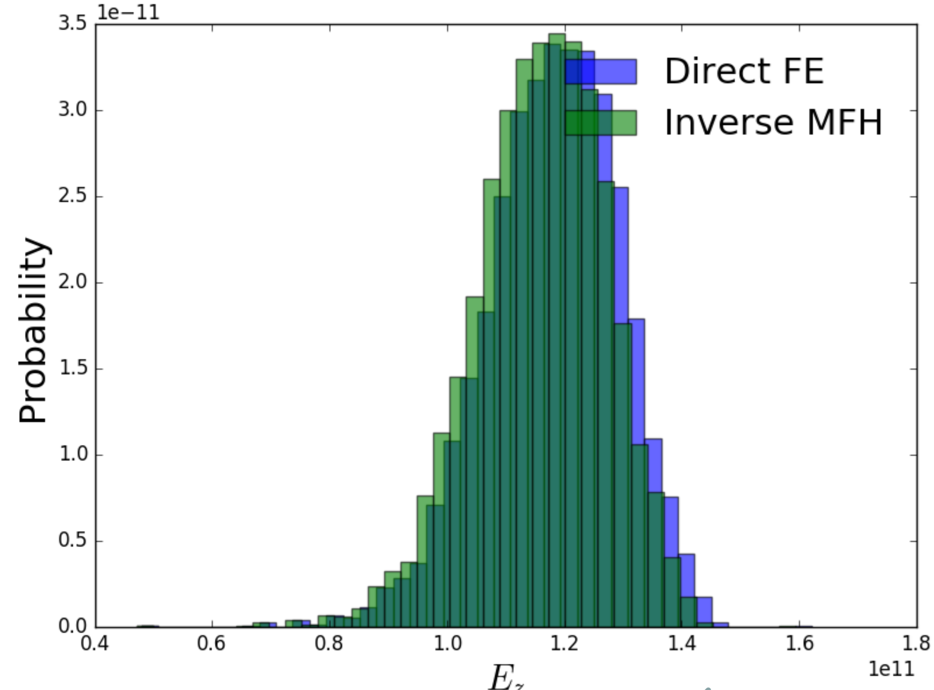

- Incremental-secant Mean-Field-homogenization
  - Virtual elastic unloading from previous state
    - Composite material unloaded to reach the stress-free state
    - Residual stress in components
  - Define Linear Comparison Composite
    - From unloaded state

$$\Delta\boldsymbol{\varepsilon}^{\mathbf{r}}_{\mathrm{I}/0} = \Delta\boldsymbol{\varepsilon}_{\mathrm{I}/0} + \Delta\boldsymbol{\varepsilon}^{\mathrm{unload}}_{\mathrm{I}/0}$$

    - Incremental-secant loading

$$\begin{cases} \boldsymbol{\sigma}_{\mathrm{M}} = \bar{\boldsymbol{\sigma}} = v_0\boldsymbol{\sigma}_0 + v_{\mathrm{I}}\boldsymbol{\sigma}_{\mathrm{I}} \\ \Delta\boldsymbol{\varepsilon}^{\mathbf{r}}_{\mathrm{M}} = \overline{\Delta\boldsymbol{\varepsilon}} = v_0\Delta\boldsymbol{\varepsilon}^{\mathbf{r}}_0 + v_{\mathrm{I}}\Delta\boldsymbol{\varepsilon}^{\mathbf{r}}_{\mathrm{I}} \\ \Delta\boldsymbol{\varepsilon}^{\mathbf{r}}_{\mathrm{I}} = \mathbb{B}^{\varepsilon}\left(\mathrm{I}, \mathbb{C}^{\mathrm{S}}_0, \mathbb{C}^{\mathrm{S}}_{\mathrm{I}}\right) : \Delta\boldsymbol{\varepsilon}^{\mathbf{r}}_0 \end{cases}$$

    - Incremental secant operator

$$\Rightarrow \Delta\boldsymbol{\sigma}_{\mathrm{M}} = \mathbb{C}^{\mathrm{S}}_{\mathrm{M}}\left(\mathrm{I}, \mathbb{C}^{\mathrm{S}}_0, \mathbb{C}^{\mathrm{S}}_{\mathrm{I}}, v_{\mathrm{I}}\right) : \Delta\boldsymbol{\varepsilon}^{\mathbf{r}}_{\mathrm{M}}$$

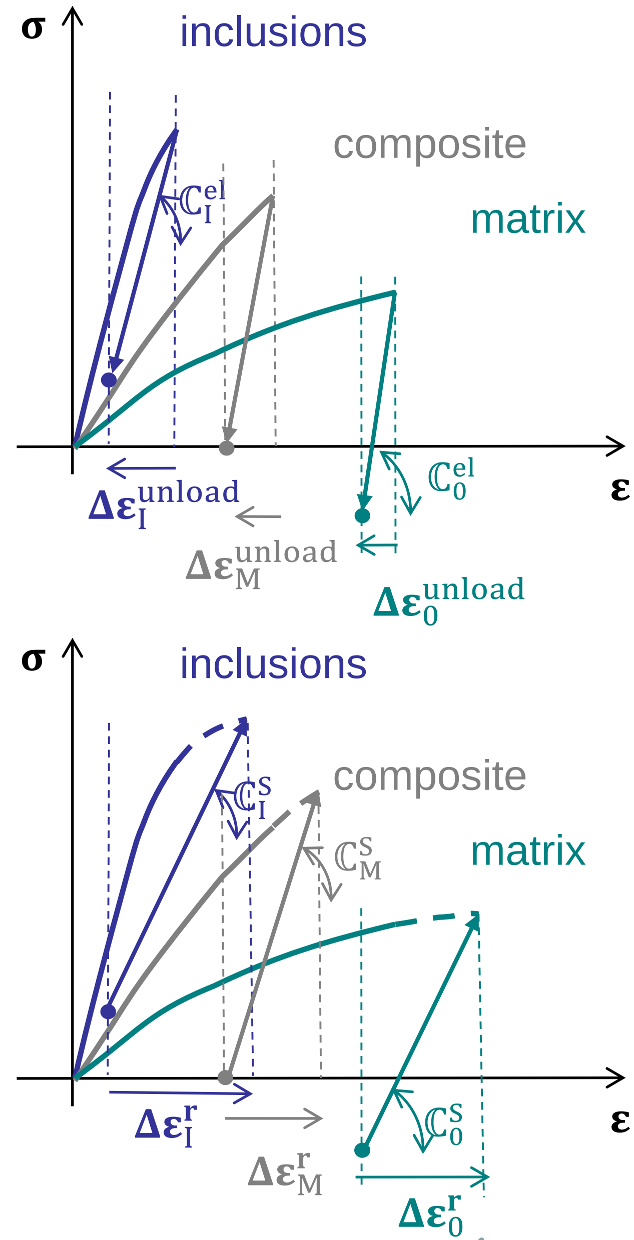

- Non-linear inverse identification
  - First step from elastic response

$$\mathbb{C}_{\mathrm{M}}^{\mathrm{el}} \simeq \hat{\mathbb{C}}_{\mathrm{M}}^{\mathrm{el}}(\hat{\mathrm{I}}, \hat{\mathbb{C}}_{0}^{\mathrm{el}}, \hat{\mathbb{C}}_{\mathrm{I}}^{\mathrm{el}}, v_{\mathrm{I}}, \theta)$$

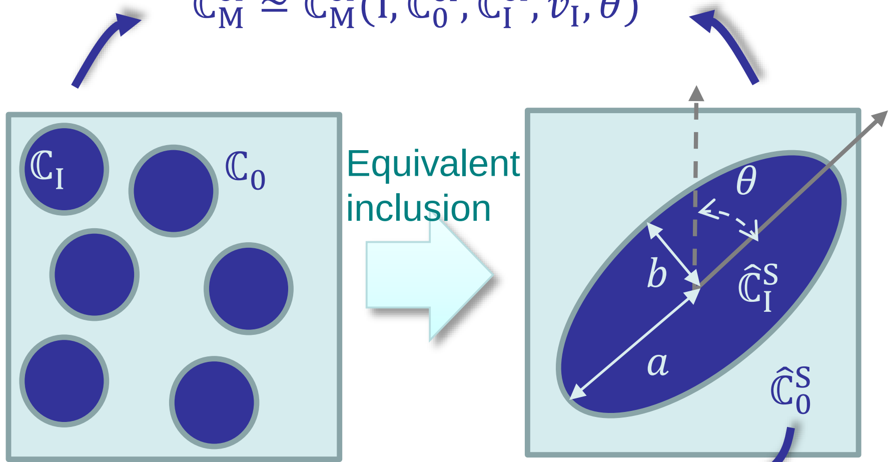

$$\mathbb{C}_{0}^{\mathrm{S}} \simeq \hat{\mathbb{C}}_{0}^{\mathrm{S}}(\hat{R}(\hat{p}_0); \hat{\mathbb{C}}_{0}^{\mathrm{el}})$$

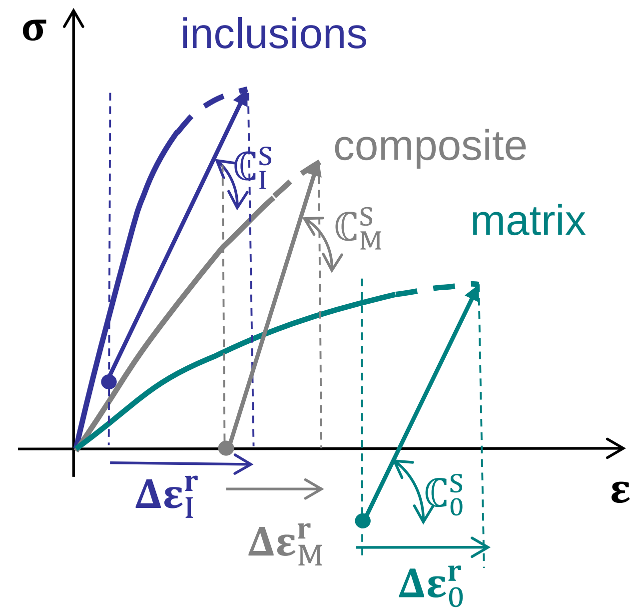

  - Second step from the LCC
    - New optimization problem

$$\Delta\boldsymbol{\sigma}_{\mathrm{M}} \simeq \hat{\mathbb{C}}_{\mathrm{M}}^{\mathrm{S}}\left(\hat{\mathrm{I}}, \hat{\mathbb{C}}_{0}^{\mathrm{S}}, \mathbb{C}_{\mathrm{I}}^{\mathrm{S}}, v_{\mathrm{I}}, \theta\right) : \Delta\boldsymbol{\varepsilon}_{\mathrm{M}}^{\mathrm{r}}$$

    - Extract the equivalent hardening $\hat{R}(\hat{p}_0)$ from the incremental secant tensor

$$\mathbb{C}_{0}^{\mathrm{S}} \simeq \hat{\mathbb{C}}_{0}^{\mathrm{S}}(\hat{R}(\hat{p}_0); \hat{\mathbb{C}}_{0}^{\mathrm{el}})$$

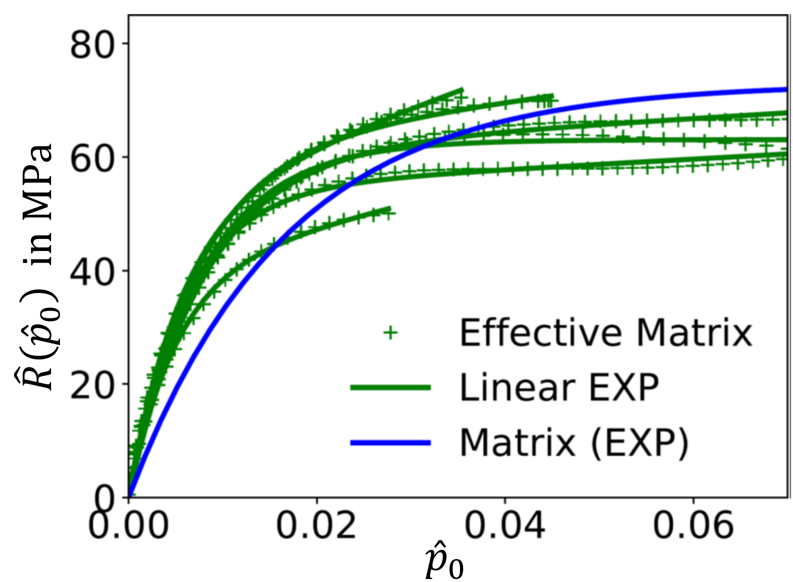

Stochastic Homogenization of Composite Materials

- Non-linear inverse identification
  - Comparison SVE vs. MFH

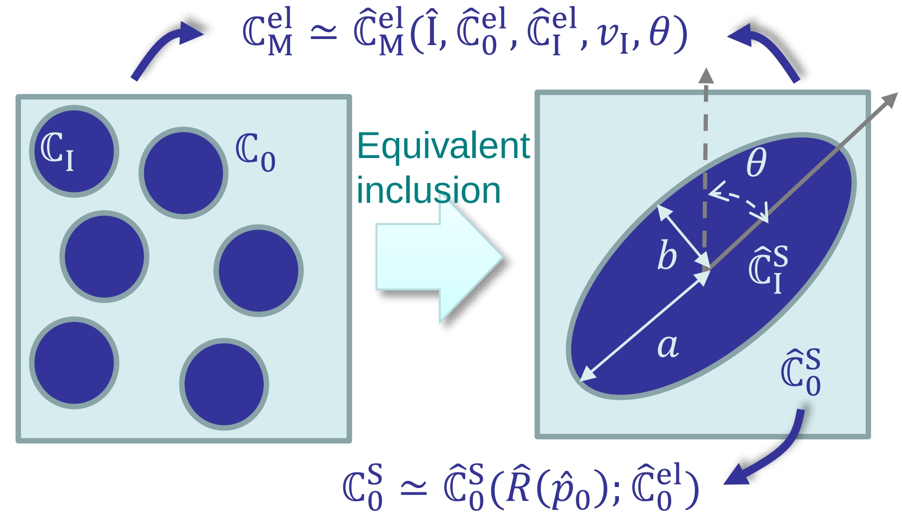

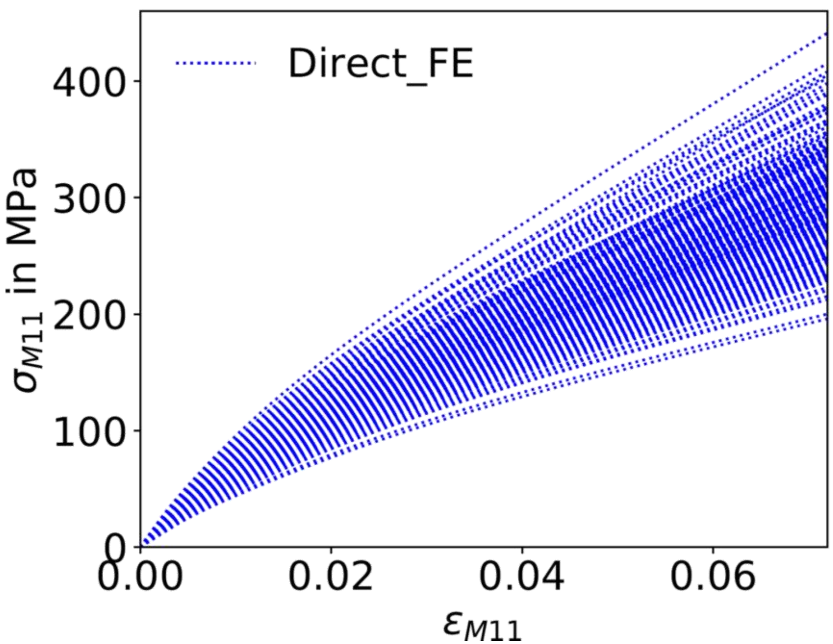

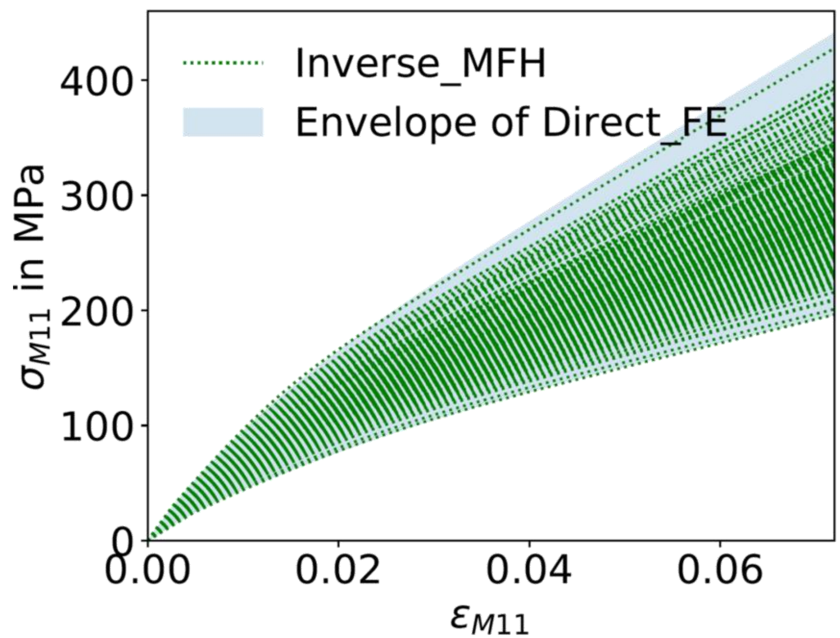

- Damage-enhanced Mean-Field-homogenization
  - Virtual elastic unloading from previous state
    - Composite material unloaded to reach the stress-free state
    - Residual stress in components
  - Define Linear Comparison Composite
    - From elastic state

$$\Delta\boldsymbol{\varepsilon}^{\mathrm{r}}_{\mathrm{I}/0} = \Delta\boldsymbol{\varepsilon}_{\mathrm{I}/0} + \Delta\boldsymbol{\varepsilon}^{\mathrm{unload}}_{\mathrm{I}/0}$$

    - Incremental-secant loading

$$\begin{cases} \boldsymbol{\sigma}_{\mathrm{M}} = \bar{\boldsymbol{\sigma}} = v_0\boldsymbol{\sigma}_0 + v_{\mathrm{I}}\boldsymbol{\sigma}_{\mathrm{I}} \\ \Delta\boldsymbol{\varepsilon}^{\mathrm{r}}_{\mathrm{M}} = \overline{\Delta\boldsymbol{\varepsilon}} = v_0\Delta\boldsymbol{\varepsilon}^{\mathrm{r}}_0 + v_{\mathrm{I}}\Delta\boldsymbol{\varepsilon}^{\mathrm{r}}_{\mathrm{I}} \\ \Delta\boldsymbol{\varepsilon}^{\mathrm{r}}_{\mathrm{I}} = \mathbb{B}^{\varepsilon}\left(\mathrm{I}, (1-D_0)\mathbb{C}^{\mathrm{S}}_0, \mathbb{C}^{\mathrm{S}}_{\mathrm{I}}\right): \Delta\boldsymbol{\varepsilon}^{\mathrm{r}}_0 \end{cases}$$

    - Incremental secant operator

$$\Rightarrow \Delta\boldsymbol{\sigma}_{\mathrm{M}} = \mathbb{C}^{\mathrm{S}}_{\mathrm{M}}\left(\mathrm{I}, (1-D_0)\mathbb{C}^{\mathrm{S}}_0, \mathbb{C}^{\mathrm{S}}_{\mathrm{I}}, v_{\mathrm{I}}\right): \Delta\boldsymbol{\varepsilon}^{\mathrm{r}}_{\mathrm{M}}$$

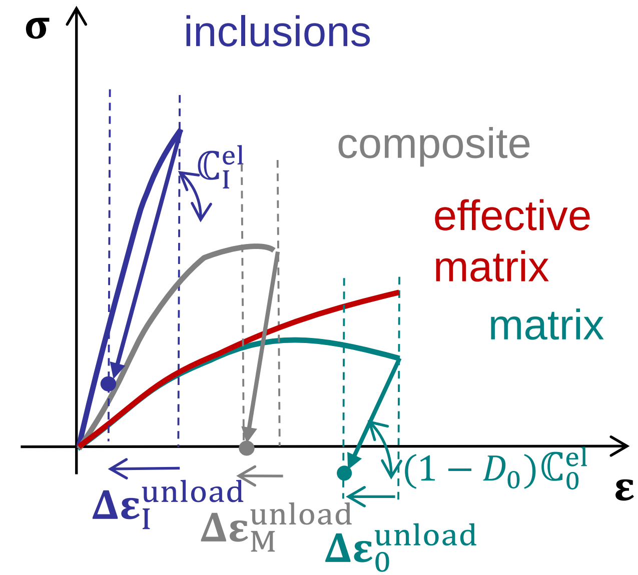

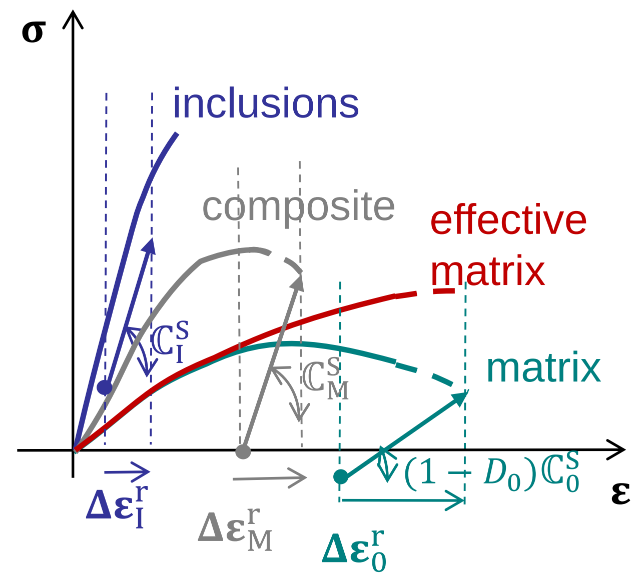

- Damage-enhanced inverse identification
  - Comparison SVE vs. MFH

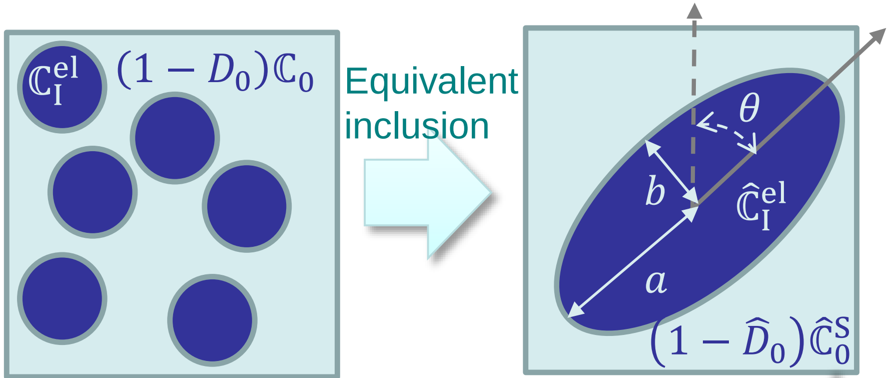

$$(1-\mathrm{D}_0)\mathbb{C}_0^S \simeq \left(1-\hat{\mathrm{D}}_0(\hat{p}_0)\right)\hat{\mathbb{C}}_0^S\left(\hat{R}(\hat{p}_0);\hat{\mathbb{C}}_0^{\mathrm{el}}\right)$$

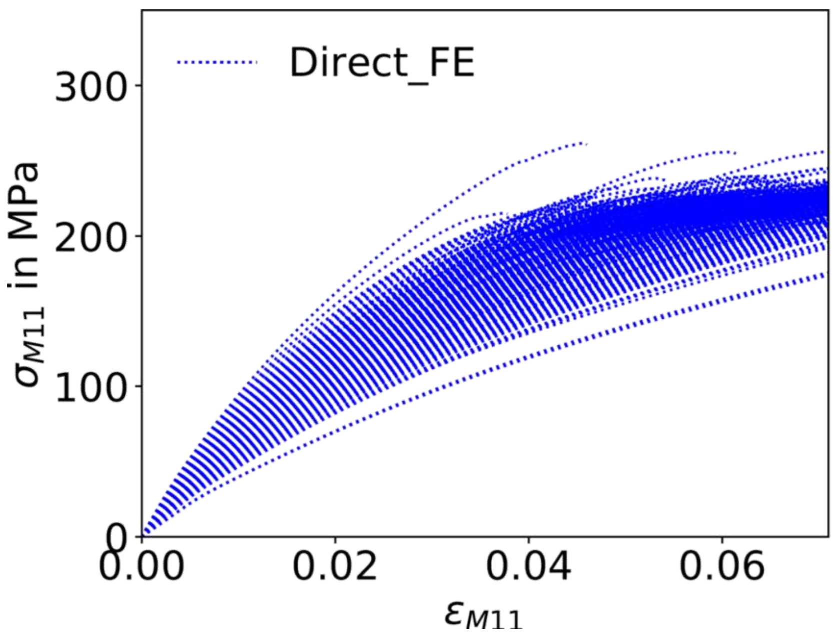

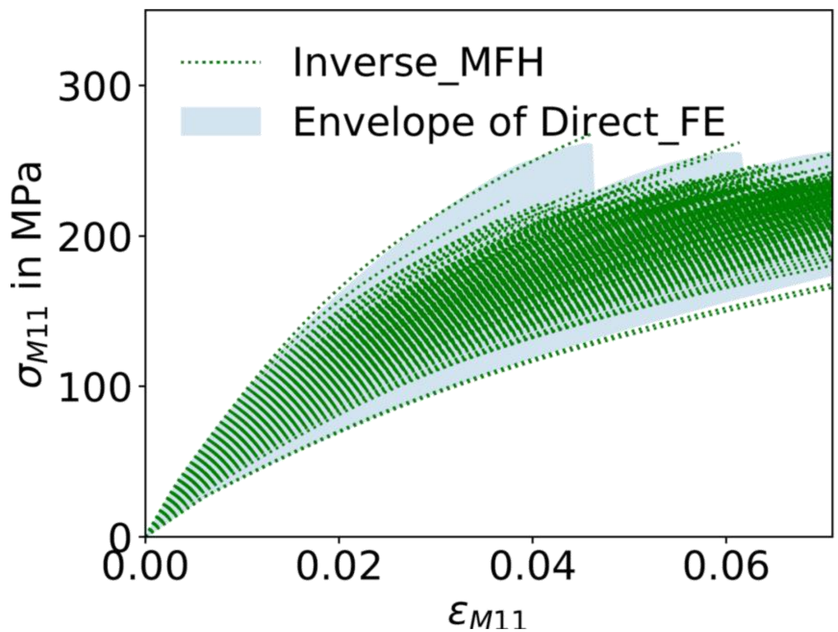

- Generation of random field
  - Comparison inverse identification vs. diffusion map –based generator

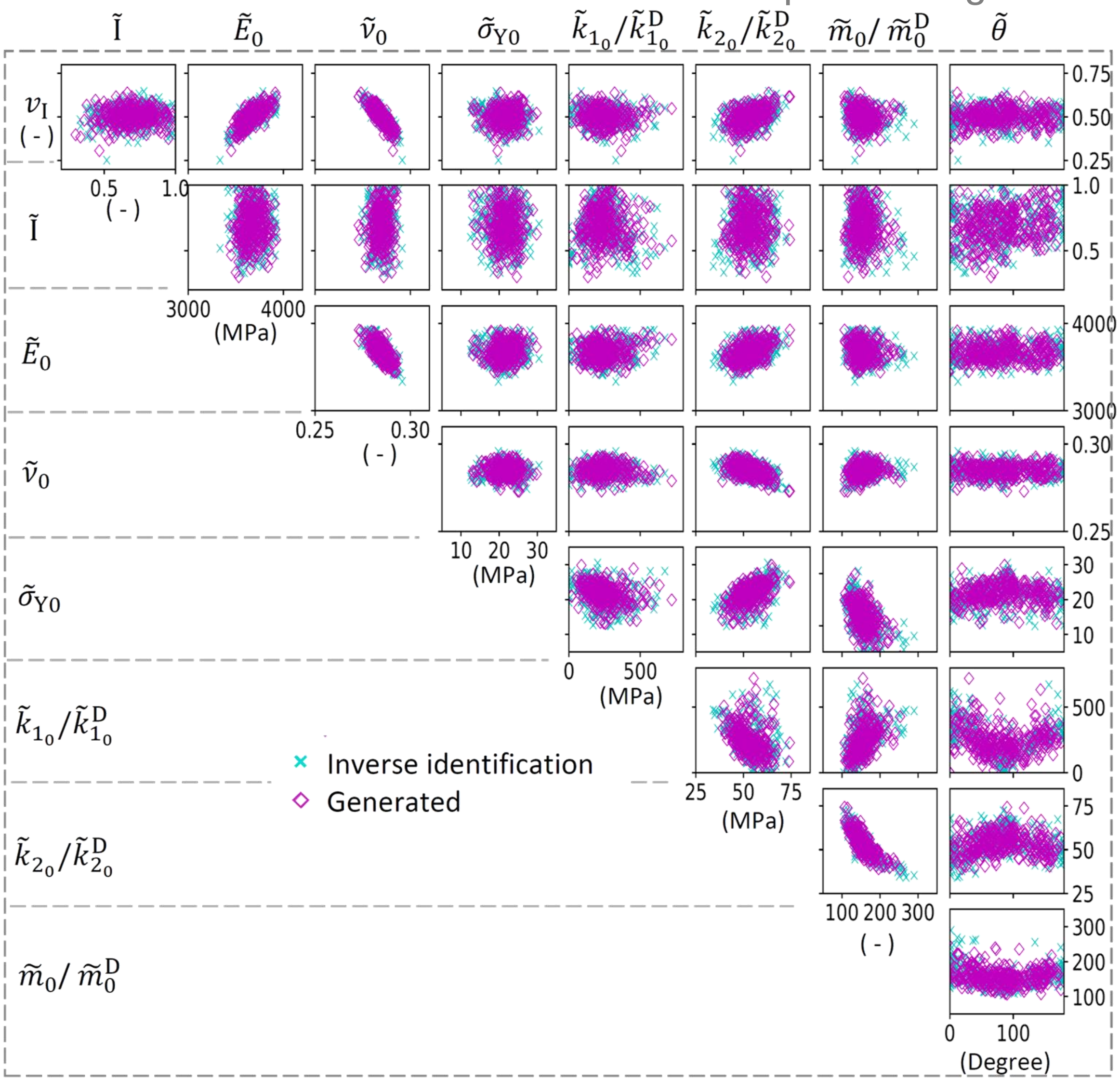

Beginning

- One single ply loading realization
  - Random field and finite elements discretizations
  - Non-uniform homogenized stress distributions
  - Creates damage localization

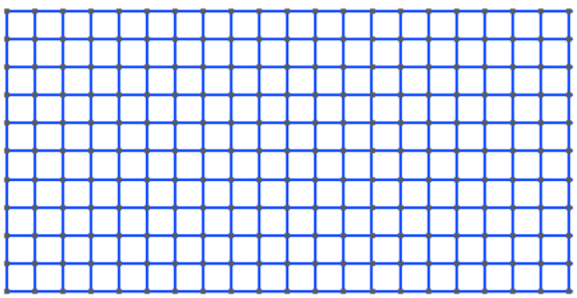

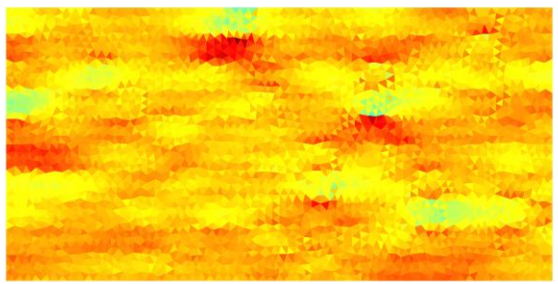

$\sigma_{M\,xx}$ [Mpa]; $\varepsilon_{M\,xx} = 2.6\%$

0 108 215

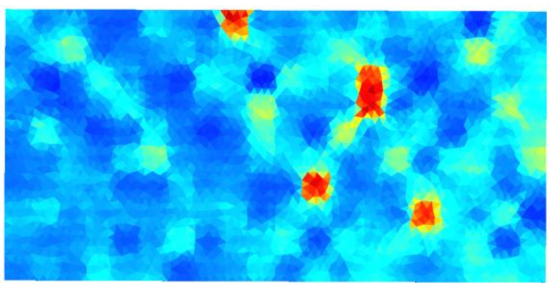

$\hat{p}_0$ [-]; $\varepsilon_{M\,xx} = 2.6\%$

0 108 215

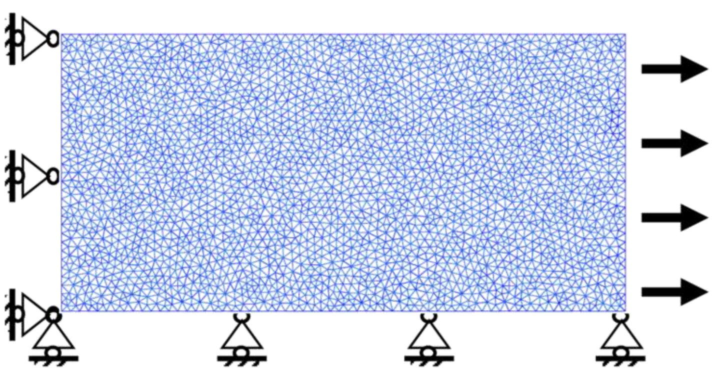

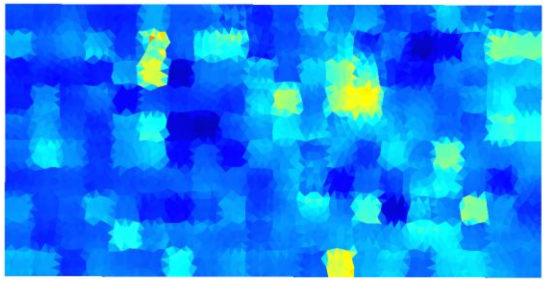

$\widehat{D}_0$[-]; $\varepsilon_{M\,xx} = 2.4\%$

0 0.025 0.05

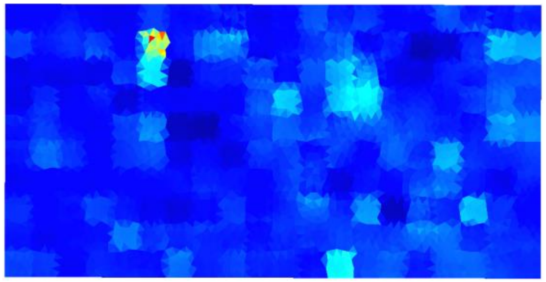

$\widehat{D}_0$[-]; $\varepsilon_{M\,xx} = 2.6\%$

0 0.025 0.05

- Ply loading realizations
  - Simple failure criterion at (homogenized stress) loss of ellipticity
  - Discrepancy in failure point

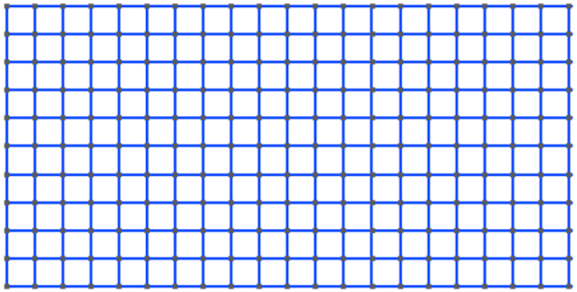

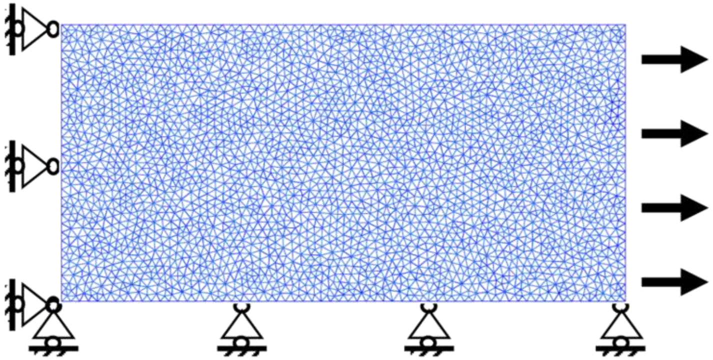

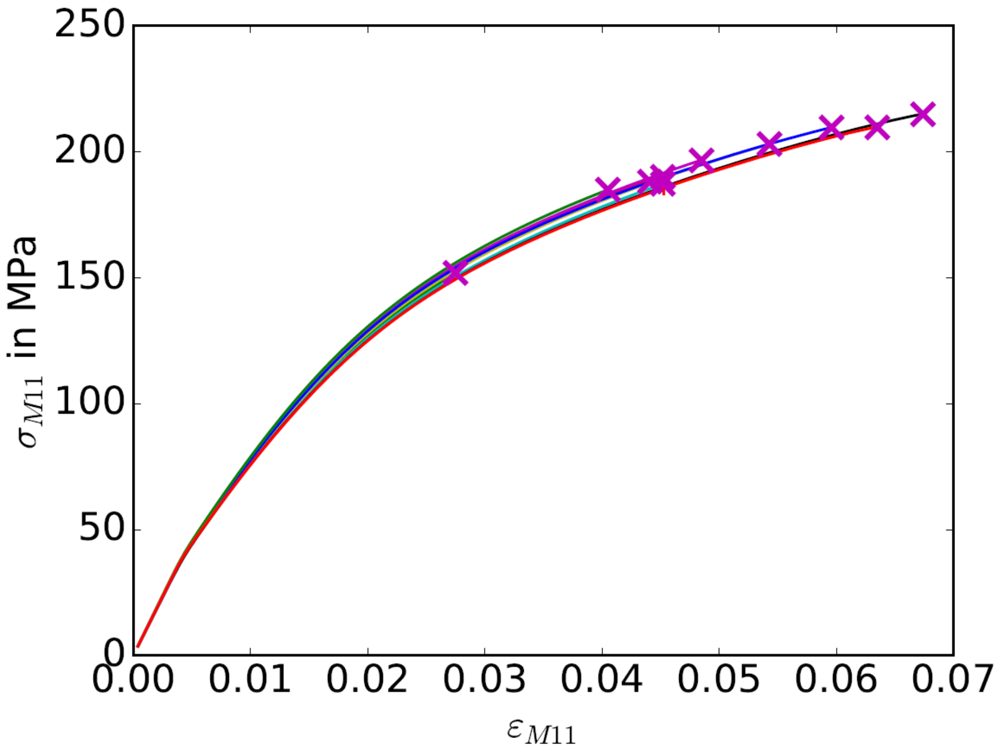

Stochastic Homogenization of Composite Materials

- STOMMMAC M.ERA-NET project (MFH for elasto-visco-plastic composites)
  - e-Xstream, ULiège (Belgium)
  - BATZ (Spain)
  - JKU, AC (Austria)
  - U Luxembourg (Luxemburg)

- Publications (doi)
  - 10.1016/j.compstruct.2018.01.051
  - 10.1002/nme.5903
  - 10.1016/j.cma.2019.01.016

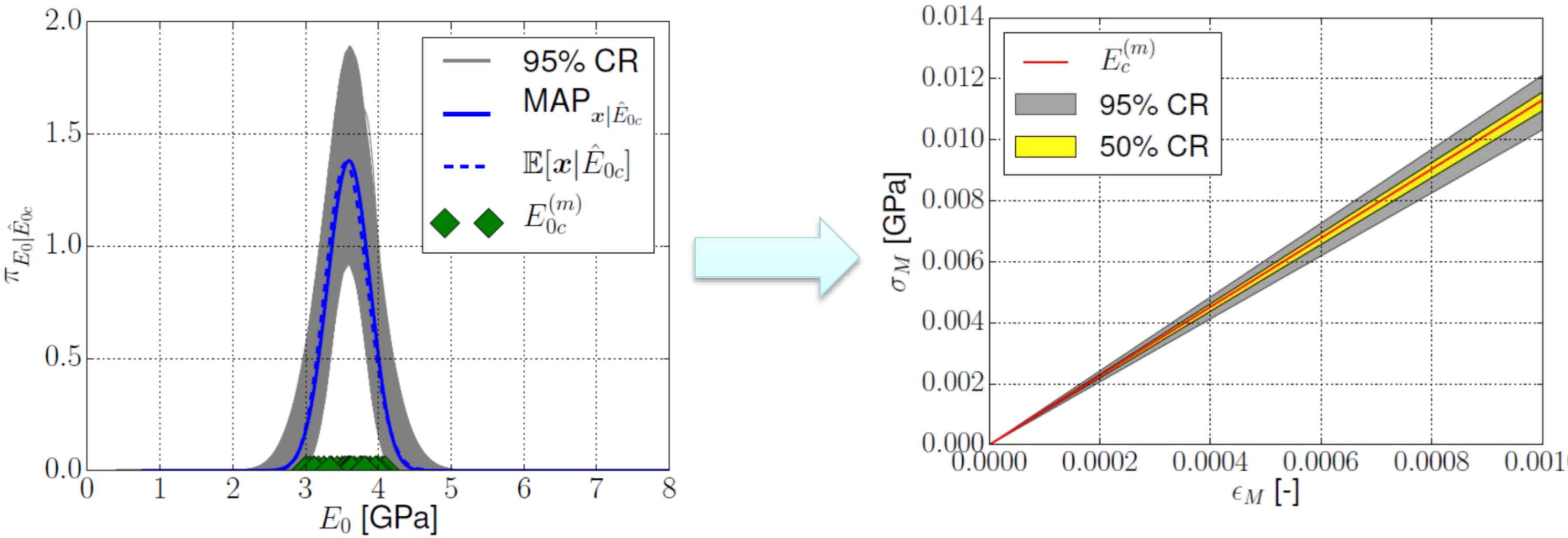

Bayesian identification of stochastic Mean-Field Homogenization model parameters

STOMMMAC The research has been funded by the Walloon Region under the agreement no 1410246-STOMMMAC (CT-INT 2013-03-28) in the context of M-ERA.NET Joint Call 2014.

Bayesian identification of stochastic MFH model parameters

- Multi-scale modeling
  - 2 problems are solved concurrently
    - The macro-scale problem
    - The meso-scale problem (on a meso-scale Volume Element)

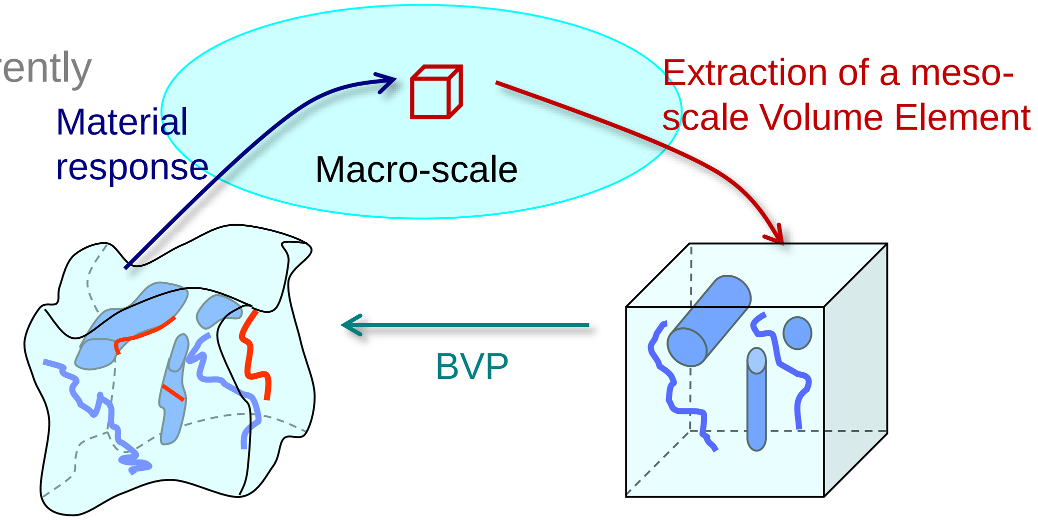

Identification: Requires identification of micro-scale geometrical and material model parameters

Bayesian identification of stochastic MFH model parameters

- Proposed methodology
  - To develop a stochastic Mean Field Homogenization method whose missing micro-constituents properties are inferred from coupons tests

Micro-structure partly characterized

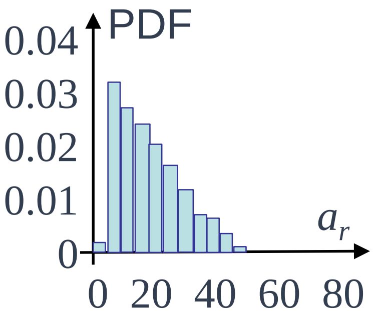

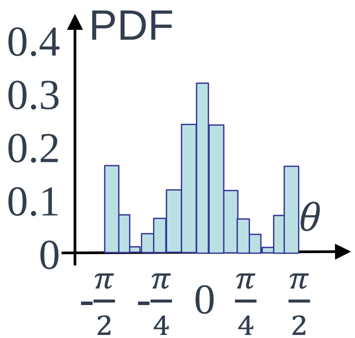

Multiscale model

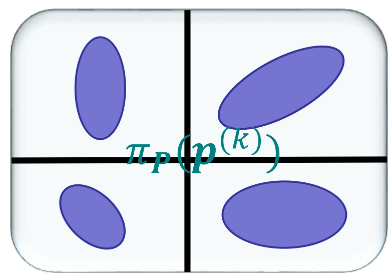

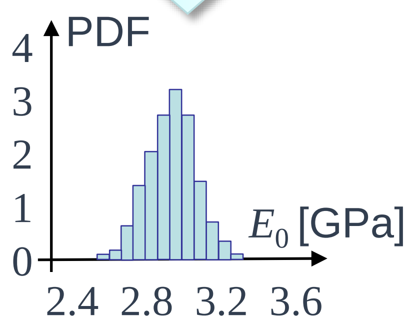

Inference of missing microconstituents properties

Macro scale response UQ

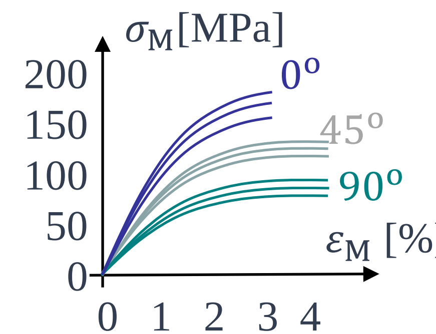

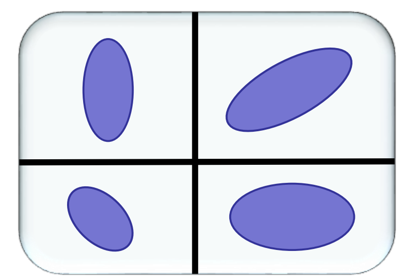

Stochastic multiscale model

- Fibre distribution effect
  - 2-step homogenization

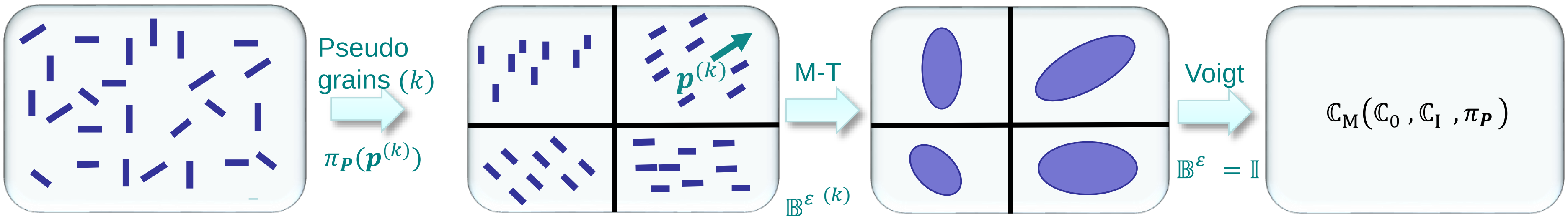

  - For uniaxial tests along direction θ: $\sigma_{\mathrm{M}} = \sigma_{\mathrm{M}}\left(\mathrm{I}(\psi(\boldsymbol{p})), \mathbb{C}_0, \mathbb{C}_{\mathrm{I}}; \theta, \varepsilon_{\mathrm{M}}\right)$

Bayesian identification of stochastic MFH model parameters

- Fibre distribution effect
  - Skin-core effect

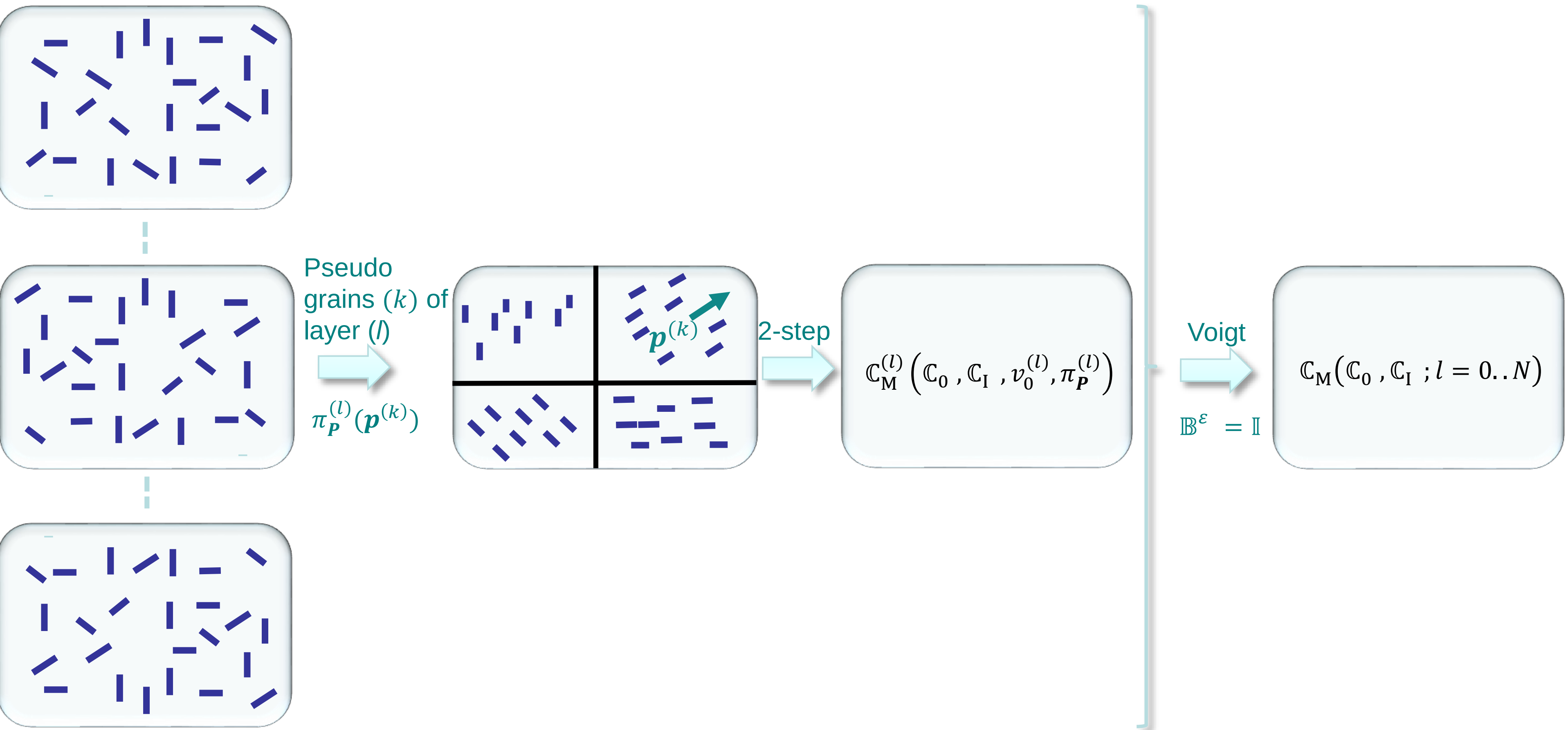

  - For uniaxial tests along direction θ: $\sigma_{\mathrm{M}} = \sigma_{\mathrm{M}}\left(\mathrm{I}(\psi(\boldsymbol{p})), \mathbb{C}_0, \mathbb{C}_{\mathrm{I}}; \theta, \varepsilon_{\mathrm{M}}\right)$

Bayesian identification of stochastic MFH model parameters

- Experimental characterization

Fiber orientation and aspect ratio (JKU)

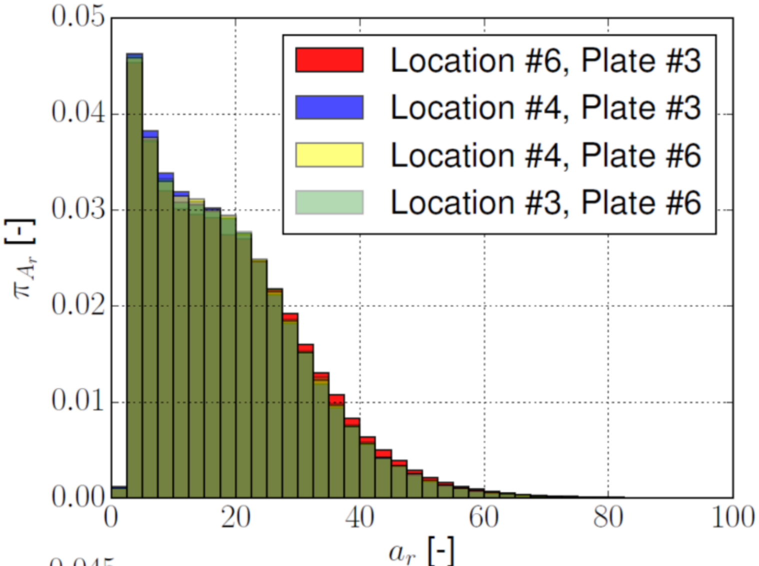

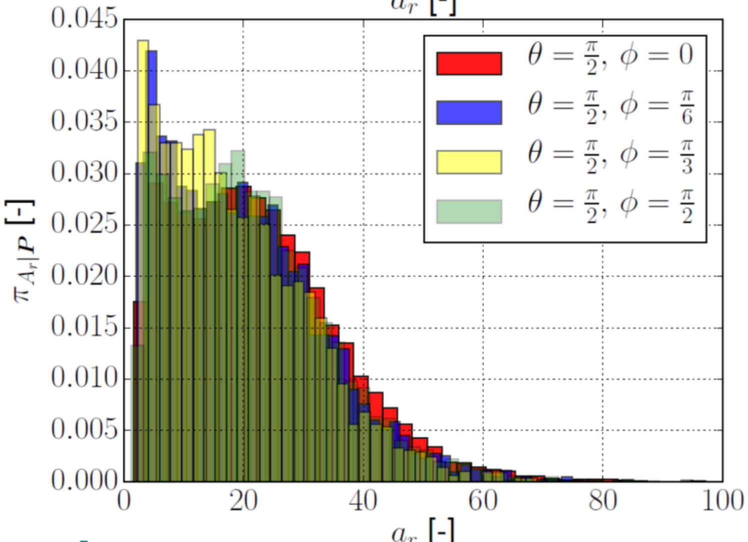

Composite material response (BATZ)

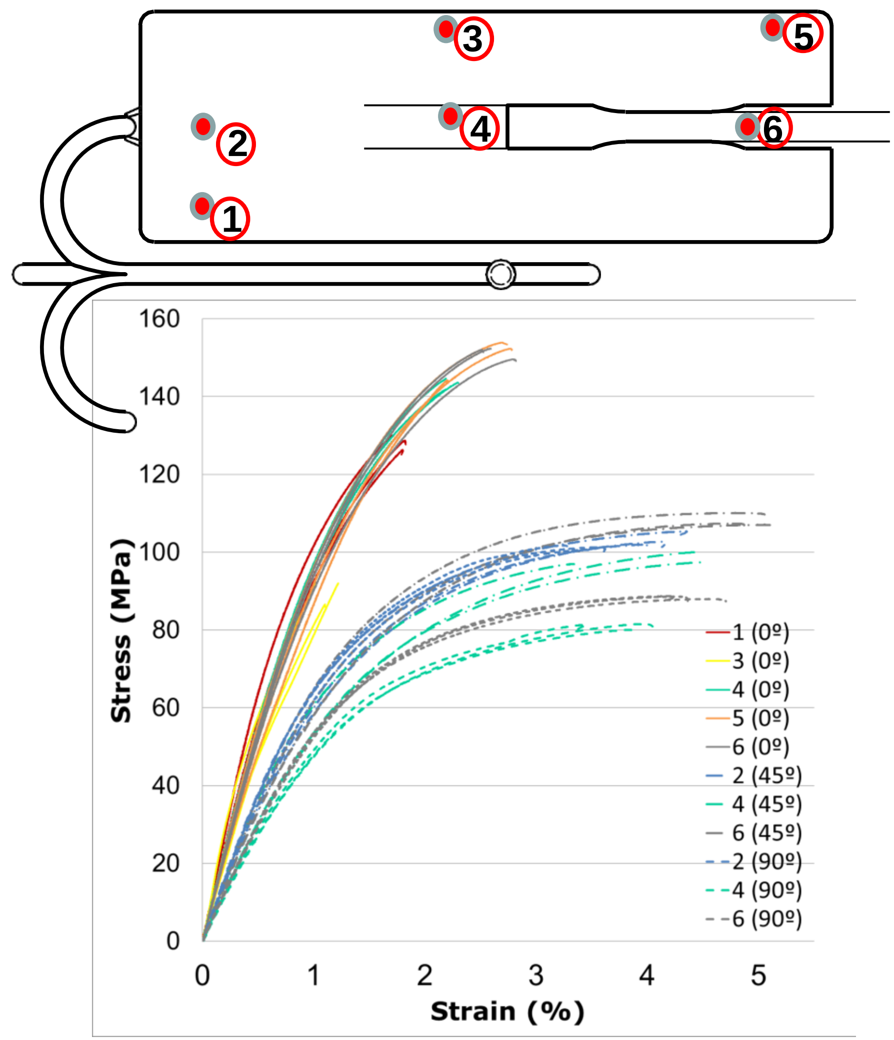

- Assume a distribution of the matrix Young's modulus
  - Beta distribution $E_0 \sim \beta_{\alpha,\beta,a,b}$ with $\beta_{\alpha,\beta,a,b}(y) = \frac{(y-a)^{\alpha-1}(y-b)^{\beta-1}}{(b-a)^{\alpha+\beta+1}B(\alpha,\beta)}$
  - Matrix Young 's modulus corresponding to experimental measurements
    - $E_{0c}^{(n)}$ with $n = 1..n_{\text{total}}$, for all directions and positions
  - Bayes' theorem

$$\pi_{\text{post}}(\alpha,\beta,a,b|\hat{E}_{0c}) \propto \pi(\hat{E}_{0c}|\alpha,\beta,a,b)\pi_{\text{prior}}(\alpha)\pi_{\text{prior}}(\beta)\pi_{\text{prior}}(a)\pi_{\text{prior}}(b)$$

- Priors: $\pi_{\text{prior}}(x) = \Gamma_{\alpha,\beta,a,c}$ with $\Gamma_{\alpha,\beta,a,c}(y) = \frac{\left(\frac{y-a}{c}\right)^{\alpha-1}\beta^{\alpha}e^{-\beta\left(\frac{y-a}{c}\right)}}{c\Gamma(\alpha)}$

- Likelihood: $\pi(\hat{E}_{0c}|\alpha,\beta,a,b) = \prod_{n=1}^{n_{\text{total}}} \beta_{\alpha,\beta,a,b}\left(E_{0c}^{(n)}\right)$

$$\Rightarrow \quad \pi_{\text{post}}(\alpha,\beta,a,b|\hat{E}_{0c}) \propto \prod_{n=1}^{n_{\text{total}}} \beta_{\alpha,\beta,a,c}\left(E_{0c}^{(n)}\right)\pi_{\text{prior}}(\alpha)\pi_{\text{prior}}(\beta)\pi_{\text{prior}}(a)\pi_{\text{prior}}(b)$$

Bayesian identification of stochastic MFH model parameters

- Assume a distribution of the matrix Young's modulus
  - Inference: $\pi_{\text{post}}(\alpha, \beta, a, b|\hat{E}_{0c}) \propto \prod_{n=1}^{n_{\text{total}}} \beta_{\alpha,\beta,a,c}\left(E_{0c}^{(n)}\right) \pi_{\text{prior}}(\alpha\ )\pi_{\text{prior}}(\beta)\pi_{\text{prior}}(a)\pi_{\text{prior}}(b)$
    - $i = 1..n_{\text{pos}}$, with n_{pos} the number of positions tested (5, positions #1-#5)

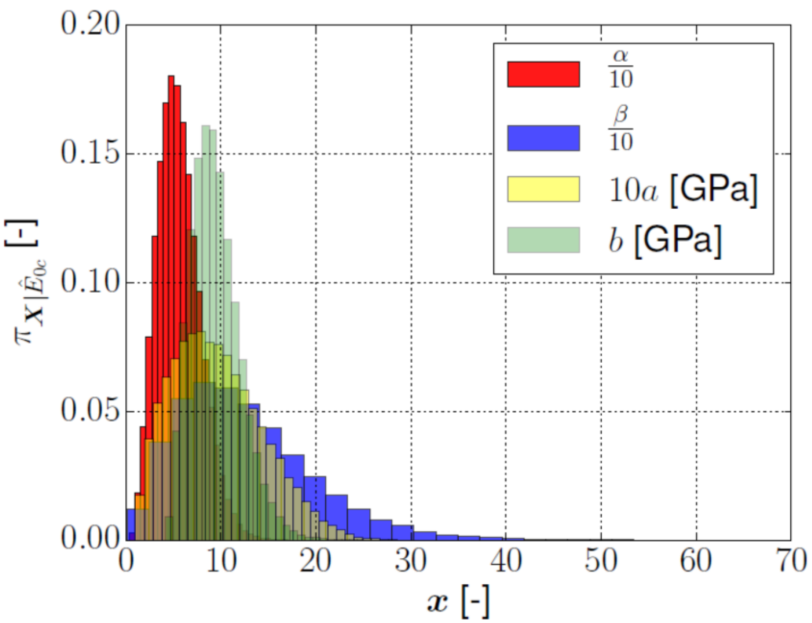

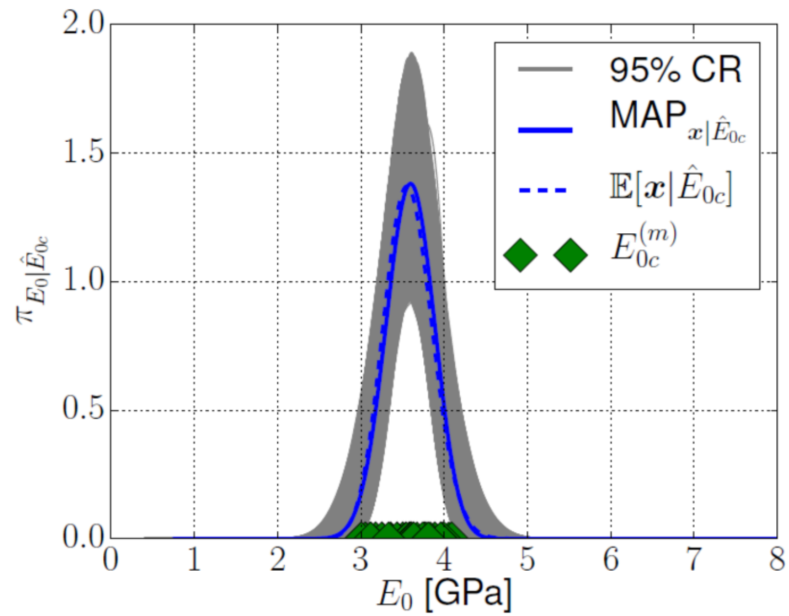

Bayesian identification of stochastic MFH model parameters

- Validation
  - Evaluate stochastic response at Position 6
    - Perform stochastic homogenization from
      $\pi_{\text{post}}(\alpha,\beta,a,b|\hat{E}_{0c})$
    - From sampling of $[\alpha,\beta,a,b]$, evaluate
      $E_0 \sim \beta_{\alpha,\beta,a,b}$
    - From sampling of $[E_0]$, evaluate composite response

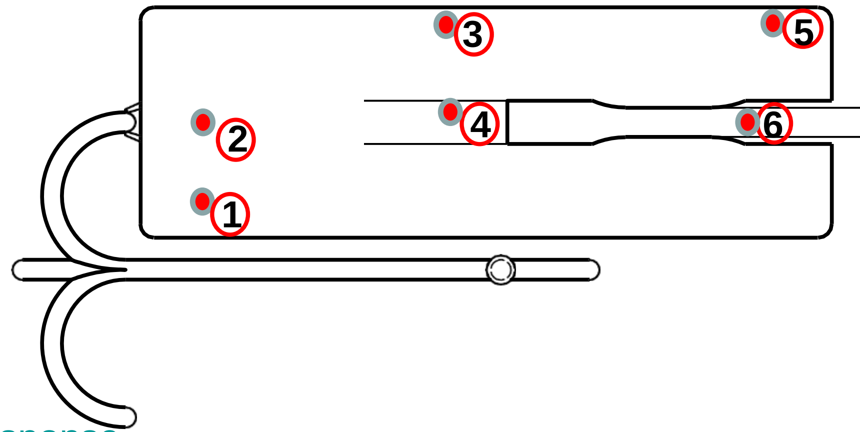

$$E_{\text{MFH}} = E_{\text{MFH}}\left(\mathrm{I}(\psi(\boldsymbol{p}),a_r),E_0\ ,\mathbb{C}_{\mathrm{I}}\ ;\theta\right)$$

- Compare with experimental measurements $\hat{E}_c^{(6,j)}$

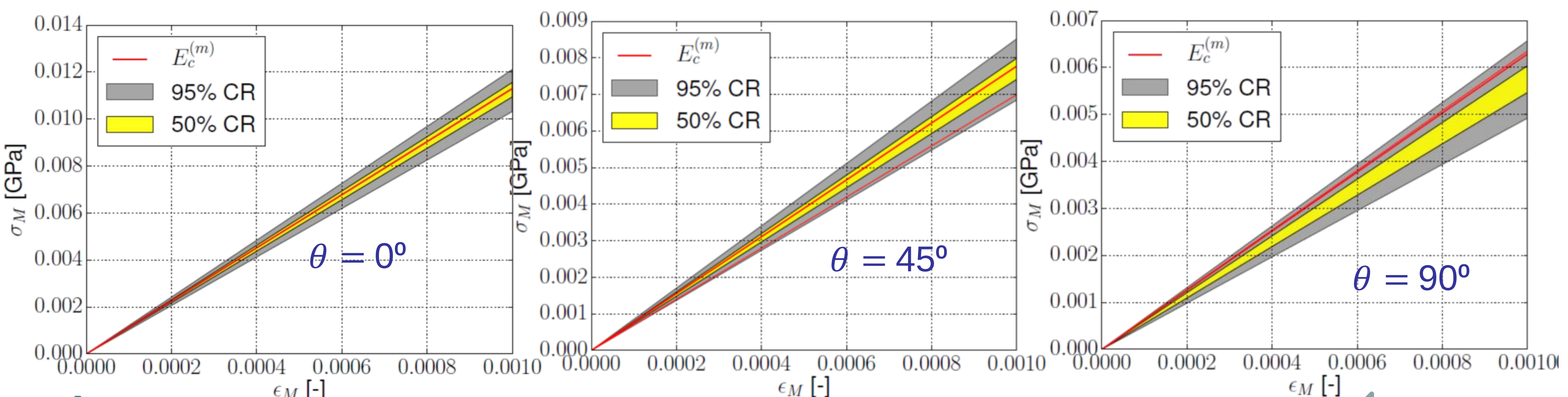

Bayesian identification of stochastic MFH model parameters

- Extension to non-linear behavior
  - More parameters to infer
    - Matrix Young's modulus E_0
    - Matrix yield stress σ_{Y0}
    - Matrix hardening law
      $$R(p_0) = h\, p_0^{m_1}(1 - \exp(-m_2 p_0))$$
    - Effective aspect ratio a_r
  - 2-Step MFH model requires many iterations
    - Incremental secant approach

$$\begin{cases} \boldsymbol{\sigma}_{\mathrm{M}} = \overline{\boldsymbol{\sigma}} = v_0 \boldsymbol{\sigma}_0 + v_{\mathrm{I}} \boldsymbol{\sigma}_{\mathrm{I}} \\ \Delta\boldsymbol{\varepsilon}_{\mathrm{M}}^{\mathrm{r}} = \overline{\Delta\boldsymbol{\varepsilon}} = v_0 \Delta\boldsymbol{\varepsilon}_0^{\mathrm{r}} + v_{\mathrm{I}} \Delta\boldsymbol{\varepsilon}_{\mathrm{I}}^{\mathrm{r}} \\ \Delta\boldsymbol{\varepsilon}_{\mathrm{I}}^{\mathrm{r}} = \mathbb{B}^{\varepsilon}\left(\mathrm{I}, \mathbb{C}_0^{\mathrm{S}}, \mathbb{C}_{\mathrm{I}}^{\mathrm{S}}\right) : \Delta\boldsymbol{\varepsilon}_0^{\mathrm{r}} \end{cases}$$

⇨ Too expensive for BI

  - Definition of parameters

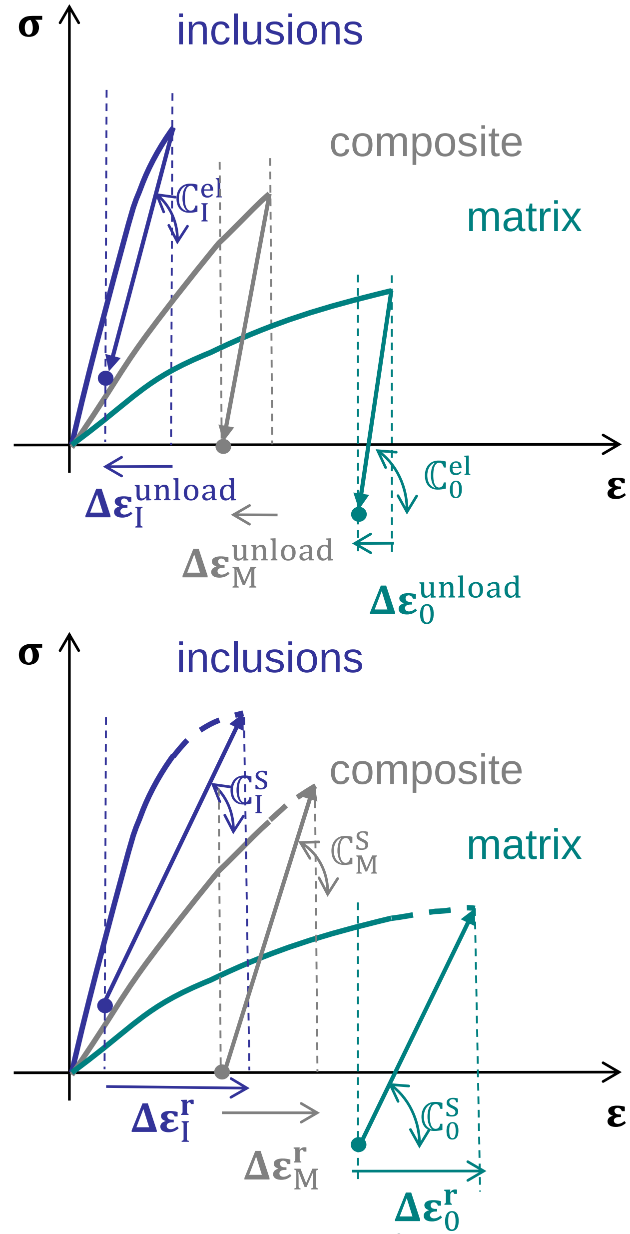

Bayesian identification of stochastic MFH model parameters

- Speed up the evaluation of the likelihood
  - Likelihood
    - $\pi(\hat{\sigma}_{\mathrm{M}}(t)|[\varepsilon_{\mathrm{M}}(t' \leq t), \boldsymbol{\vartheta}])$
    - With $\boldsymbol{\vartheta} = [E_0, \sigma_{Y_0}, h, m_1, m_2, a_r]$
    - 2-Step MFH model

      $\sigma_{\mathrm{MFH}}(t)$
      $= \sigma_{\mathrm{MFH}}\big(\mathrm{I}(\psi(\boldsymbol{p}), a_r), E_0$

    Too expensive for BI
  - Use of a surrogate
    - $\sigma_{\mathrm{NNW}}(t) = \sigma_{\mathrm{NNW}}\big(\boldsymbol{\varepsilon}_{\mathbf{M}}(t), \boldsymbol{\vartheta}, \mathbb{C}_{\mathrm{I}}\ ; \theta\big)$
    - Constructed using artificial Neural Network
    - Trained fusing the 2-Step MFH model

      $\sigma_{\mathrm{MFH}}(t)$
      $= \sigma_{\mathrm{MFH}}\big(\mathrm{I}(\psi(\boldsymbol{p}), a_r), E_0$
      $, \qquad \mathbb{C}_{\mathrm{I}}\ , \varepsilon_{\mathrm{M}}(t'$

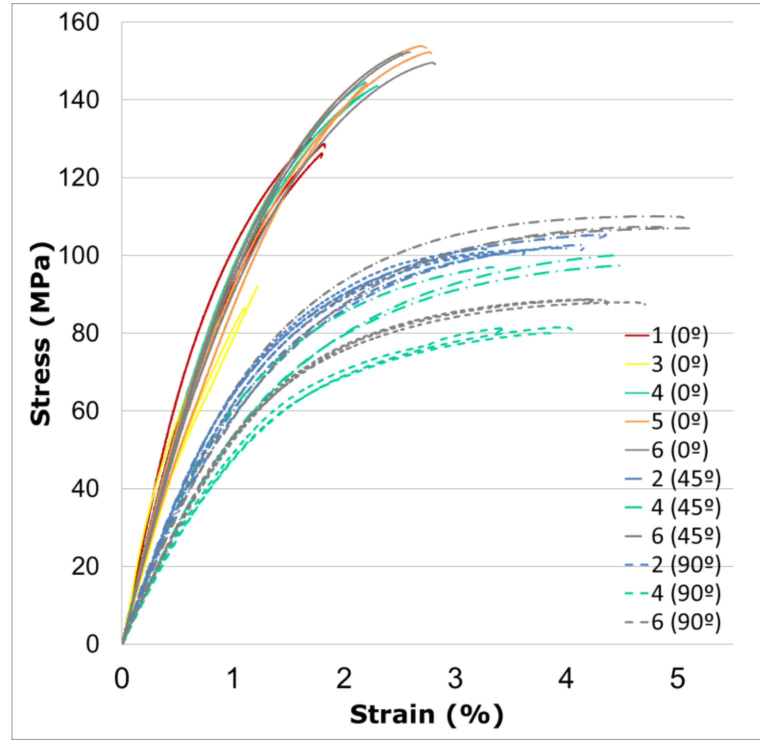

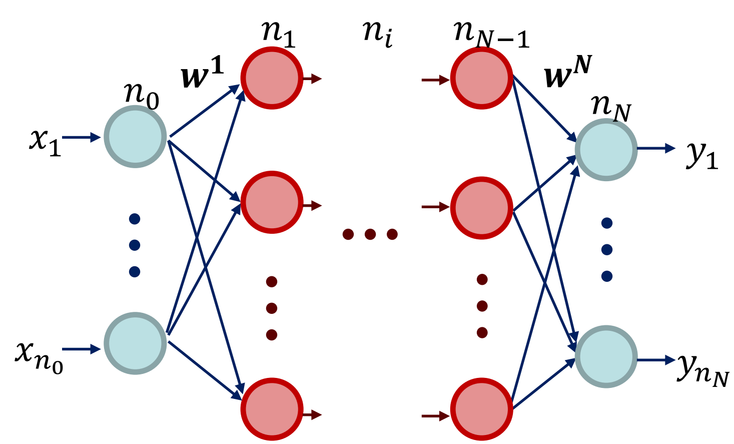

Beginning

Bayesian identification of stochastic MFH model parameters

- Assume a noise in the measurements & use surrogate model
  - Measurements at strain i in direction θ_j:

$$\Sigma_c^{(i,j,k)} = \sigma_{\mathrm{NNW}}^{(i,j)}\left(\boldsymbol{\varepsilon}_{\mathbf{M}}^{(\boldsymbol{i},\boldsymbol{j})}, \boldsymbol{\vartheta}, \mathbb{C}_{\mathrm{I}}\ ; \theta_j\right) + \mathrm{noise}^{(i,j)}$$

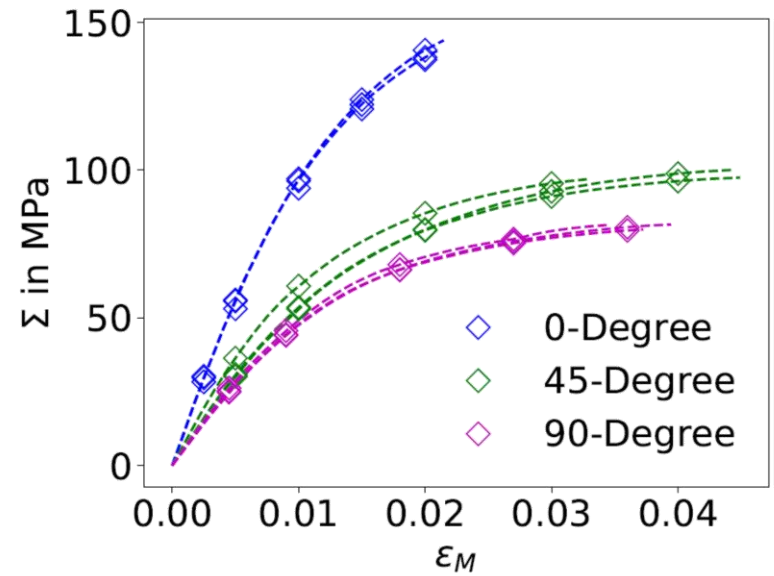

$$\pi\left(\Sigma_c^{(i,j,k)} \middle| \left[\boldsymbol{\varepsilon}_{\mathbf{M}}^{(\boldsymbol{i},\boldsymbol{j})}, \boldsymbol{\vartheta}\right]\right) = \pi_{\mathrm{noise}}^{(i,j)}\left(\Sigma_c^{(i,j,k)} - \sigma_{\mathrm{NNW}}^{(i,j)}\left(\boldsymbol{\varepsilon}_{\mathbf{M}}^{(\boldsymbol{i},\boldsymbol{j})}, \boldsymbol{\vartheta}, \mathbb{C}_{\mathrm{I}}\ ; \theta_j\right)\right)$$

    - $j = 1..n_{\mathrm{dir}}$, with
      n_{dir} the number of directions θ_j tested
    - $i = 1..n_\varepsilon^{(j)}$, with
      n_ε the number of stress-strain points
    - $k = 1..n_{\mathrm{test}}^{(i,j)}$, with
      $n_{\mathrm{test}}^{(i,j)}$ the number of samples tested at point i along direction θ_j

  - Noise function from $n_{\mathrm{test},i,j}$ measurements at strain i in direction θ_j:

$$\pi_{\mathrm{noise}^{(i,j)}}(y) = \frac{1}{\sqrt{2\pi}\,\sigma_{\Sigma_c^{(i,j)}}} \exp\left(-\frac{y^2}{2\sigma^2_{\Sigma_c^{(i,j)}}}\right)$$

  - Bayes' theory:

$$\pi_{\mathrm{post}}\left(\boldsymbol{\vartheta} \middle| \hat{\boldsymbol{\varepsilon}}_{\mathbf{M}}, \hat{\boldsymbol{\Sigma}}_{\mathrm{c}}\ \right) \propto \pi_{\mathrm{prior}}(\boldsymbol{\vartheta})\ \prod_{j=1}^{n_{\mathrm{dir}}} \prod_{i=1}^{n_\varepsilon^{(j)}} \prod_{k=1}^{n_{\mathrm{test}}^{(i,j)}} \pi_{\mathrm{noise}}^{(i,j)}\left(\Sigma_c^{(i,j,k)} - \sigma_{\mathrm{NNW}}^{(i,j)}\left(\boldsymbol{\varepsilon}_{\mathbf{M}}^{(\boldsymbol{i},\boldsymbol{j})}, \boldsymbol{\vartheta}, \mathbb{C}_{\mathrm{I}}\ ; \theta_j\right)\right)$$

- Results

$$\pi_{\text{post}}\left(\boldsymbol{\vartheta}|\hat{\boldsymbol{\varepsilon}}_{\mathbf{M}},\widehat{\boldsymbol{\Sigma}}_{\mathrm{c}}\right) \propto \pi_{\text{prior}}(\boldsymbol{\vartheta}) \prod_{j=1}^{n_{\text{dir}}} \prod_{i=1}^{n_{\varepsilon}^{(j)}} \prod_{k=1}^{n_{\text{test}}^{(i,j)}} \pi_{\text{noise}}^{(i,j)}\left(\Sigma_c^{(i,j,k)} - \sigma_{\text{NNW}}^{(i,j)}\left(\boldsymbol{\varepsilon}_{\mathbf{M}}^{(\boldsymbol{i},\boldsymbol{j})},\boldsymbol{\vartheta},\mathbb{C}_{\mathrm{I}}\ ;\theta_j\right)\right)$$

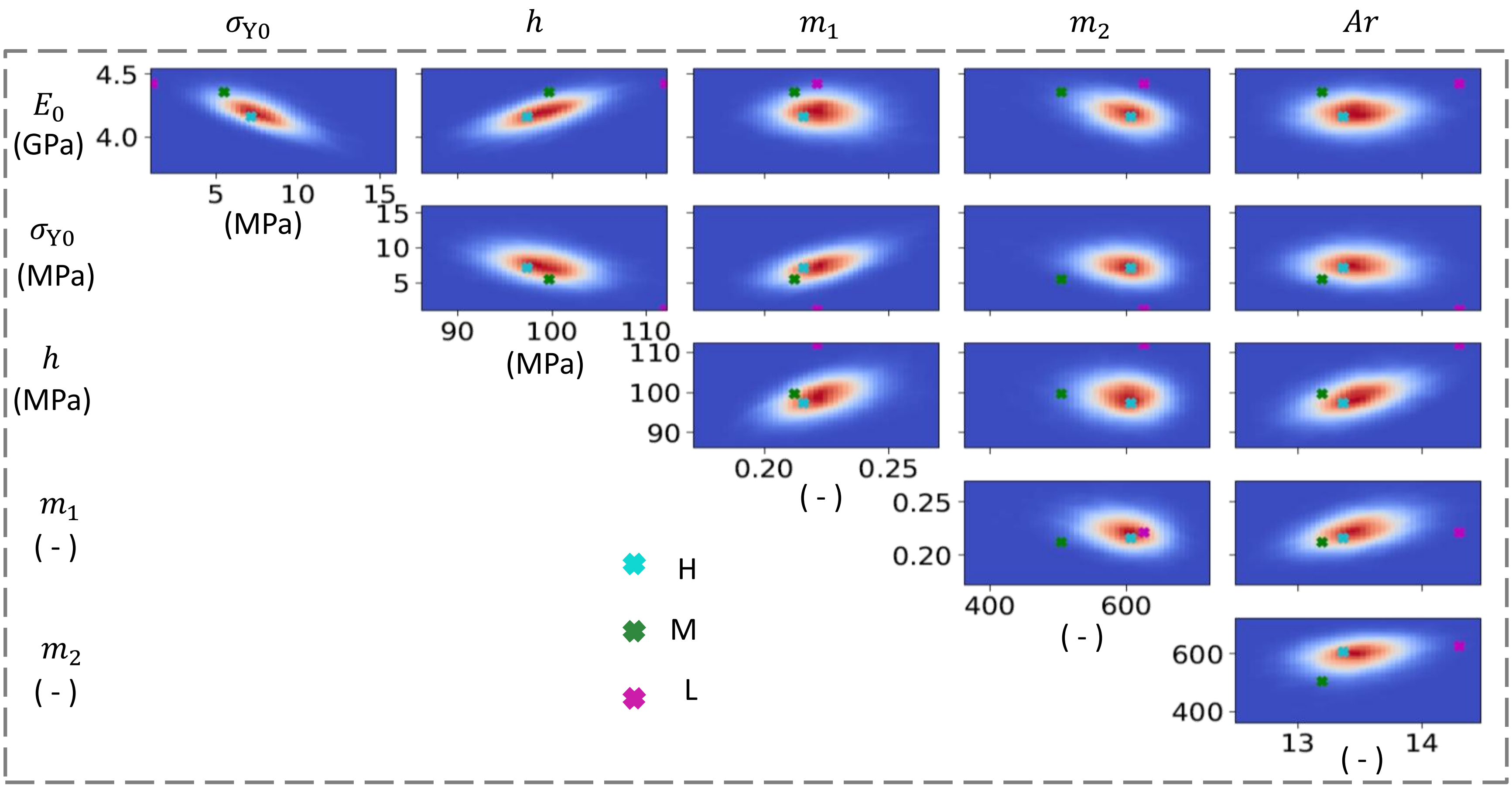

- Verification

$$\pi_{\text{post}}\left(\boldsymbol{\vartheta}|\hat{\boldsymbol{\varepsilon}}_{\mathbf{M}},\hat{\boldsymbol{\Sigma}}_{\text{c}}\right) \propto \pi_{\text{prior}}(\boldsymbol{\vartheta}) \prod_{j=1}^{n_{\text{dir}}} \prod_{i=1}^{n_{\varepsilon}^{(j)}} \prod_{k=1}^{n_{\text{test}}^{(i,j)}} \pi_{\text{noise}}^{(i,j)}\left(\Sigma_c^{(i,j,k)} - \sigma_{\text{NNW}}^{(i,j)}\left(\boldsymbol{\varepsilon}_{\mathbf{M}}^{(\boldsymbol{i},\boldsymbol{j})},\boldsymbol{\vartheta},\mathbb{C}_{\text{I}}\ ;\theta_j\right)\right)$$

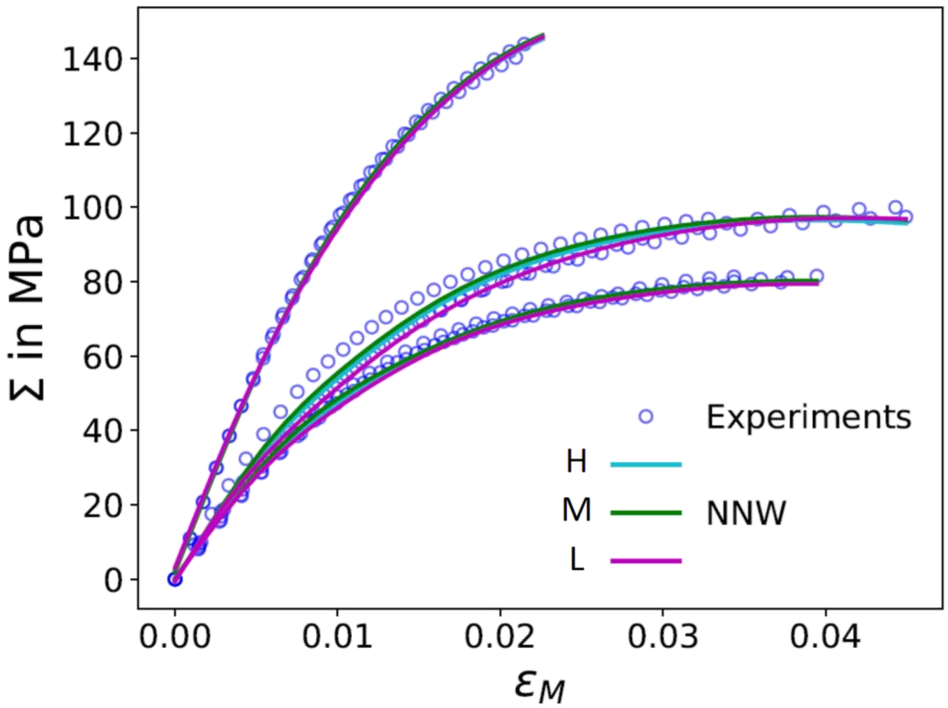

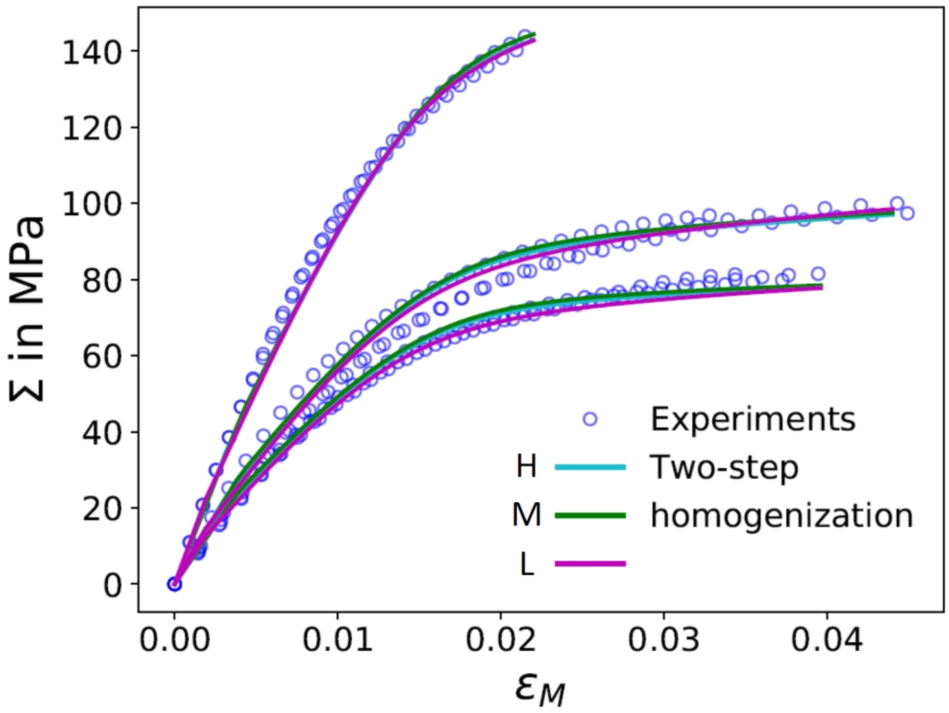

Bayesian identification of stochastic MFH model parameters

- STOMMMAC M.ERA-NET project (MFH for elasto-visco-plastic composites)
  - e-Xstream, ULiège (Belgium)
  - BATZ (Spain)
  - JKU, AC (Austria)
  - U Luxembourg (Luxemburg)

- Publications (doi)
  - 10.1016/j.cma.2019.112693 data on 10.5281/zenodo.3740410
  - 10.1016/j.compstruct.2019.03.066

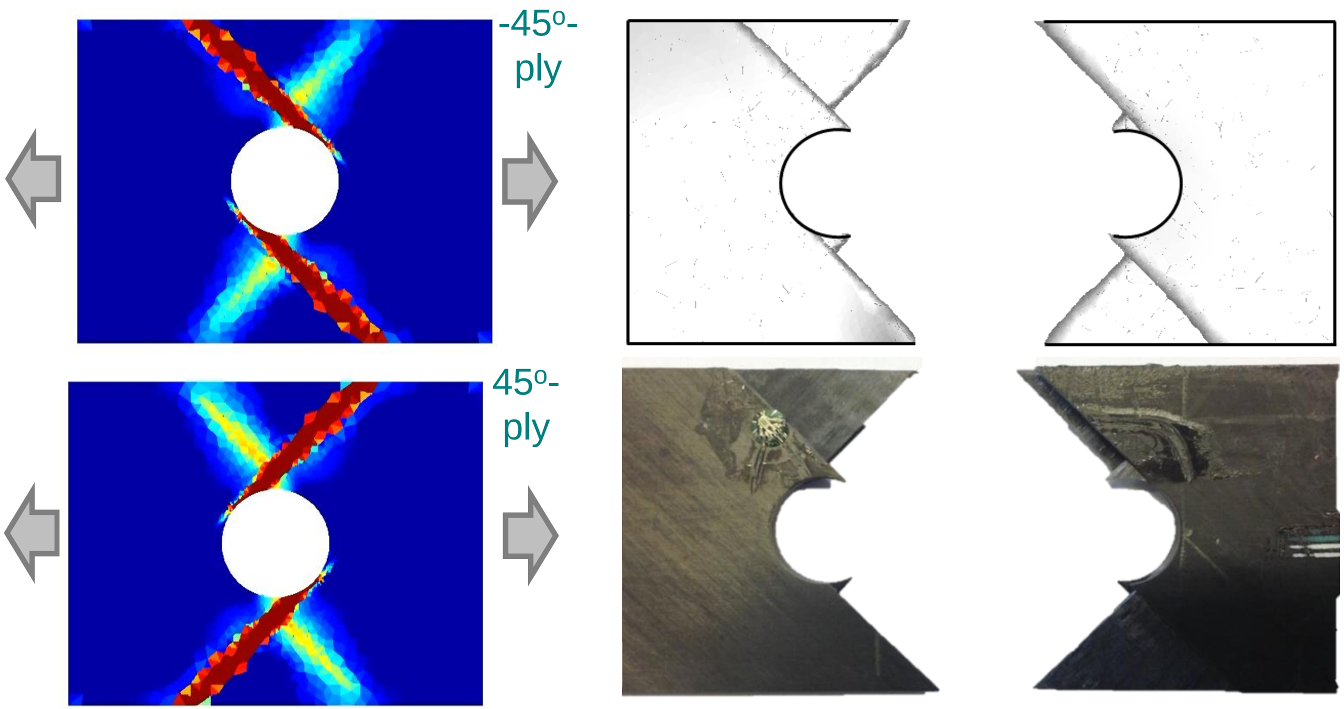

Non-Local Damage Mean-Field-Homogenization

SIMUCOMP The research has been funded by the Walloon Region under the agreement no 1017232 (CT-EUC 2010-10-12) in the context of the ERA-NET +, Matera + framework.

- Multi-scale modeling
  - 2 problems are solved concurrently
    - The macro-scale problem
    - The meso-scale problem (on a meso-scale Volume Element)

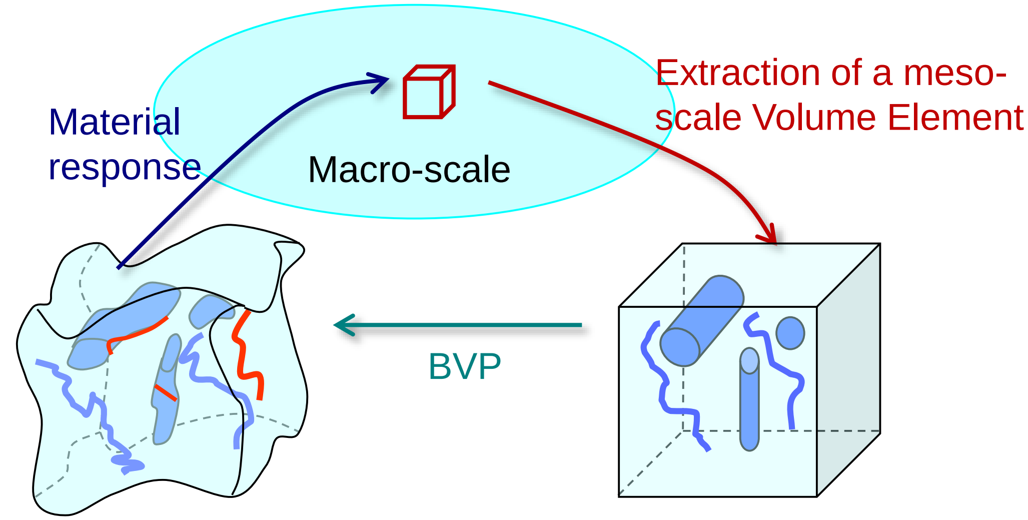

- Length-scales separation

$$L_{macro} >> L_{VE} >> L_{micro}$$

For accuracy: Size of the meso-scale volume element smaller than the characteristic length of the macro-scale loading

To be statistically representative: Size of the meso-scale volume element larger than the characteristic length of the micro-structure

Non-Local Damage Mean-Field-Homogenization

- Materials with strain softening
  - Incremental forms
    - Strain increments in the same direction

$$\Delta\boldsymbol{\varepsilon}_{\mathrm{I}} = \mathbf{B}^{\varepsilon}\left(\mathrm{I}, \bar{\mathbf{C}}_0^{\mathrm{alg}}, \bar{\mathbf{C}}_{\mathrm{I}}^{\mathrm{alg}}\right) : \Delta\boldsymbol{\varepsilon}_0$$

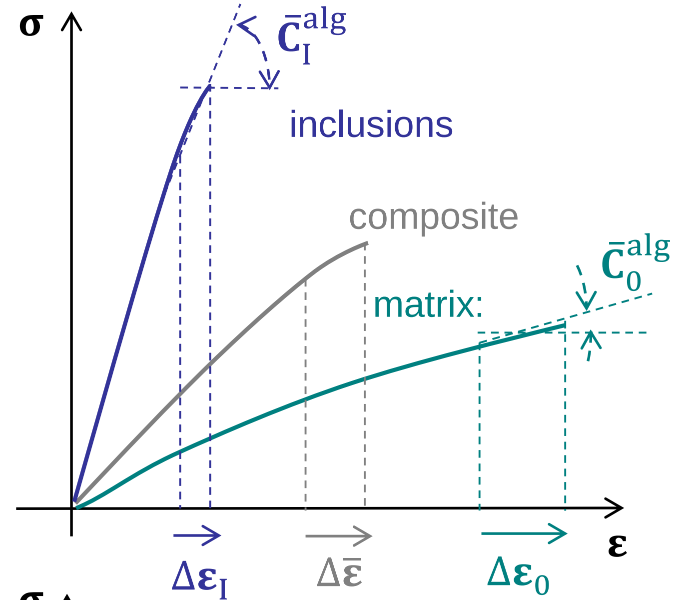

  - Because of the damaging process, the fiber phase is elastically unloaded during matrix softening

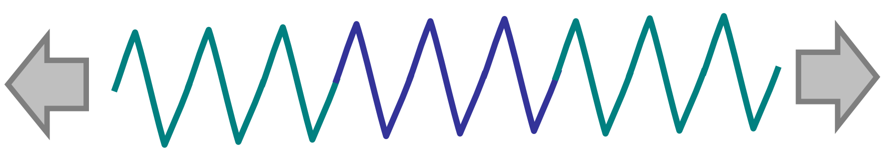

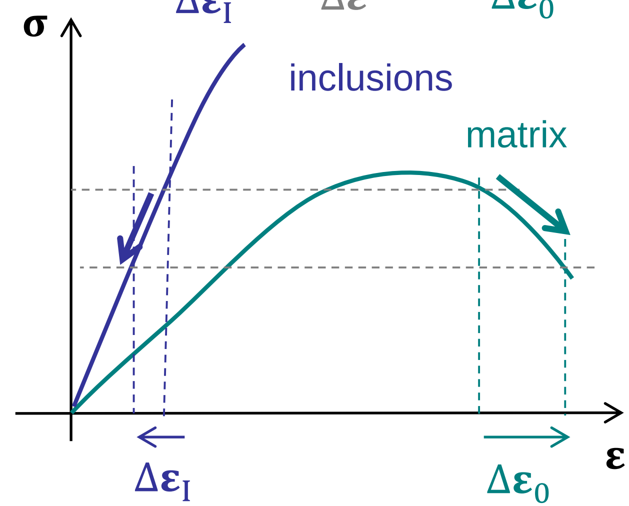

- Solution: new incremental-secant method
  - We need to define the LCC from another stress state

- Based on the incremental-secant approach
  - Perform a virtual elastic unloading from previous solution
    - Composite material unloaded to reach the stress-free state
    - Residual stress in components
  - Apply MFH from unloaded state
    - New strain increments (>0)

$$\Delta\boldsymbol{\varepsilon}^{\mathrm{r}}_{\mathrm{I}/0} = \Delta\boldsymbol{\varepsilon}_{\mathrm{I}/0} + \Delta\boldsymbol{\varepsilon}^{\mathrm{unload}}_{\mathrm{I}/0}$$

    - Use of secant operators

$$\Delta\boldsymbol{\varepsilon}^{\mathrm{r}}_{\mathrm{I}} = \mathbf{B}^{\varepsilon}\left(\mathrm{I}, (1-D)\bar{\mathbf{C}}^{\mathrm{Sr}}_{0}, \bar{\mathbf{C}}^{\mathrm{S0}}_{\mathrm{I}}\right) : \Delta\boldsymbol{\varepsilon}^{\mathrm{r}}_{0}$$

    - Possibility of unloading

$$\begin{cases} \Delta\boldsymbol{\varepsilon}^{\mathrm{r}}_{\mathrm{I}} > \mathbf{0} \\ \Delta\boldsymbol{\varepsilon}_{\mathrm{I}} < \mathbf{0} \end{cases}$$

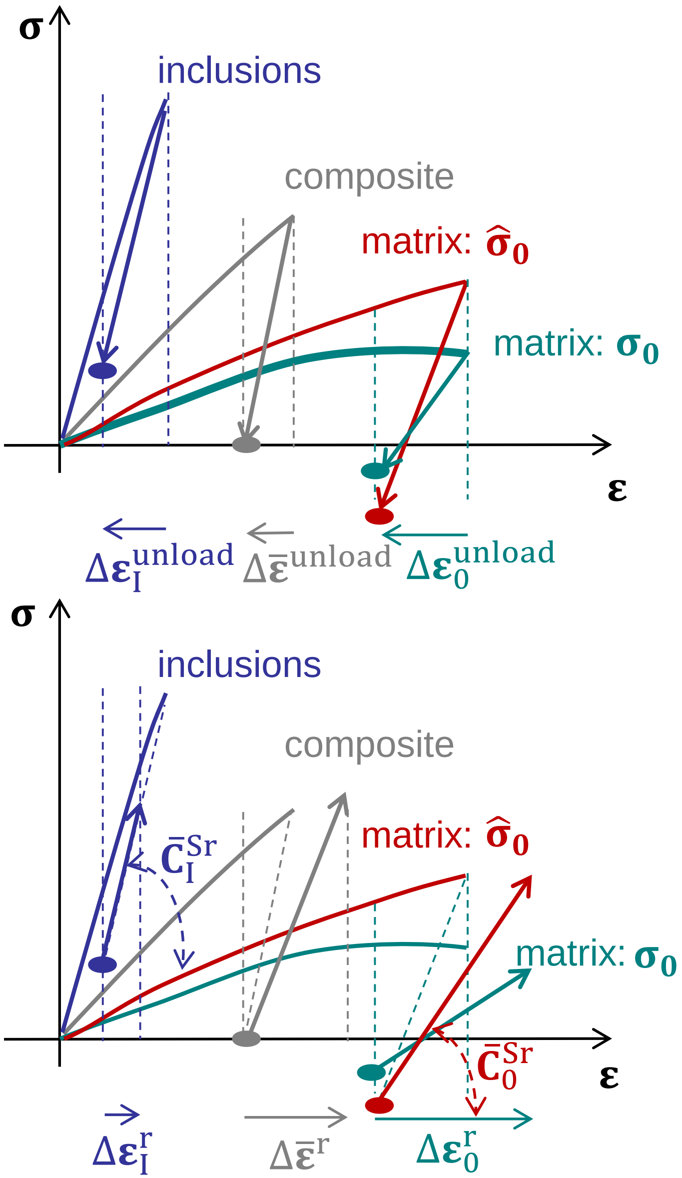

- New results for damage
  - Fictitious composite
    - 50%-UD fibres
  - Elasto-plastic matrix with damage

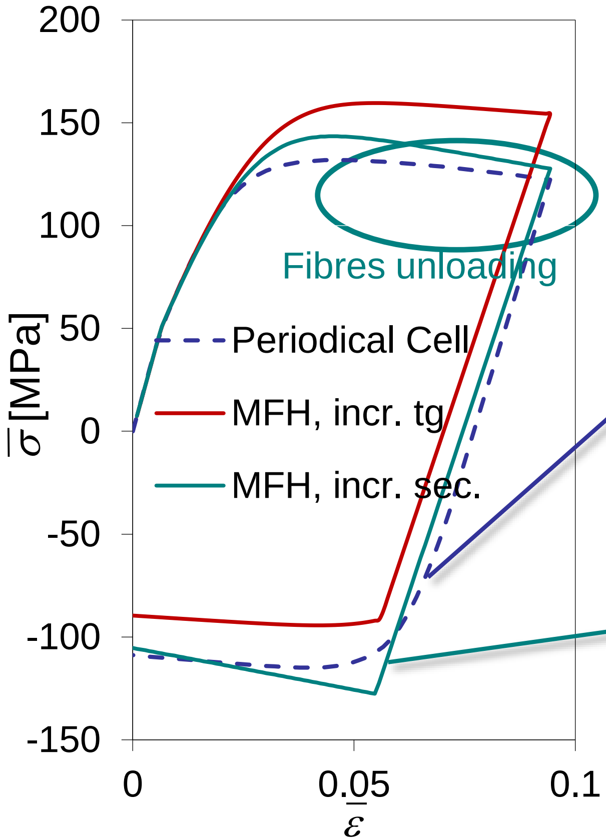

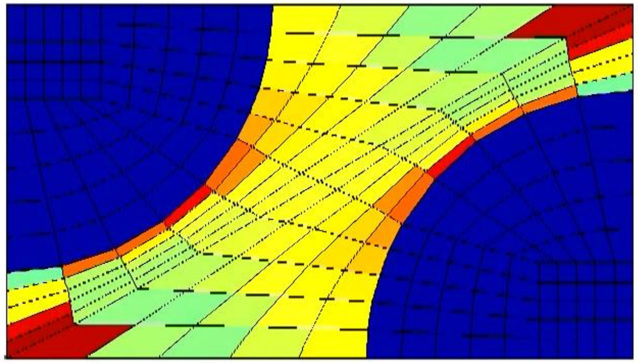

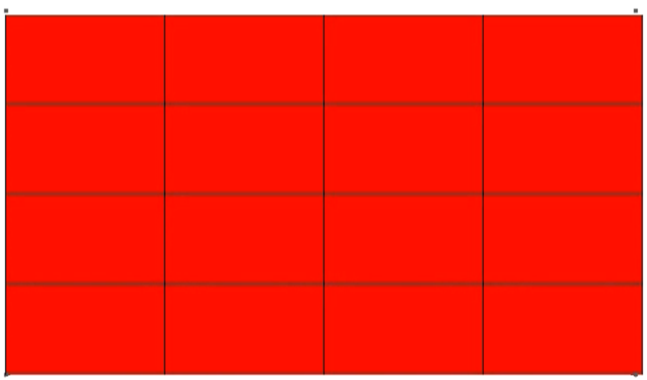

- Material models
  - Elasto-plastic material
    - Stress tensor $\boldsymbol{\sigma} = \mathbf{C}^{\mathrm{el}} : (\boldsymbol{\varepsilon} - \boldsymbol{\varepsilon}^{\mathrm{pl}})$
    - Yield surface $f(\boldsymbol{\sigma}, p) = \boldsymbol{\sigma}^{\mathrm{eq}} - \sigma^{Y} - R(p) \leq 0$
    - Plastic flow $\Delta\boldsymbol{\varepsilon}^{\mathbf{pl}} = \Delta p \mathbf{N}$ & $\mathbf{N} = \frac{\partial f}{\partial \boldsymbol{\sigma}}$
  - Local damage model
    - Apparent-effective stress tensors $\boldsymbol{\sigma} = (1 - D)\hat{\boldsymbol{\sigma}}$
    - Plastic flow in the effective stress space
    - Damage evolution $\Delta D = F_D(\boldsymbol{\varepsilon}, \Delta p)$
  - Non-Local damage model [Peerlings et al., 1996]
    - Damage evolution $\Delta D = F_D(\boldsymbol{\varepsilon}, \Delta \tilde{p})$
    - Anisotropic governing equation $\tilde{p} - \nabla \cdot (\mathbf{c}_{\mathrm{g}} \cdot \nabla \tilde{p}) = p$

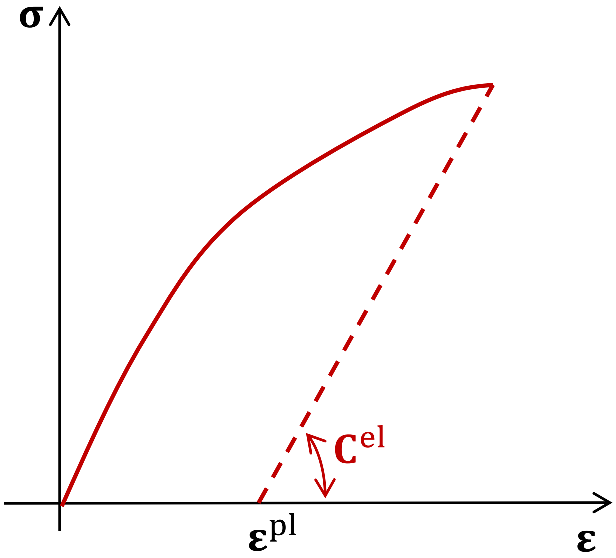

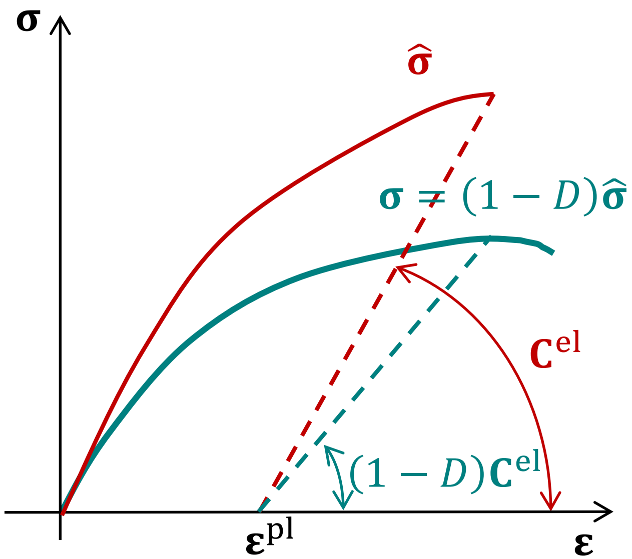

- Laminate studies
  - Bulk material law
    - Non-local damage-enhanced MFH
    - Intra-laminar failure
    - Account for anisotropy
  - Interface
    - DG/Cohesive zone model
    - Inter-laminar failure

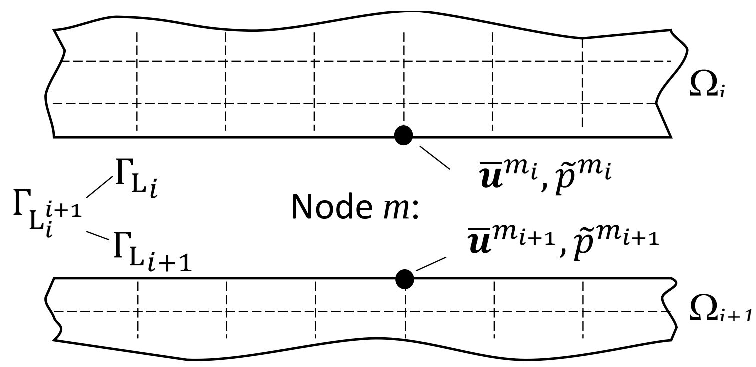

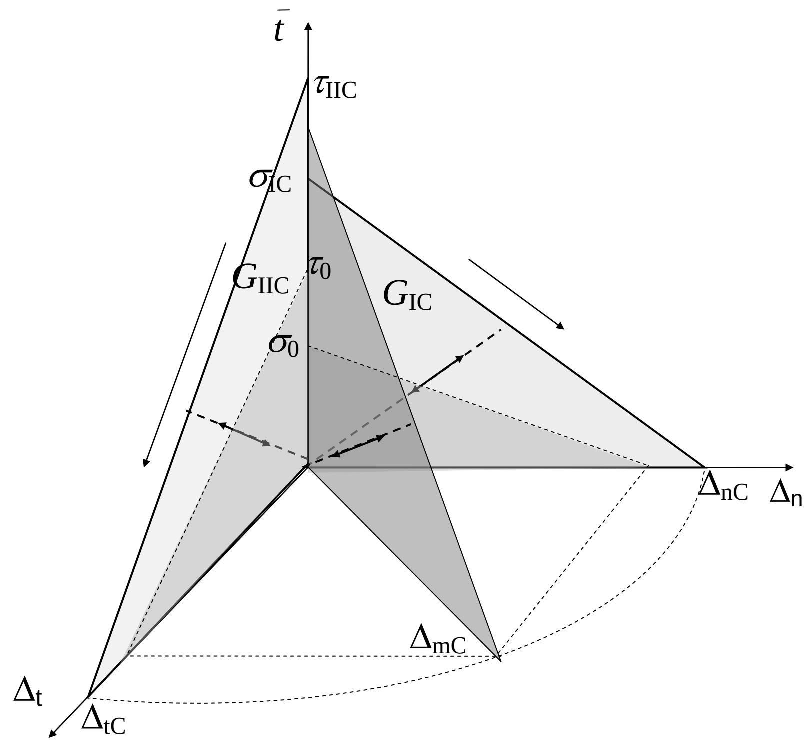

Non-Local Damage Mean-Field-Homogenization

- $[45^o{}_4 / -45^o{}_4]_S$- open hole laminate (epoxy- with 60% UD CF)

Intra-laminar failure along fiber directions

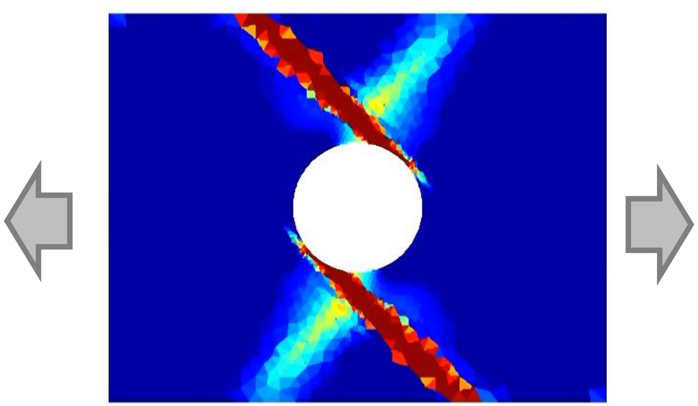

-45º-ply

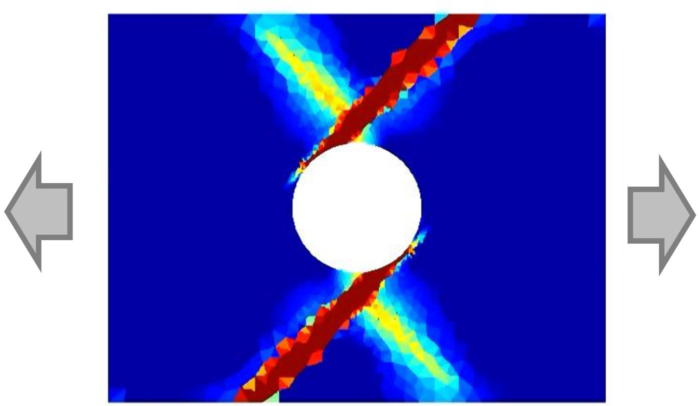

45º-ply

Inter-laminar failure matches experimental results

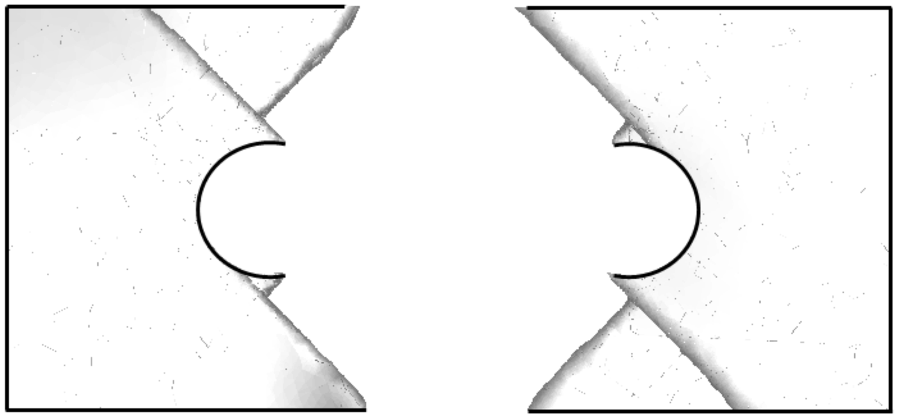

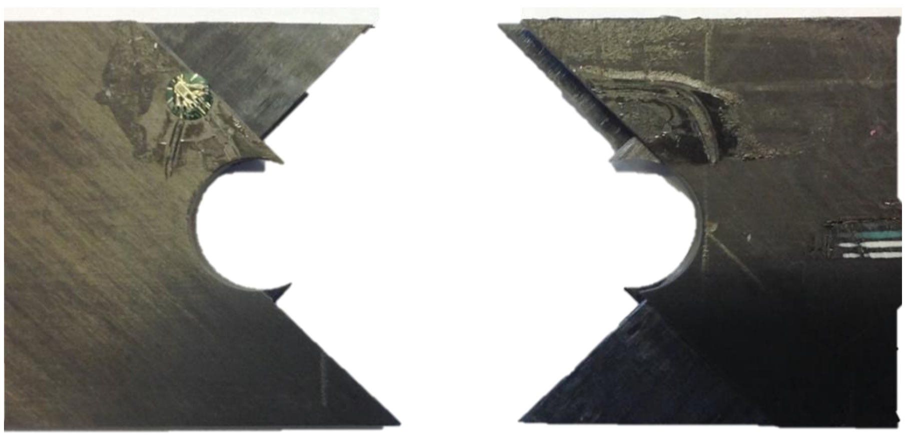

Non-Local Damage Mean-Field-Homogenization

- $[90^o / 45^o / -45^o / 90^o / 0^o]_S$- open hole laminate
  - Intra-laminar failure along fiber directions (experiments: IMDEA Materials)

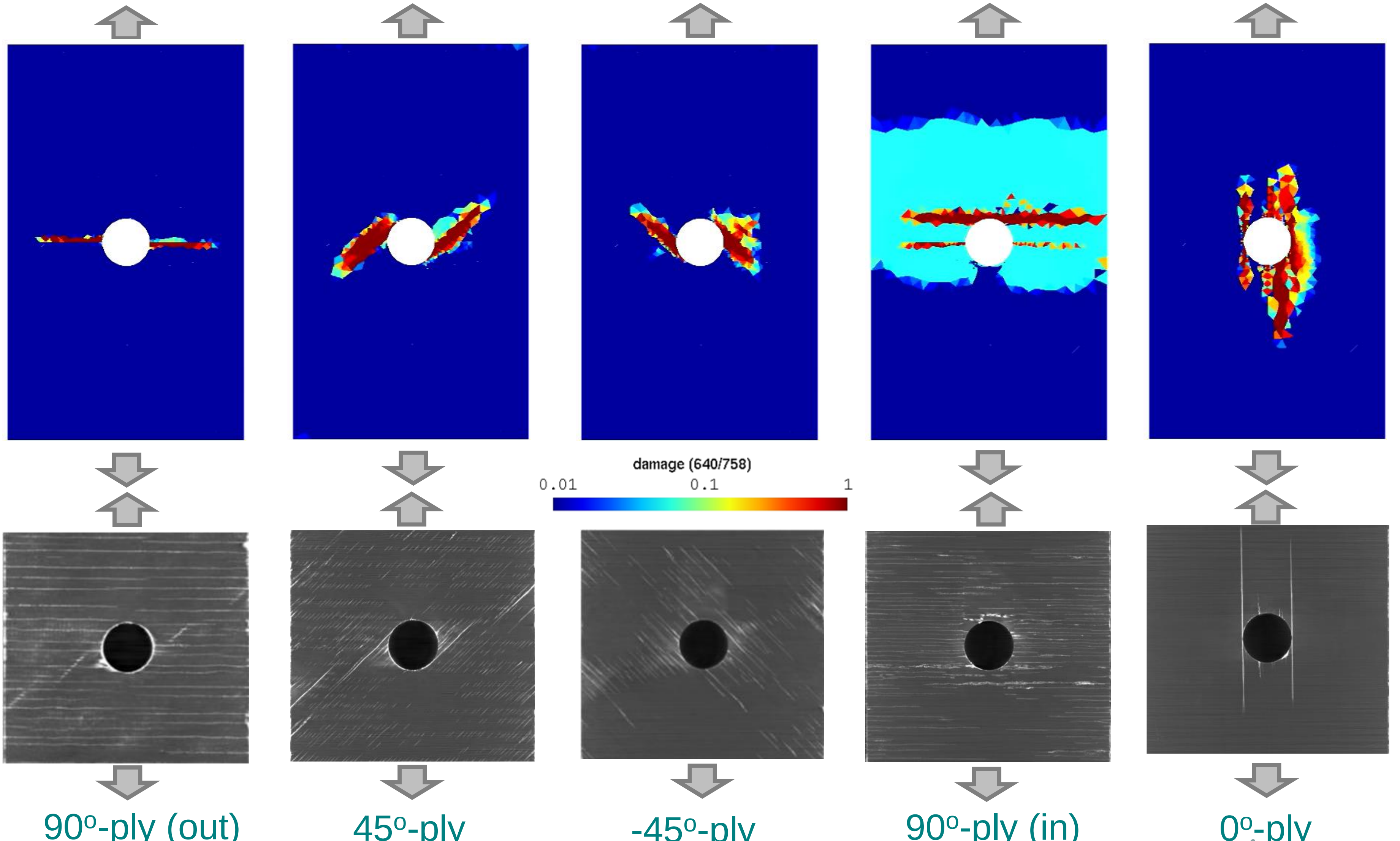

Non-Local Damage Mean-Field-Homogenization

- [90º / 45º / -45º / 90º / 0º]$_S$- open hole laminate
  - Inter-laminar failure compared to experimental results (experiments: IMDEA Materials)

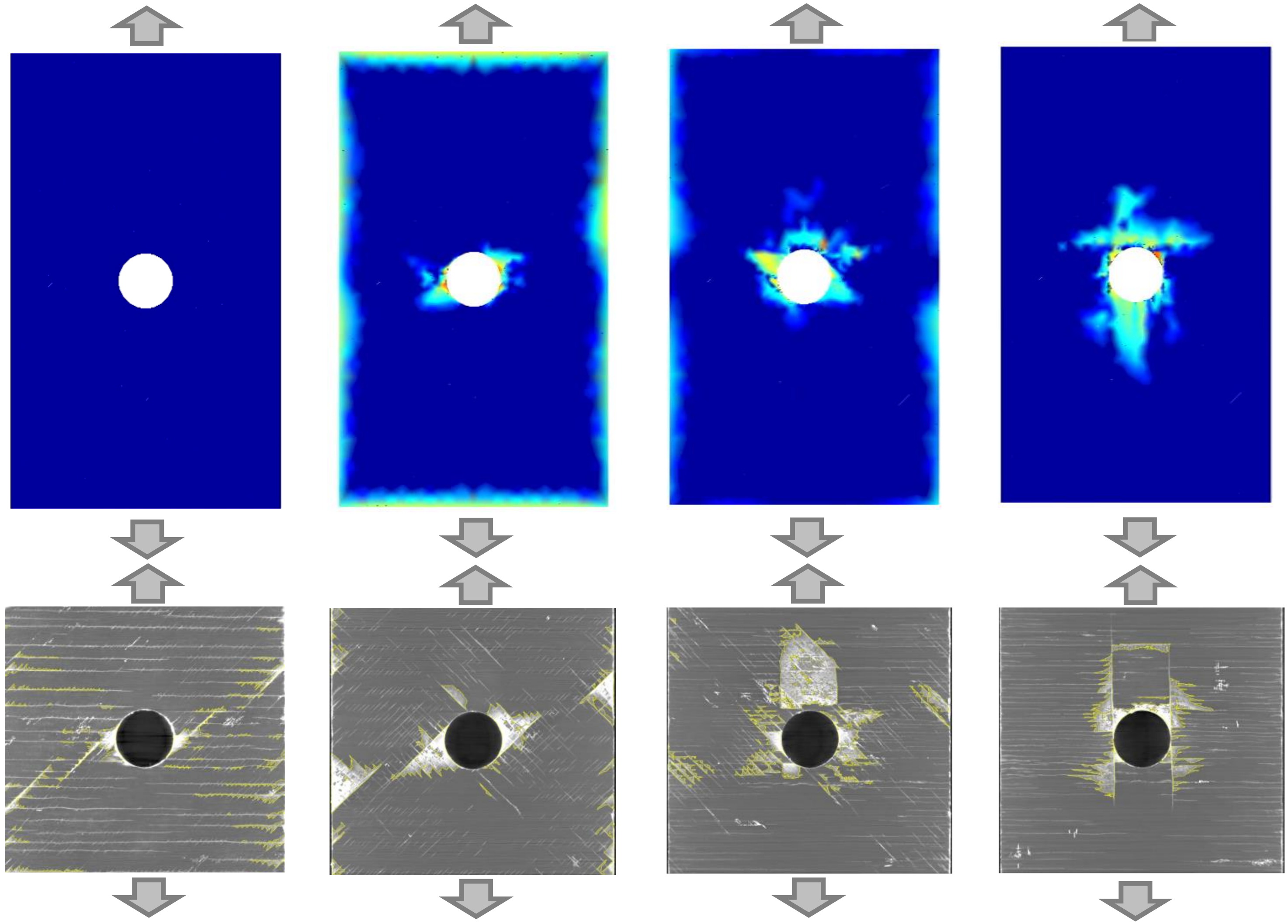

90º (out) / 45º | 45º / -45º | -45º / 90º (in) | 90º (in) / 0º

Non-Local Damage Mean-Field-Homogenization

- SIMUCOMP ERA-NET project
  - e-Xstream, CENAERO, ULiège (Belgium)
  - IMDEA Materials (Spain)
  - CRP Henri-Tudor (Luxemburg)
- Publications (doi)
  - 10.1016/j.compstruct.2015.02.070
  - 10.1016/j.ijsolstr.2013.07.022
  - 10.1016/j.ijplas.2013.06.006
  - 10.1016/j.cma.2012.04.011
  - 10.1007/978-1-4614-4553-1_13

Boundary conditions and tangent operator in multi-physics computational homogenization

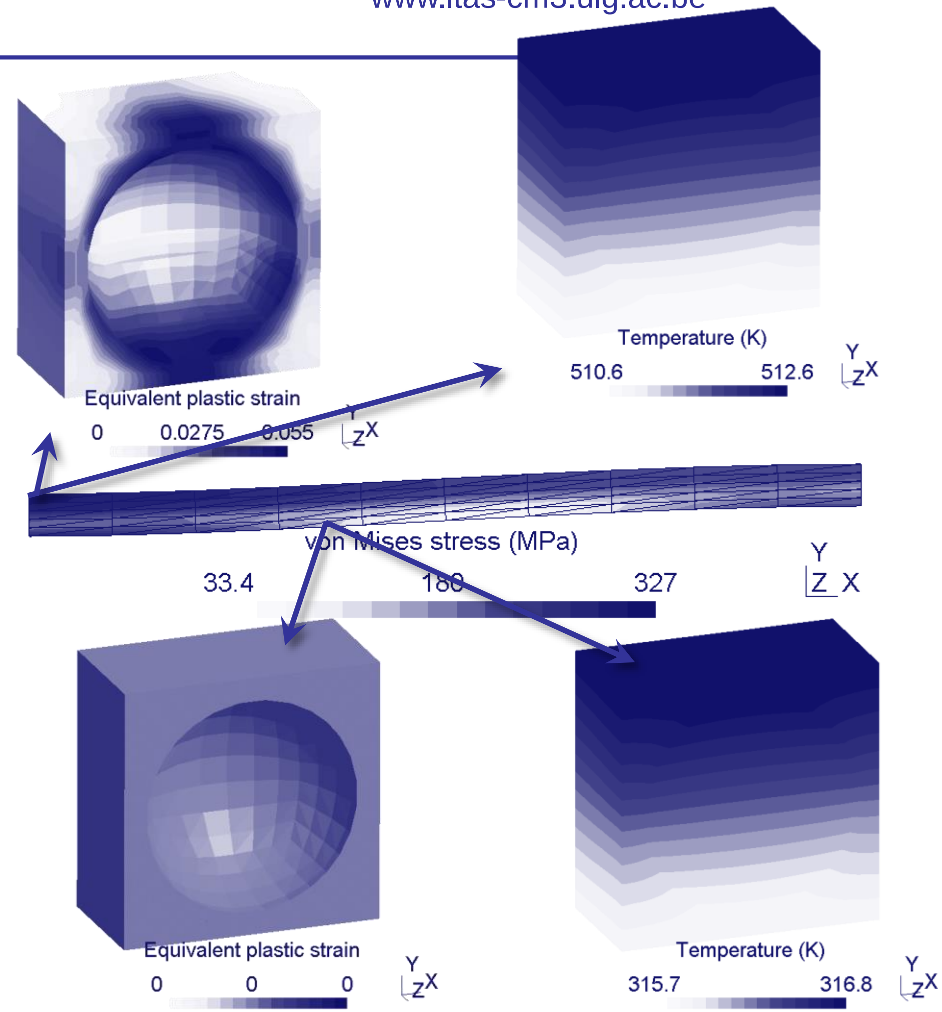

ARC 09/14-02 BRIDGING - From imaging to geometrical modelling of complex micro structured materials: Bridging computational engineering and material science

The authors gratefully acknowledge the financial support from F.R.S-F.N.R.S. under the project number PDR T.1015.14

- Multi-scale modeling
  - 2 problems are solved concurrently
    - The macro-scale problem
    - The meso-scale problem (on a meso-scale Volume Element)

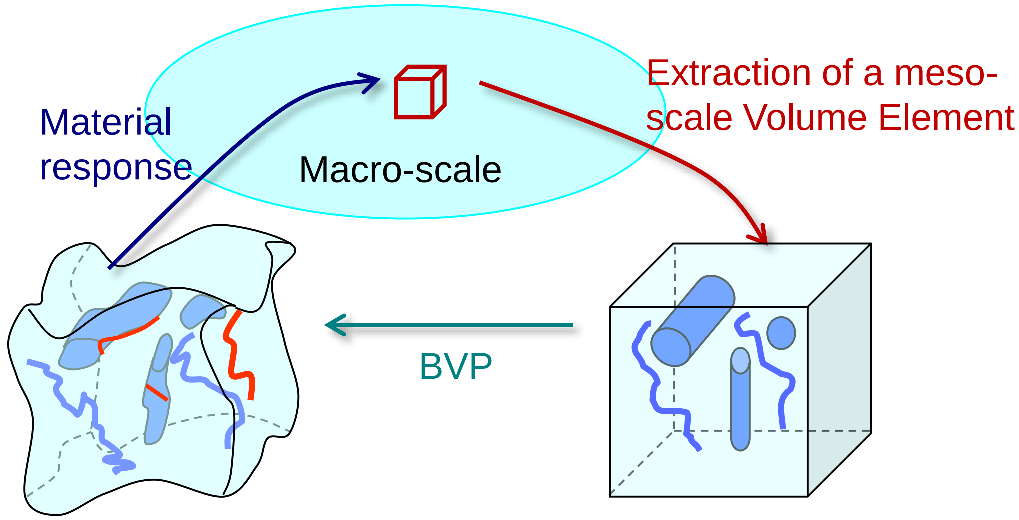

- Length-scales separation

$$L_{\text{macro}} >> L_{\text{VE}} >> L_{\text{micro}}$$

For accuracy: Size of the meso-scale volume element smaller than the characteristic length of the macro-scale loading

To be statistically representative: Size of the meso-scale volume element larger than the characteristic length of the micro-structure

- Generalized multi-physics representation
  - Strong form $\mathcal{P} \cdot \nabla_0 = 0$
  - Fully-coupled constitutive law $\mathcal{P} = \mathcal{P}\left(\mathcal{X}^C, \mathcal{F}; \mathcal{Z}\right)$
    - $\mathcal{F}$: generalized deformation gradient, $\mathcal{X}^C$: fields appearing in the constitutive relations
    - $\mathcal{Z}$: internal variables
    - Tangent operators $\mathcal{L} = \frac{\partial \mathcal{P}}{\partial \mathcal{F}}$ & $\mathcal{J} = \frac{\partial \mathcal{P}}{\partial \mathcal{X}^C}$ but also $\mathcal{Y}_\mathcal{F} = \frac{\partial \mathcal{Z}}{\partial \mathcal{F}}$ & $\mathcal{Y}_{\mathcal{X}^C} = \frac{\partial \mathcal{Z}}{\partial \mathcal{X}^C}$
- Two-scale procedure

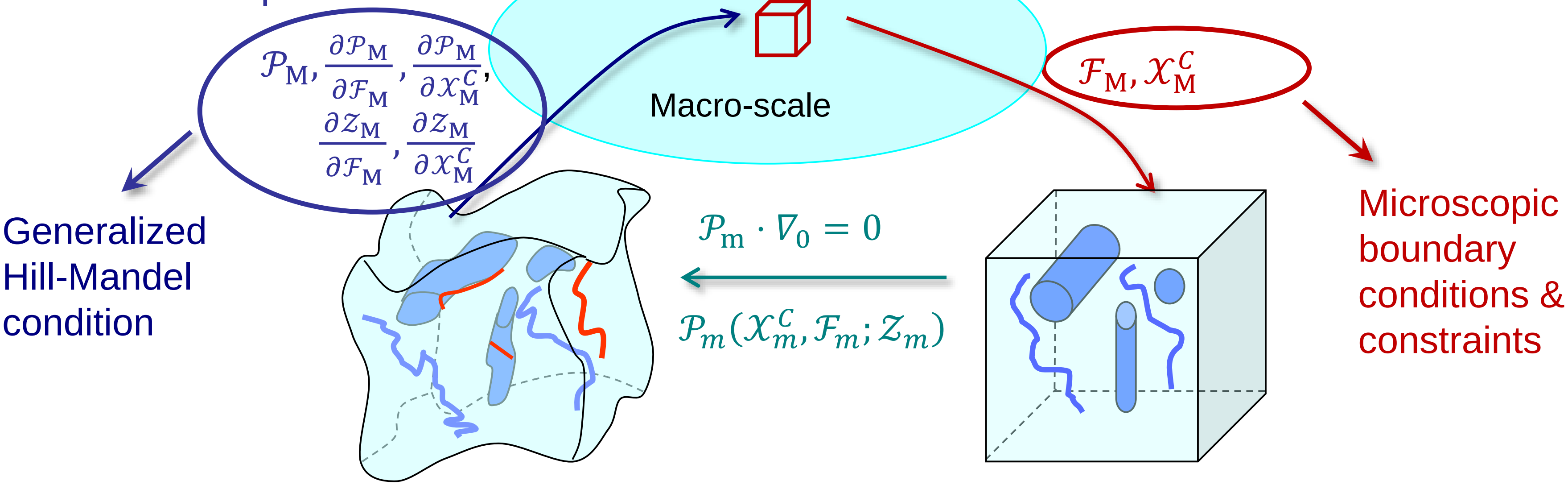

Boundary conditions and tangent operator in FE^2

- Generalized microscopic boundary conditions
  - Arbitrary field k kinematics: $\mathcal{X}^k_{\mathrm{m}} = \mathcal{X}^k_{\mathrm{M}} + \mathcal{F}^k_{\mathrm{M}} \cdot \mathrm{X}_{\mathrm{m}} + \mathcal{W}^k_{\mathrm{m}}$

    Fluctuation
  - Constrained field k equivalence: $\int_{\omega_0} C^k_m \mathcal{X}^{C^k}_{\mathrm{m}}\, d\omega = \int_{\omega_0} C^k_m d\omega\, \mathcal{X}^{C^k}_{\mathrm{M}}$
  - E.g. periodic boundary conditions

    Define an interpolant map

    $$\mathbb{S}^i = \sum \mathbb{N}^i_k(\boldsymbol{X}_m) a^i_k$$

    Substitute fluctuation fields

    $$W^k_m(\boldsymbol{X}^+_m) = \mathbb{S}^i(\boldsymbol{X}^-_m) = W^k_m(\boldsymbol{X}^-_m)$$

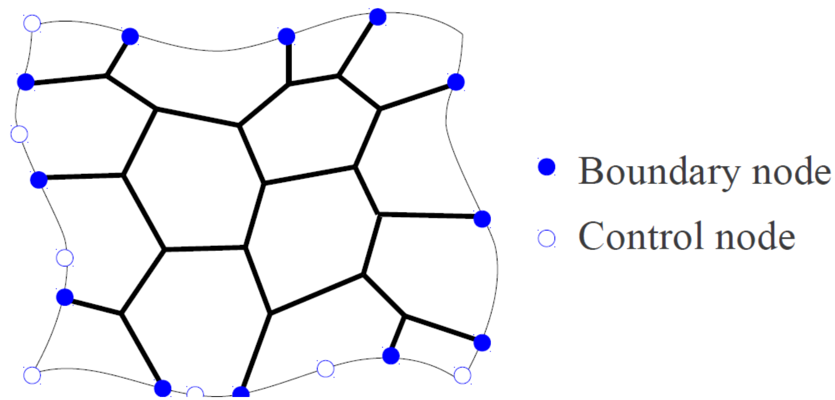

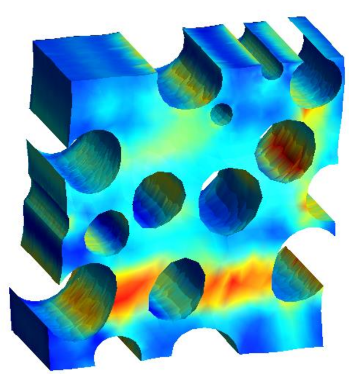

- Microscale BVP
  - Weak formulation

$$\begin{cases} \mathcal{P}_\mathrm{m}\cdot\nabla_0 = 0 \qquad \text{with } \mathcal{P}_m(\mathcal{X}_m^C, \mathcal{F}_m; \mathcal{Z}_m) \\ \mathcal{X}_\mathrm{m}^k = \mathcal{X}_\mathrm{M}^k + \mathcal{F}_\mathrm{M}^k \cdot \mathrm{X}_\mathrm{m} + \mathcal{W}_\mathrm{m}^k \\ \int_{\omega_0} C_m^k {\mathcal{X}_\mathrm{m}^C}^k \, d\omega = \int_{\omega_0} C_m^k d\omega \, {\mathcal{X}_\mathrm{M}^C}^k \end{cases}$$

  - Weak finite element constrained form ($\omega_0 = \cup_e \, \omega^e$)

$$\begin{cases} \mathbf{f}_\mathrm{m}(\boldsymbol{\mathcal{U}}_m) - \mathbf{C}^\mathrm{T}\boldsymbol{\lambda} = 0 \\ \mathbf{C}\boldsymbol{\mathcal{U}}_m - \mathbf{S}\begin{bmatrix} \mathcal{F}_\mathrm{M} \\ \mathcal{X}_\mathrm{M}^C \end{bmatrix} = 0 \end{cases}$$

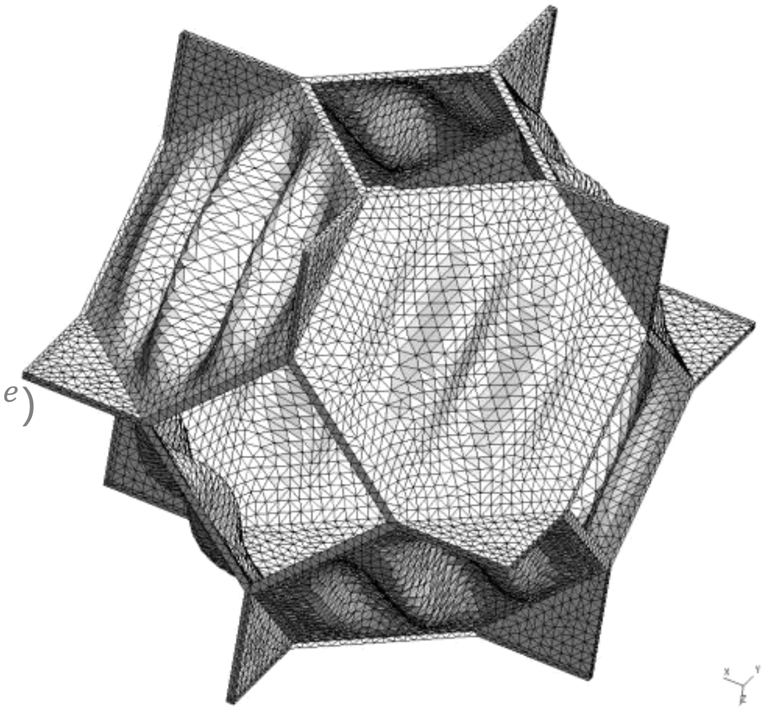

  - System linearization

$$\begin{cases} \mathbf{Q}^\mathrm{T}\dfrac{\partial \mathbf{f}_\mathrm{m}}{\partial \boldsymbol{\mathcal{U}}_m}\mathbf{Q}\delta\boldsymbol{\mathcal{U}}_m + \mathbf{r} - \mathbf{Q}^\mathrm{T}\dfrac{\partial \mathbf{f}_\mathrm{m}}{\partial \boldsymbol{\mathcal{U}}_m}\mathbf{C}^\mathrm{T}(\mathbf{C}\mathbf{C}^\mathrm{T})^{-1}\left(\mathbf{r}_c - \mathbf{S}\begin{bmatrix} \delta\mathcal{F}_\mathrm{M} \\ \delta\mathcal{X}_\mathrm{M}^C \end{bmatrix}\right) = 0 \\ \mathbf{C}\delta\boldsymbol{\mathcal{U}}_m + \mathbf{r}_\mathrm{c} - \mathbf{S}\begin{bmatrix} \delta\mathcal{F}_\mathrm{M} \\ \delta\mathcal{X}_\mathrm{M}^C \end{bmatrix} = 0 \qquad \& \qquad \mathbf{Q} = \mathbf{I} - \mathbf{C}^\mathrm{T}(\mathbf{C}\mathbf{C}^\mathrm{T})^{-1}\mathbf{C} \end{cases}$$

Boundary conditions and tangent operator in FE^2

- Multi-scale resolution
  - System linearization

$$\begin{cases} \mathbf{Q}^{\mathrm{T}} \dfrac{\partial \mathbf{f}_{\mathrm{m}}}{\partial \boldsymbol{\mathcal{U}}_m} \mathbf{Q} \delta \boldsymbol{\mathcal{U}}_m + \mathbf{r} - \mathbf{Q}^{\mathrm{T}} \dfrac{\partial \mathbf{f}_{\mathrm{m}}}{\partial \boldsymbol{\mathcal{U}}_m} \mathbf{C}^{\mathrm{T}} \left(\mathbf{C}\mathbf{C}^{\mathrm{T}}\right)^{-\mathbf{1}} \left(\mathbf{r}_c - \mathbf{S} \begin{bmatrix} \delta \mathcal{F}_{\mathrm{M}} \\ \delta \mathcal{X}_{\mathrm{M}}^{C} \end{bmatrix} \right) = 0 \\ \mathbf{C} \delta \boldsymbol{\mathcal{U}}_m + \mathbf{r}_{\mathrm{c}} - \mathbf{S} \begin{bmatrix} \delta \mathcal{F}_{\mathrm{M}} \\ \delta \mathcal{X}_{\mathrm{M}}^{C} \end{bmatrix} = 0 \qquad \& \qquad \mathbf{Q} = \mathbf{I} - \mathbf{C}^{\mathrm{T}} \left(\mathbf{C}\mathbf{C}^{\mathrm{T}}\right)^{-\mathbf{1}} \mathbf{C} \end{cases}$$

  - FEM resolution: $\delta \mathcal{F}_{\mathrm{M}} = \delta \mathcal{X}_{\mathrm{M}}^{C} = 0$

$$\delta \boldsymbol{\mathcal{U}}_m = -\widetilde{\mathbf{K}}^{-1} \left(\mathbf{r} + \left(\mathbf{C}^{\mathrm{T}} - \mathbf{Q}^{\mathrm{T}} \frac{\partial \mathbf{f}_{\mathrm{m}}}{\partial \boldsymbol{\mathcal{U}}_m} \mathbf{C}^{\mathrm{T}} \left(\mathbf{C}\mathbf{C}^{\mathrm{T}}\right)^{-1} \right) \mathbf{r}_c \right)$$

  - Constraints effect: $\mathbf{r} = \mathbf{r}_c = 0$

$$\frac{\partial \boldsymbol{\mathcal{U}}_m}{\partial \left[\mathcal{F}_{\mathrm{M}} \quad \mathcal{X}_{\mathrm{M}}^{C} \right]^{T}} = \widetilde{\mathbf{K}}^{-1} \left(\mathbf{C}^{\mathrm{T}} - \mathbf{Q}^{\mathrm{T}} \frac{\partial \mathbf{f}_{\mathrm{m}}}{\partial \boldsymbol{\mathcal{U}}_m} \mathbf{C}^{\mathrm{T}} \left(\mathbf{C}\mathbf{C}^{\mathrm{T}}\right)^{-1} \right) \mathbf{S}$$

Only one matrix to factorize

$$\widetilde{\mathbf{K}} = \mathbf{C}^{\mathrm{T}} \mathbf{C} + \mathbf{Q}^{\mathrm{T}} \frac{\partial \mathbf{f}_{\mathrm{m}}}{\partial \boldsymbol{\mathcal{U}}_m} \mathbf{Q}$$

  - Macro-scale operators at low cost

$$\begin{bmatrix} \dfrac{\partial \mathcal{P}_{\mathrm{M}}}{\partial \mathcal{F}_{\mathrm{M}}} & \dfrac{\partial \mathcal{P}_{\mathrm{M}}}{\partial \mathcal{X}_{\mathrm{M}}^{C}} \\ \dfrac{\partial \mathcal{Z}_{\mathrm{M}}}{\partial \mathcal{F}_{\mathrm{M}}} & \dfrac{\partial \mathcal{Z}_{\mathrm{M}}}{\partial \mathcal{X}_{\mathrm{M}}^{C}} \end{bmatrix} = \left(\bigwedge_{\omega^e} \frac{1}{V(\omega_0)} \int_{\omega_0^e} \begin{bmatrix} \dfrac{\partial \mathcal{P}_{\mathrm{m}}}{\partial \mathcal{F}_{\mathrm{m}}} \mathbf{B}^e & \dfrac{\partial \mathcal{P}_{\mathrm{m}}}{\partial \mathcal{X}_{\mathrm{m}}^{C}} \mathbf{N}^e \\ \dfrac{\partial \mathcal{Z}_{\mathrm{m}}}{\partial \mathcal{F}_{\mathrm{m}}} \mathbf{B}^e & \dfrac{\partial \mathcal{Z}_{\mathrm{m}}}{\partial \mathcal{X}_{\mathrm{m}}^{C}} \mathbf{N}^e \end{bmatrix} d\omega \right) \frac{\partial \boldsymbol{\mathcal{U}}_m}{\partial \left[\mathcal{F}_{\mathrm{M}} \quad \mathcal{X}_{\mathrm{M}}^{C} \right]^{T}}$$

- Thermo-elasto-plasticity

$$\left\{\begin{aligned} &\mathbf{P}_{\mathrm{M}} \cdot \boldsymbol{\nabla}_0 = 0 \\ &\rho_{\mathrm{M}} C_{v\mathrm{M}} \dot{\vartheta}_{\mathrm{M}} - \mathcal{D}_{\mathrm{M}} + \mathbf{q}_{\mathrm{M}} \cdot \boldsymbol{\nabla}_0 = 0 \end{aligned}\right.$$

$$\left\{\begin{aligned} &\mathbf{P}_{\mathrm{M}} = \frac{1}{V(\omega_0)} \int_{\omega_0} \mathbf{P}_{\mathrm{m}} d\omega \\ &\boldsymbol{q}_{\mathrm{M}} = \frac{1}{V(\omega_0)} \int_{\omega_0} \boldsymbol{q}_{\mathrm{m}} d\omega \\ &\rho_{\mathrm{M}} C_{v\mathrm{M}} = \frac{1}{V(\omega_0)} \int \rho_{\mathrm{m}} C_{v\mathrm{m}} d\omega \\ &\mathcal{D}_{\mathrm{M}} = \frac{1}{V(\omega_0)} \int \mathcal{D}_{\mathrm{m}} d\omega \\ &\quad \& \\ &\frac{\partial \mathbf{P}_{\mathrm{M}}}{\partial \mathbf{F}_{\mathrm{M}}}, \frac{\partial \mathbf{P}_{\mathrm{M}}}{\partial \vartheta_{\mathrm{M}}}, \frac{\partial \mathbf{P}_{\mathrm{M}}}{\partial \boldsymbol{\nabla}_0 \vartheta_{\mathrm{M}}}, \\ &\frac{\partial \mathbf{q}_{\mathrm{M}}}{\partial \mathbf{F}_{\mathrm{M}}}, \frac{\partial \mathbf{q}_{\mathrm{M}}}{\partial \vartheta_{\mathrm{M}}}, \frac{\partial \mathbf{q}_{\mathrm{M}}}{\partial \boldsymbol{\nabla}_0 \vartheta_{\mathrm{M}}}, \\ &\frac{\partial \mathcal{D}_{\mathrm{M}}}{\partial \mathbf{F}_{\mathrm{M}}}, \frac{\partial \mathcal{D}_{\mathrm{M}}}{\partial \vartheta_{\mathrm{M}}}, \frac{\partial \mathcal{D}_{\mathrm{M}}}{\partial \boldsymbol{\nabla}_0 \vartheta_{\mathrm{M}}} \end{aligned}\right.$$

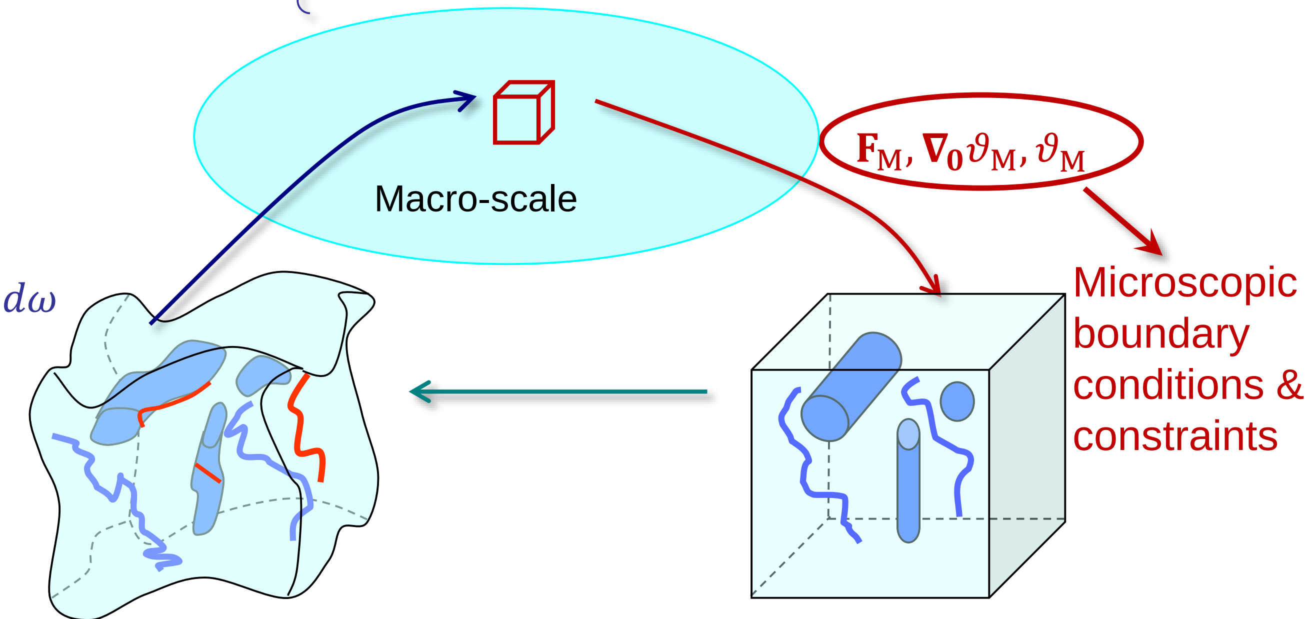

$$\left\{\begin{aligned} &\mathbf{P}_{\mathrm{m}} = \mathbf{P}_{\mathrm{m}}\left(\mathbf{F}_{\mathrm{m}}, \boldsymbol{\nabla}_0 \vartheta_{\mathrm{m}}, \vartheta_{\mathrm{m}} ; p, \mathbf{F}_{\mathrm{m}}^{\mathbf{p}}\right) \\ &\mathbf{q}_{\mathrm{m}} = \mathbf{q}_{\mathrm{m}}\left(\mathbf{F}_{\mathrm{m}}, \boldsymbol{\nabla}_0 \vartheta_{\mathrm{m}}, \vartheta_{\mathrm{m}} ; p, \mathbf{F}_{\mathrm{m}}^{\mathbf{p}}\right) \\ &\mathcal{D}_{\mathrm{m}} = \beta \dot{p} \tau + \vartheta \frac{\partial \dot{W}^{\mathrm{el}}}{\partial \vartheta} \\ &\mathbf{P}_{\mathrm{m}} \cdot \boldsymbol{\nabla}_0 = 0 \\ &\mathbf{q}_{\mathrm{m}} \cdot \boldsymbol{\nabla}_0 = 0 \end{aligned}\right.$$

Boundary conditions and tangent operator in FE²

- Thermo-elasto-plasticity
  - Thermal-softening hardening
    $\tau = (\sigma_0 + Hp)\,(1 - \omega_T(T - T_0))$

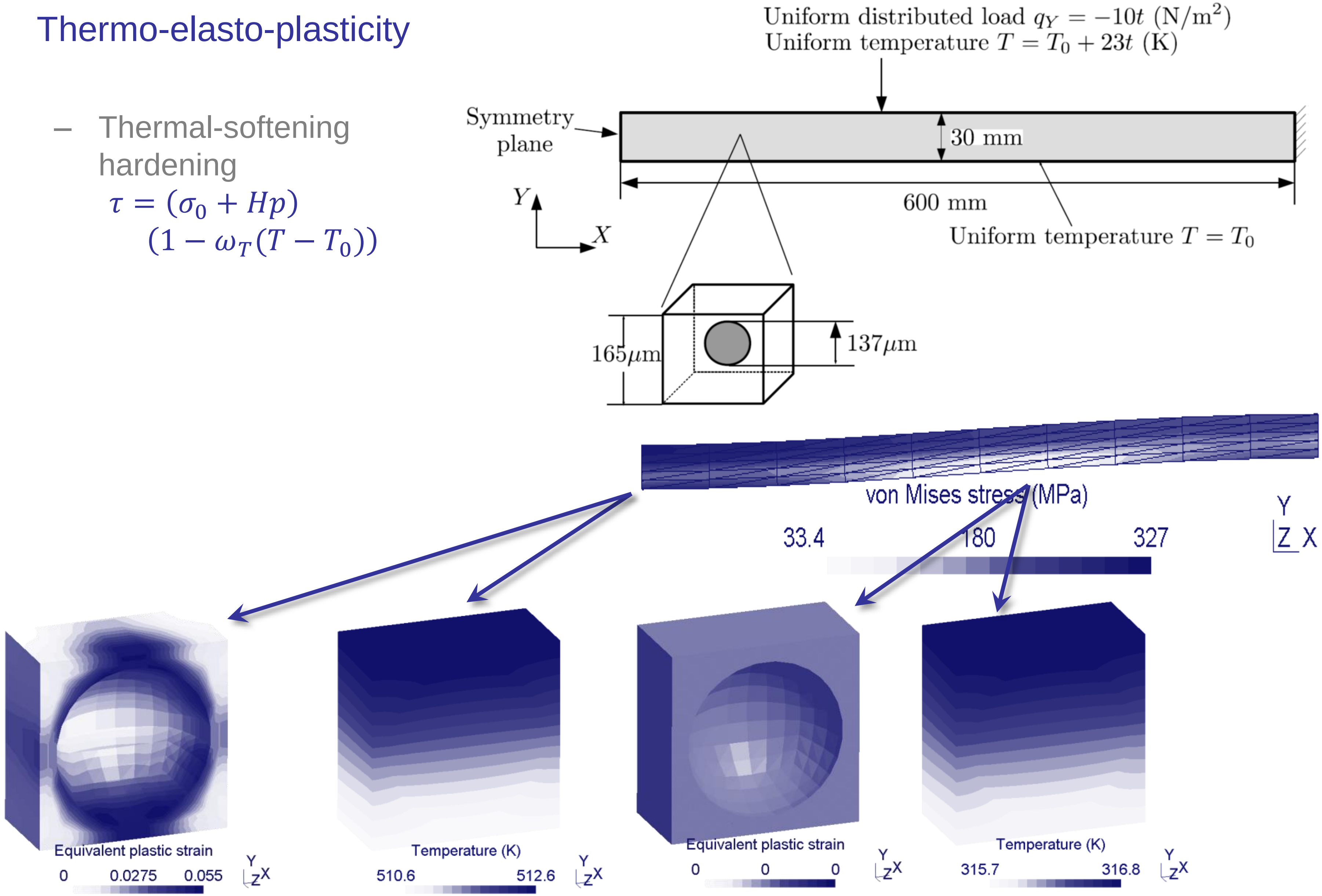

Boundary conditions and tangent operator in FE^2

- BRIDGING ARC project (Periodic boundary conditions)
  - ULiège, Applied Sciences (A&M, EEI, ICD)
  - ULiège, Sciences (CERM)

- PDR T.1015.14 project (MFH with second-order moments)
  - ULiège, UCL (Belgium)

- Publications
  - 10.1007/s00466-016-1358-z
  - 10.1016/j.commatsci.2011.10.017

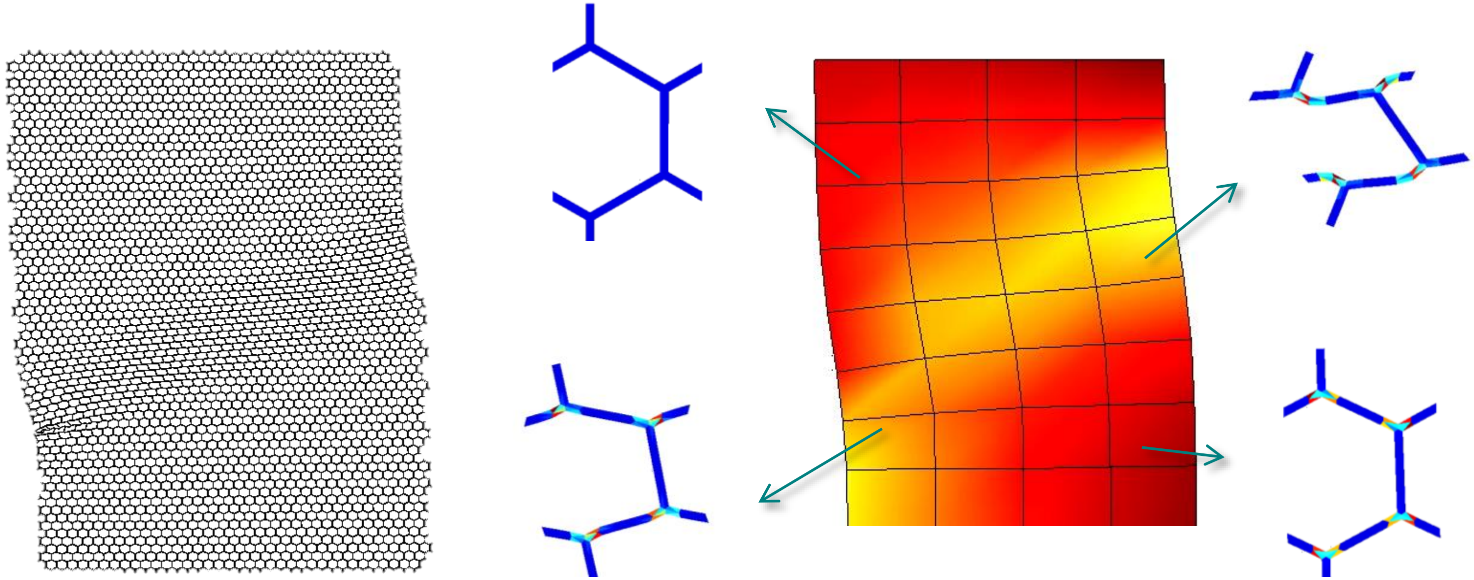

Computational Homogenization For Cellular Materials

ARC 09/14-02 BRIDGING - From imaging to geometrical modelling of complex micro structured materials: Bridging computational engineering and material science

- Multi-scale modeling
  - 2 problems are solved concurrently
    - The macro-scale problem
    - The meso-scale problem (on a meso-scale Volume Element)

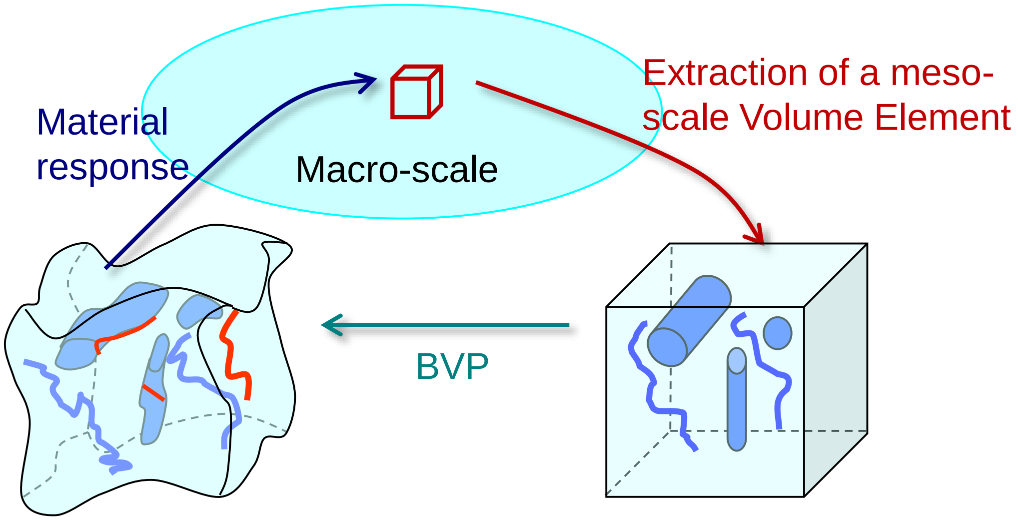

- What if homogenized properties loose ellipticity?
  - Buckling of honeycomb structures

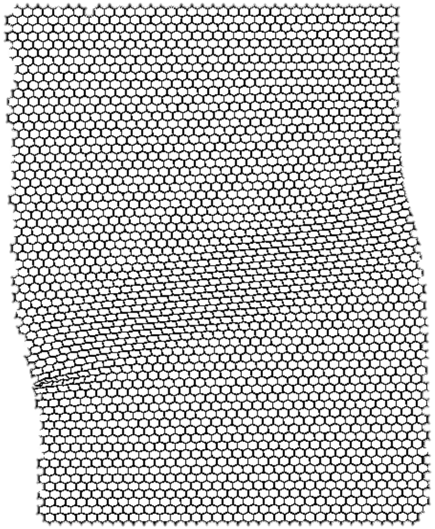

- DG-based second-order FE^2
  - Macro-scale
    - High-order Strain-Gradient formulation
    - C^1 weakly enforced by DG
    - Partitioned mesh (//)
  - Transition
    - Gauss points on different processors
    - Each Gauss point is associated to one mesh and one solver
  - Micro-scale
    - Usual 3D finite elements
    - High-order periodic boundary conditions
      - Non-conforming mesh
      - Use of interpolant functions

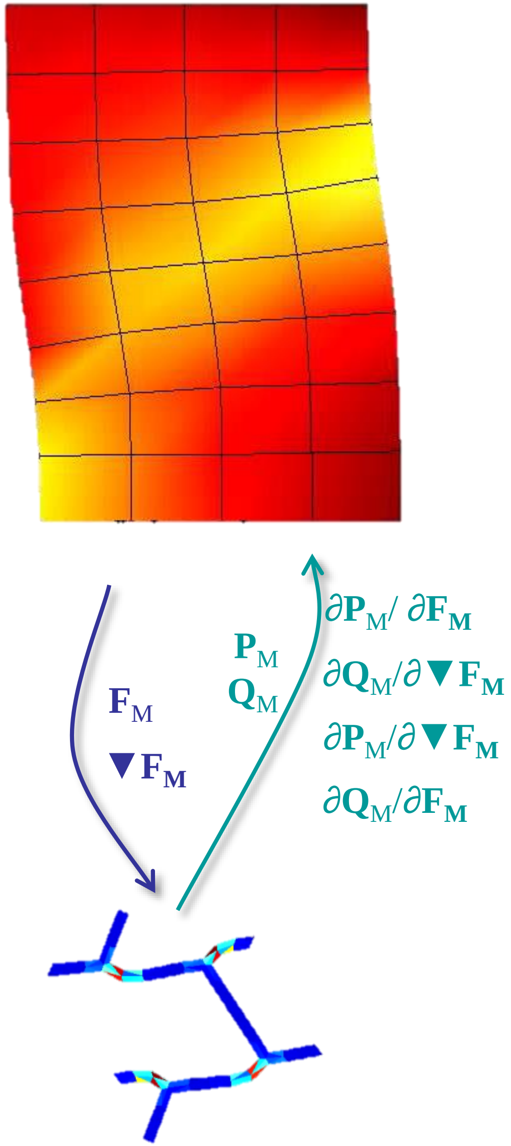

Computational Homogenization For Cellular Materials

- Instabilities
  - Micro-scale: buckling
  - Macro-scale: localization bands
  - Captured owing to
    - Second-order homogenization
    - Ad-hoc periodic boundary conditions
    - Path following method

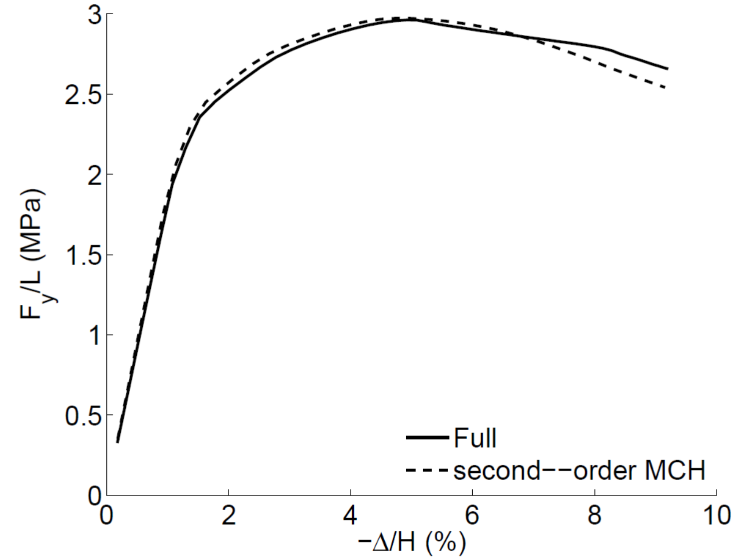

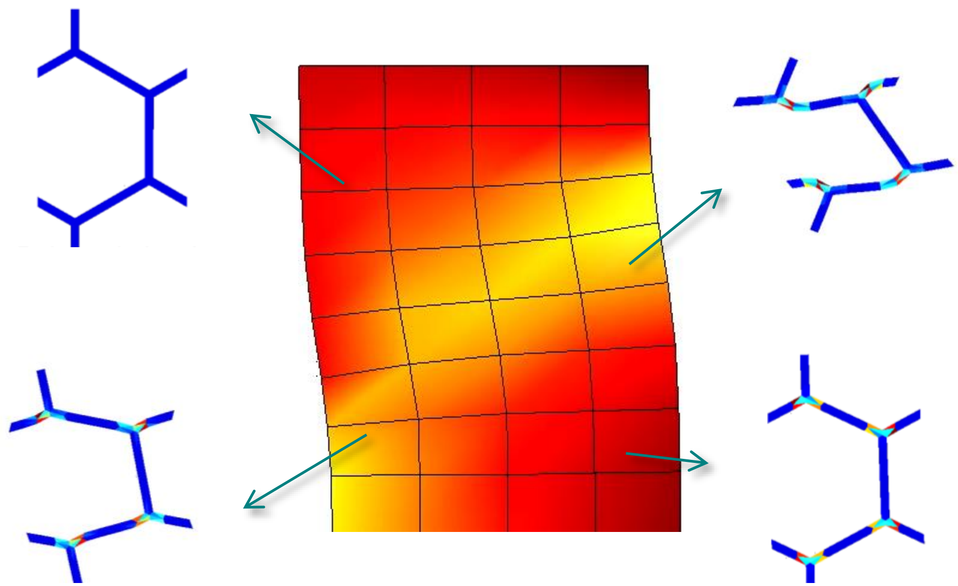

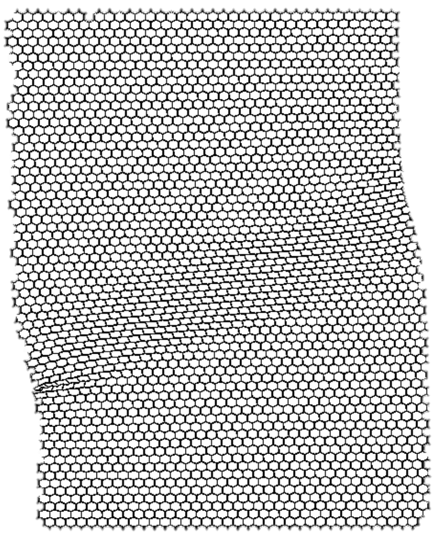

Computational Homogenization For Cellular Materials

- Open-hole plate

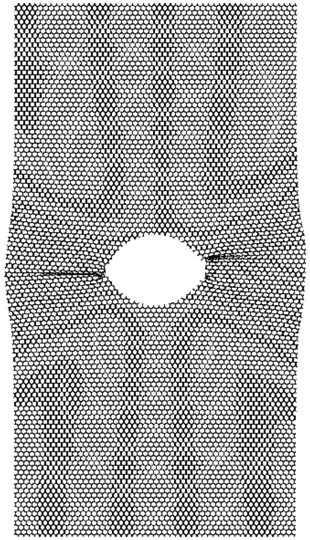

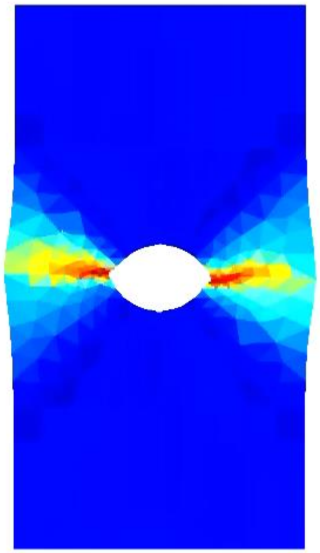

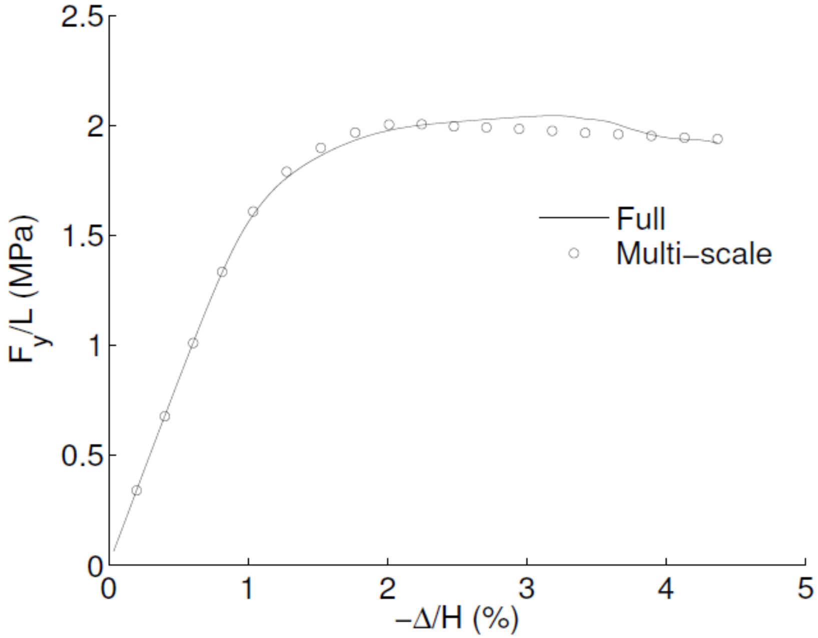

- BRIDGING ARC project
  - ULiège, Applied Sciences (A&M, EEI, ICD)
  - ULiège, Sciences (CERM)
- Publications
  - 10.1016/j.mechmat.2015.07.004
  - 10.1016/j.ijsolstr.2014.02.029
  - 10.1016/j.cma.2013.03.024

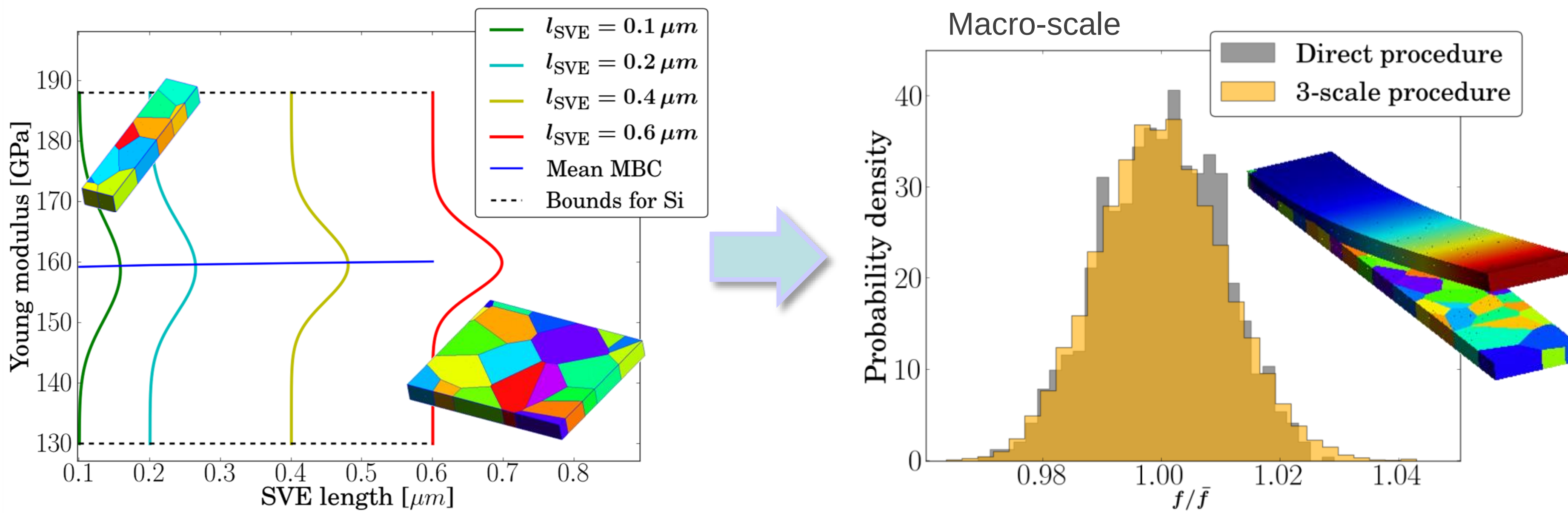

Stochastic 3-Scale Models for Polycrystalline Materials

3SMVIB: The research has been funded by the Walloon Region under the agreement no 1117477 (CT-INT 2011-11-14) in the context of the ERA-NET MNT framework.

Stochastic 3-Scale Models

- Multi-scale modeling
  - 2 problems are solved concurrently
    - The macro-scale problem
    - The meso-scale problem (on a meso-scale Volume Element)

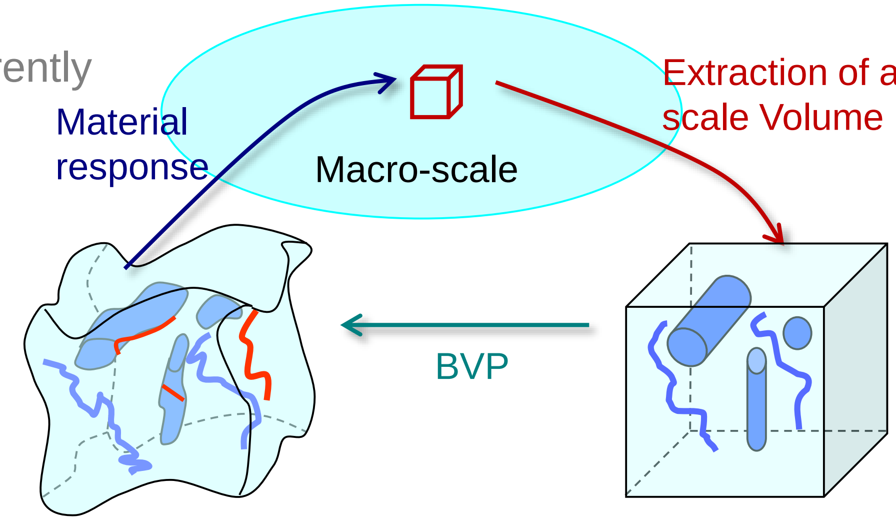

- For structures not several orders larger than the micro-structure size

$L_{macro} >> L_{VE} >\sim L_{micro}$

For accuracy: Size of the meso-scale volume element smaller than the characteristic length of the macro-scale loading

Meso-scale volume element no longer statistically representative:
- **Stochastic Volume Elements**

Stochastic 3-Scale Models

- Key idea

Micro-scale	Meso-scale	Macro-scale
➢ Samples of stochastic volume elements ➢ Random microstructure	➢ Intermediate scale ➢ The distribution of the material property $\mathbb{P}(C)$ is defined	➢ Uncertainty quantification of the macro-scale quantity ➢ Quantity of interest distribution $\mathbb{P}(Q)$

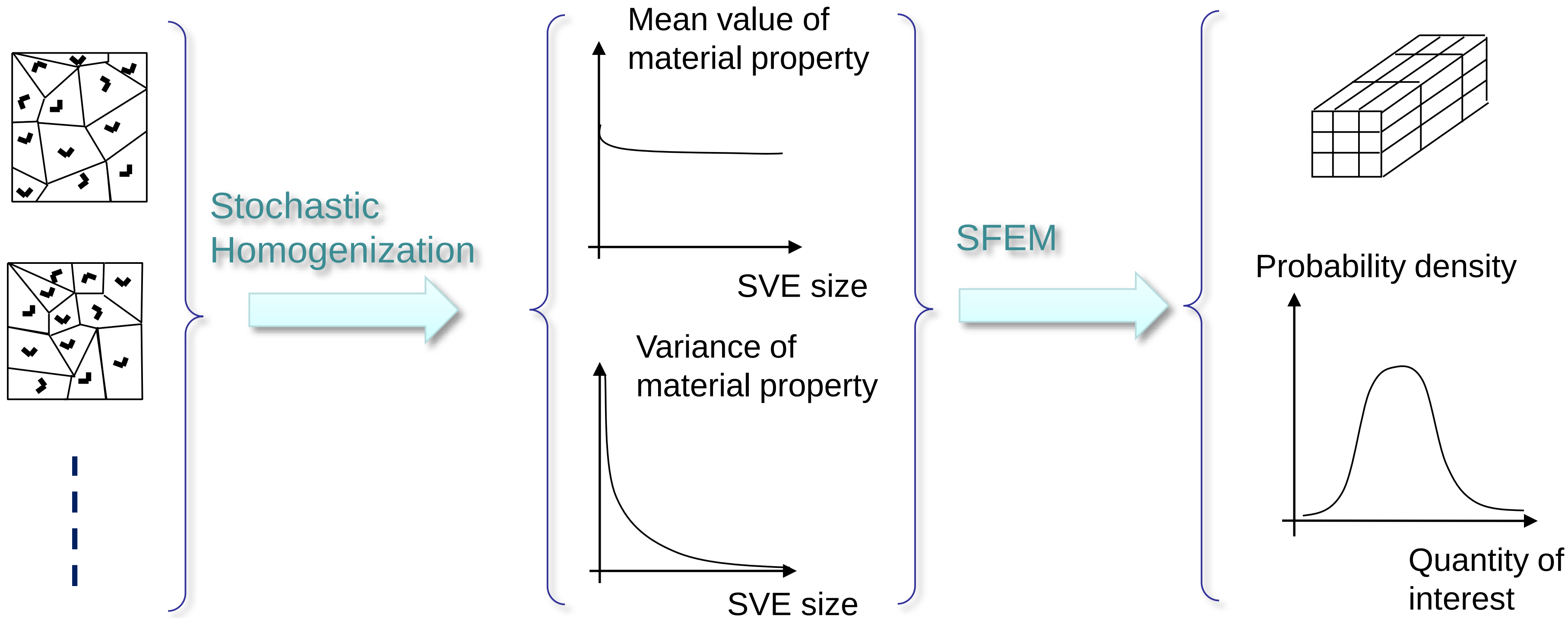

Stochastic 3-Scale Models

- Material structure: grain orientation distribution
  - Grain orientation by XRD (X-ray Diffraction) measurements on 2 µm-thick poly-silicon films

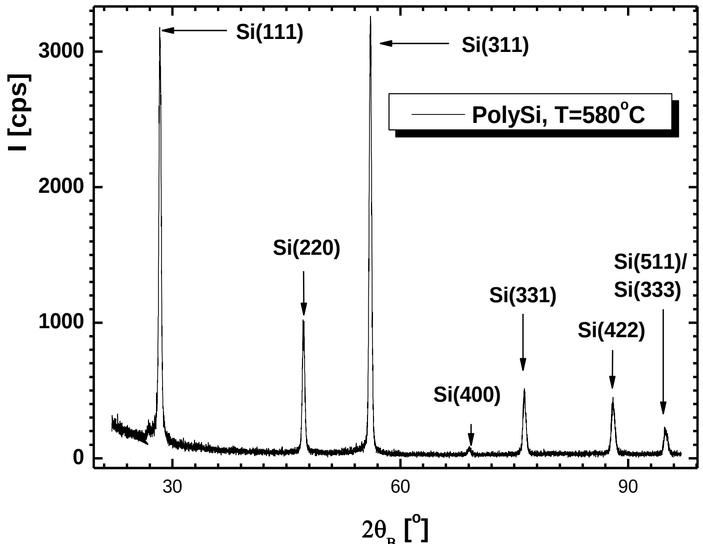

Deposition temperature: 580 ºC

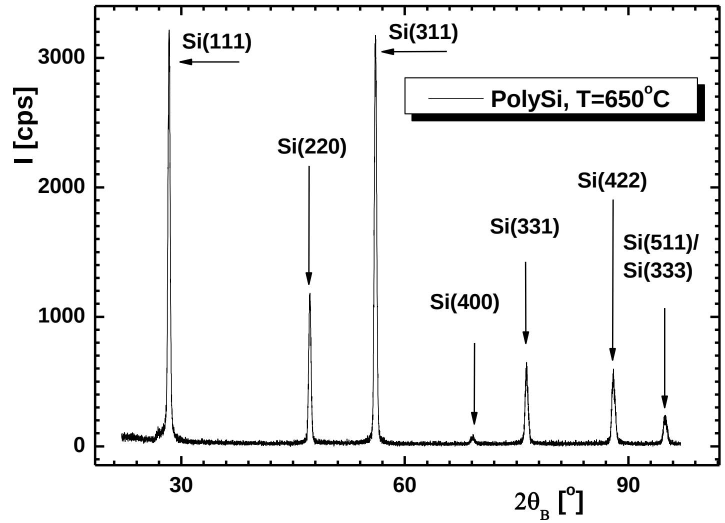

Deposition temperature: 630 ºC

Deposition temperature [ºC]	580	610	630	650
<111> [%]	12.57	19.96	12.88	11.72
<220> [%]	7.19	13.67	7.96	7.59
<311> [%]	42.83	28.83	39.08	38.47
<400> [%]	4.28	5.54	3.13	3.93
<331> [%]	17.97	18.14	21.32	20.45
<422> [%]	15.15	13.86	15.63	17.84

XRD images provided by IMT Bucharest, Rodica Voicu, Angela Baracu, Raluca Muller

- Application to polycrystalline materials: The micro-scale to meso-scale transition
  - Stochastic homogenization

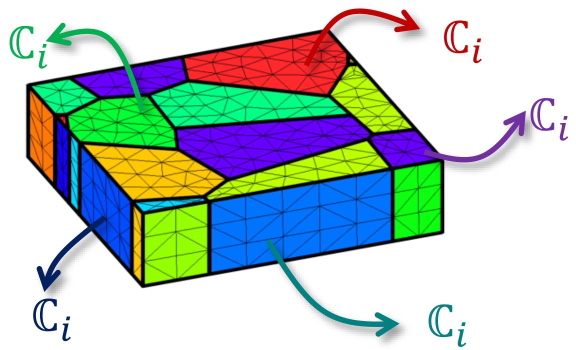

$$\boldsymbol{\sigma}_{m^i} = \mathbb{C}_i : \boldsymbol{\epsilon}_{m^i} \quad , \forall i$$

Stochastic Homogenization

$$\boldsymbol{\sigma}_M = \mathbb{C}_M : \boldsymbol{\epsilon}_M$$

Samples of the meso-scale homogenized elasticity tensors

  - Homogenized Young's modulus distribution

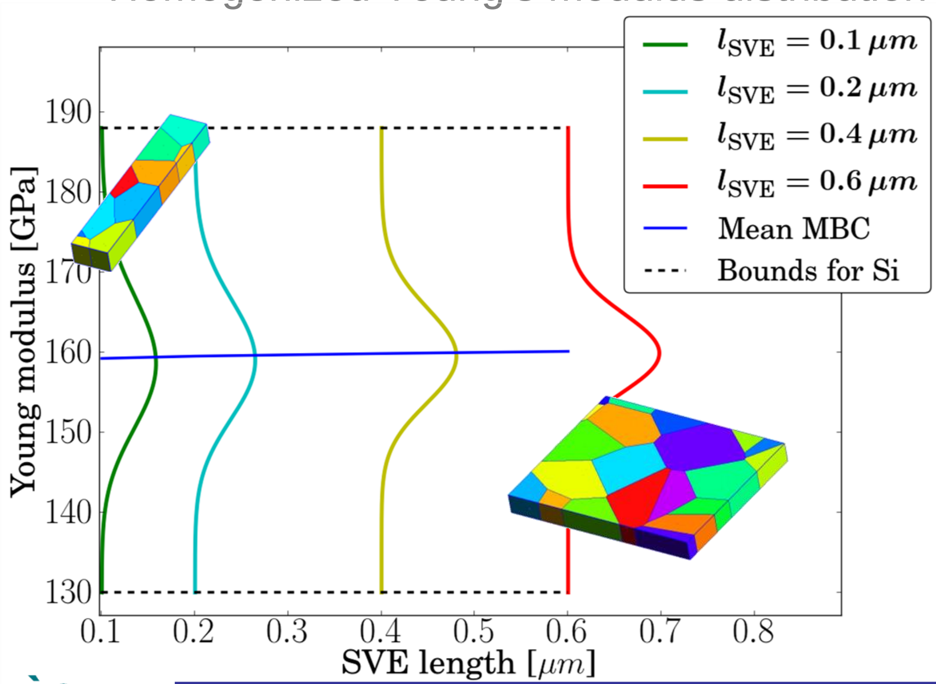

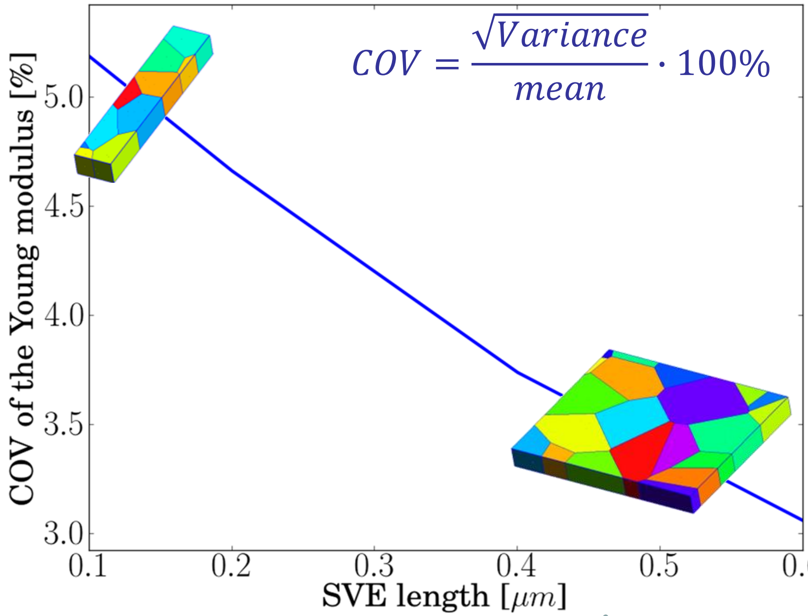

- Application to polycrystalline materials: The meso-scale spatial correlation
  - Use of the window technique

$$R_{\mathbb{C}}^{(rs)}(\boldsymbol{\tau}) = \frac{\mathbb{E}\left[\left(\mathbb{C}^{(r)}(\boldsymbol{x}) - \mathbb{E}\left(\mathbb{C}^{(r)}\right)\right)\left(\mathbb{C}^{(s)}(\boldsymbol{x}+\boldsymbol{\tau}) - \mathbb{E}\left(\mathbb{C}^{(s)}\right)\right)\right]}{\sqrt{\mathbb{E}\left[\left(\mathbb{C}^{(r)} - \mathbb{E}\left(\mathbb{C}^{(r)}\right)\right)^2\right]\mathbb{E}\left[\left(\mathbb{C}^{(s)} - \mathbb{E}\left(\mathbb{C}^{(s)}\right)\right)^2\right]}}$$

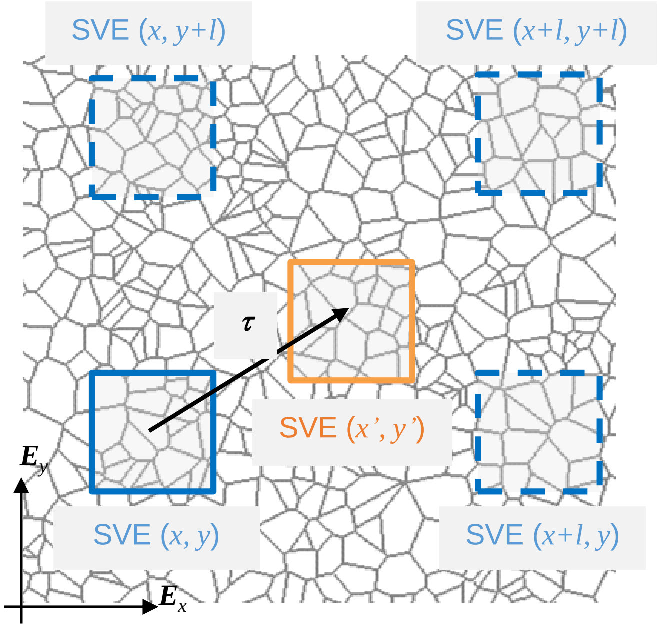

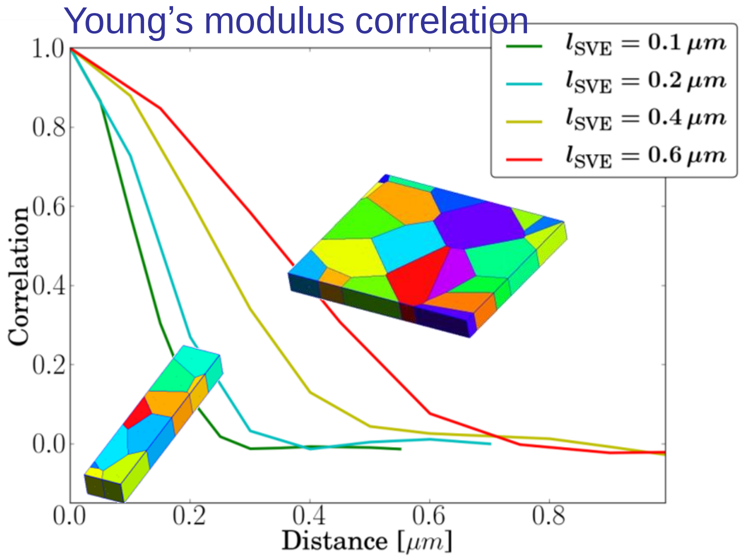

  - Definition of the correlation length $L_{\mathbb{C}}^{(rs)} = \frac{\int_{-\infty}^{\infty} R_{\mathbb{C}}^{(rs)}}{R_{\mathbb{C}}^{(rs)}(0)}$

- Application to polycrystalline materials: The meso-scale random field
  - Accounts for the meso-scale distribution & spatial correlation

Random field with different SVEs sizes

$l_{\mathrm{SVE}} = 0.1\ \mu m$

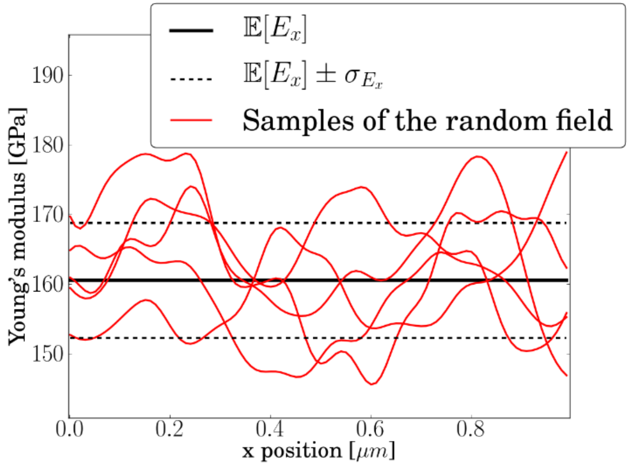

$l_{\mathrm{SVE}} = 0.4\ \mu m$

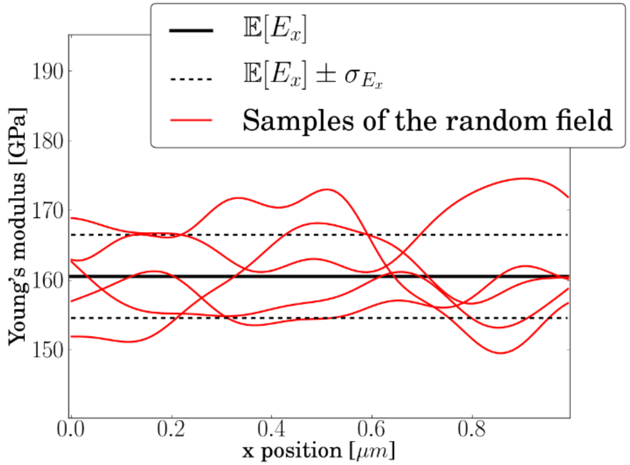

  - Needs to be generated using a stochastic model

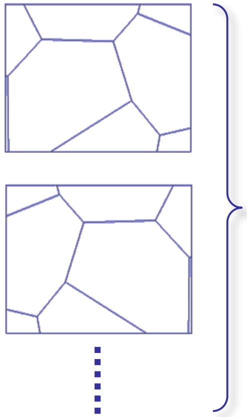

Stochastic model

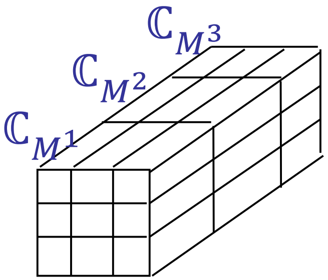

- Stochastic model of Gaussian meso-scale random fields
  - Define the homogenous zero-mean random field $\mathcal{A}'(\boldsymbol{x},\boldsymbol{\theta})$
    - Elasticity tensor $\mathbb{C}_{\mathrm{M}}(x,\theta)$ (matrix form $\boldsymbol{C}_M$) is bounded

$$\boldsymbol{\varepsilon}:(\mathbb{C}_{\mathrm{M}}-\mathbb{C}_{\mathrm{L}}):\boldsymbol{\varepsilon}>0 \qquad \forall\boldsymbol{\varepsilon}$$

    - Use a Cholesky decomposition

$$\boldsymbol{C}_{\mathrm{M}}(\boldsymbol{x},\boldsymbol{\theta})=\boldsymbol{C}_{\mathrm{L}}+\left(\bar{\mathcal{A}}+\mathcal{A}'(\boldsymbol{x},\boldsymbol{\theta})\right)^T\left(\bar{\mathcal{A}}+\mathcal{A}'(\boldsymbol{x},\boldsymbol{\theta})\right)$$

  - Evaluate the covariance function

$$\tilde{R}^{(rs)}_{\mathcal{A}'}(\boldsymbol{\tau})=\sigma_{\mathcal{A}'(r)}\sigma_{\mathcal{A}'(s)}R^{(rs)}_{\mathcal{A}'}(\boldsymbol{\tau}) = \mathbb{E}\left[\left(\mathcal{A}'^{(r)}(\boldsymbol{x})\right)\left(\mathcal{A}'^{(s)}(\boldsymbol{x}+\boldsymbol{\tau})\right)\right]$$

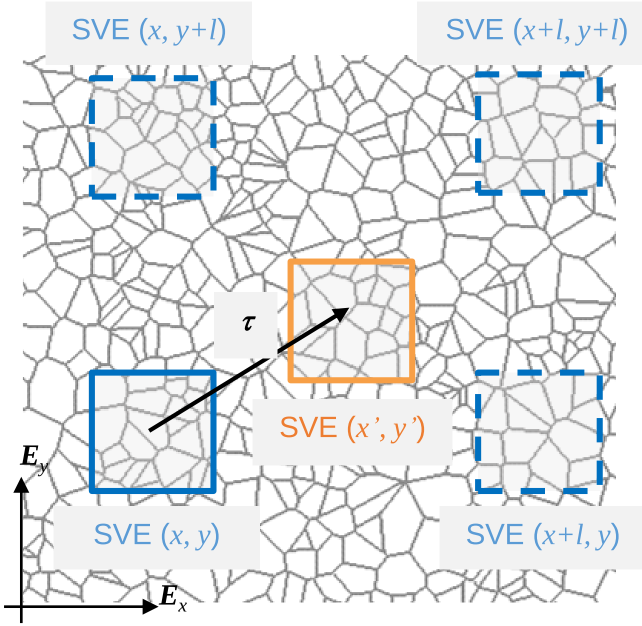

  - Evaluate the spectral density matrix from periodized zero-padded matrix $\tilde{\boldsymbol{R}}^{\mathrm{P}}_{\mathcal{V}'}(\boldsymbol{\tau})$

$$\boldsymbol{S}^{(rs)}_{\mathcal{A}'}\left[\boldsymbol{\omega}^{(\boldsymbol{m})}\right]=\sum_{n}\tilde{R}^{\mathrm{P}\ (rs)}_{\mathcal{A}'}\left[\boldsymbol{\tau}^{(n)}\right]e^{-2\pi i\boldsymbol{\tau}^{(n)}\cdot\boldsymbol{\omega}^{(\boldsymbol{m})}} \ \& \ \ \boldsymbol{S}_{\mathcal{A}'}\left[\boldsymbol{\omega}^{(\boldsymbol{m})}\right]=\boldsymbol{H}_{\mathcal{A}'}\left[\boldsymbol{\omega}^{(\boldsymbol{m})}\right]\boldsymbol{H}^{*}_{\mathcal{A}'}\left[\boldsymbol{\omega}^{(\boldsymbol{m})}\right]$$

  - Generate a Gaussian random field $\mathcal{A}'(\boldsymbol{x},\boldsymbol{\theta})$

$$\mathcal{A}'^{(r)}(\boldsymbol{x},\boldsymbol{\theta})=\sqrt{2\Delta\omega}\,\Re\left(\sum_{s}\sum_{\boldsymbol{m}}\boldsymbol{H}^{(rs)}_{\mathcal{A}'}\left[\boldsymbol{\omega}^{(\boldsymbol{m})}\right]\eta^{(s,\boldsymbol{m})}\,e^{2\pi i\left(\boldsymbol{x}\cdot\boldsymbol{\omega}^{(\boldsymbol{m})}+\boldsymbol{\theta}^{(s,\boldsymbol{m})}\right)}\right)$$

- Stochastic model of non-Gaussian meso-scale random fields
  - Start from micro-sampling of the stochastic homogenization
    - The continuous form of the targeted PSD function

$$\boldsymbol{S}^{\mathrm{T}^{(rs)}}(\boldsymbol{\omega}) = \boldsymbol{\Delta\tau S}_{\mathcal{V}'}^{(rs)}\left[\boldsymbol{\omega}^{(m)}\right] = \boldsymbol{\Delta\tau}\sum_{n}\widetilde{R}^{\mathrm{P}}_{\mathcal{A}'}{}^{(rs)}\left[\boldsymbol{\tau}^{(n)}\right]e^{-2\pi i\boldsymbol{\tau}^{(n)}\cdot\boldsymbol{\omega}^{(m)}}$$

    - The targeted marginal distribution density function $\boldsymbol{F}^{\mathrm{NG}(r)}$ of the random variable $\mathcal{A}'^{(r)}$
    - A marginal Gaussian distribution $\boldsymbol{F}^{G(r)}$ of zero-mean and targeted variance $\boldsymbol{\sigma}_{\mathcal{A}'^{(r)}}$
  - Iterate

Generate Gaussian random vector $\mathcal{A}'^{\mathrm{G}}(\boldsymbol{x})$ from $\boldsymbol{S}^{(rs)}(\boldsymbol{\omega})$

Map $\mathcal{A}'^{G}(\boldsymbol{x})$ to a non-Gaussian field:

$$\mathcal{A}'^{\mathrm{NG}^{(r)}}(\boldsymbol{x}) = \boldsymbol{F}^{\mathrm{NG}(r)^{-1}}\left(\boldsymbol{F}^{\mathrm{G}(r)}\left(\mathcal{A}'^{\mathrm{G}^{(r)}}(\boldsymbol{x})\right)\right)$$

Evaluate the PSD $\boldsymbol{S}^{\mathrm{NG}^{(rs)}}(\boldsymbol{\omega})$ of $\boldsymbol{\mathcal{V}}^{\mathrm{NG}}(\boldsymbol{x})$

$$\boldsymbol{S}^{\mathrm{NG}^{(rs)}} \simeq \boldsymbol{S}^{\mathrm{T}^{(rs)}}?$$

No

$$\boldsymbol{S}^{(rs)}(\boldsymbol{\omega}) \leftarrow \boldsymbol{S}^{(rs)}(\boldsymbol{\omega})\frac{\boldsymbol{S}^{\mathrm{T}^{(rr)}}(\boldsymbol{\omega})\boldsymbol{S}^{\mathrm{T}^{(ss)}}(\boldsymbol{\omega})}{\boldsymbol{S}^{\mathrm{NG}^{(rr)}}(\boldsymbol{\omega})\boldsymbol{S}^{\mathrm{NG}^{(ss)}}(\boldsymbol{\omega})}$$

- The meso-scale stochastic model
  - Application to film deposited at 610 ºC:
  - Comparison between micro-samples and generated fields

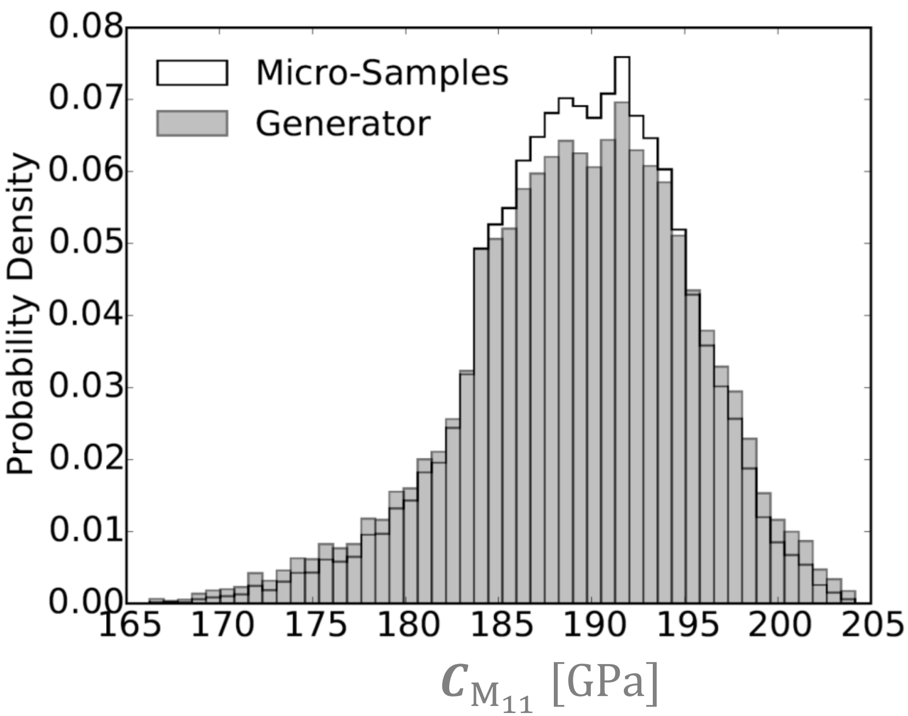

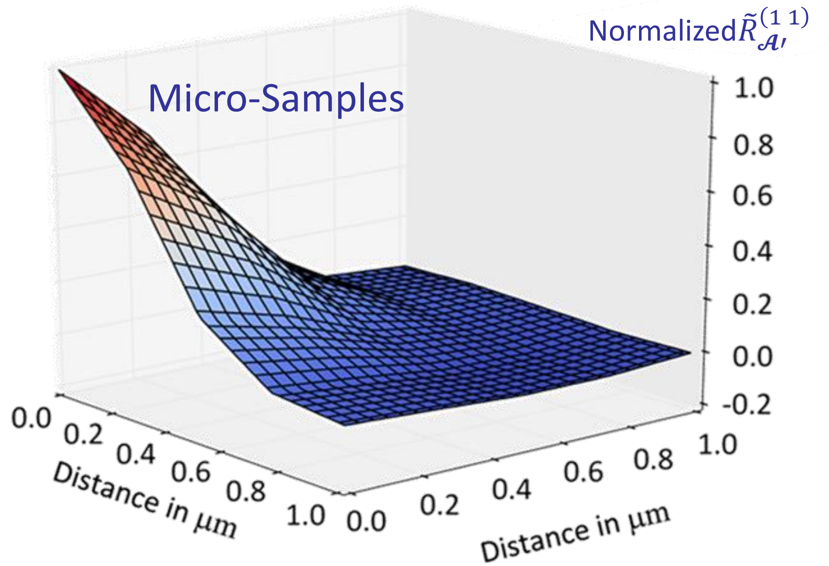

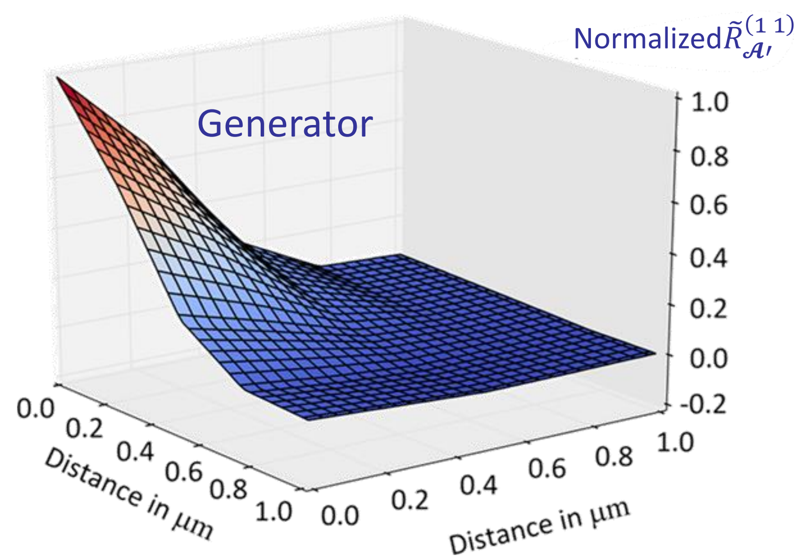

Beginning

- Application to polycrystalline materials: The meso-scale to macro-scale transition
  - Convergence in terms of $\alpha = \frac{l_{\mathbb{C}}}{l_{\text{mesh}}}$, the correlation length and macro-mesh ratio
  - The results converge
    - With the mesh size for all the SVE sizes
    - Toward the direct Monte Carlo simulations results

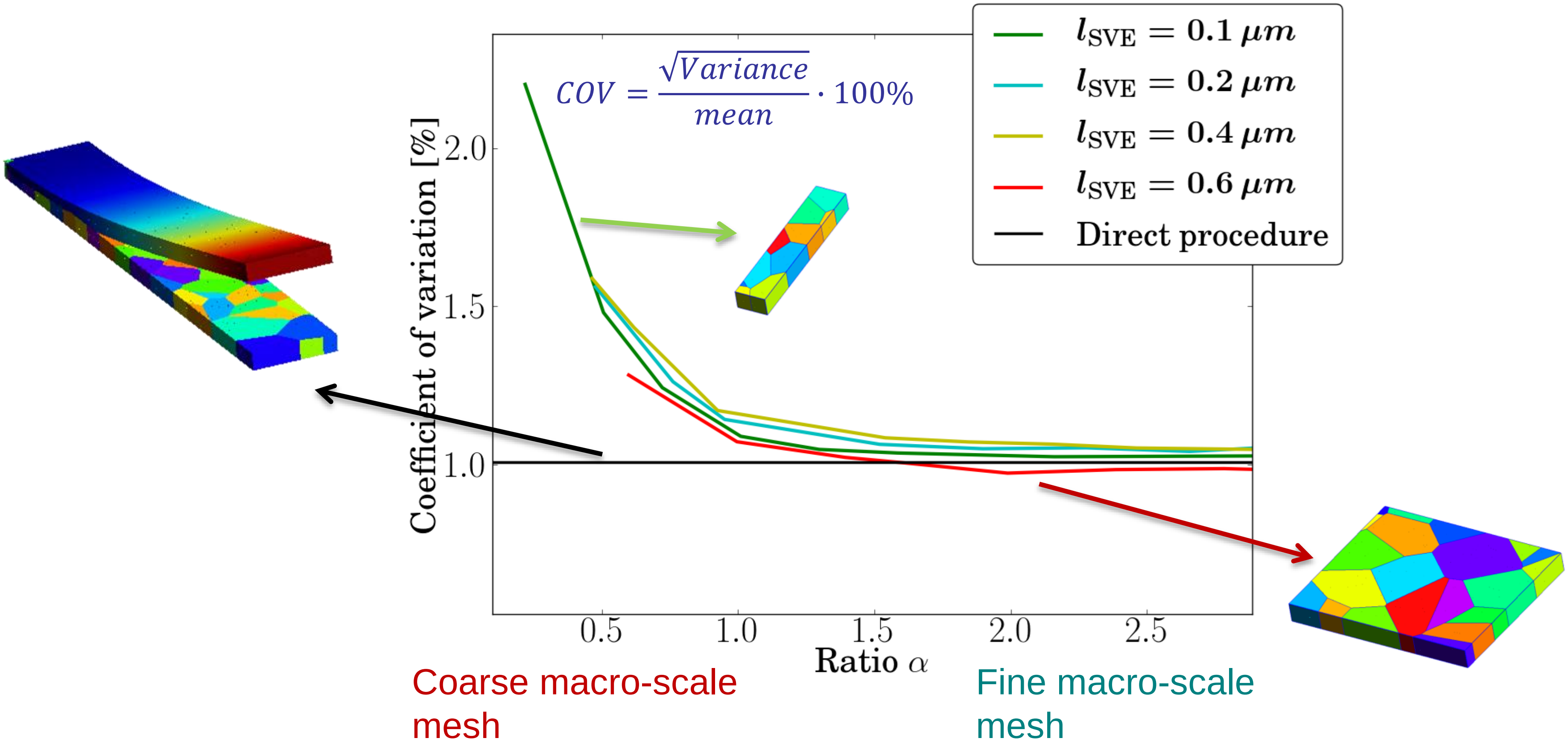

Stochastic 3-Scale Models

- Application to polycrystalline materials: The meso-scale to macro-scale transition
  - Comparison with direct Monte Carlo simulations

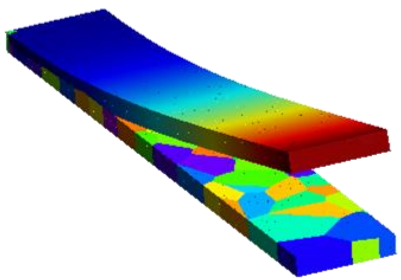

Relative difference in the mean: 0.57 %

Eigen frequency

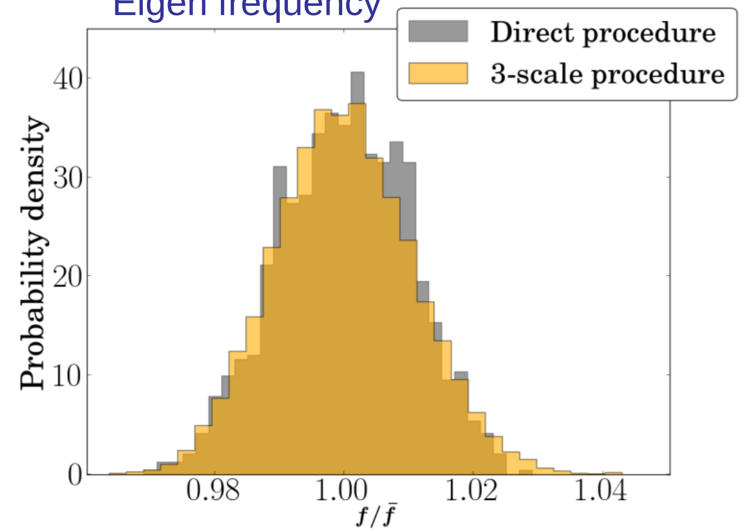

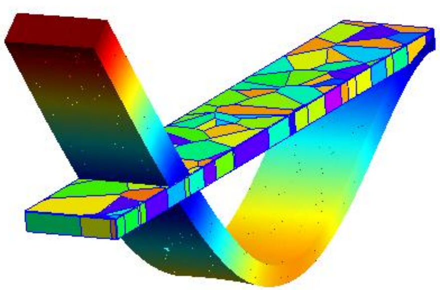

Relative difference in the mean: 0.44 %

Eigen frequency

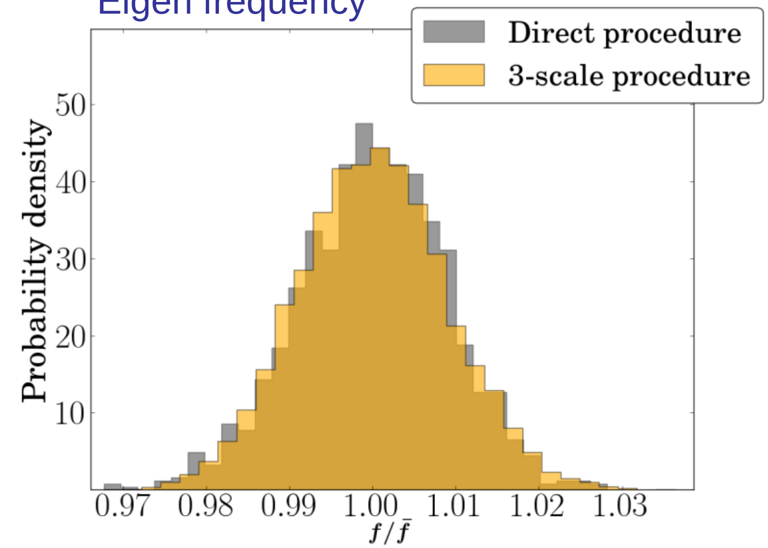

- Thermo-mechanical homogenization
  - Down-scaling

$$\begin{cases} \boldsymbol{\varepsilon}_{\mathrm{M}} = \frac{1}{V(\omega)} \int_{\omega} \boldsymbol{\varepsilon}_{\mathrm{m}} d\omega \\ \nabla_{\mathrm{M}} \vartheta_{\mathrm{M}} = \frac{1}{V(\omega)} \int_{\omega} \nabla_{\mathrm{m}} \vartheta_{\mathrm{m}} d\omega \\ \vartheta_{\mathrm{M}} = \frac{1}{V(\omega)} \int_{\omega} \frac{\rho_{\mathrm{m}} C_{v\mathrm{m}}}{\rho_{\mathrm{M}} C_{v\mathrm{M}}} \vartheta_{\mathrm{m}} d\omega \end{cases}$$

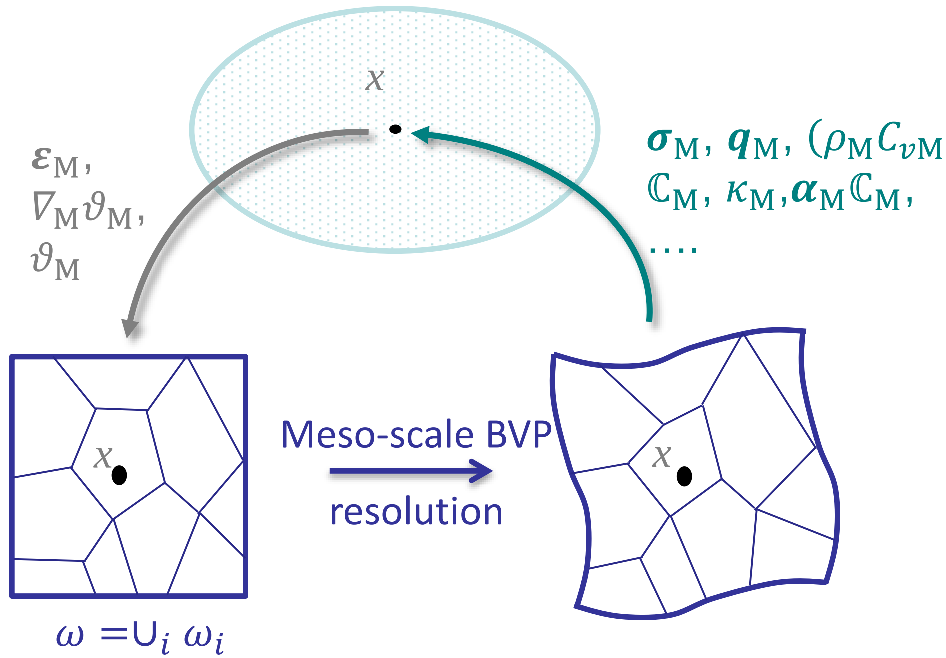

  - Up-scaling

$$\begin{cases} \boldsymbol{\sigma}_{\mathrm{M}} = \frac{1}{V(\omega)} \int_{\omega} \boldsymbol{\sigma}_{\mathrm{m}} d\omega \\ \boldsymbol{q}_{\mathrm{M}} = \frac{1}{V(\omega)} \int_{\omega} \boldsymbol{q}_{\mathrm{m}} d\omega \\ \rho_{\mathrm{M}} C_{v\mathrm{M}} = \frac{1}{V(\omega)} \int \rho_{\mathrm{m}} C_{v\mathrm{m}} dV \end{cases} \longrightarrow \begin{cases} \mathbb{C}_{\mathrm{M}} = \frac{\partial \boldsymbol{\sigma}_{\mathrm{M}}}{\partial \boldsymbol{u}_{\mathrm{M}} \otimes \boldsymbol{\nabla}_{\mathrm{M}}} \quad \& \quad \boldsymbol{\alpha}_{\mathrm{M}} : \mathbb{C}_{\mathrm{M}} = -\frac{\partial \boldsymbol{\sigma}_{\mathrm{M}}}{\partial \vartheta_{\mathrm{M}}} \\ \boldsymbol{\kappa}_{\mathrm{M}} = -\frac{\partial \boldsymbol{q}_{\mathrm{M}}}{\partial \nabla_{\mathrm{M}} \vartheta_{\mathrm{M}}} \end{cases}$$

  - Consistency $\longrightarrow$ Satisfied by periodic boundary conditions

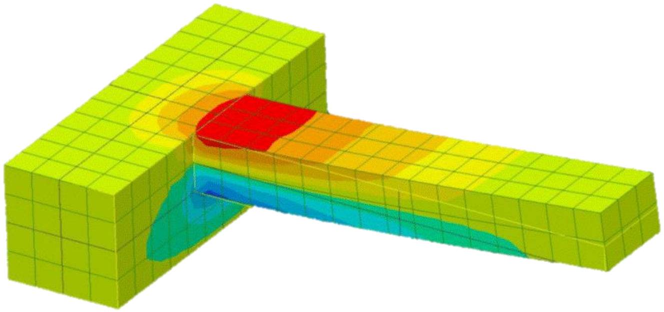

- Quality factor
  - Micro-resonators
    - Temperature changes with compression/traction
    - Energy dissipation
  - Eigen values problem
    - Governing equations

$$\begin{bmatrix}\mathbf{M} & \mathbf{0}\\ \mathbf{0} & \mathbf{0}\end{bmatrix}\begin{bmatrix}\ddot{\mathbf{u}}\\ \ddot{\boldsymbol{\vartheta}}\end{bmatrix}+\begin{bmatrix}\mathbf{0} & \mathbf{0}\\ \mathbf{D}_{\mathrm{u}\vartheta}(\boldsymbol{\theta}) & \mathbf{D}_{\vartheta\vartheta}\end{bmatrix}\begin{bmatrix}\dot{\mathbf{u}}\\ \dot{\boldsymbol{\vartheta}}\end{bmatrix}+\begin{bmatrix}\mathbf{K}_{\mathrm{uu}}(\boldsymbol{\theta}) & \mathbf{K}_{\mathrm{u}\vartheta}(\boldsymbol{\theta})\\ \mathbf{0} & \mathbf{K}_{\vartheta\vartheta}(\boldsymbol{\theta})\end{bmatrix}\begin{bmatrix}\mathbf{u}\\ \boldsymbol{\vartheta}\end{bmatrix}=\begin{bmatrix}\boldsymbol{F}_{\mathrm{u}}\\ \boldsymbol{F}_{\vartheta}\end{bmatrix}$$

    - Free vibrating problem

$$\begin{bmatrix}\mathbf{u}(t)\\ \boldsymbol{\vartheta}(t)\end{bmatrix}=\begin{bmatrix}\mathbf{u}_0\\ \boldsymbol{\vartheta}_0\end{bmatrix}e^{i\omega t}$$

$$\begin{bmatrix}-\mathbf{K}_{\mathrm{uu}}(\boldsymbol{\theta}) & -\mathbf{K}_{\mathrm{u}\vartheta}(\boldsymbol{\theta}) & \mathbf{0}\\ \mathbf{0} & -\mathbf{K}_{\vartheta\vartheta}(\boldsymbol{\theta}) & \mathbf{0}\\ \mathbf{0} & \mathbf{0} & \mathbf{I}\end{bmatrix}\begin{bmatrix}\mathbf{u}\\ \boldsymbol{\vartheta}\\ \dot{\mathbf{u}}\end{bmatrix}=i\omega\begin{bmatrix}\mathbf{0} & \mathbf{0} & \mathbf{M}\\ \mathbf{D}_{\vartheta\mathrm{u}}(\boldsymbol{\theta}) & \mathbf{D}_{\vartheta\vartheta} & \mathbf{0}\\ \mathbf{I} & \mathbf{0} & \mathbf{0}\end{bmatrix}\begin{bmatrix}\mathbf{u}\\ \boldsymbol{\vartheta}\\ \dot{\mathbf{u}}\end{bmatrix}$$

  - Quality factor
    - From the dissipated energy per cycle
    - $Q^{-1}=\dfrac{2|\Im\omega\,|}{\sqrt{(\Im\omega)^2+(\Re\omega)^2}}$

- Application of the 3-Scale method to extract the quality factor distribution
  - 3D models readily available
  - The effect of the anchor can be studied

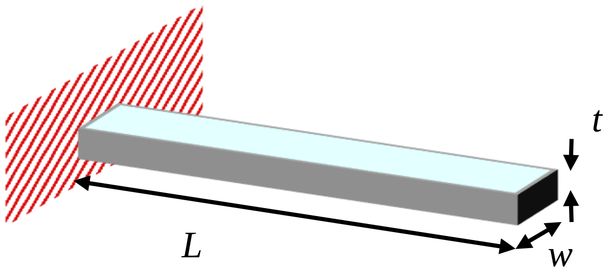

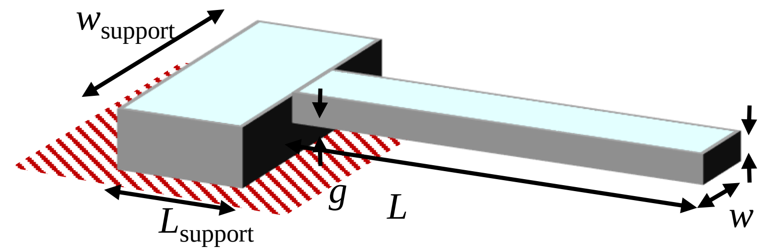

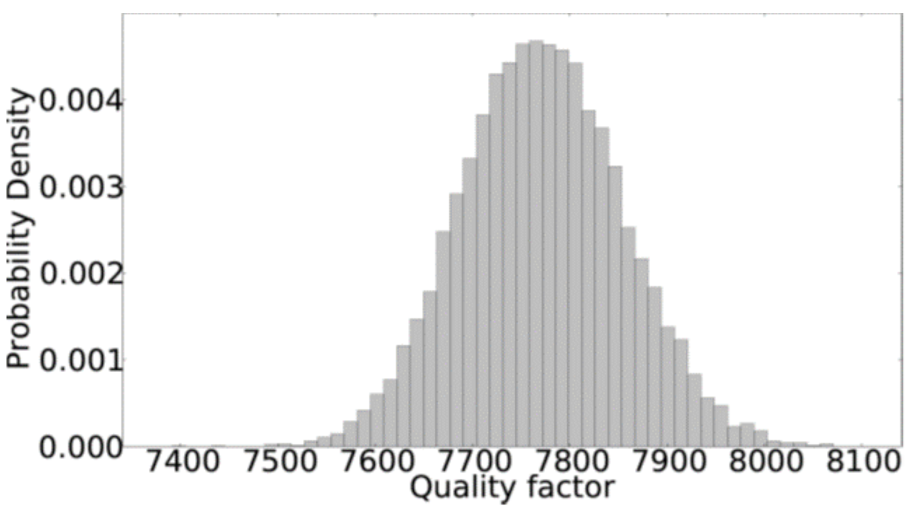

15 x 3 x 2 μm^3-beam,

deposited at 610 ºC

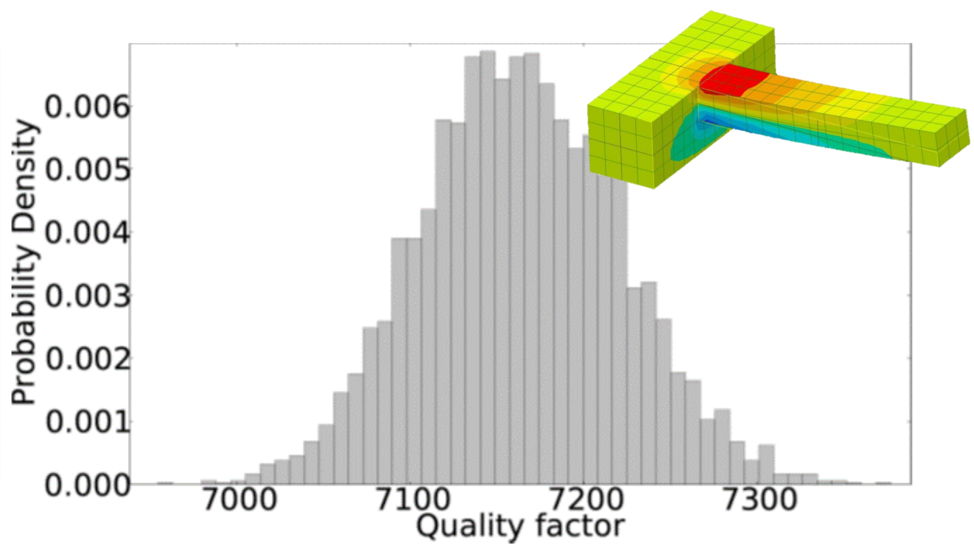

15 x 3 x 2 μm^3-beam & anchor,

deposited at 610 ºC

- Surface topology: asperity distribution
  - Upper surface topology by AFM (Atomic Force Microscope) measurements on 2 µm-thick poly-silicon films

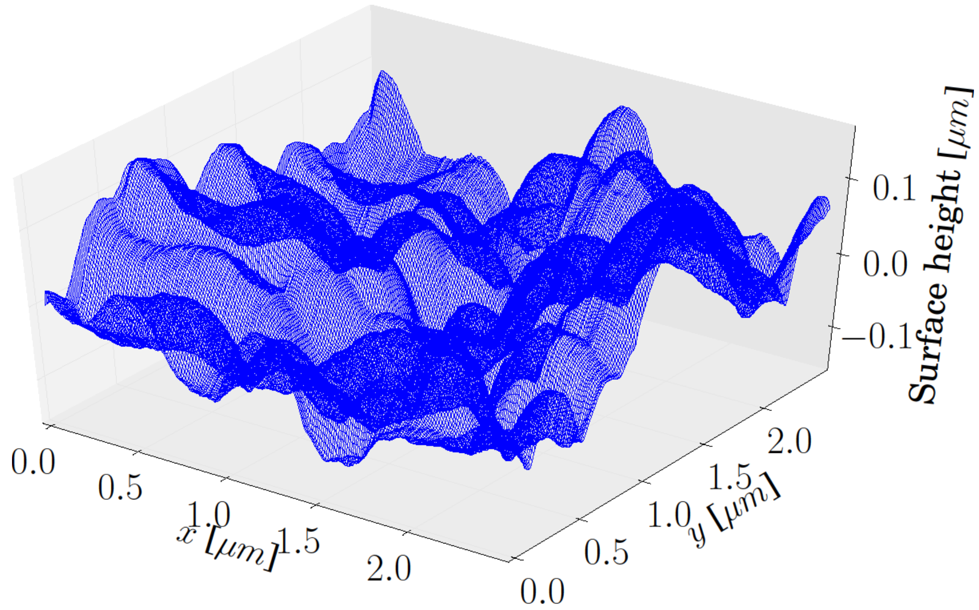

Deposition temperature [^{o}C]	580	610	630	650
Std deviation [nm]	35.6	60.3	90.7	88.3

AFM data provided by IMT Bucharest, Rodica Voicu, Angela Baracu, Raluca Muller

Stochastic 3-Scale Models

- Accounting for roughness
  - Second-order homogenization

$$\begin{cases} \tilde{\boldsymbol{n}}_{\mathrm{M}} = \mathbb{C}_{\mathrm{M}_1} : \boldsymbol{\varepsilon}_{\mathrm{M}} + \mathbb{C}_{\mathrm{M}_2} : \boldsymbol{\kappa}_{\mathrm{M}} \\ \tilde{\boldsymbol{m}}_{\mathrm{M}} = \mathbb{C}_{\mathrm{M}_3} : \boldsymbol{\varepsilon}_{\mathrm{M}} + \mathbb{C}_{\mathrm{M}_4} : \boldsymbol{\kappa}_{\mathrm{M}} \end{cases}$$

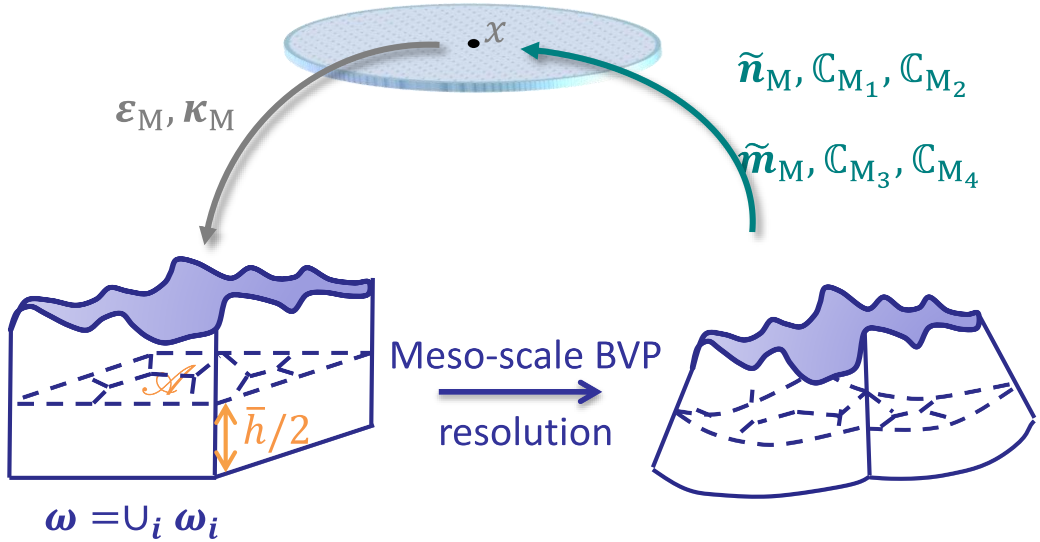

  - Stochastic homogenization
    - Several SVE realizations
    - For each SVE $\omega_j = \cup_i \omega_i$
    - The density per unit area is now non-constant

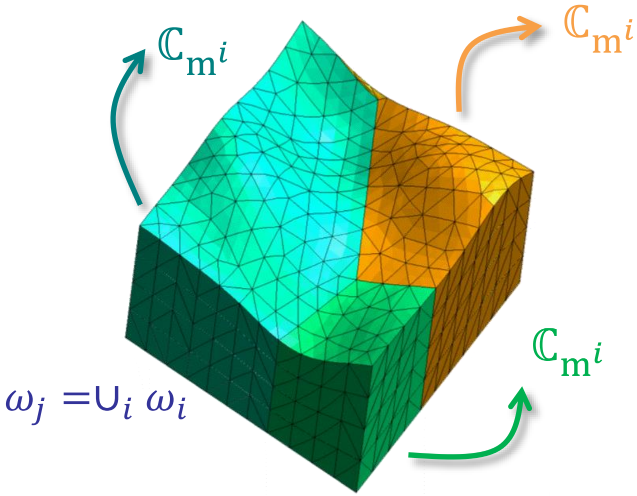

$$\mathbb{C}_{\mathrm{m}^i}\ \forall i \longrightarrow \mathbb{C}_{\mathrm{M}_1^j}, \mathbb{C}_{\mathrm{M}_2^j}, \mathbb{C}_{\mathrm{M}_3^j}, \mathbb{C}_{\mathrm{M}_4^j} \longrightarrow \mathrm{U}_{\mathrm{M}^j}$$

Computational homogenization

$\bar{\boldsymbol{\rho}}_{\mathrm{M}^j}$

Samples of the meso-scale homogenized elasticity matrix U_{M} & density $\bar{\boldsymbol{\rho}}_{\mathrm{M}}$

Stochastic 3-Scale Models

- Accounting for roughness
  - Cantilever of 8 x 3 x t $\mu\mathrm{m}^3$ deposited at 610 ºC

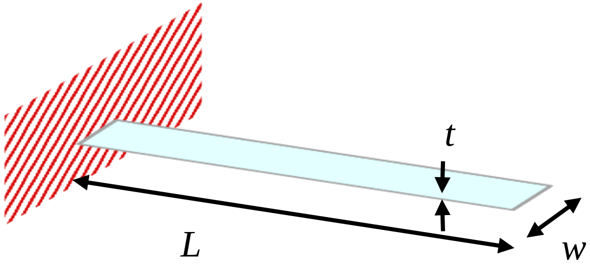

Flat SVEs (no roughness) - F

Rough SVEs (Polysilicon film deposited at 610 ºC) - R

Grain orientation following XRD measurements – Si_{pref}

Grain orientation uniformly distributed – Si_{uni}

Reference isotropic material – Iso

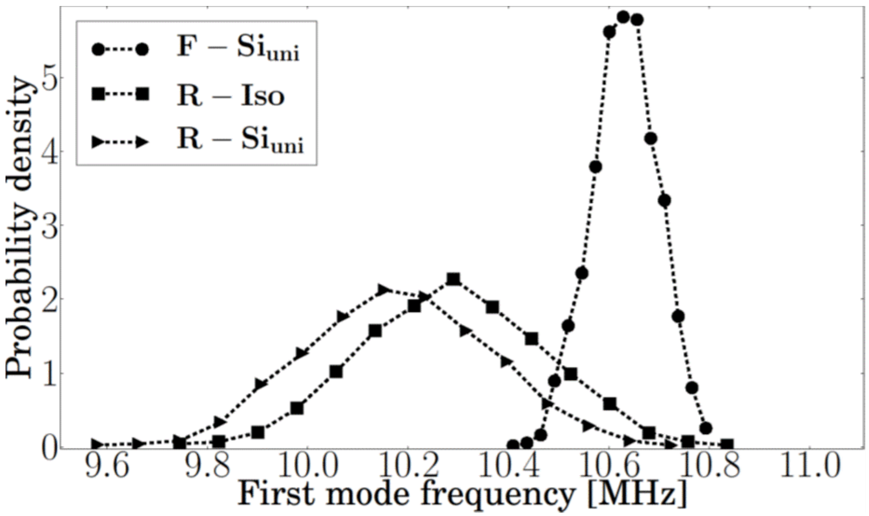

Roughness effect is the most important for 8 x 3 x 0.5 $\mu\mathrm{m}^3$ cantilevers

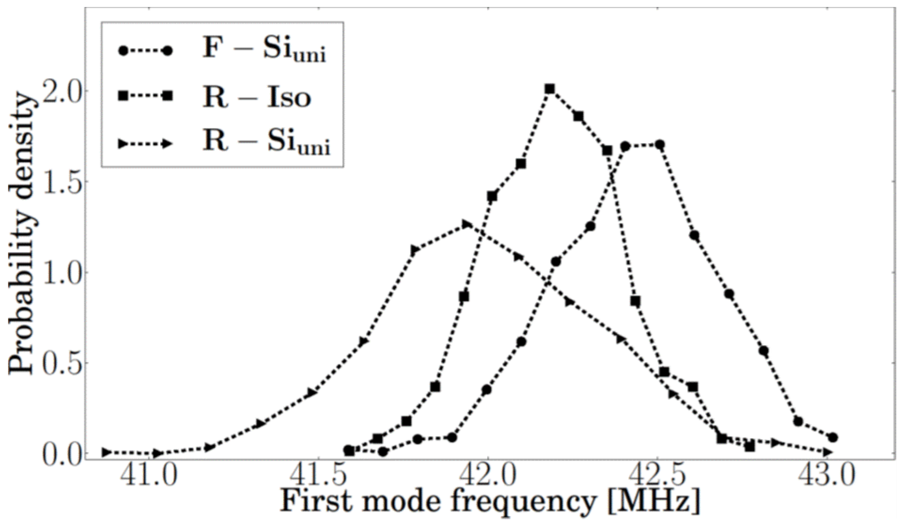

Roughness effect is of same importance as orientation for 8 x 3 x 2 $\mu\mathrm{m}^3$ cantilevers

- Application to robust design
  - Determination of probabilistic meso-scale properties
  - Propagate uncertainties to higher scale
  - Vibro-meter sensors:
    - Uncertainties in resonance frequency / Q factor

- 3SMVIB MNT.ERA-NET project
  - Open-Engineering, V2i, ULiège (Belgium)
  - Polit. Warszawska (Poland)
  - IMT, Univ. Cluj-Napoca (Romania)

- Publications (doi)
  - 10.1002/nme.5452
  - 10.1016/j.cma.2016.07.042
  - 10.1016/j.cma.2015.05.019

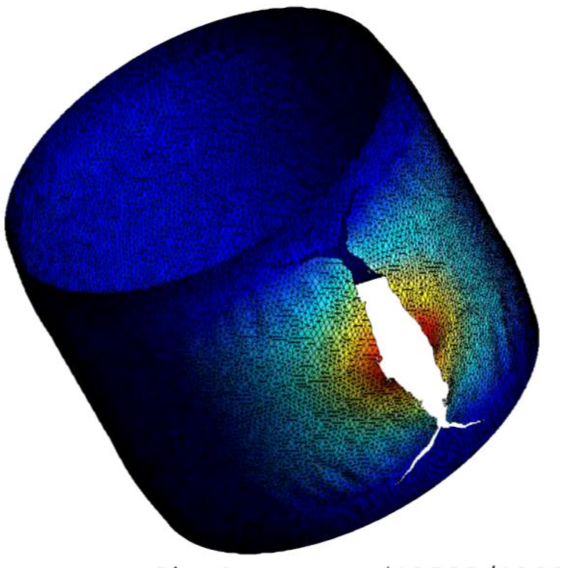

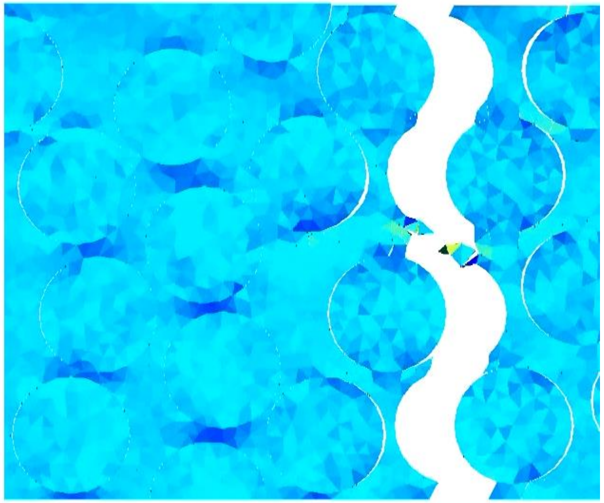

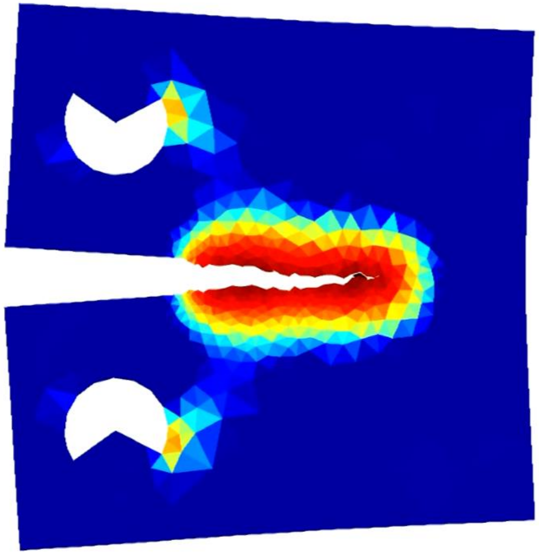

DG-Based (Multi-Scale) Fracture

The research has been funded by the Belgian National Fund for Education at the Research in Industry and Farming.
SIMUCOMP The research has been funded by the Walloon Region under the agreement no 1017232 (CT-EUC 2010-10-12) in the context of the ERA-NET +, Matera + framework.
The research has been funded by the Walloon Region under the agreement no.7581-MRIPF in the context of the 16th MECATECH call.

DG-Based Fracture

- Hybrid DG/cohesive law formulation
  - Discontinuous Galerkin method
    - Finite-element discretization
    - Same **discontinuous** polynomial approximations for the
      - **Test** functions φ_h and
      - **Trial** functions $\delta\varphi$

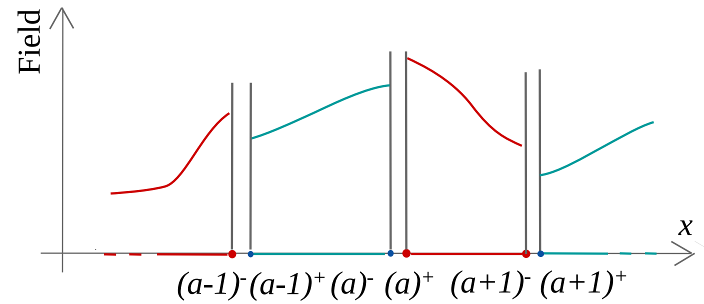

  - Can easily be combined with a cohesive law for fracture analyses
    - Interface elements already exist
    - Easy to shift from un-fractured to fractured states
    - Remains accurate before fracture onset (DG formulation)
    - Efficient // implementation

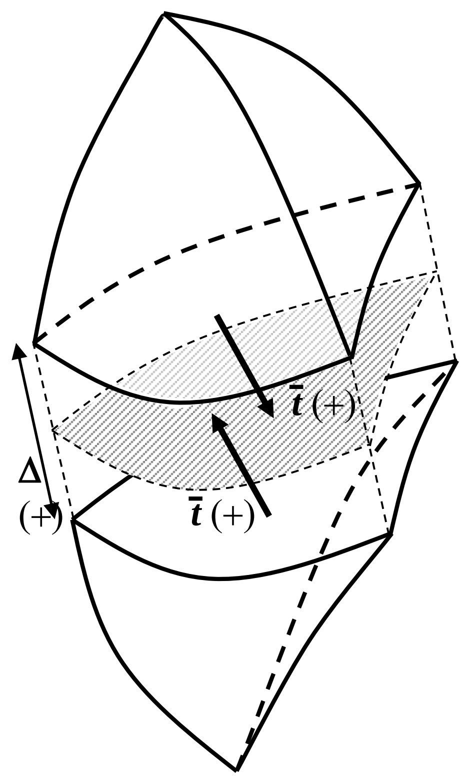

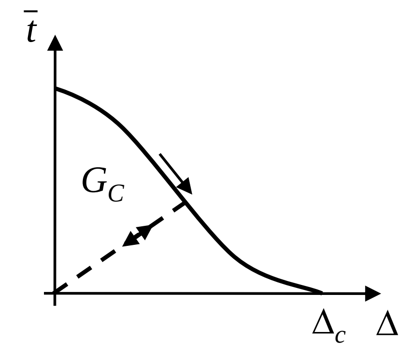

- Publications (doi)
  - [10.1016/j.cma.2010.08.014](https://doi.org/10.1016/j.cma.2010.08.014)

- Multi-scale modeling
  - 2 problems are solved concurrently
    - The macro-scale problem
    - The meso-scale problem (on a meso-scale Volume Element)

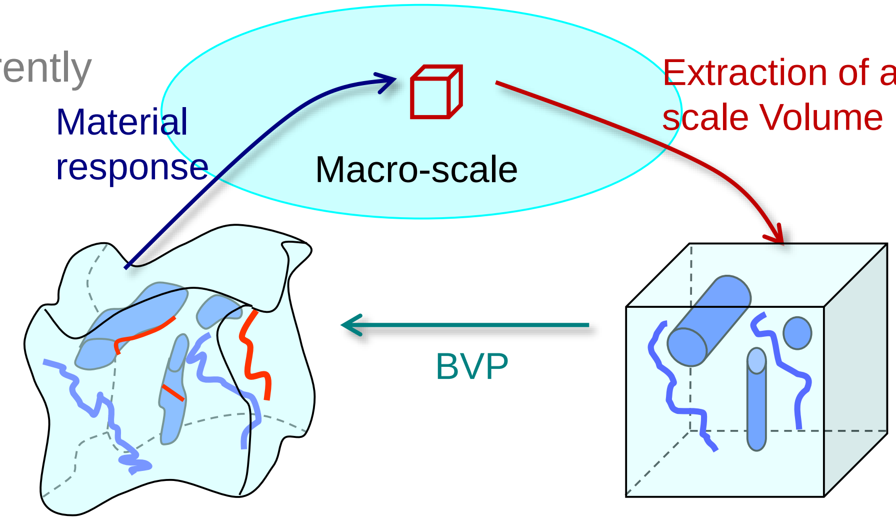

- For meso-scale volume elements embedding crack propagation

$L_{macro} >> L_{VE} ? L_{micro}$

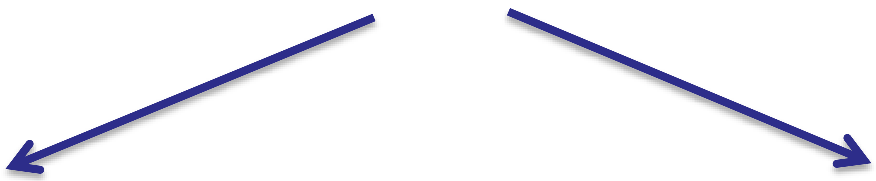

For accuracy: Size of the meso-scale volume element smaller than the characteristic length of the macro-scale loading

The crack induces a loss of statistical representativeness
- **Should recover consistency lost due to the discontinuity**

DG-Based Multi-Scale Fracture

- Micro-Meso fracture model for intra-laminar failure
  - Epoxy-CF (60%), transverse loading
  - 3 stages captured

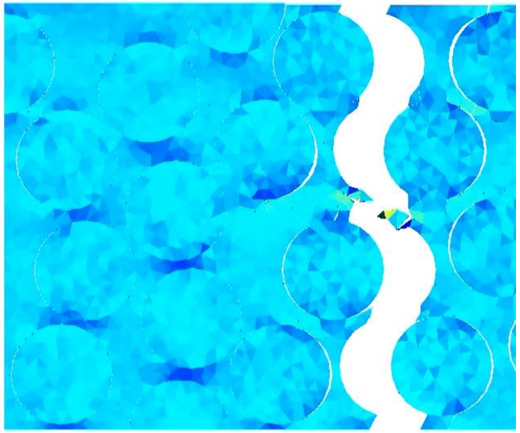

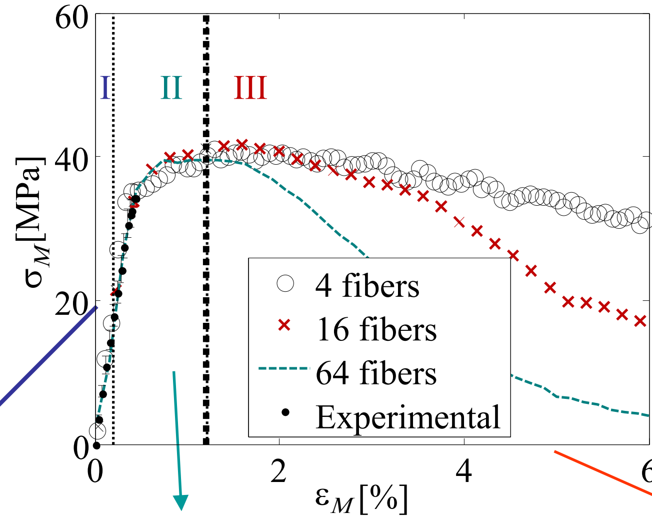

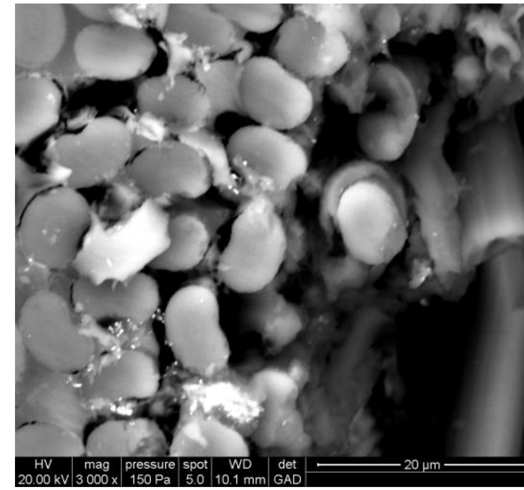

Elastic response

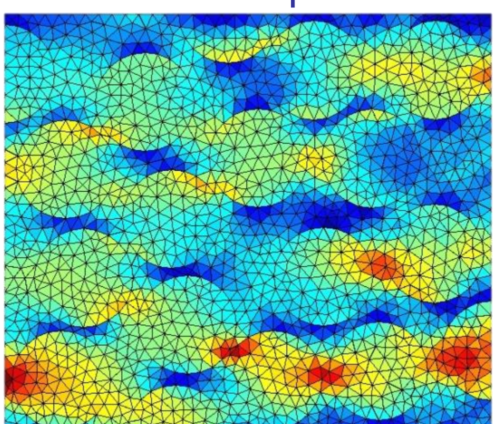

Damage due to debonding

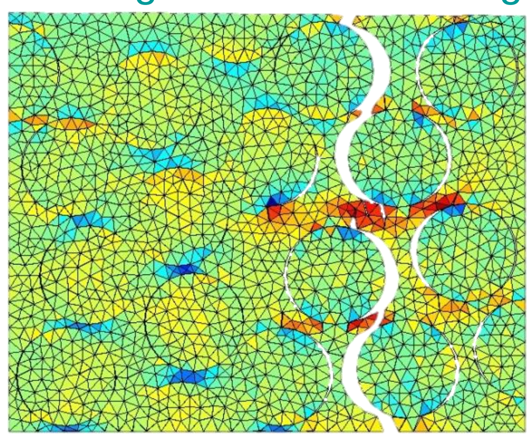

Meso-crack

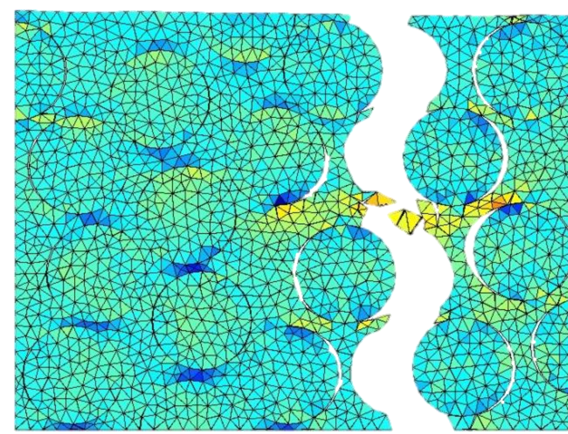

- Micro-Meso fracture model for intra-laminar failure (2)
  - Scale transition after softening onset
    - Should not depend on the RVE size
    - Extraction of the meso-scale TSL ($\bar{t}_M$ vs. Δ_M)

[Verhoosel et al., IJNME 2010]

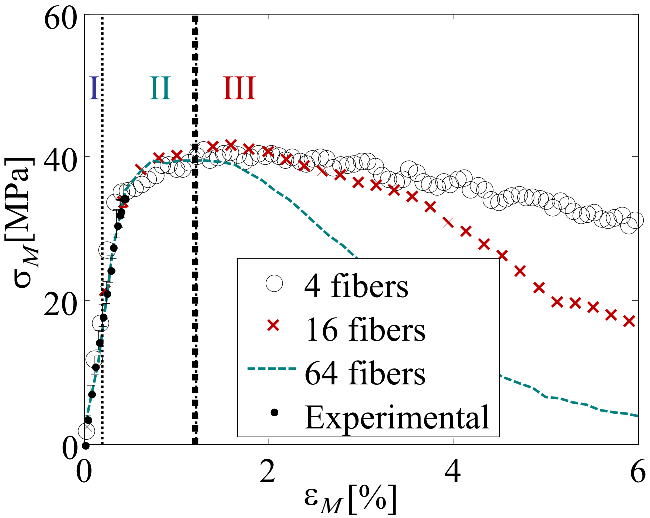

$$\delta\bar{t}_M = \boldsymbol{\delta\sigma_M} \cdot \boldsymbol{e_X}$$

$$\delta\boldsymbol{\Delta}_M = \delta\boldsymbol{u}^m - L_{\text{cell}}\boldsymbol{C_M}^{-1} : \boldsymbol{e_X} \otimes \boldsymbol{e_X} \cdot \boldsymbol{\delta\bar{t}_M}$$

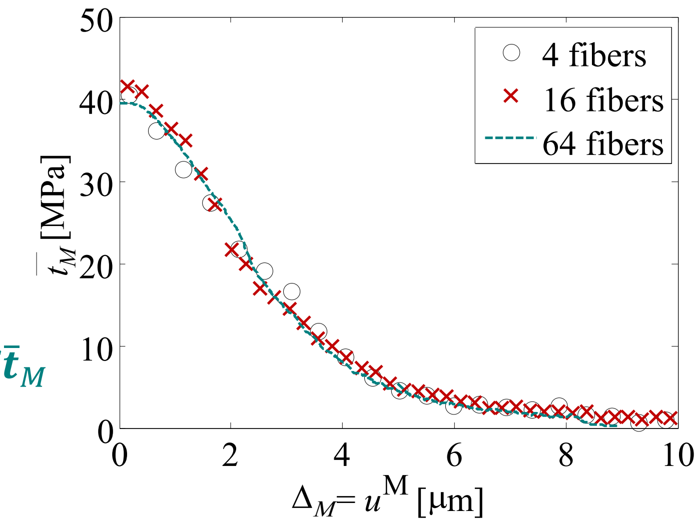

- SIMUCOMP ERA-NET project
  - e-Xstream, CENAERO, ULiège (Belgium)
  - IMDEA Materials (Spain)
  - CRP Henri-Tudor (Luxemburg)
- Publication (doi)
  - 10.1016/j.engfracmech.2013.03.018

DG-Based Dynamic Fracture

- Fracture of thin structures

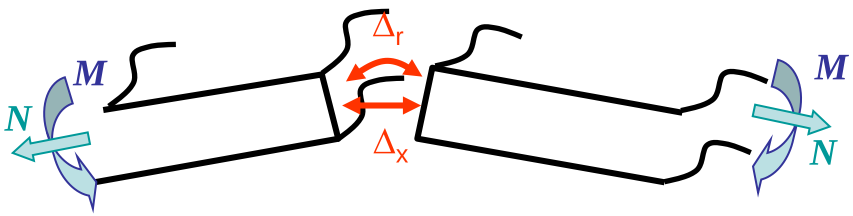

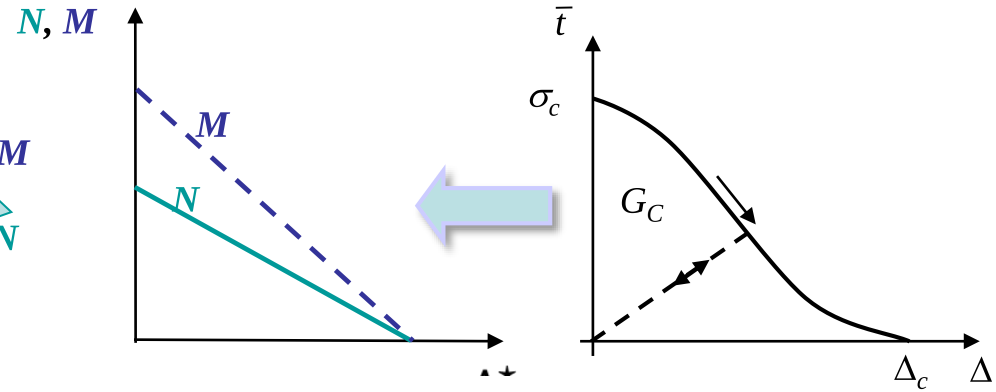

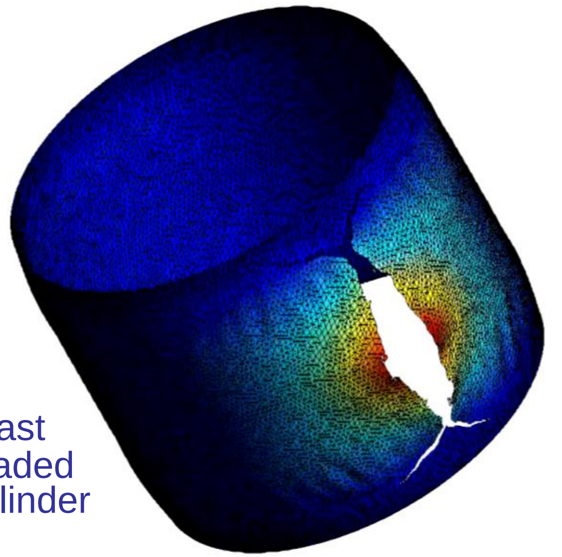

Blast loaded cylinder

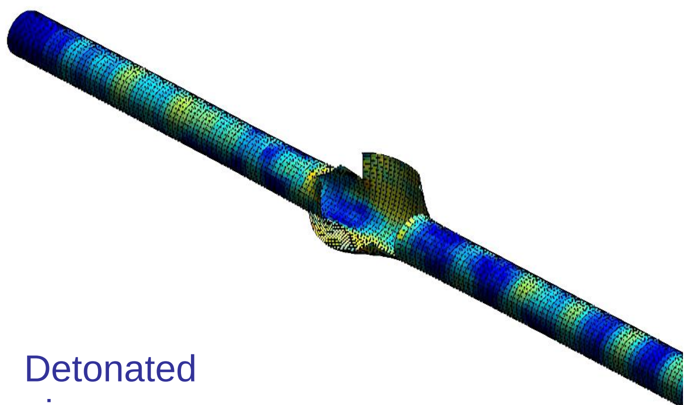

Detonated pipe

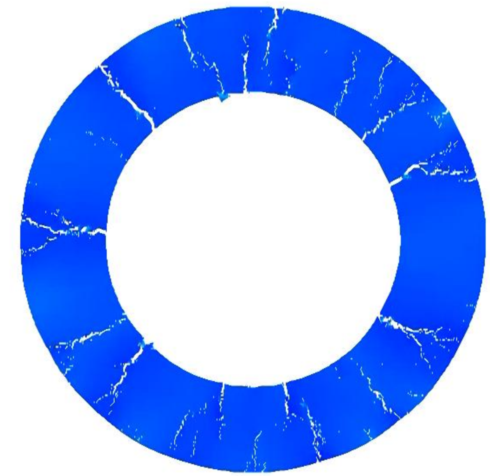

Fragmented disk

- FNRS-FRIA fellowship
- Publications (doi)
  - [10.1002/nme.4381]
  - [10.1007/s10704-012-9748-5]
  - [10.1016/j.cma.2011.07.008]
  - [10.1002/nme.3008]

- Capture triaxiality effects: Cohesive Band Model (CBM)
  - Introduction of a uniform band of given thickness h_b [Remmers et al. 2013]

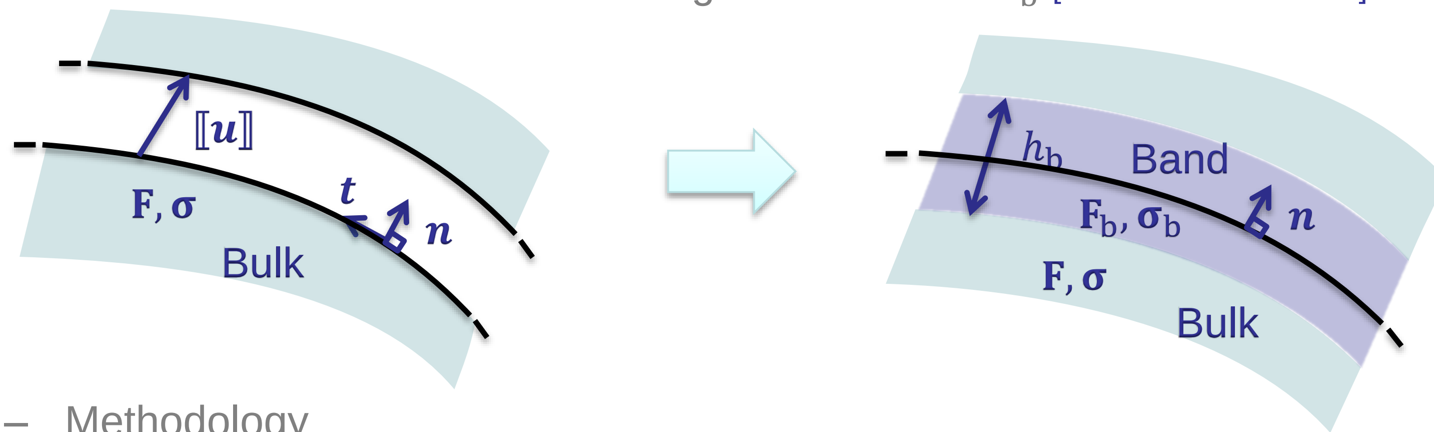

  - Methodology
    1. Bulk stress $\boldsymbol{\sigma}$ using non-local damage law
    2. Compute a "band" deformation gradient
    $$\mathbf{F}_b = \mathbf{F} + \frac{[\![\boldsymbol{u}]\!] \otimes \boldsymbol{N}}{h_b} + \frac{1}{2}\boldsymbol{\nabla}_T [\![\boldsymbol{u}]\!]$$
    3. Band stress $\boldsymbol{\sigma}_b$ using the (local) damage law
    4. Recover traction forces $\boldsymbol{t}([\![\boldsymbol{u}]\!], \mathbf{F}) = \boldsymbol{\sigma}_b . \boldsymbol{n}$

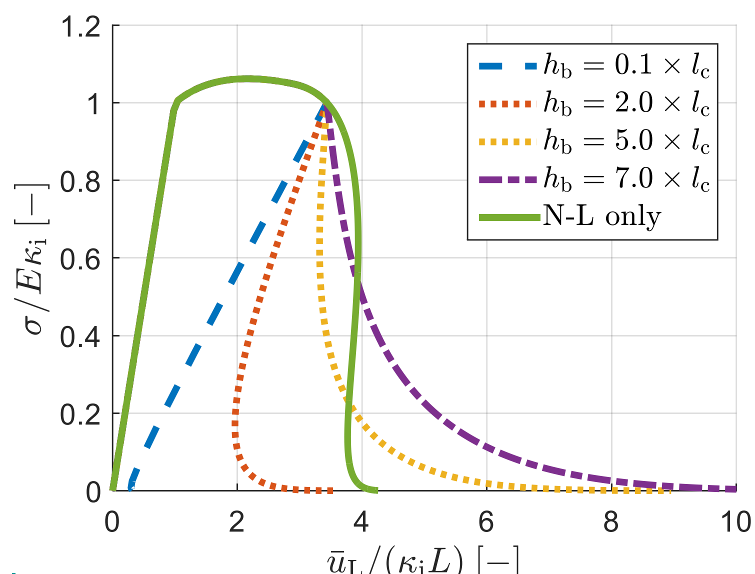

  - The cohesive band thickness
    - Evaluated to ensure energy consistency
    - Same dissipated energy as with a damage model

DG-Based elastic damage to crack transition

- Slit plate

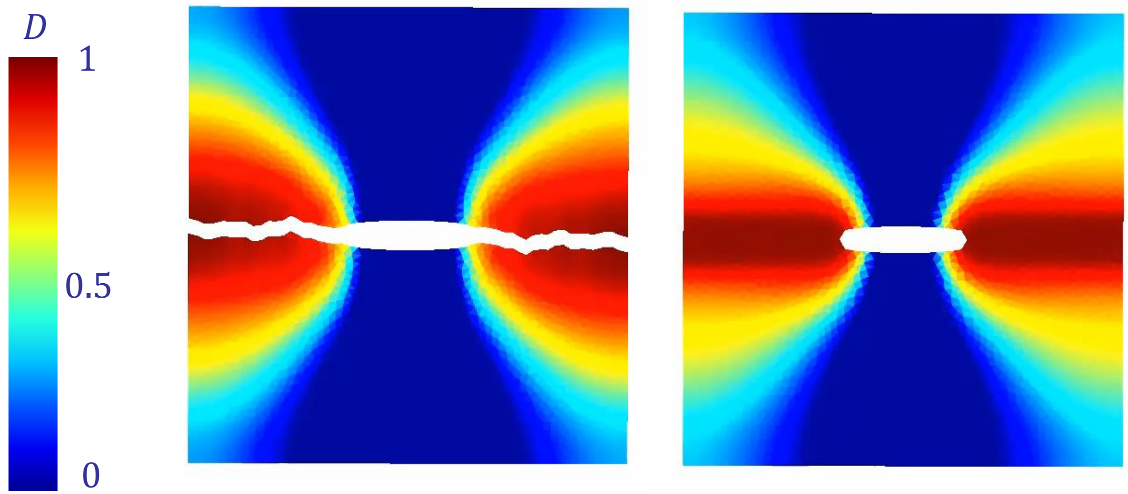

Non-Local+ CBM

Non-Local

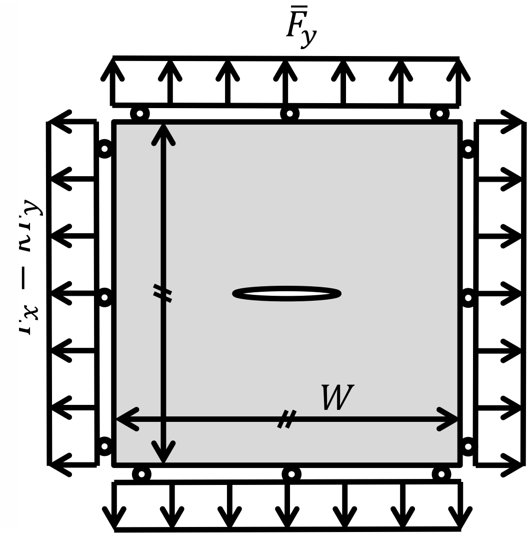

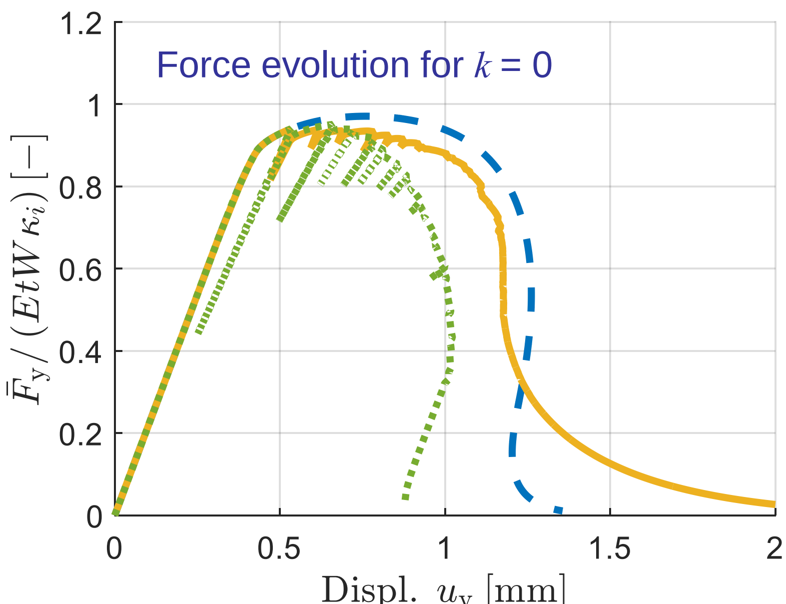

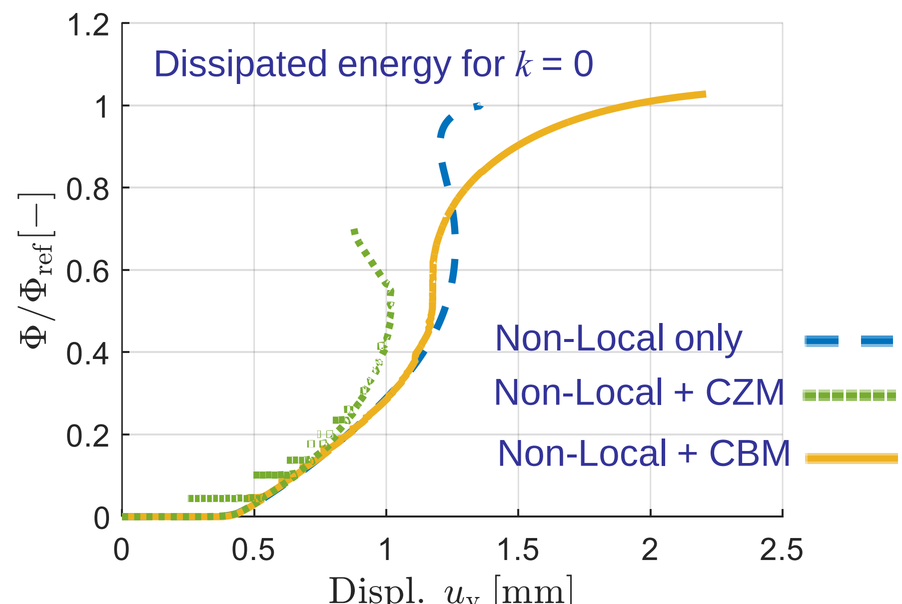

- Slit plate
  - Triaxiality effect through ratio k

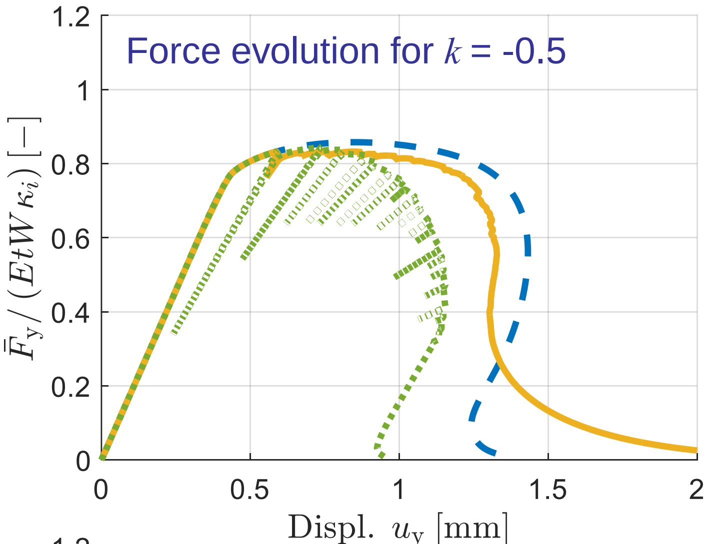

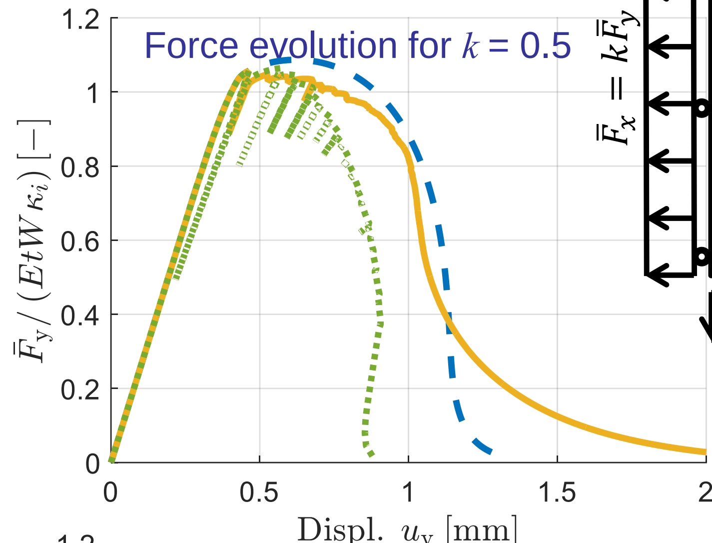

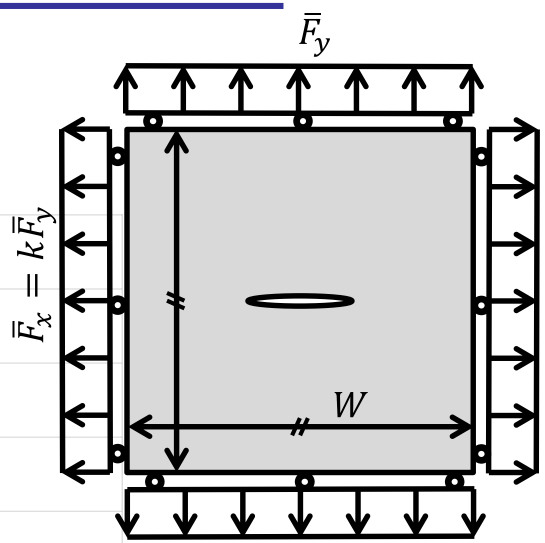

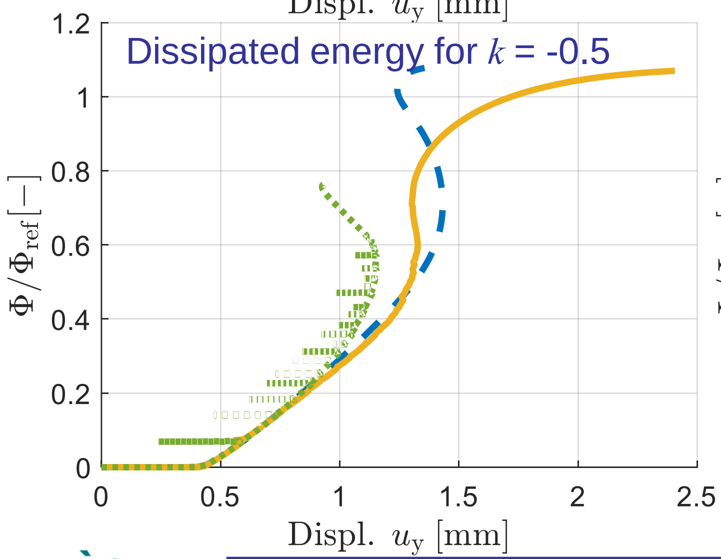

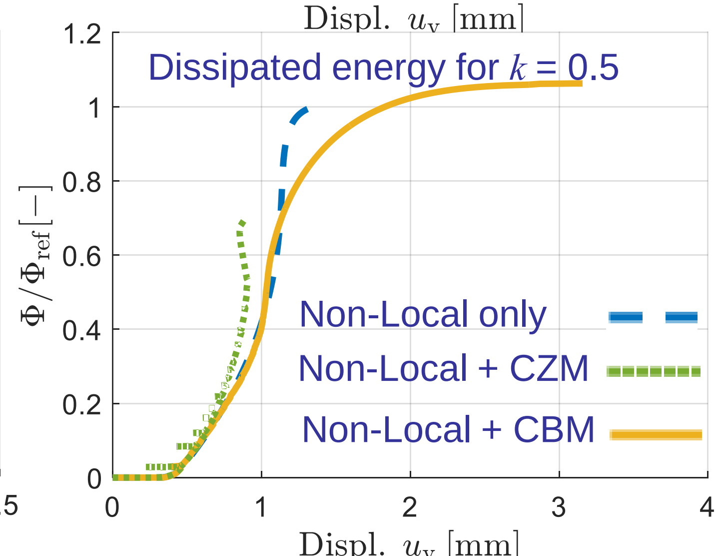

DG-Based elastic damage to crack transition

- Comparison with phase field
  - Single edge notched specimen [Miehe et al. 2010]
    - Calibration of damage and CBM parameters with 1D case [Leclerc et al. 2018]

Non-local model | Cohesive band model | Force-displacement curve

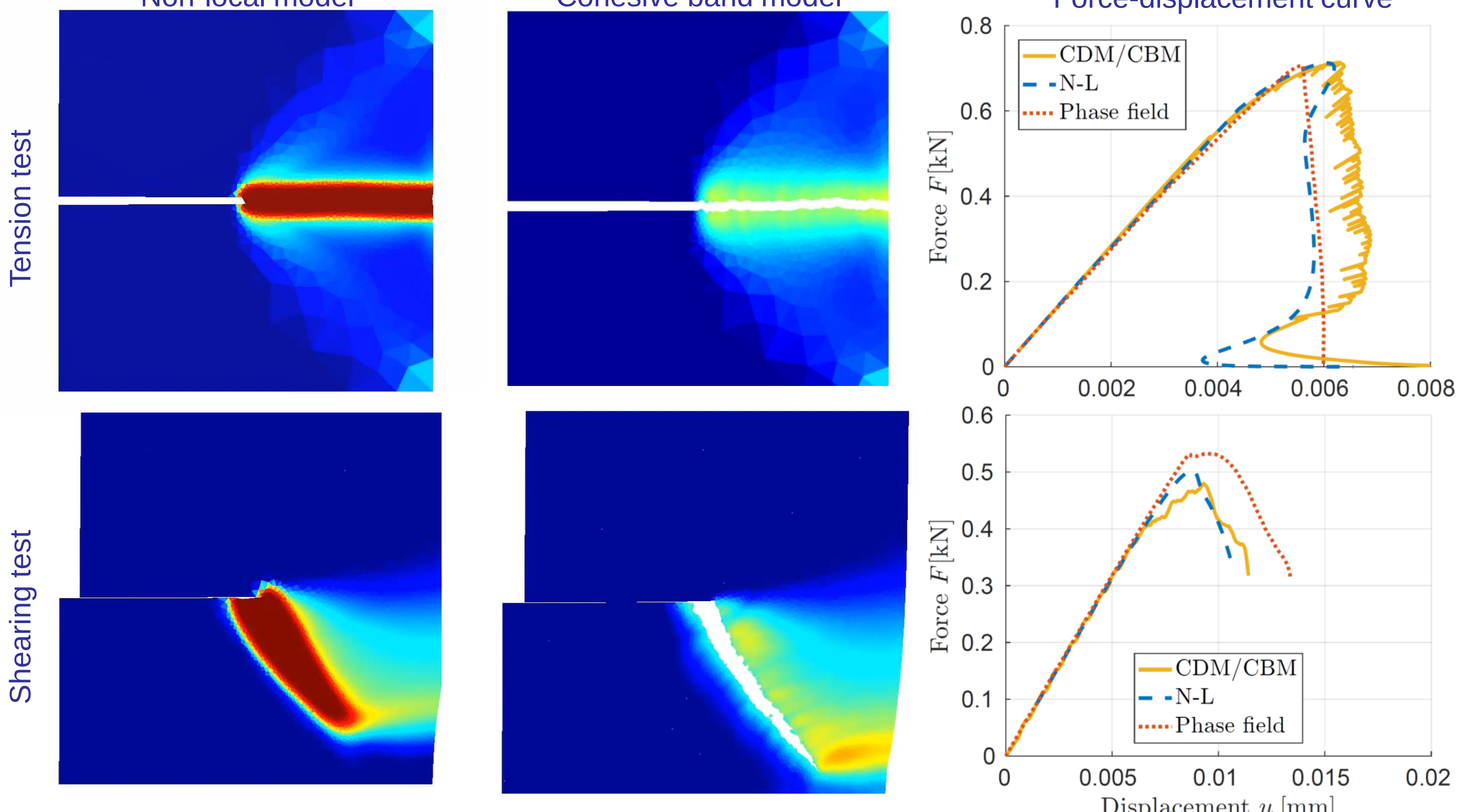

DG-Based elastic damage to crack transition

- Compact Tension Specimen:
  - Non-Local damage law combined to cohesive band model improves accuracy

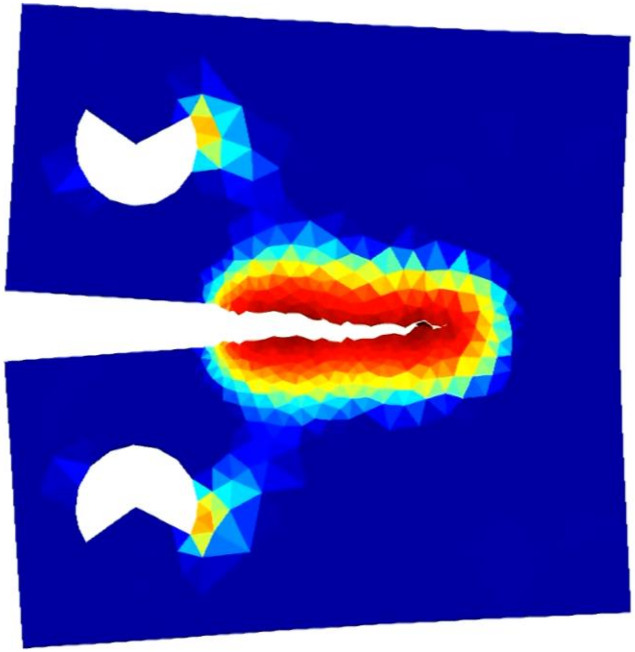

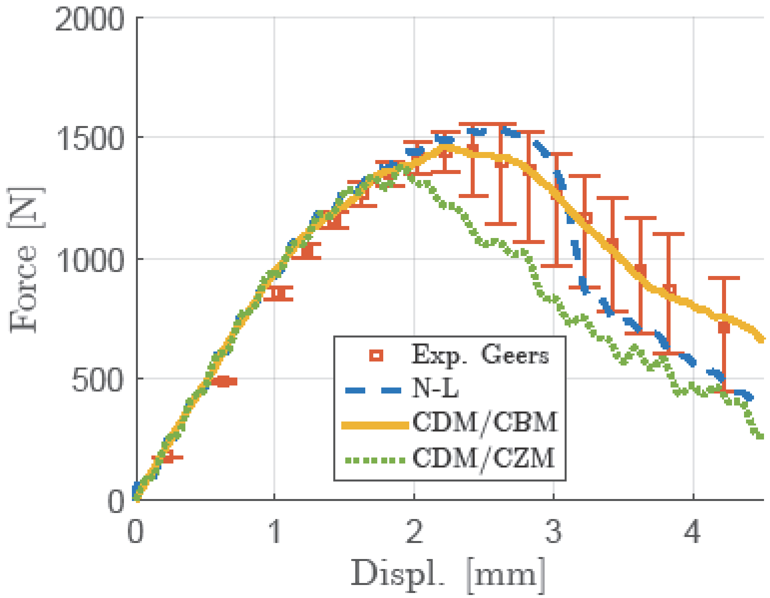

- MRIPF MECATECH project
  - GDTech, UCL, FZ, MECAR, Capital People (Belgium)
- Publication (doi)
  - 10.1002/nme.5618
  - 10.1016/j.cma.2014.06.031

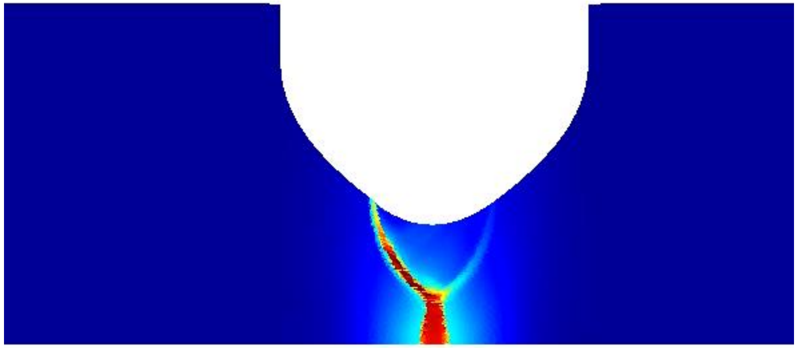

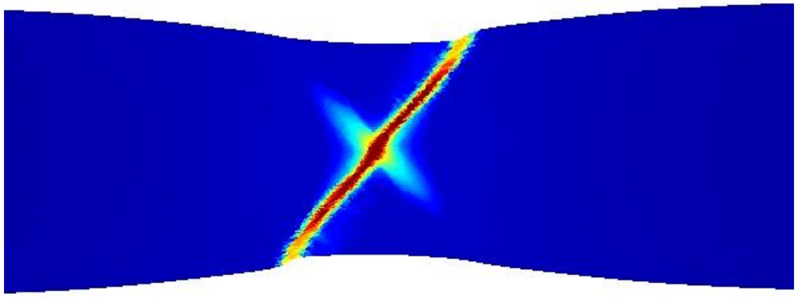

Shear and necking coalescence mechanisms for porous materials

The research has been funded by the Walloon Region under the agreement no. 1610154- EntroTough in the context of the 2016 WalInnov call

Shear and necking coalescence mechanisms for porous materials

- Objective:
  - To develop a non-local ductile failure model accounting for complex loading stress states
- Porous plasticity

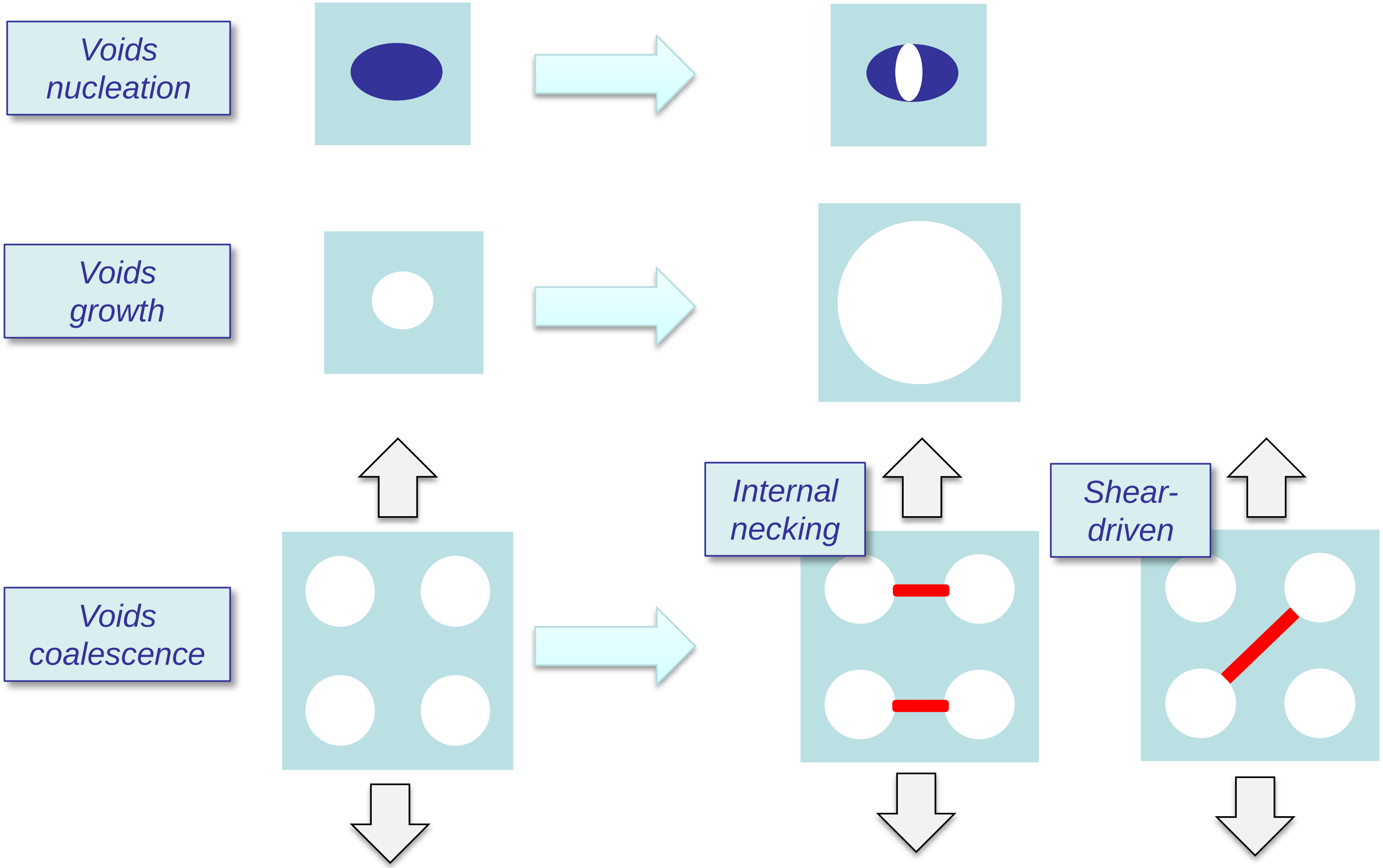

- Ductile failure: stress-state dependent fracture strain
  - Stress triaxiality dependent

$$\eta = \frac{p'}{\sigma_{eq}} \in]-\infty\ \infty[\qquad p = \frac{\mathrm{tr}\,(\boldsymbol{\sigma})}{3} \qquad \sigma_{eq} = \sqrt{\frac{3}{2}\mathrm{dev}(\boldsymbol{\sigma}):\mathrm{dev}(\boldsymbol{\sigma})}$$

  - Lode dependent

$$\theta = \frac{1}{3}\arccos\left(\frac{27J_3}{2\sigma_{eq}{}^3}\right) \qquad J_3 = \det(\mathrm{dev}(\boldsymbol{\sigma})\ )$$

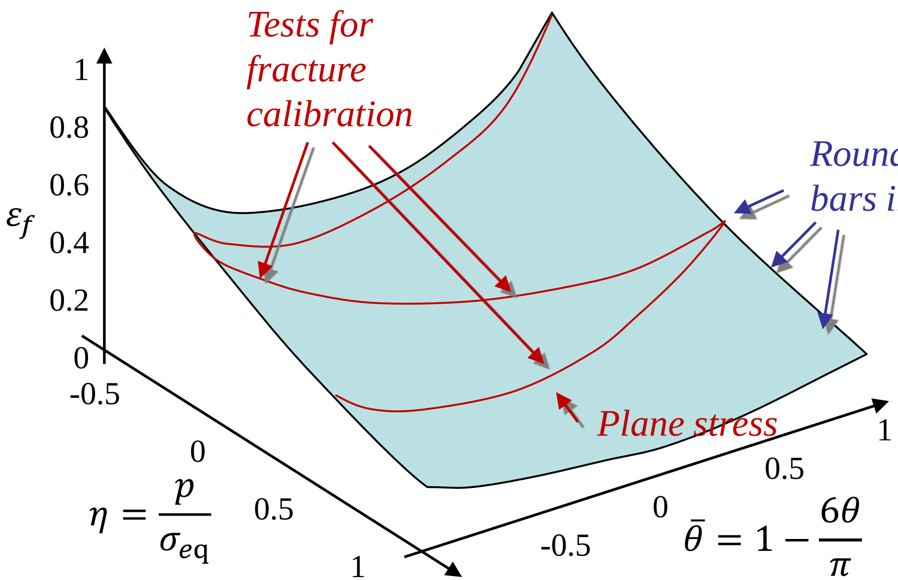

Fracture locus for 2024-T351 aluminum alloy

(Bai & Wierzbicki 2010)

Shear and necking coalescence mechanisms for porous materials

- Hyperelastic-based formulation
  - Multiplicative decomposition

    $\mathbf{F} = \mathbf{F}^{\mathrm{e}} \cdot \mathbf{F}^{\mathrm{p}}, \quad \mathbf{C}^{\mathrm{e}} = \mathbf{F}^{\mathrm{e}^T} \cdot \mathbf{F}^{\mathrm{e}}, \quad J^{e} = \det(\mathbf{F}^{\mathrm{e}})$
  - Stress tensor definition
    - Elastic potential $\psi(\mathbf{C}^{\mathrm{e}})$
    - First Piola-Kirchhoff stress tensor

      $$\mathbf{P} = 2\mathbf{F}^{\mathrm{e}} \cdot \frac{\partial\psi(\mathbf{C}^{\mathrm{e}})}{\partial\mathbf{C}^{\mathrm{e}}} \cdot \mathbf{F}^{\mathrm{p}^{-T}}$$
    - Kirchhoff stress tensors
      - In current configuration

        $$\boldsymbol{\kappa} = \mathbf{P} \cdot \mathbf{F}^{T} = 2\mathbf{F}^{\mathrm{e}} \cdot \frac{\partial\psi(\mathbf{C}^{\mathrm{e}})}{\partial\mathbf{C}^{\mathrm{e}}} \cdot \mathbf{F}^{\mathrm{e}^T}$$
      - In co-rotational space

        $$\boldsymbol{\tau} = \mathbf{C}^{\mathrm{e}} \cdot \mathbf{F}^{\mathrm{e}^{-1}} \cdot \boldsymbol{\kappa} \cdot \mathbf{F}^{\mathrm{e}^{-T}} = 2\mathbf{C}^{\mathrm{e}} \cdot \frac{\partial\psi(\mathbf{C}^{\mathrm{e}})}{\partial\mathbf{C}^{\mathrm{e}}}$$
- Logarithmic deformation
  - Elastic potential ψ:

    $$\psi(\mathbf{C}^{\mathrm{e}}) = \frac{K}{2}\ln^2(J^{e}) + \frac{G}{4}(\ln(\mathbf{C}^{\mathrm{e}}))^{\mathrm{dev}} : (\ln(\mathbf{C}^{\mathrm{e}}))^{\mathrm{dev}}$$
  - Stress tensor in co-rotational space

    $$\boldsymbol{\tau} = \underbrace{K\ln(J^{e})}_{p}\,\mathbf{I} + G(\ln(\mathbf{C}^{\mathrm{e}}))^{\mathrm{dev}}$$

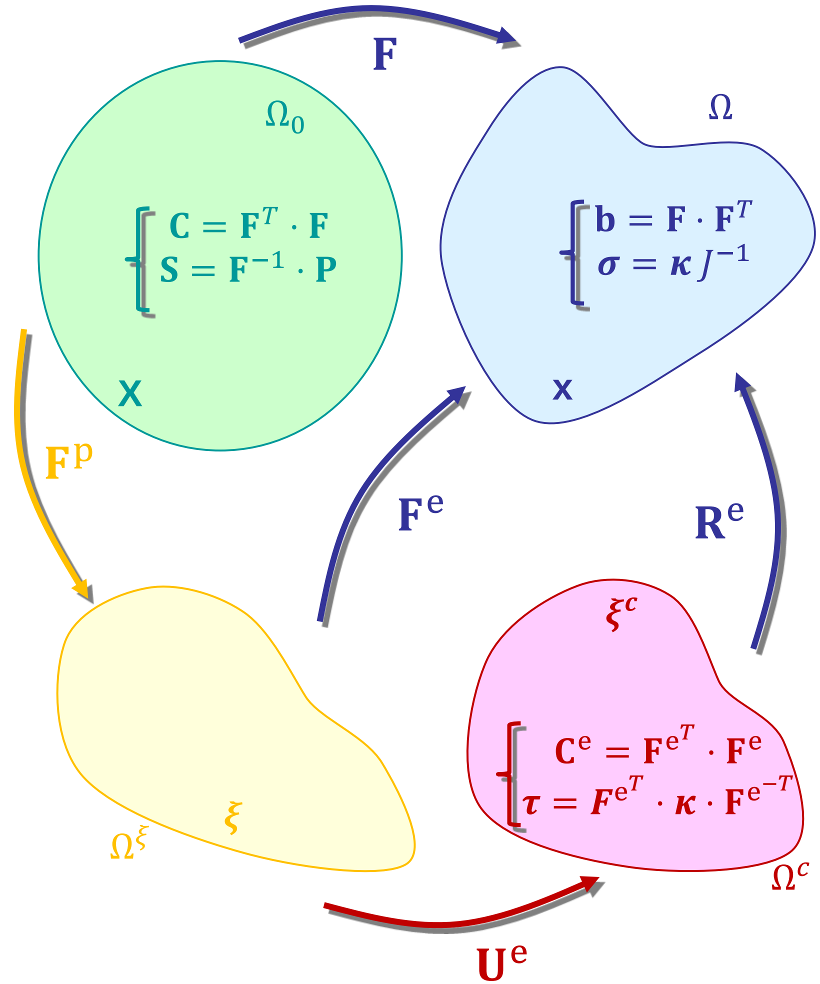

Beginning

Shear and necking coalescence mechanisms for porous materials

- Material changes represented via internal variables
  - Constitutive law $\boldsymbol{\sigma}\left(\boldsymbol{\varepsilon};\boldsymbol{Z}(t')\right)$
  - Internal variables $\boldsymbol{Z}(t')$
    - Plastic flow normal to yield surface Φ

$$\mathbf{D}^{\mathrm{p}} = \dot{\mathbf{F}}^{\mathrm{p}}\mathbf{F}^{\mathrm{p}-1} = \dot{\mu}\frac{\partial\Phi}{\partial\boldsymbol{\sigma}}$$

    - Matrix plastic strain rate $\dot{\varepsilon}_m = \dfrac{\boldsymbol{\sigma}:\mathbf{D}^{\mathrm{p}}}{(1-f)\sigma_Y}$
    - Volumetric plastic deformation $\dot{\varepsilon}_v = \mathrm{tr}\,(\mathbf{D}^{\mathrm{p}})$
    - Deviatoric plastic deformation $\dot{\varepsilon}_d = \sqrt{\frac{2}{3}\mathrm{dev}(\mathbf{D}^{\mathrm{p}}):\mathrm{dev}(\mathbf{D}^{\mathrm{p}})}$
  - Voids characteristics **Y**
    - Porosity : f
    - Void ligament ratio: χ
    - Void aspect ratio: W
    - Void spacing ratio: λ

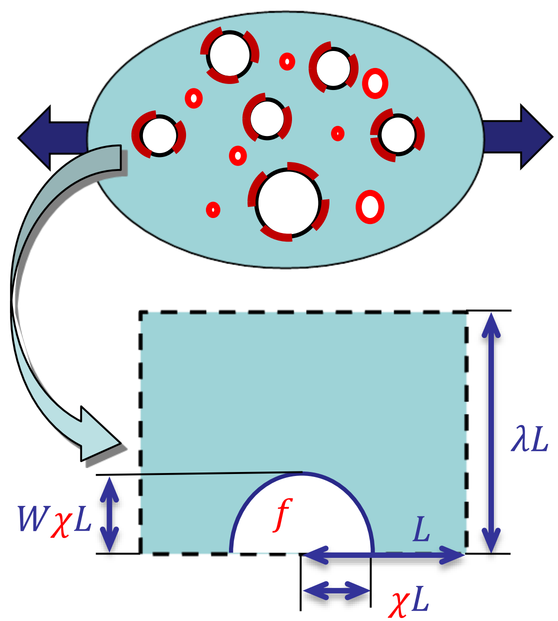

Shear and necking coalescence mechanisms for porous materials

- Non-local formalism
  - Local form
    - Mesh dependency
  - Requires non-local form [Bažant 1988]
    - Introduction of characteristic length l_c
    - Weighted average: $\tilde{Z}_k(\boldsymbol{x}) = \int_{V_C} W(\boldsymbol{y};\boldsymbol{x},l_c)\ Z_k(\mathbf{y})d\boldsymbol{y}$
  - Implicit form [Peerlings et al. 1998]
    - New degrees of freedom: $\tilde{Z}_k$
    - New Helmholtz-type equations: $\tilde{Z}_k - l_c^2\ \Delta\tilde{Z}_k = Z_k$
  - Constitutive law $\boldsymbol{\sigma}\left(\boldsymbol{\varepsilon},\widetilde{\boldsymbol{Z}}(t');\boldsymbol{Z}(t')\right)$

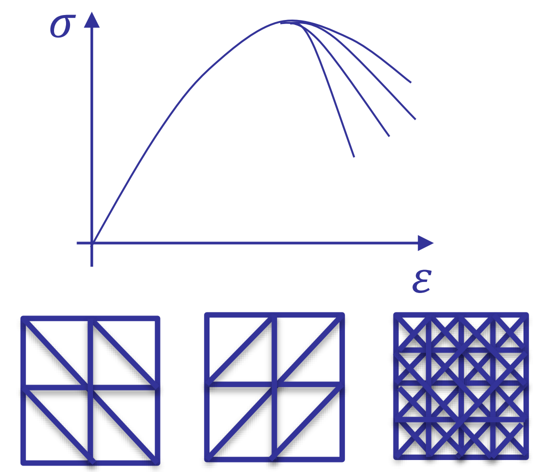

The numerical results change without convergence

- Non-local multi-mechanisms

$$\begin{cases} \dot{\varepsilon}_m = \dfrac{\boldsymbol{\sigma}:\mathbf{D}^{\mathrm{p}}}{(1-f)\sigma_Y} \\ \dot{\varepsilon}_v = \mathrm{tr}\,(\mathbf{D}^{\mathrm{p}}) \\ \dot{\varepsilon}_d = \sqrt{\dfrac{2}{3}\mathrm{dev}(\mathbf{D}^{\mathrm{p}}):\mathrm{dev}(\mathbf{D}^{\mathrm{p}})} \end{cases} \Rightarrow \begin{cases} \tilde{\varepsilon}_m - l_c^2\ \Delta\tilde{\varepsilon}_m = \varepsilon_m \\ \tilde{\varepsilon}_v - l_c^2\ \Delta\tilde{\varepsilon}_v = \varepsilon_v \\ \tilde{\varepsilon}_d - l_c^2\ \Delta\tilde{\varepsilon}_d = \varepsilon_d \end{cases}$$

- Different yield surfaces: void growth
  - Classical GTN model
    - Non-local porosity evolution

$$\dot{f} = \dot{f}_{\mathrm{gr}} + \dot{f}_{\mathrm{nu}} + \dot{f}_{\mathrm{sh}}$$

$$\begin{cases} \dot{f}_{\mathrm{gr}} = (1-f)\dot{\tilde{\varepsilon}}_v \\ \dot{f}_{\mathrm{nu}} = A_n(\tilde{\varepsilon}_m)\dot{\tilde{\varepsilon}}_m \\ \dot{f}_{\mathrm{sh}} = k_w \phi_\eta\left(\dfrac{p}{\sigma_{\mathrm{eq}}}\right)\phi_\omega(\cos 3\theta) f \dot{\tilde{\varepsilon}}_d \end{cases}$$

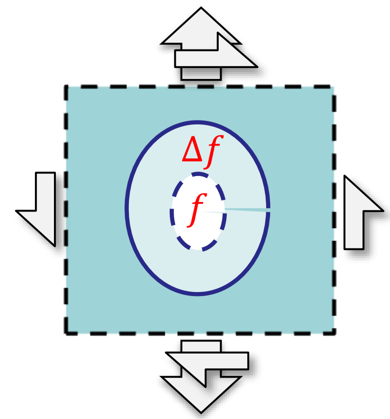

    - Yield surface

$$\phi_{\mathrm{G}} = \frac{\sigma_{\mathrm{eq}}^2}{\sigma_{\mathrm{Y}}^2} + 2q_1 f \cosh\left(\frac{q_2 p}{2\sigma_{\mathrm{Y}}}\right) - 1 - q_3^2 f^2 \leq 0$$

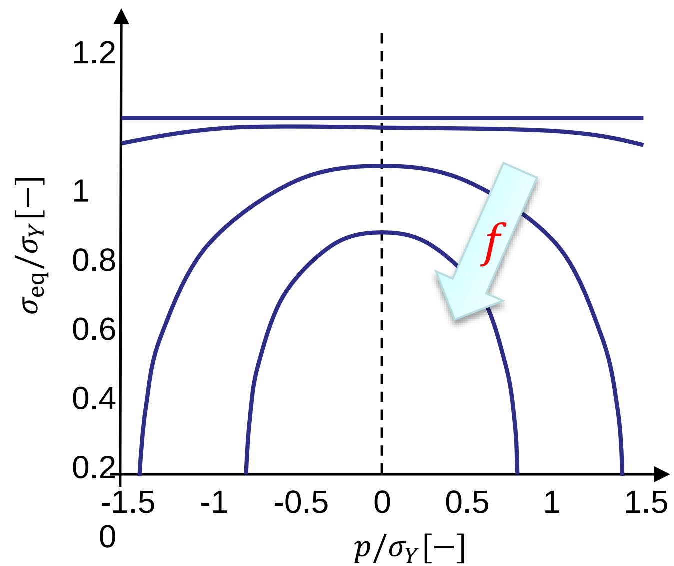

- Different yield surfaces: coalescence
  - Coalescence by necking
    - Yield surface

$$\phi_{\mathrm{T}} = \frac{2}{3}\sigma_{\mathrm{eq}}\cos\theta + |p| - C_{\mathrm{T}}^{f}(\chi, \mathrm{W})\sigma_{\mathrm{Y}} \leq 0$$

Max Principal Stress

    - Limit load factor

$$C_{\mathrm{T}}^{f}(\chi, W) = (1-\chi^2)\left[h\left(\frac{1-\chi}{W\chi}\right)^2 + g\sqrt{\frac{1}{\chi}}\right]$$

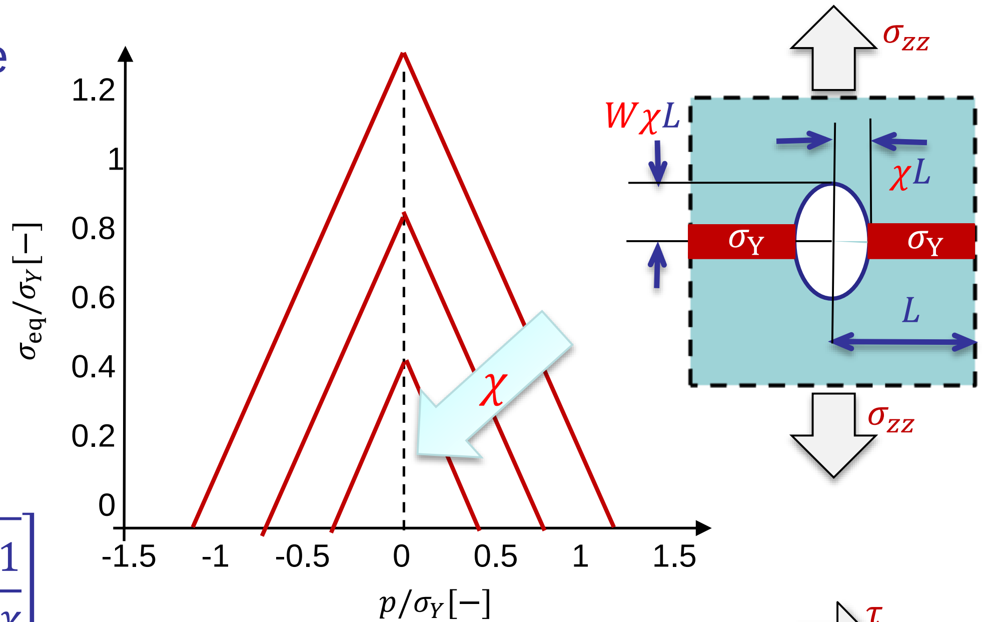

  - Coalescence by shearing
    - Yield surface

$$\phi_{\mathrm{S}} = \sqrt{3}\tau - C_{\mathrm{S}}^{f}(\chi)\sigma_{\mathrm{Y}} = \sigma_{\mathrm{eq}}\left(\frac{\sin\theta}{2} + \frac{\sqrt{3}\cos\theta}{2}\right) - C_{\mathrm{S}}^{f}(\chi)\sigma_{\mathrm{Y}} \leq 0$$

Max Shear Stress

    - Limit load factor

$$C_{\mathrm{S}}^{f}(\chi) = \xi(1-\chi^2)$$

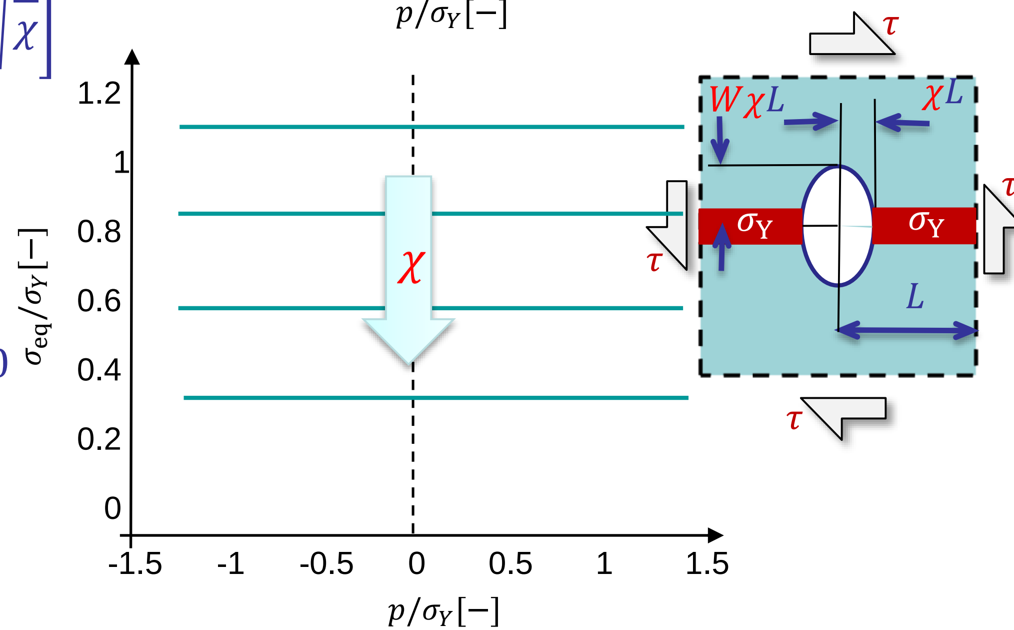

Shear and necking coalescence mechanisms for porous materials

- Multi-surface model
  - Effective yield surface

$$\phi_{\mathrm{e}} = \begin{pmatrix} (\phi_{\mathrm{G}}+1)^m + \\ (\phi_{\mathrm{T}}+1)^m + \\ (\phi_{\mathrm{S}}+1)^m \end{pmatrix}^{1/m}$$

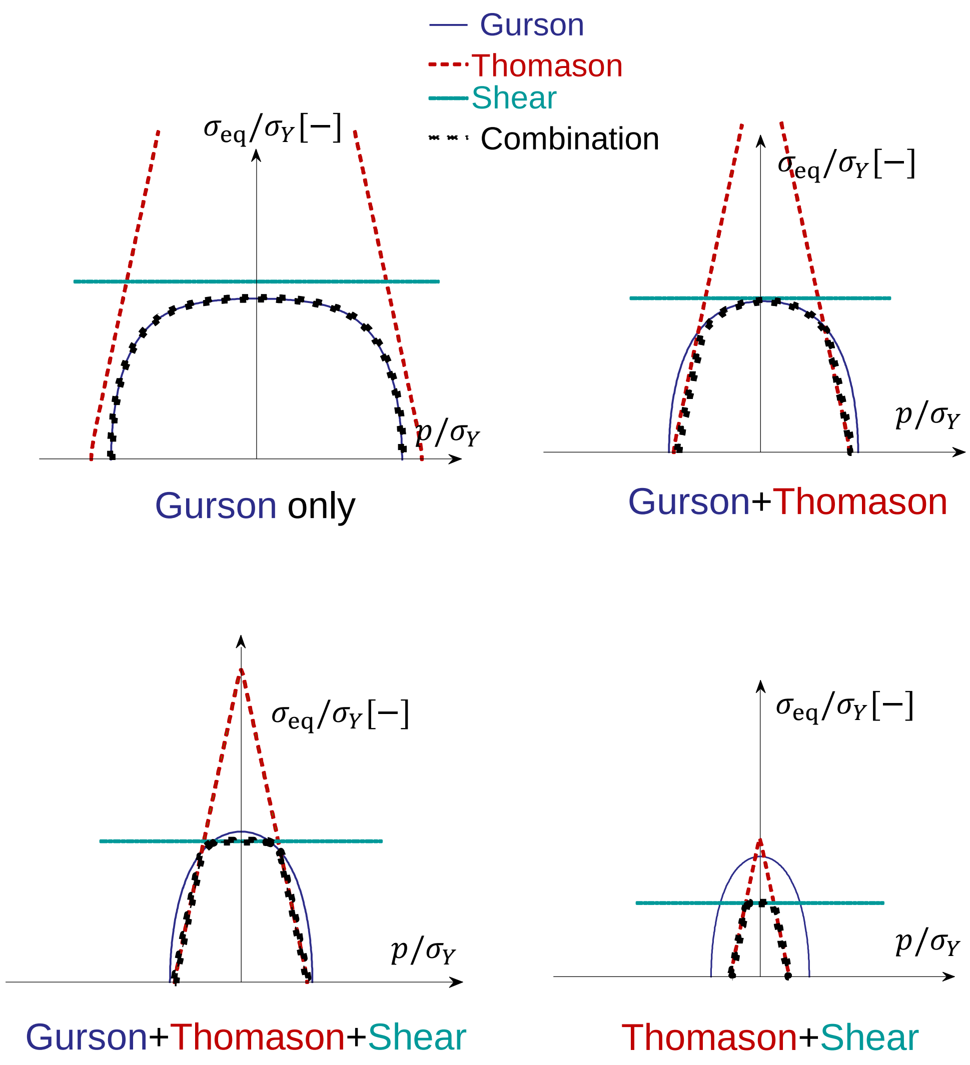

Shear and necking coalescence mechanisms for porous materials

- Solution under proportional loadings
  - Constant
    - Stress triaxiality ($\frac{p}{\sigma_{\mathrm{eq}}}$); and
    - Normalized Lode angle ($\bar{\theta} = 1 - \frac{6\theta}{\pi}$)
  - $\varepsilon_{\mathrm{dc}}$- ductility = plastic deformation at coalescence onset

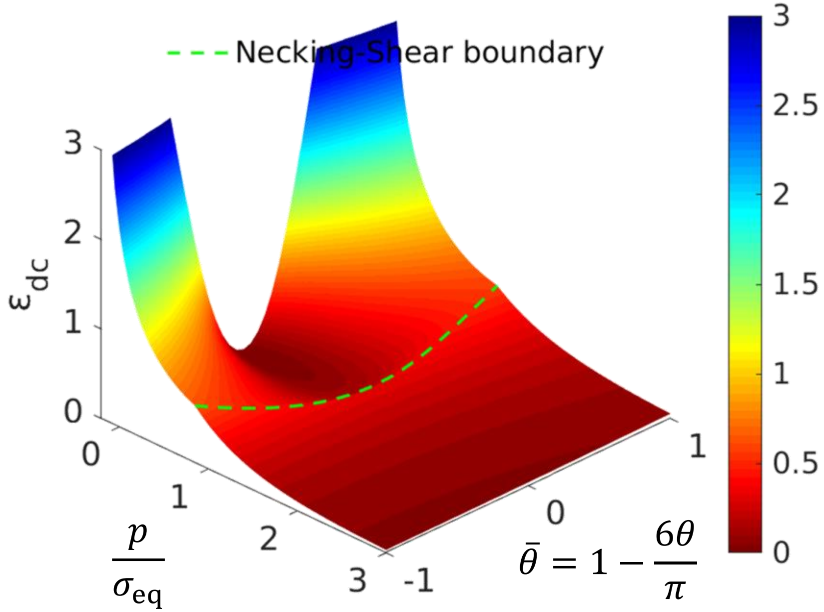

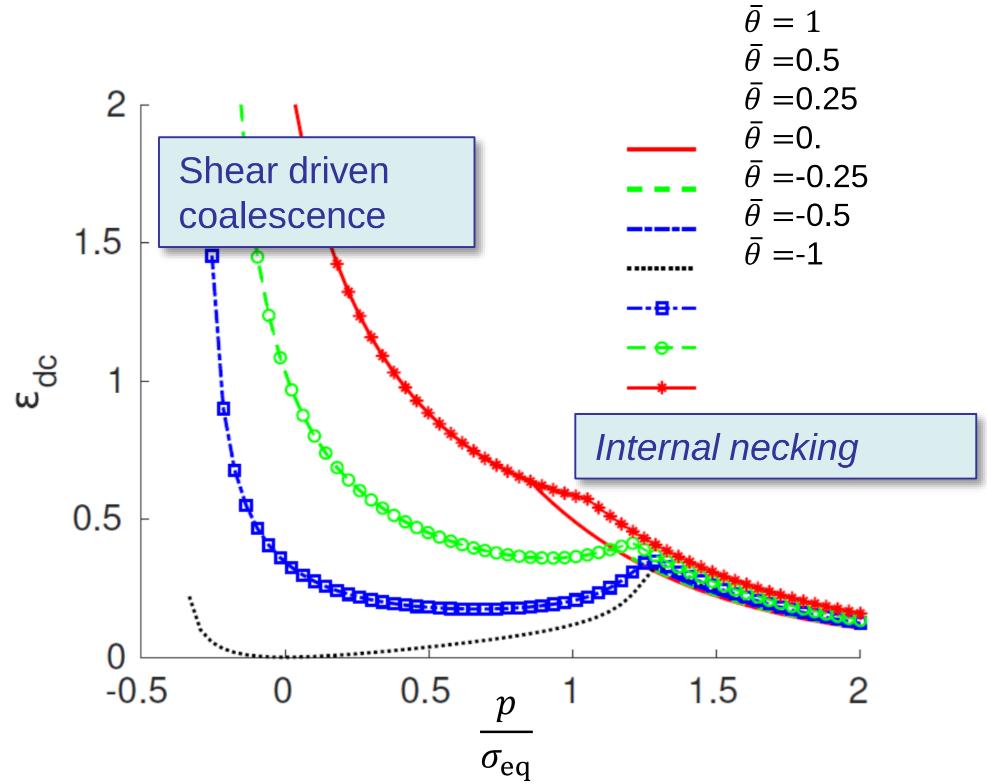

Shear and necking coalescence mechanisms for porous materials

- Plane strain smooth specimen under tensile loading
  - Verification of the nonlocal model: mesh convergence

$L = 12.5$ mm
$e_0 = 3$ mm
$\xi = 1.015$ ($\varepsilon_{ds} = 0.95$)

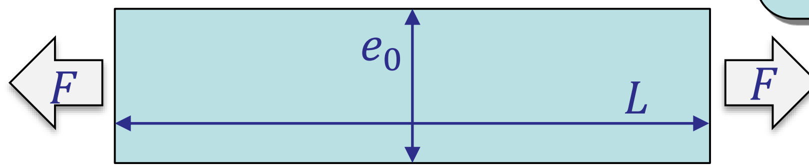

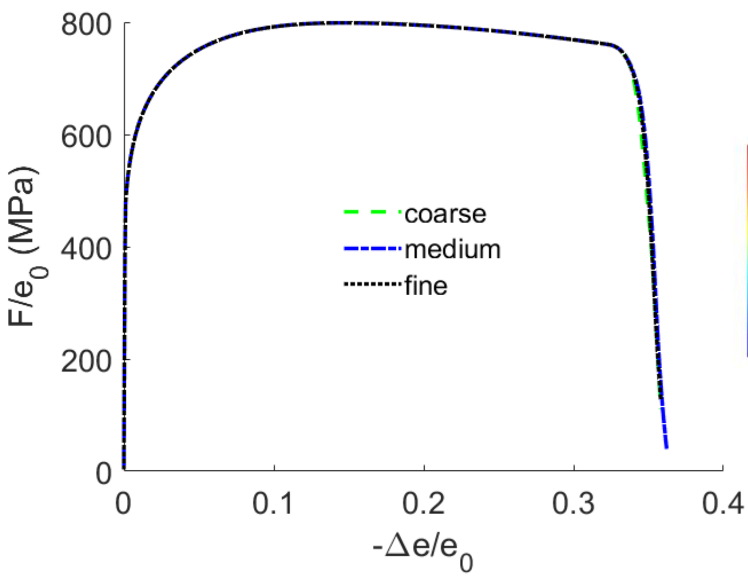

Distribution of void ligament ratio χ

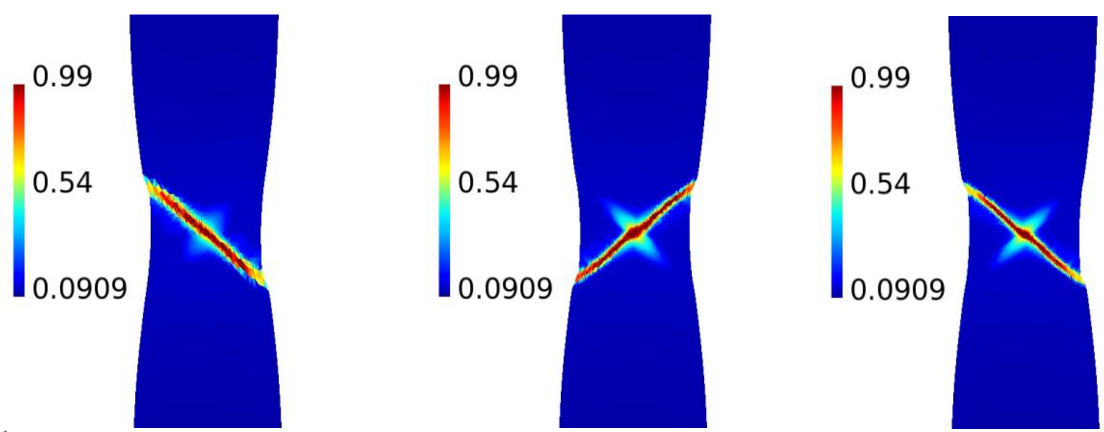

Coarse Medium Fine

Capture slant fracture

Shear and necking coalescence mechanisms for porous materials

- Plane strain smooth specimen under tensile loading
  - Effect of ξ

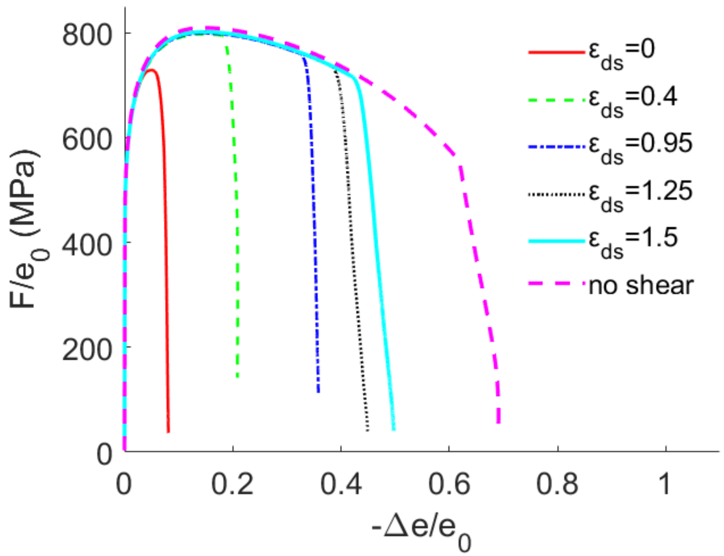

$L = 12.5$ mm
$e_0 = 3$ mm

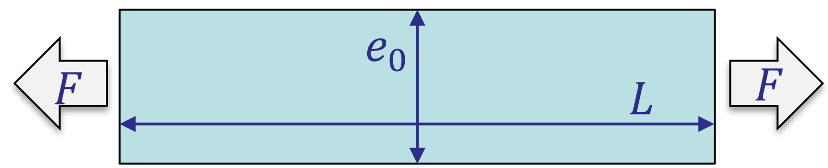

Distribution of void ligament ratio χ

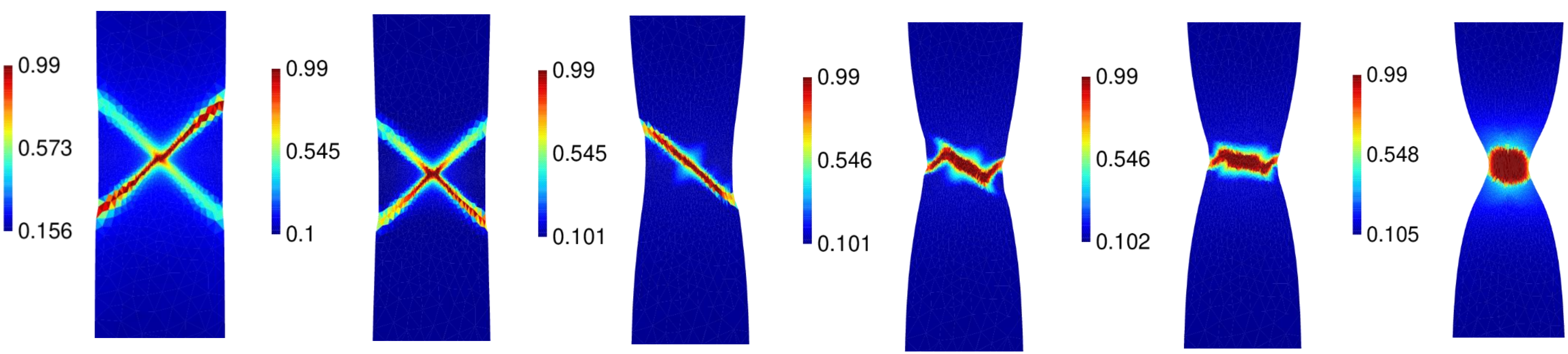

$\varepsilon_{ds} = 0$ | $\varepsilon_{ds} = 0.4$ | $\varepsilon_{ds} = 0.95$ | $\varepsilon_{ds} = 1.25$ | $\varepsilon_{ds} = 1.5$ | no shear

Shear and necking coalescence mechanisms for porous materials

- Axisymmetric (notched) specimens under tensile loading
  - Different notch radii: $R_0/R_n = 0, 0.2, 0.6, 1, 1.5$

$R_0 = 3$ mm
$R_1 = 6$ mm
$L = 25$ mm
$\xi = 1.015$ ($\varepsilon_{ds} = 0.95$)

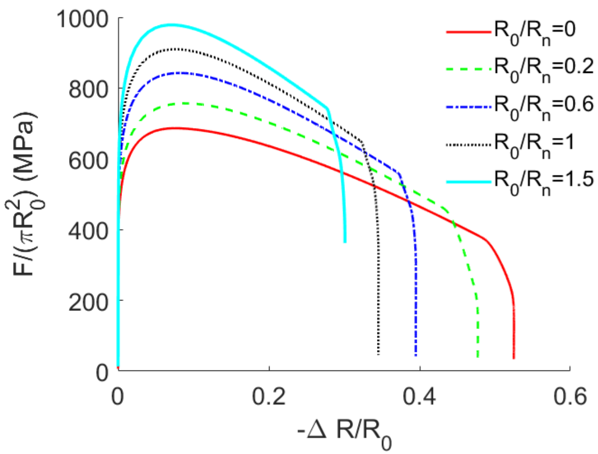

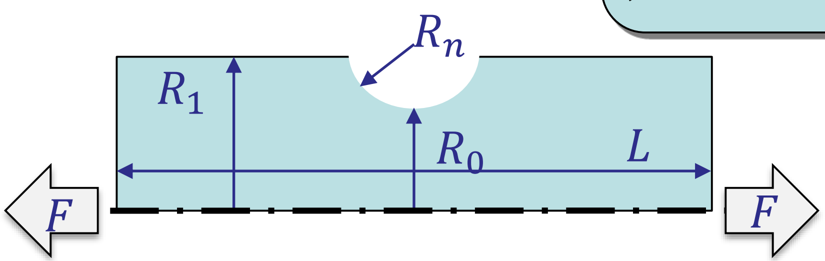

Distribution of void ligament ratio χ

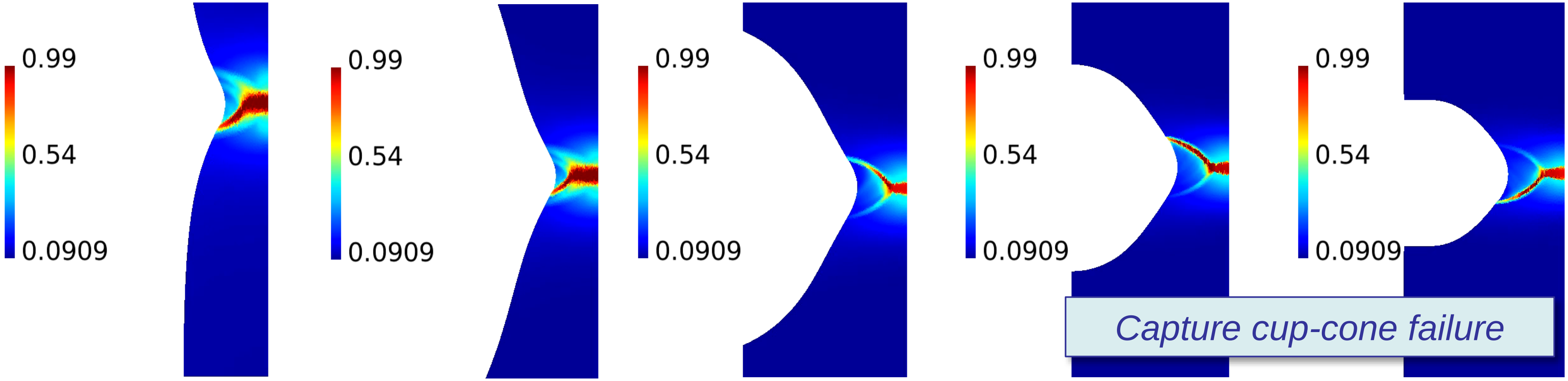

- EntroTough WalInnov project: UCL, ULB (Belgium)
  - Publication (doi): 10.1016/j.jmps.2020.103891

Shear and necking coalescence mechanisms for porous materials

- Grooved plate

- EntroTough WalInnov project
  - UCL, ULB (Belgium)
- Publication (doi)
  - 10.1016/j.jmps.2020.103891

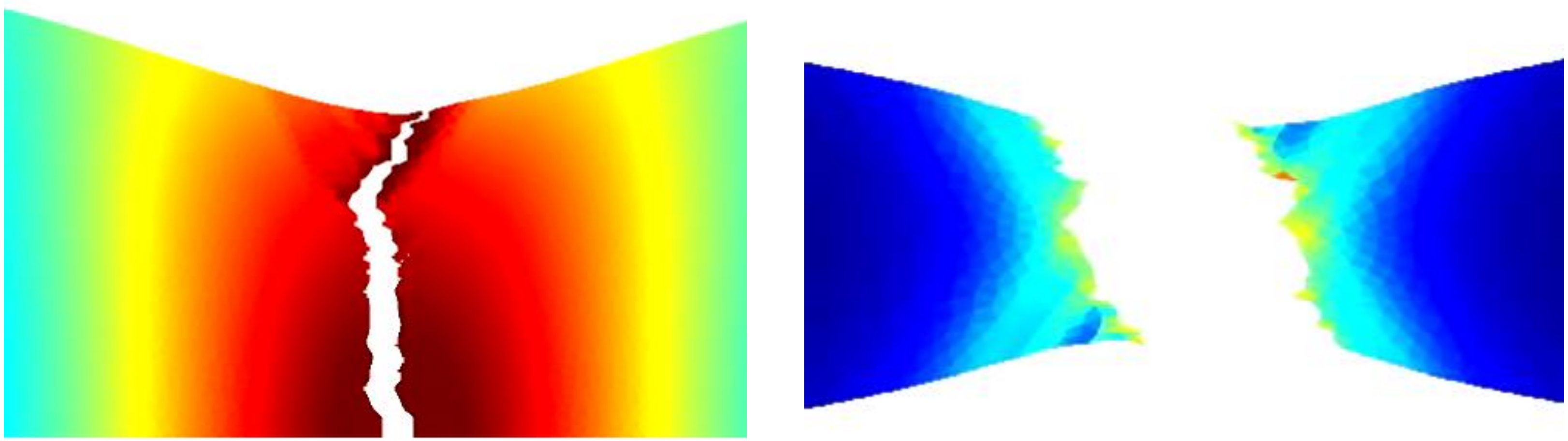

Non-local Gurson damage model to crack transition

The research has been funded by the Walloon Region under the agreement no.7581-MRIPF in the context of the 16th MECATECH call.

Non-local Gurson damage model to crack transition

- Objective:
  - To develop high fidelity numerical methods for ductile failure

- Numerical approach:
  - Combination of 2 complementary methods in a single finite element framework:
    - continuous (damage model)

      + transition to
    - discontinuous (cohesive band model including triaxiality / strain rate effects)

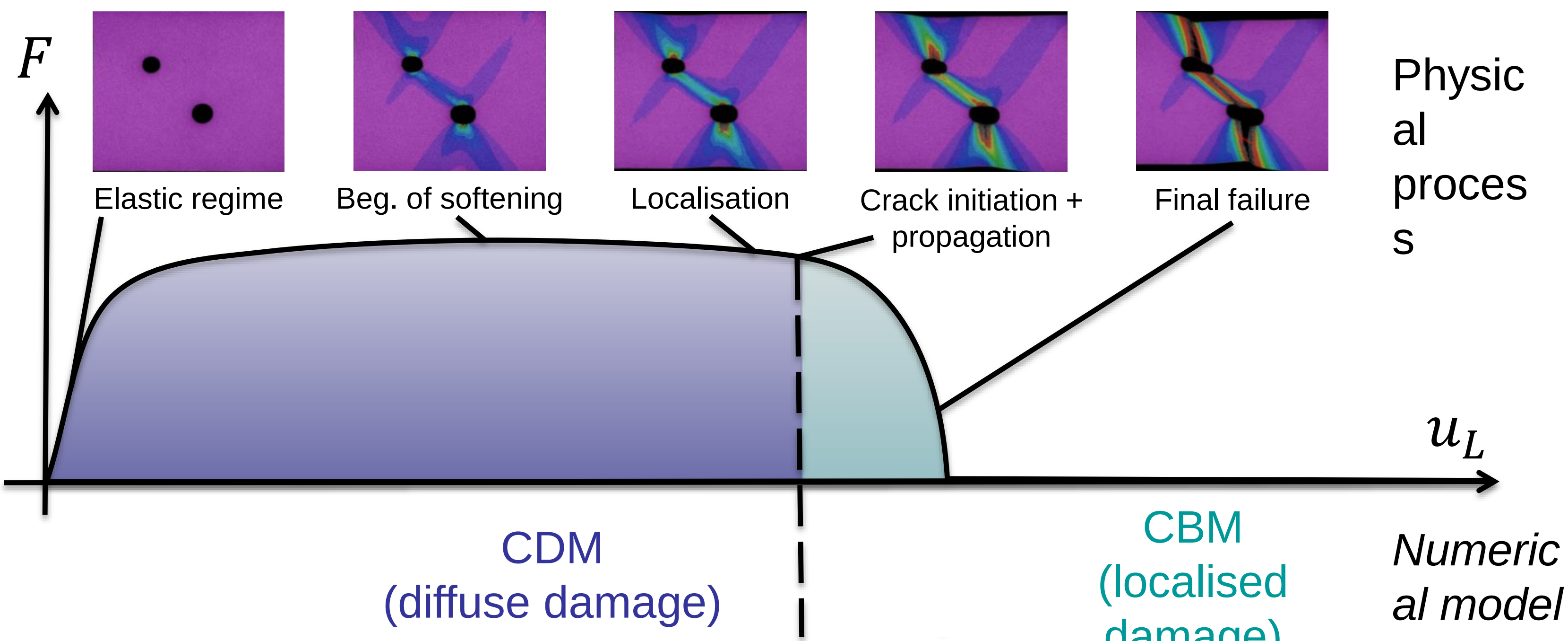

Non-local Gurson damage model to crack transition

- Material changes represented via internal variables
  - Constitutive law $\boldsymbol{\sigma}\left(\boldsymbol{\varepsilon};\boldsymbol{Z}(t')\right)$
    - Internal variables $\boldsymbol{Z}(t')$
  - Different models
    - Lemaitre-Chaboche (degraded properties)
    - Gurson model (yield surface in terms of porosity f)

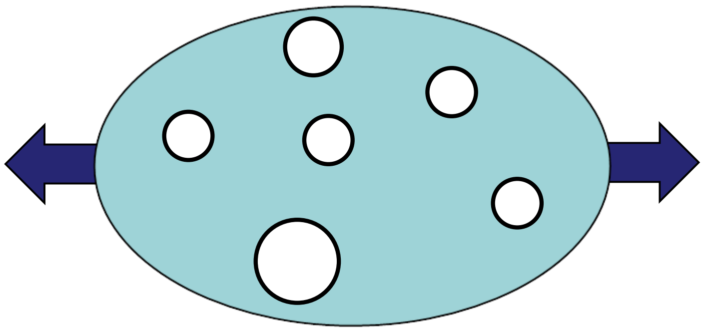

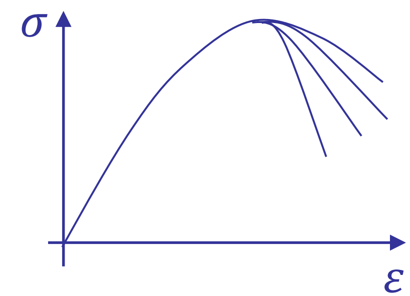

- Model implementation:
  - Local form
    - Mesh dependency
  - Requires non-local form [Bažant 1988]
    - Introduction of characteristic length l_c
    - Weighted average: $\tilde{Z}(\boldsymbol{x}) = \int_{V_C} W(\boldsymbol{y};\boldsymbol{x},l_c)\; Z(\mathbf{y})d\boldsymbol{y}$
  - Implicit form [Peerlings et al. 1998]
    - New degrees of freedom: $\tilde{Z}$
    - New Helmholtz-type equations: $\tilde{Z} - l_c^2\,\Delta\tilde{Z} = Z$

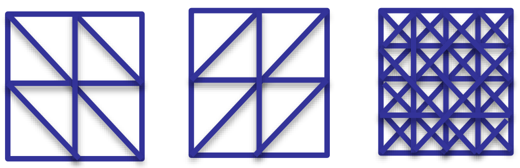

The numerical results change without convergence

Non-local Gurson damage model to crack transition

- Hyperelastic-based formulation
  - Multiplicative decomposition
    $\mathbf{F} = \mathbf{F}^{\mathrm{e}} \cdot \mathbf{F}^{\mathrm{p}}, \quad \mathbf{C}^{\mathrm{e}} = \mathbf{F}^{\mathrm{e}^T} \cdot \mathbf{F}^{\mathrm{e}}, \quad J^{e} = \det(\mathbf{F}^{\mathrm{e}})$
  - Stress tensor definition
    - Elastic potential $\psi(\mathbf{C}^{\mathrm{e}})$
    - First Piola-Kirchhoff stress tensor
      $$\mathbf{P} = 2\mathbf{F}^{\mathrm{e}} \cdot \frac{\partial \psi(\mathbf{C}^{\mathrm{e}})}{\partial \mathbf{C}^{\mathrm{e}}} \cdot \mathbf{F}^{\mathrm{p}^{-T}}$$
    - Kirchhoff stress tensors
      - In current configuration
        $$\boldsymbol{\kappa} = \mathbf{P} \cdot \mathbf{F}^{T} = 2\mathbf{F}^{\mathrm{e}} \cdot \frac{\partial \psi(\mathbf{C}^{\mathrm{e}})}{\partial \mathbf{C}^{\mathrm{e}}} \cdot \mathbf{F}^{\mathrm{e}^T}$$
      - In co-rotational space
        $$\boldsymbol{\tau} = \mathbf{C}^{\mathrm{e}} \cdot \mathbf{F}^{\mathrm{e}^{-1}} \cdot \boldsymbol{\kappa} \cdot \mathbf{F}^{\mathrm{e}^{-T}} = 2\mathbf{C}^{\mathrm{e}} \cdot \frac{\partial \psi(\mathbf{C}^{\mathrm{e}})}{\partial \mathbf{C}^{\mathrm{e}}}$$
- Logarithmic deformation
  - Elastic potential ψ:
    $$\psi(\mathbf{C}^{\mathrm{e}}) = \frac{K}{2} \ln^2(J^{e}) + \frac{G}{4} (\ln(\mathbf{C}^{\mathrm{e}}))^{\mathrm{dev}} : (\ln(\mathbf{C}^{\mathrm{e}}))^{\mathrm{dev}}$$
  - Stress tensor in co-rotational space
    $$\boldsymbol{\tau} = \underbrace{K \ln(J^{e})}_{p} \, \mathbf{I} + G (\ln(\mathbf{C}^{\mathrm{e}}))^{\mathrm{dev}}$$

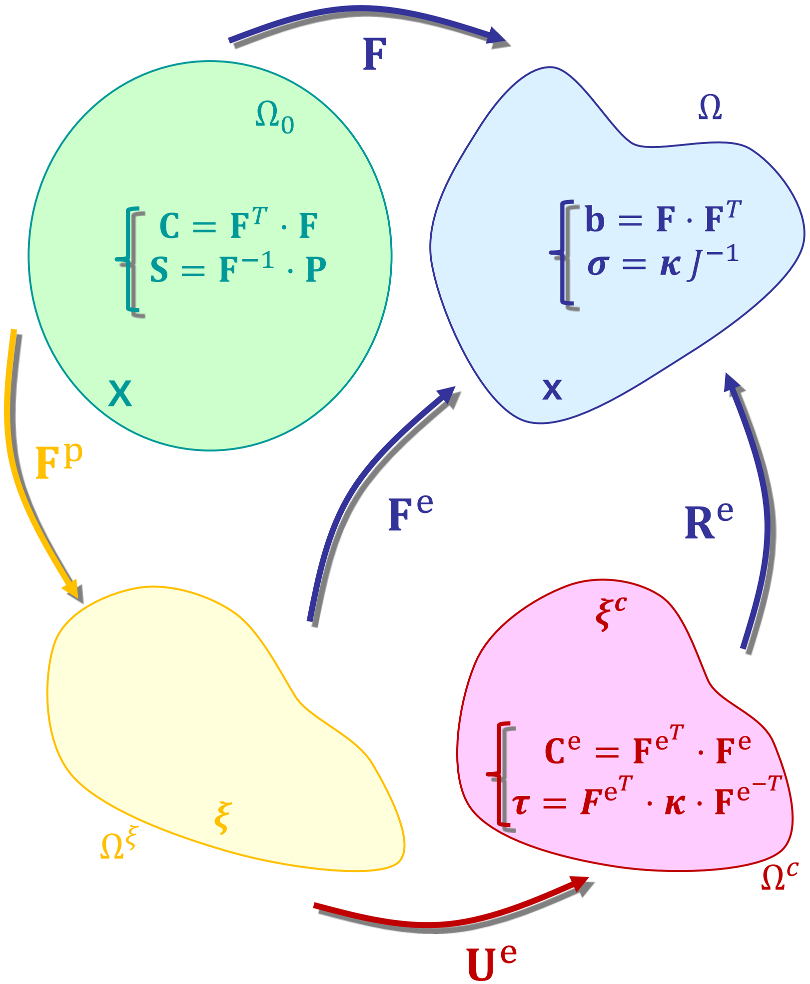

- Porous plasticity (or Gurson) approach
  - Competition between 2 plastic modes:

Growth mode: Gurson model

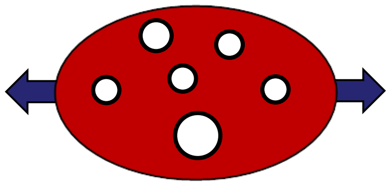

Coalescence mode: Thomason model

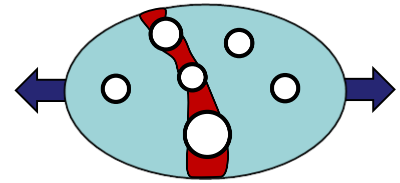

$$\phi_{\mathrm{G}} = \frac{\tau_{\mathrm{eq}}^2}{\tau_{\mathrm{Y}}^2} + 2q_1\tilde{f}\cosh\left(\frac{q_2 p}{2\tau_{\mathrm{Y}}}\right) - 1 - q_3^2\tilde{f}^2 \leq 0$$

vs

$$\phi_{\mathrm{T}} = \frac{2}{3}\tau_{\mathrm{eq}} + |p| - C_{\mathrm{T}}^{f}(\chi)\tau_{\mathrm{Y}} \leq 0$$

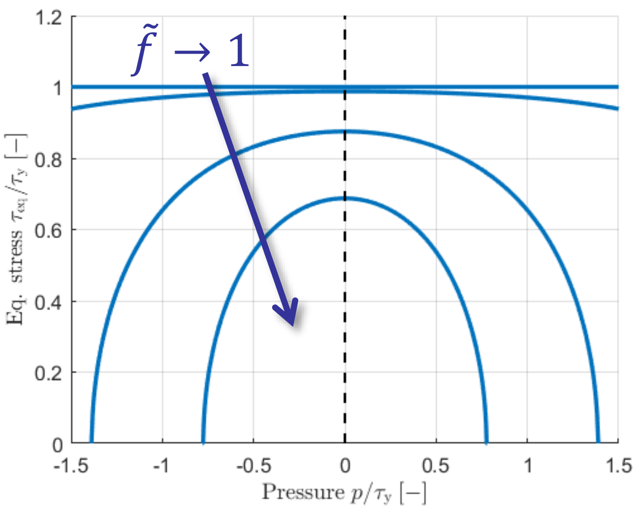

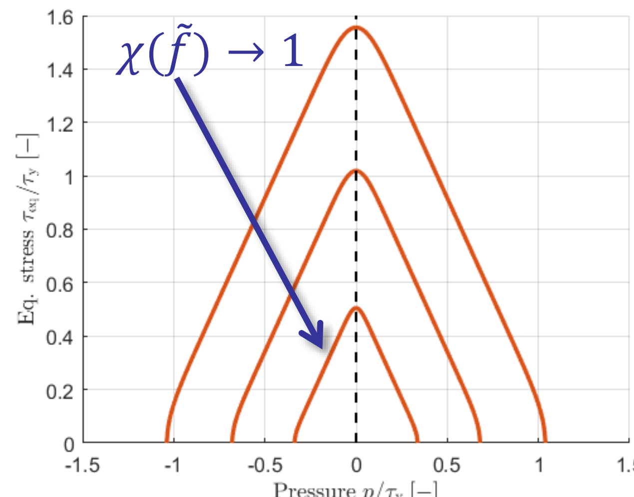

- Hybrid DG model: use of a Cohesive Band Model (CBM)
  - Principles
    - Substitute TSL of CZM by the behavior of a uniform band of thickness h_{b} [Remmers et al. 2013]

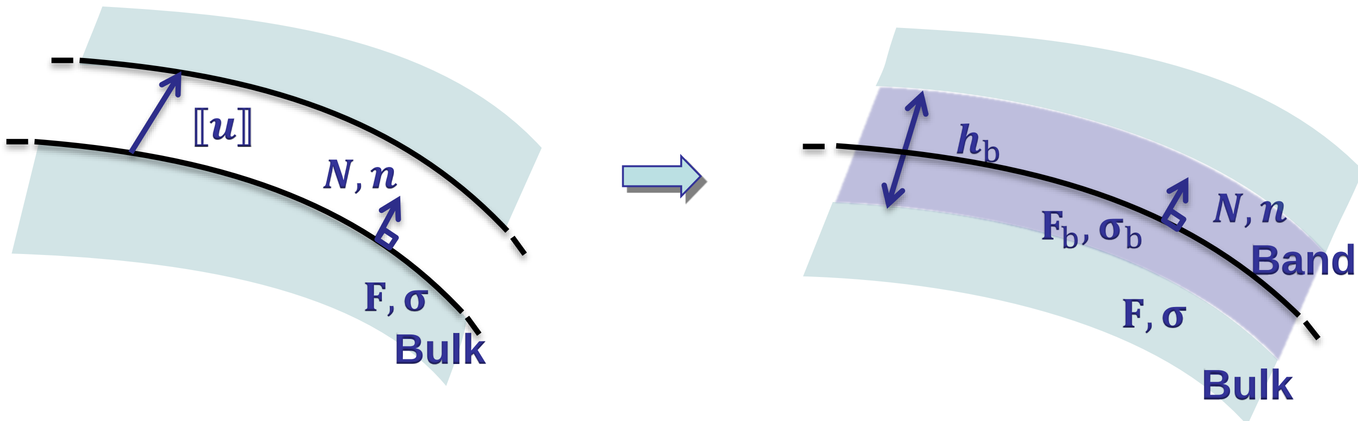

  - Localization criterion
    - Thomason: $\boldsymbol{N} \cdot \boldsymbol{\tau} \cdot \boldsymbol{N} - C_I^f \tau_y \geq 0$
  - Methodology [Leclerc et al. 2018]
    1. Compute a band strain tensor $\mathbf{F}_{\mathrm{b}} = \mathbf{F} + \frac{[\![\boldsymbol{u}]\!] \otimes \boldsymbol{N}}{h_b} + \frac{1}{2} \boldsymbol{\nabla}_T [\![\boldsymbol{u}]\!]$
    2. Compute a band stress tensor $\boldsymbol{\sigma}_{\mathrm{b}}\left(\mathbf{F}_{\mathrm{b}}; \mathrm{Z}(\tau)\right)$ using the same CDM as bulk elements
    3. Recover a surface traction $\boldsymbol{t}([\![\boldsymbol{u}]\!], \mathbf{F}) = \boldsymbol{\sigma}_{\mathrm{b}}.\boldsymbol{n}$
  - What is the effect of h_{b} (band thickness)
    - Recover the fracture energy

Non-local Gurson damage model to crack transition

- Comparison with literature [Huespe2012,Besson2003]

Slanted plane strain specimen

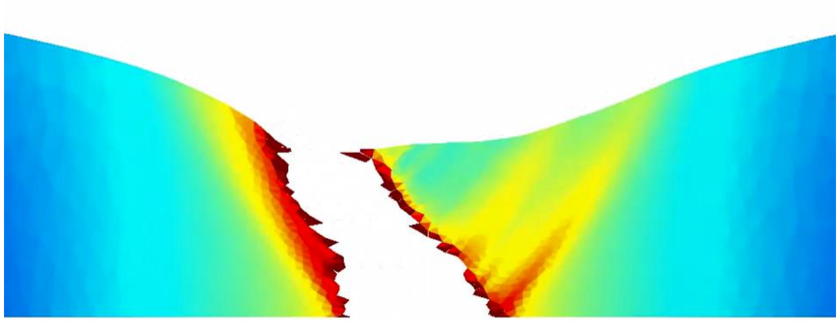

Cup-cone in round bar

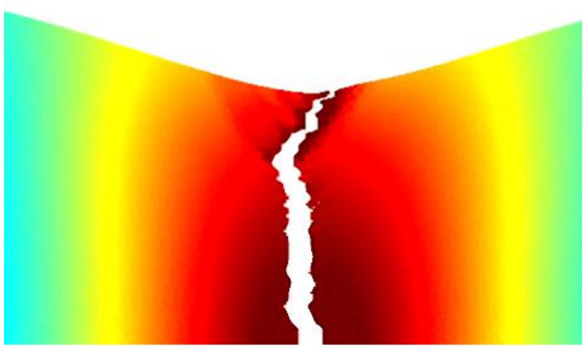

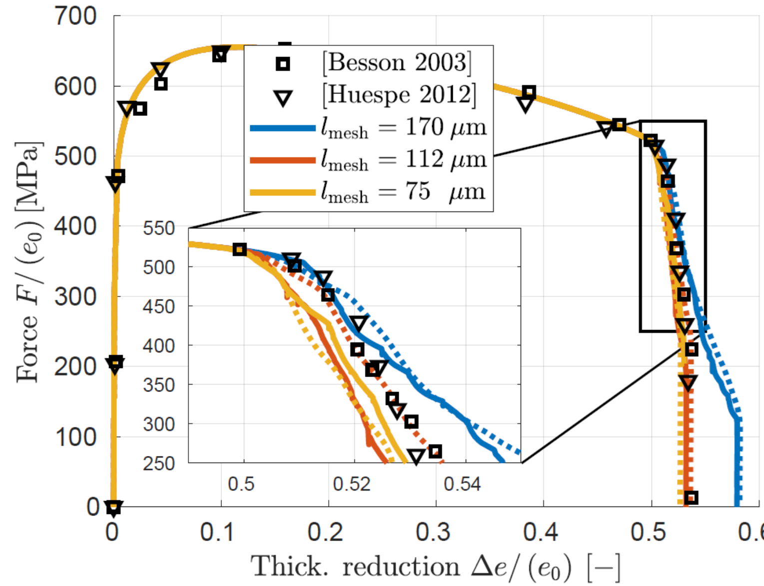

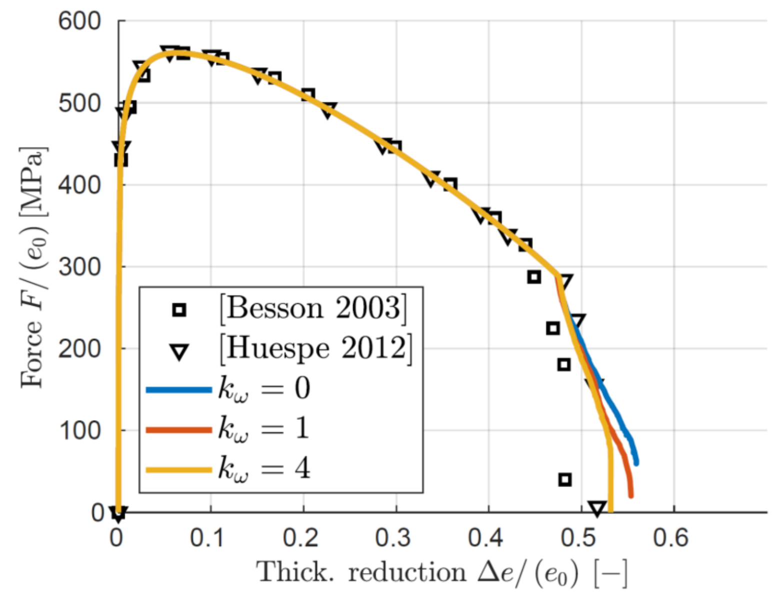

Non-local Gurson damage model to crack transition

- Grooved plate

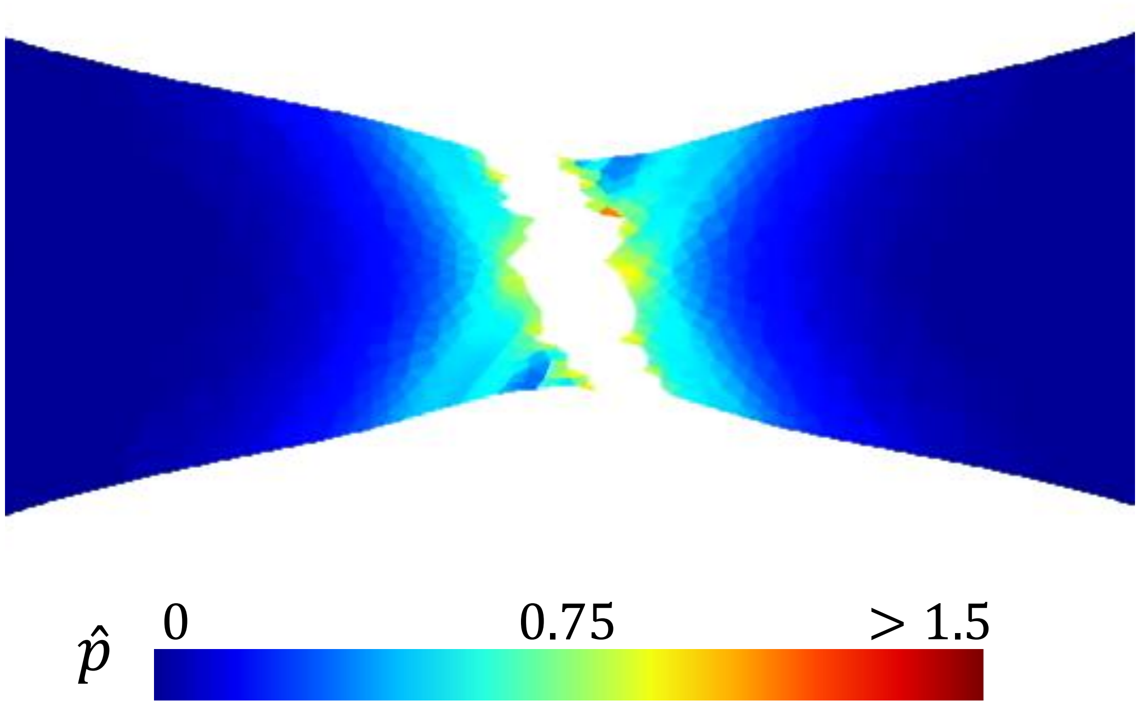

- MRIPF MECATECH project
  - GDTech, UCL, FZ, MECAR, Capital People (Belgium)
- Publication (doi)
  - 10.1002/nme.5618
  - 10.1016/j.ijplas.2019.11.010

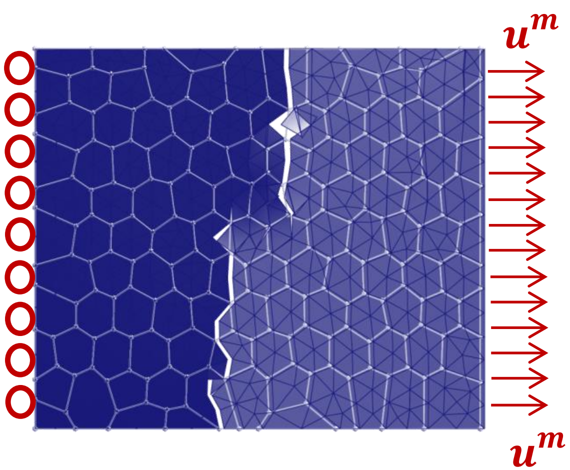

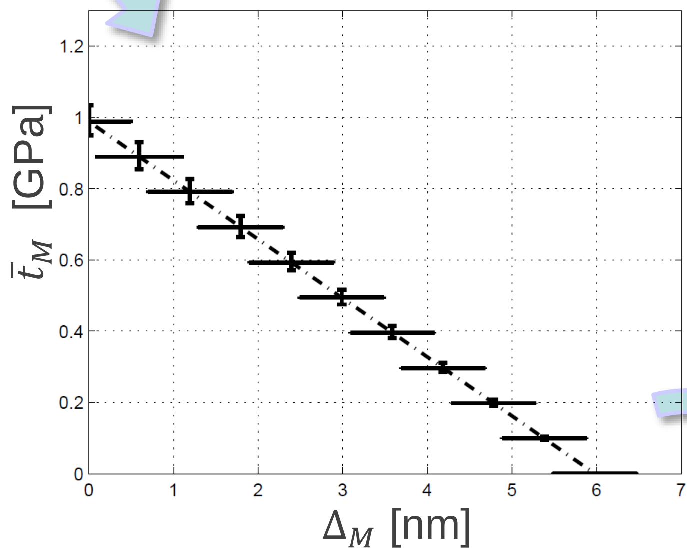

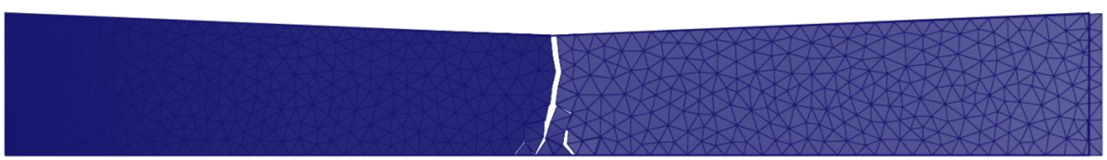

Stochastic Multi-Scale Fracture of Polycrystalline Films

Robust design of MEMS: Financial support from F. R. S. - F. N. R. S. under the project number FRFC 2.4508.11

Stochastic Multi-Scale Fracture of Polycrystalline Films

- Multi-scale modeling
  - 2 problems are solved concurrently
    - The macro-scale problem
    - The meso-scale problem (on a meso-scale Volume Element)

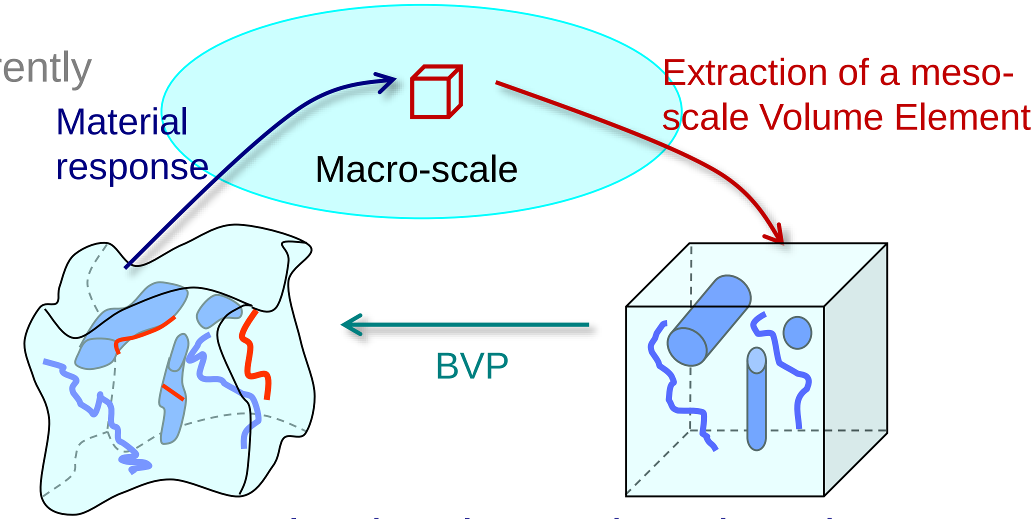

- For meso-scale volume elements not several orders larger than the micro-structure size and embedding crack propagations

$$L_{macro} >> L_{VE} \sim ?\ L_{micro}$$

For accuracy: Size of the meso-scale volume element smaller than the characteristic length of the macro-scale loading

Meso-scale volume element no longer statistically representative:
- **Stochastic Volume Elements**
- **Should recover consistency lost due to the discontinuity**

- Micro-scale model: Silicon crystal
  - Different fracture strengths and critical energy release rates

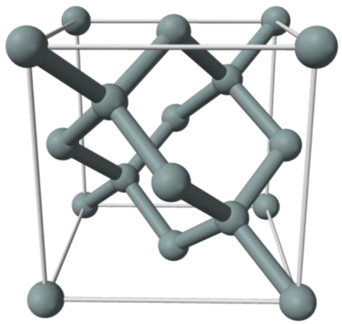

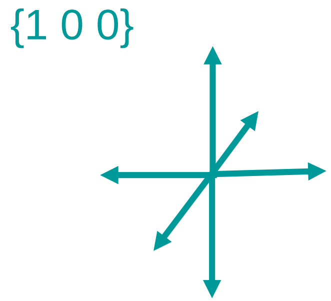

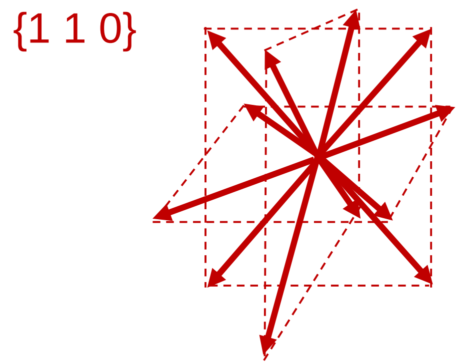

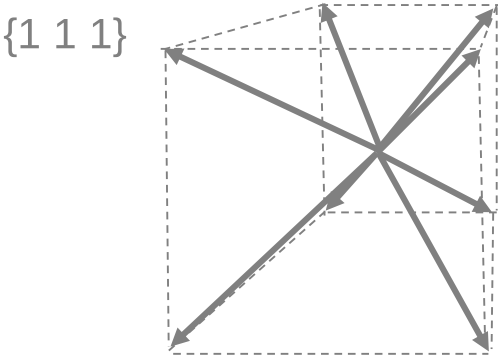

  - Define a “continuous” strength mapping

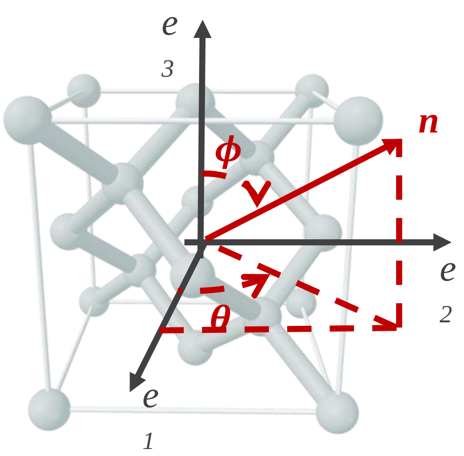

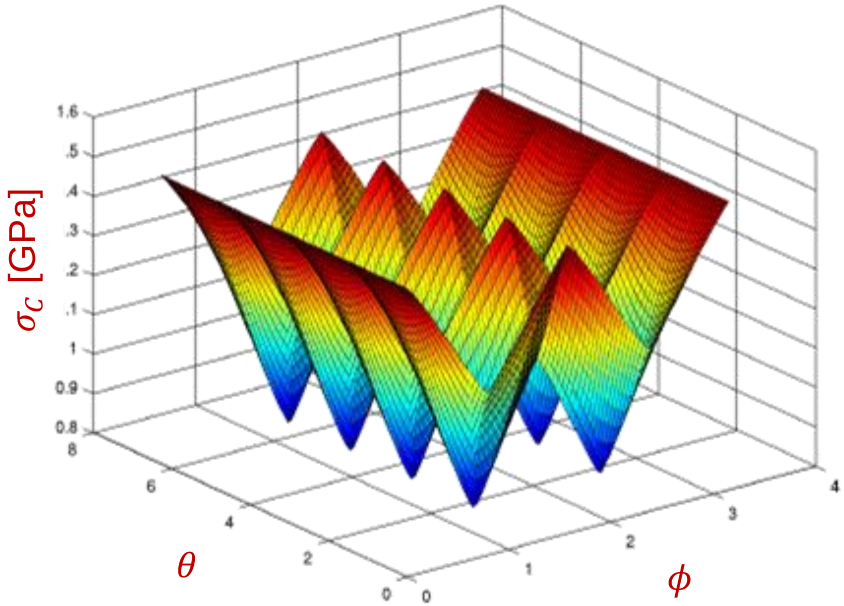

Stochastic Multi-Scale Fracture of Polycrystalline Films

- Micro-scale model: Polycrsytalline films
  - Discontinuous Galerkin method
  - Extrinsic cohesive law
  - Intra/Inter granular fracture
  - Accounts for interface orientation

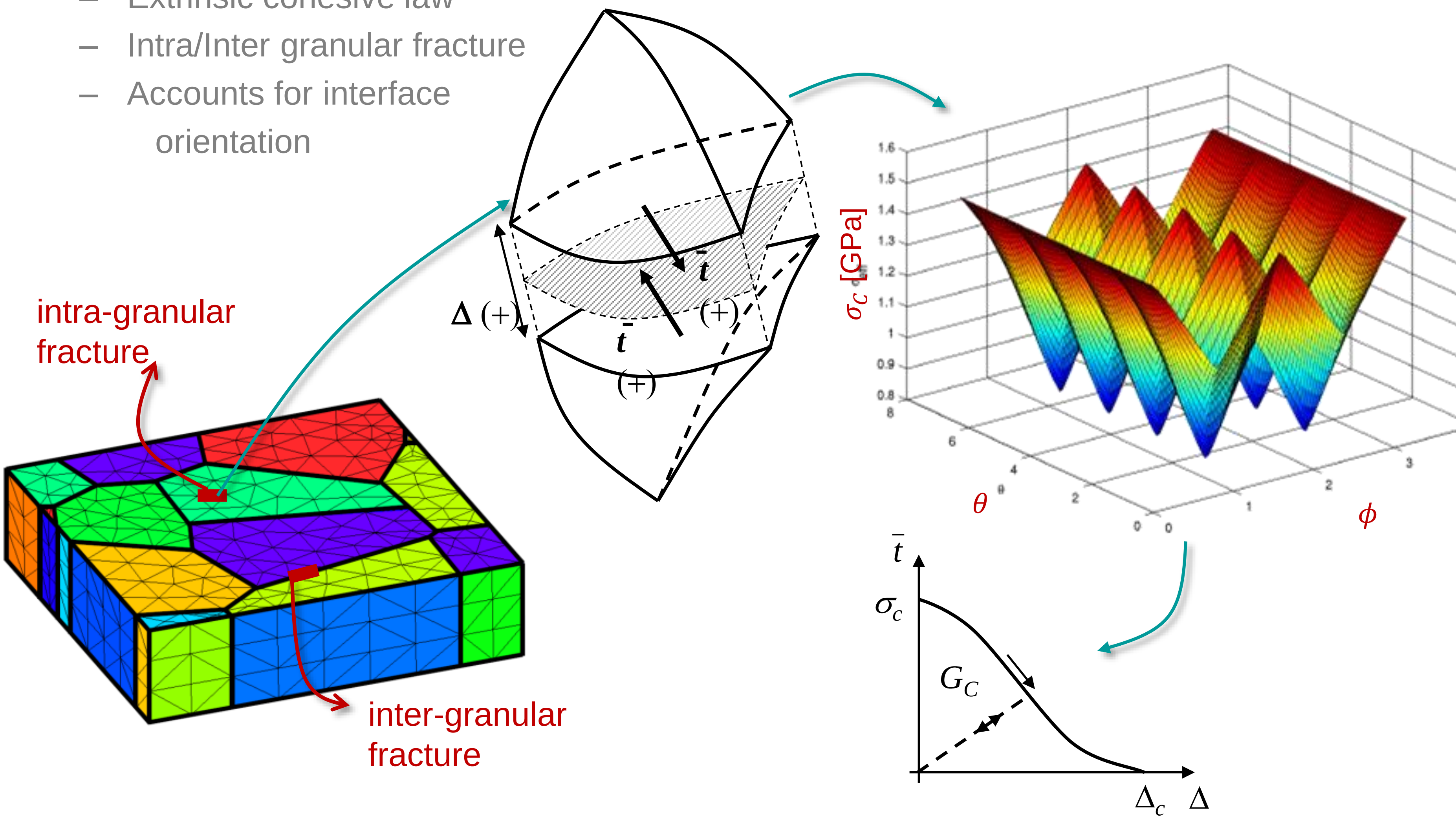

- Stochastic micro-scale to meso-scale model
  - Several SVE realizations (random grain orientation)
  - Extraction of consistent meso-scale cohesive laws
    - $\bar{t}_M$ vs. Δ_M
    - for each SVE sample
  - Resulting meso-scale cohesive law distribution

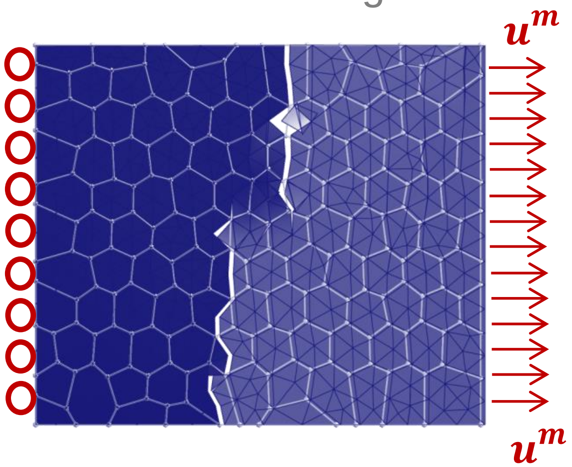

$$\delta\bar{\boldsymbol{t}}_M = \boldsymbol{\delta\sigma_M} \cdot \boldsymbol{e}_X$$

$$\delta\boldsymbol{\Delta}_M = \delta\boldsymbol{u}^m - L_{\text{cell}}\boldsymbol{C_M}^{-1}: \boldsymbol{e}_X \otimes \boldsymbol{e}_X \cdot \boldsymbol{\delta}\bar{\boldsymbol{t}}_M$$

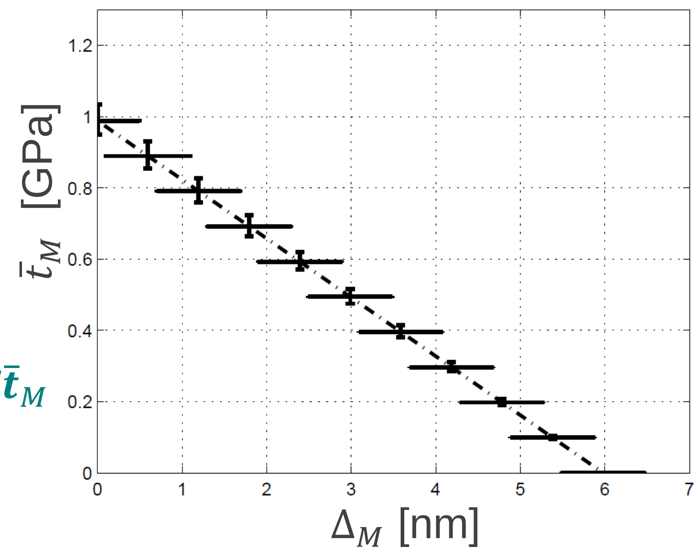

Stochastic Multi-Scale Fracture of Polycrystalline Films

- Macro-scale simulation
  - Finite element model non-conforming to the grains
  - Use homogenized (random) meso-scale cohesive laws as input

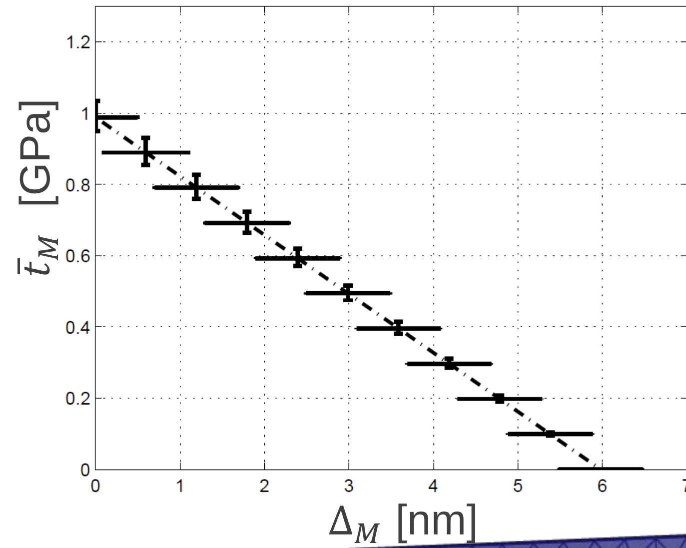

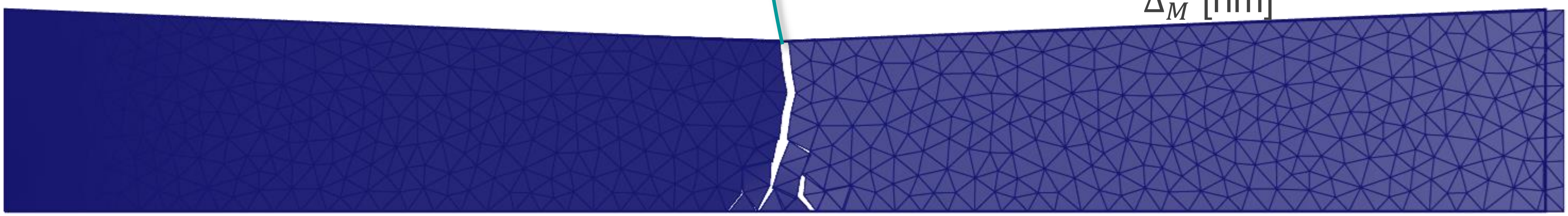

- Collaboration for experiments
  - UcL (T. Pardoen, J.-P Raskin)
- Publications
  - 10.1007/s00466-014-1083-4

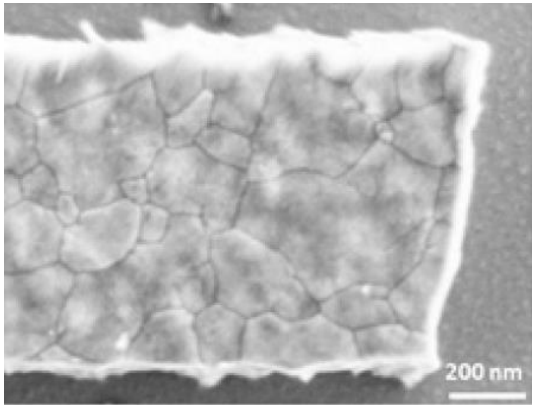

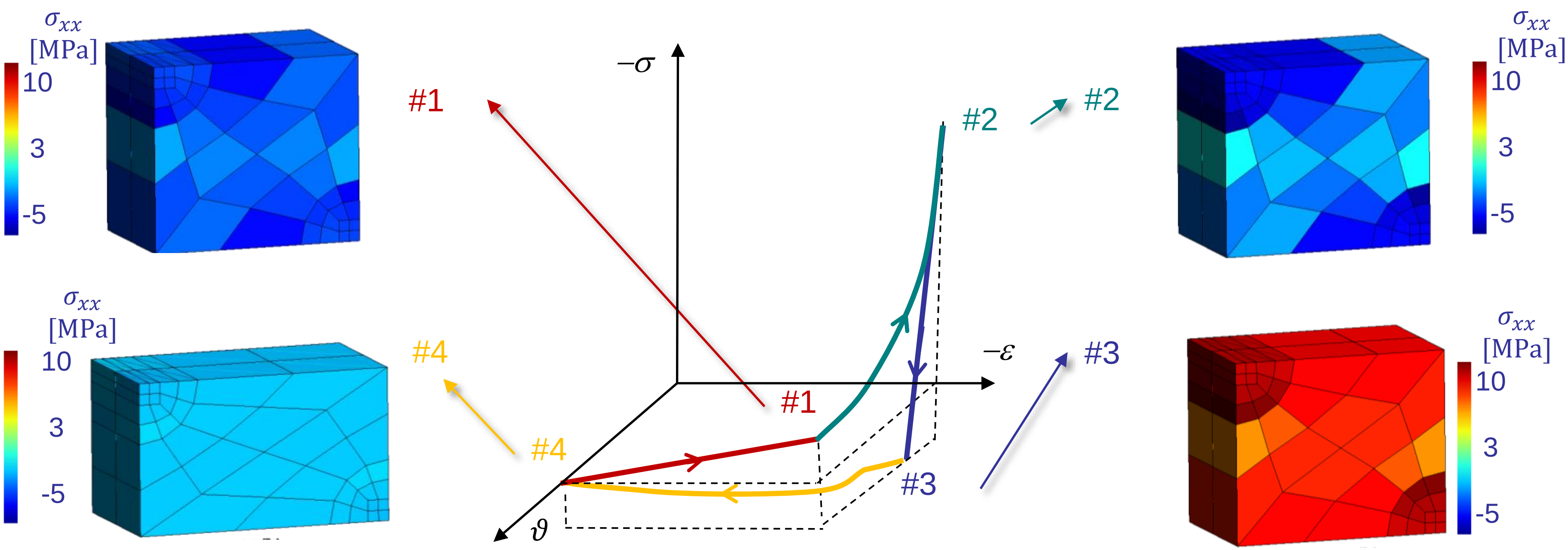

Smart Composite Materials

This project has been funded with support of the European Commission under the grant number 2012-2624/001-001-EM. This publication reflects the view only of the author, and the Commission cannot be held responsible for any use which may be made of the information contained therein.

- Electro-thermo-mechanical coupling
  - Finite field variation formulation
  - Strong coupling

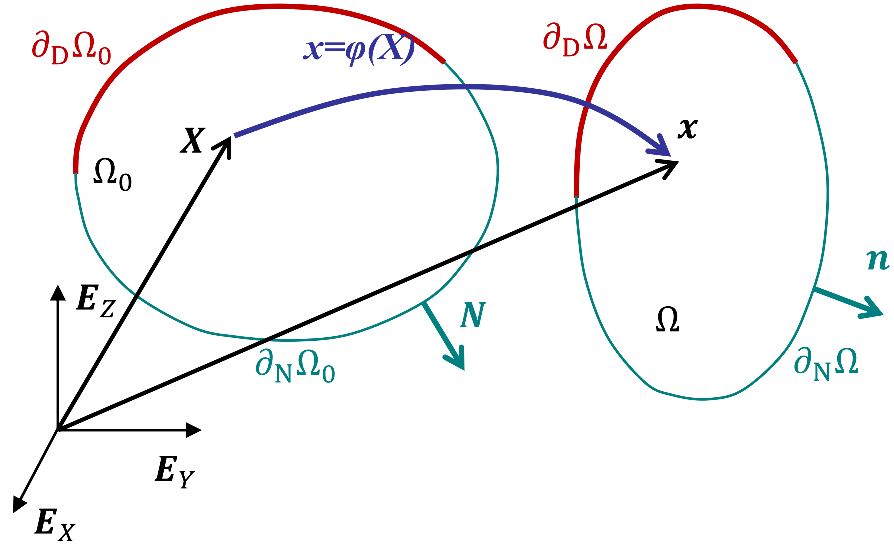

Conservation of electric charge	Conservation of energy	Conservation of momentum balance
$\mathbf{J}_e \cdot \boldsymbol{\nabla}_0 = 0$ $\mathbf{J}_e = \mathbf{J}_e(\mathbf{F}, \boldsymbol{\nabla}_0 V, V, \boldsymbol{\nabla}_0 \vartheta, \vartheta; \boldsymbol{Z})$	$\rho C_v \dot{\vartheta} - \mathcal{D} + \mathbf{J}_y \cdot \boldsymbol{\nabla}_0 = 0$ $\mathbf{J}_y = \mathbf{q} + V\mathbf{J}_e$ $\mathbf{q} = \mathbf{q}(\mathbf{F}, V, \boldsymbol{\nabla}_0 \vartheta, \vartheta; \boldsymbol{Z})$	$\mathbf{P} \cdot \boldsymbol{\nabla}_0 = 0$ $\mathbf{P} = \mathbf{P}(\mathbf{F}, \vartheta; \boldsymbol{Z})$ $\mathcal{D} = \beta \dot{p} \tau + \vartheta \dfrac{\partial \dot{W}^{\mathrm{el}}}{\partial \vartheta}$

- Two-way electro-thermal coupling
  - Seebeck coefficient α
  - Finite strain conductivities $\mathbf{K}(V,\vartheta) = \mathbf{F}^{-1}\cdot\mathbf{k}(V,\vartheta)\cdot\mathbf{F}^{-T}J$ & $\mathbf{L}(V,\vartheta) = \mathbf{F}^{-1}\cdot\mathbf{l}(V,\vartheta)\cdot\mathbf{F}^{-T}J$

$$\begin{pmatrix}\mathbf{J}_e\\ \mathbf{J}_y\end{pmatrix} = \begin{pmatrix}\mathbf{L}(V,\vartheta) & \alpha\mathbf{L}(V,\vartheta)\\ V\mathbf{L}(V,\vartheta)+\alpha T\mathbf{L}(V,\vartheta) & \mathbf{K}(V,\vartheta)+\alpha V\mathbf{L}(V,\vartheta)+\alpha^2 T\mathbf{L}(V,\vartheta)\end{pmatrix}\begin{pmatrix}-\boldsymbol{\nabla}_0 V\\ -\boldsymbol{\nabla}_0\vartheta\end{pmatrix}$$

Non energetically conjugated

[Liu IJES, 2012]

Change of variables

$$\begin{cases} f_V = -\dfrac{V}{\vartheta}\\ f_\vartheta = \dfrac{1}{\vartheta}\end{cases}$$

$$\begin{pmatrix}\mathbf{J}_e\\ \mathbf{J}_y\end{pmatrix} = \mathbf{Z}(\mathbf{F}, f_V, f_\vartheta)\begin{pmatrix}\boldsymbol{\nabla}_0 f_V\\ \boldsymbol{\nabla}_0 f_\vartheta\end{pmatrix}$$

  - The coefficients matrix $\mathbf{Z}(\mathbf{F}, f_V, f_\vartheta)$ is symmetric and definite positive

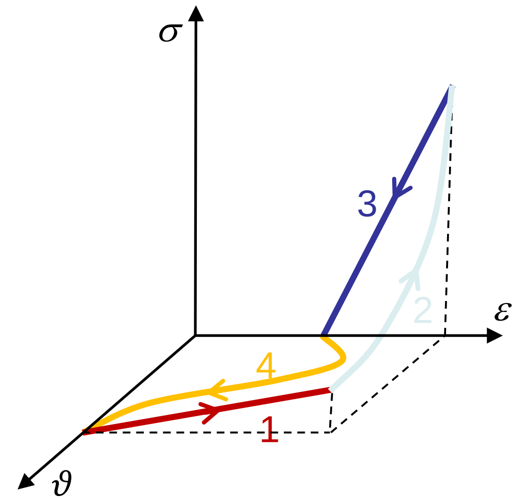

- Thermo-mechanical shape memory polymer
  - Deformations above glass transition temperature ϑ_g (1)
  - Fixed once cooled down below ϑ_g (2 & 3)
  - Recovery once heated up (4)

- Elasto-visco-plastic model constitutive behavior
  - Different mechanisms (α)
    - Multiplicative decomposition
      $$\mathbf{F}^{(\alpha)} = \mathbf{F}^{\mathrm{e}(\alpha)}\mathbf{F}^{\mathrm{p}(\alpha)}$$
    - Free energy
      $$\psi = \sum_{\alpha} \psi^{(\alpha)}\left(\mathbf{C}^{\mathrm{e}(\alpha)}, \vartheta\right)$$
    - Thermo-visco-plasticity
      $$\tau^{(\alpha)} = \mathcal{T}\left(\mathbf{C}^{\mathrm{e}(\alpha)}, \mathbf{F}^{\mathrm{p}(\alpha)}, \dot{p}^{(\alpha)}, \vartheta, \xi^{(\alpha)}\right)$$
  - Stress and dissipation
    $$\begin{cases} \mathbf{P} = \mathbf{P}\left(\mathbf{F}, \vartheta; \mathbf{F}^{\mathrm{p}(\alpha)}, p^{(\alpha)}, \xi^{(\alpha)}\right) \\ \mathcal{D} = \beta \dot{p}^{(\alpha)} \tau^{(\alpha)} \end{cases}$$

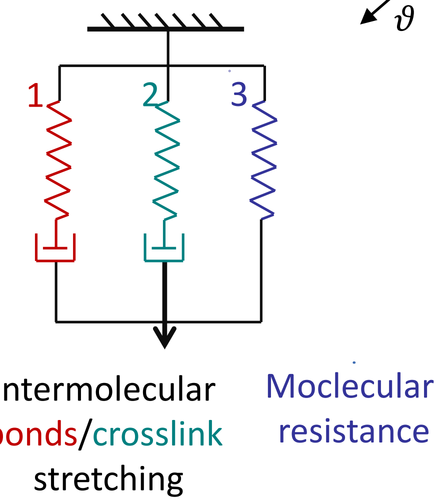

[V. Srivastav et. al, 2010]

- Elasto-visco-plastic behavior of thermo-mechanical shape memory polymer

Refs. by [V. Srivastav et. al, 2010]

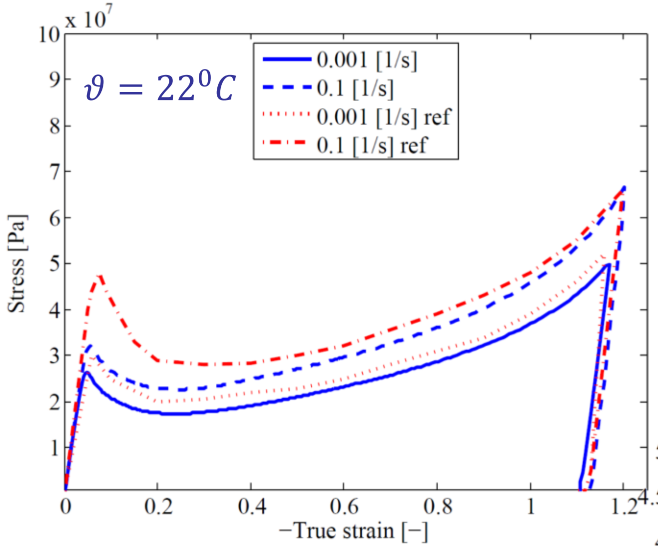

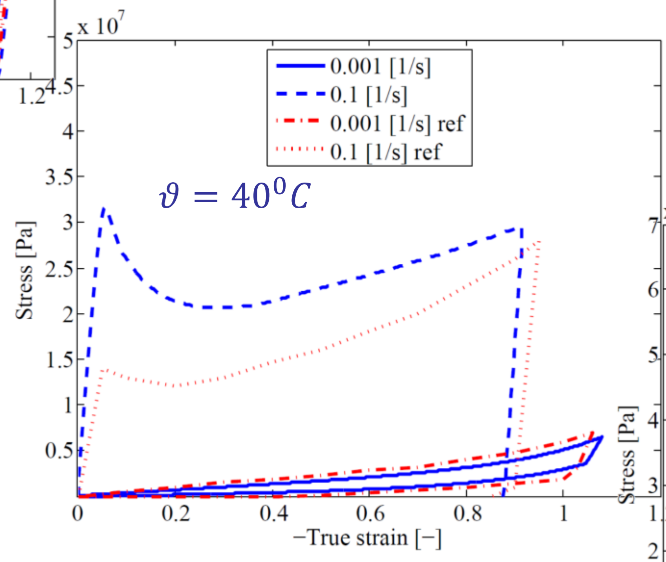

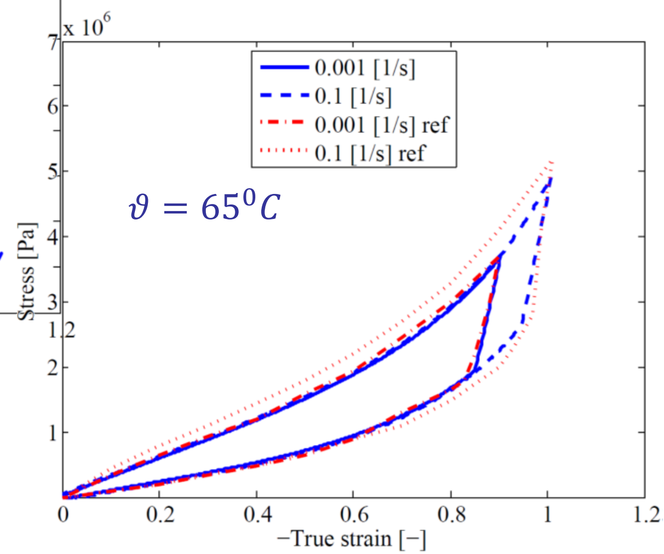

- Recovery of a shape memory composite unit cell
  - Carbon Fiber reinforced SMP
  - Shape memory effect triggered by Joule effect
  - Test with compressive force recovery:
    - #1: Compression deformation obtained above ϑ_g
    - #2: Fixation of the deformation above ϑ_g
    - #3: Reheat above ϑ_g at constant deformation:

      → recovery force, the cell wants to expend
    - #4: Release deformation/stress

      → recovery force vanishes

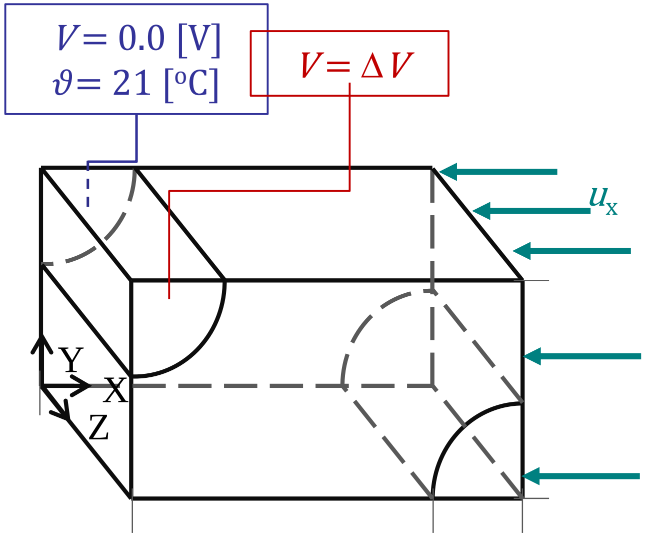

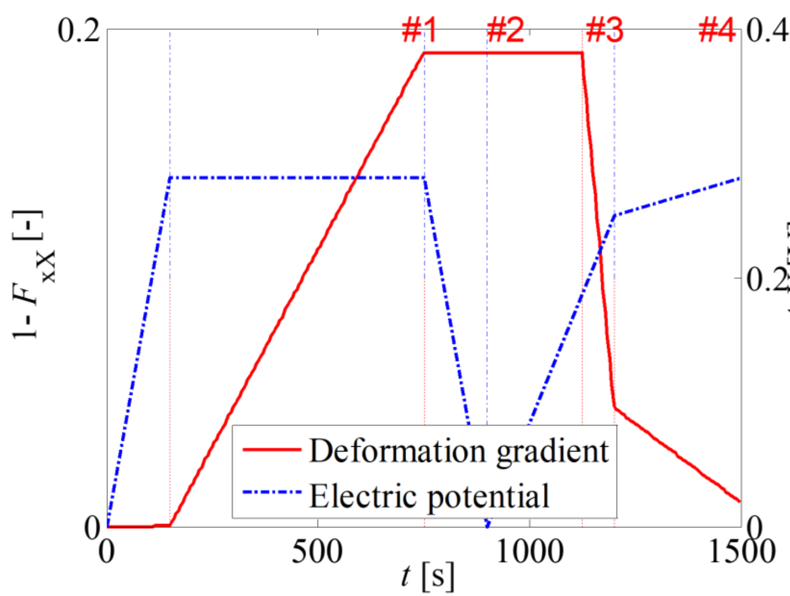

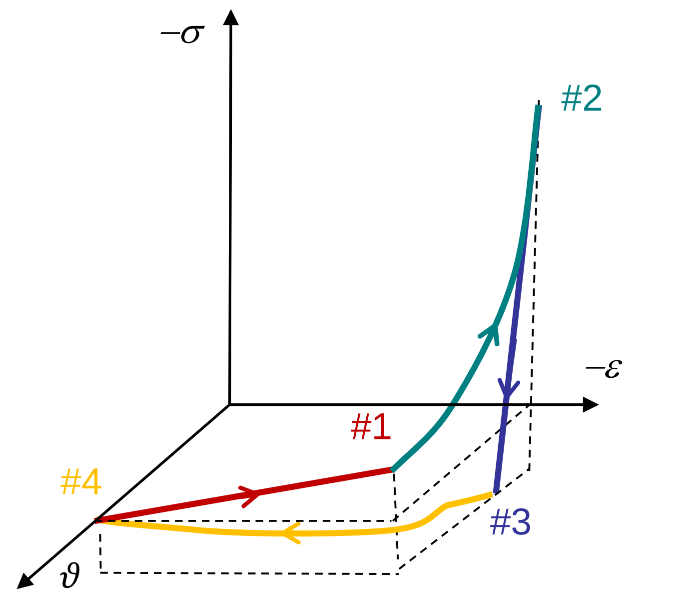

Smart Composite Materials

- Recovery of a shape memory composite unit cell
  - Carbon Fiber reinforced SMP
  - Triggered by Joule effecy

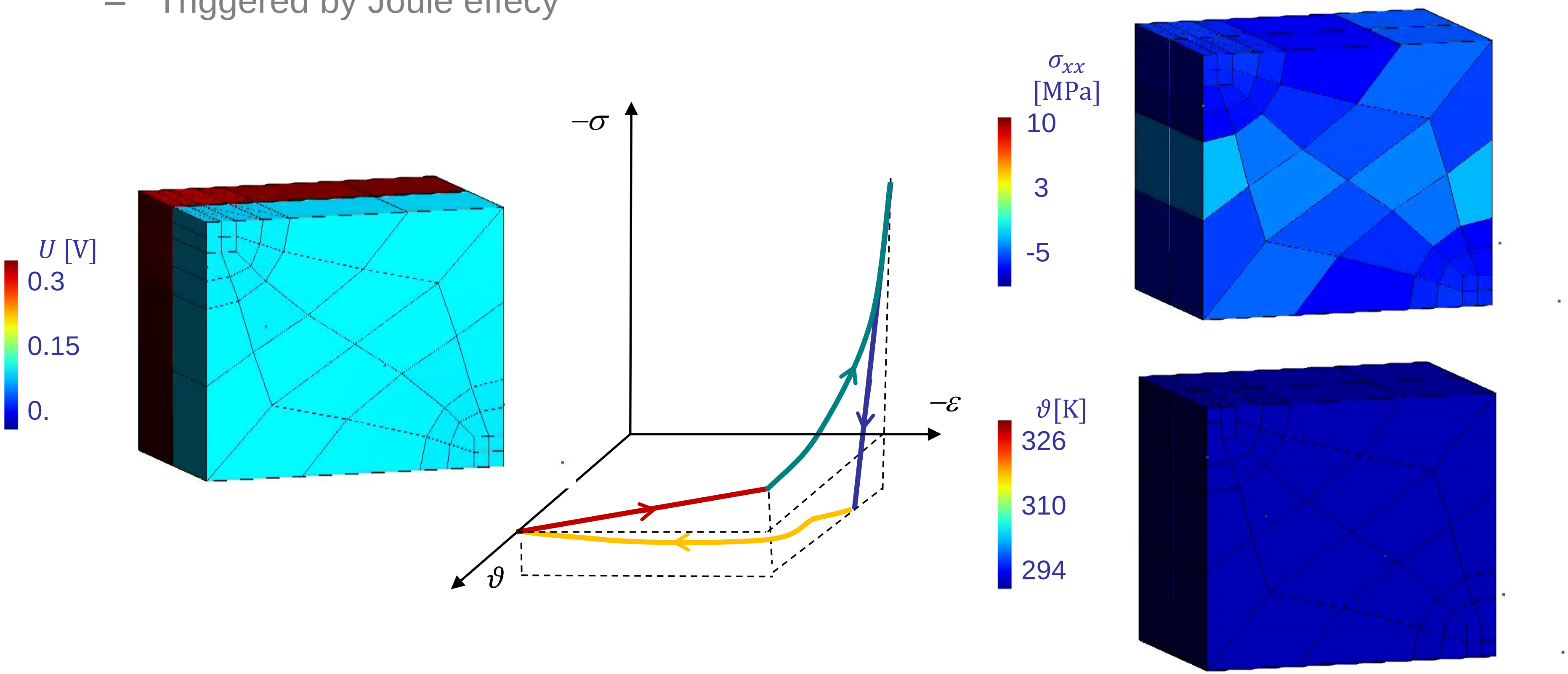

- Discontinuous Galerkin implementation
  - Finite-element discretization
  - Same **discontinuous** polynomial approximations for the
    - **Test** functions φ_h and
    - **Trial** functions $\delta\varphi$
  - Extended to non-linear electro-thermo-mechanical coupling

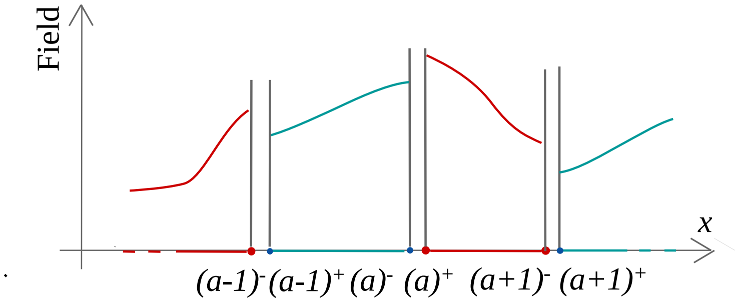

- Publication (doi)
  - 10.1007/s11012-017-0743-9
  - 10.1016/j.jcp.2017.07.028

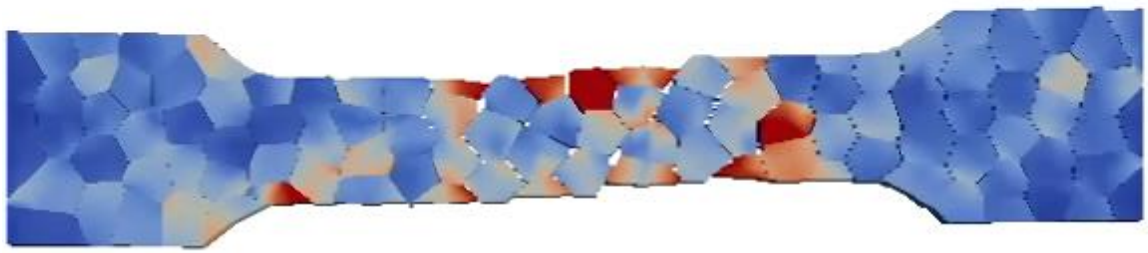

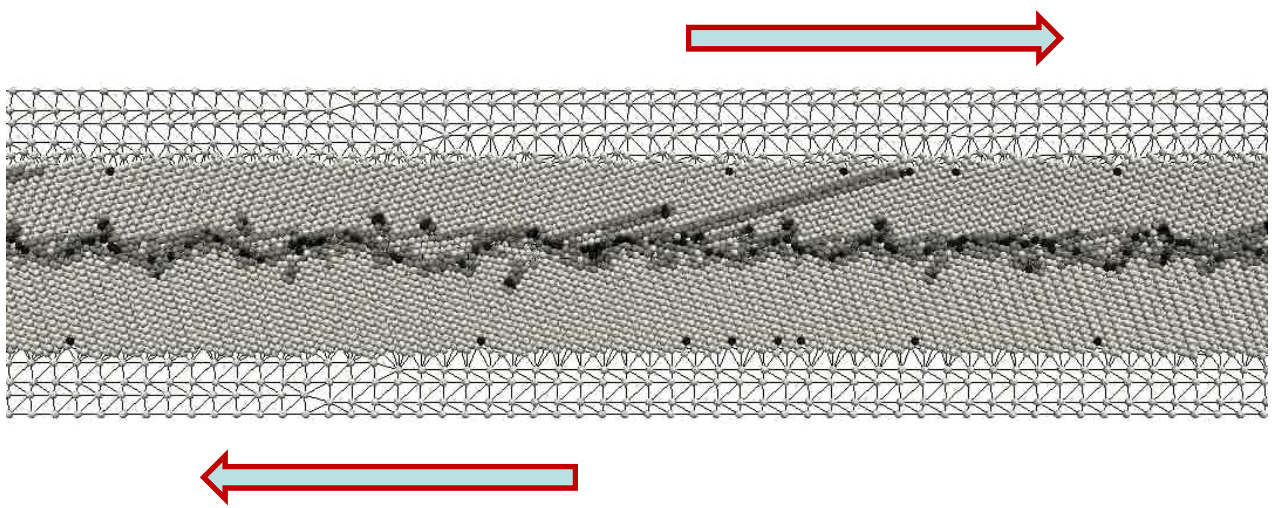

Multi-Scale Modeling of Nano-Crystal Grain Boundary Sliding

Multi-Scale Modeling of Nano-Crystal Grain Boundary Sliding

- 2-scale framework
  - Macro-scale: Finite Elements
  - Micro-scale: Quasi-Continuum

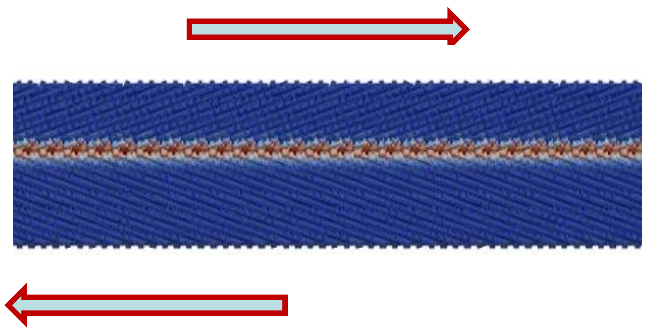

Grain-boundary sliding/opening characterization

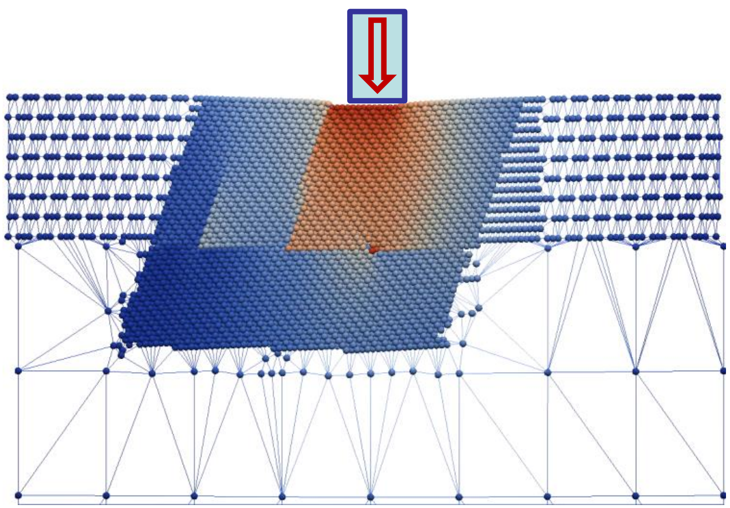

Crystal plasticity characterization by nano-indentation

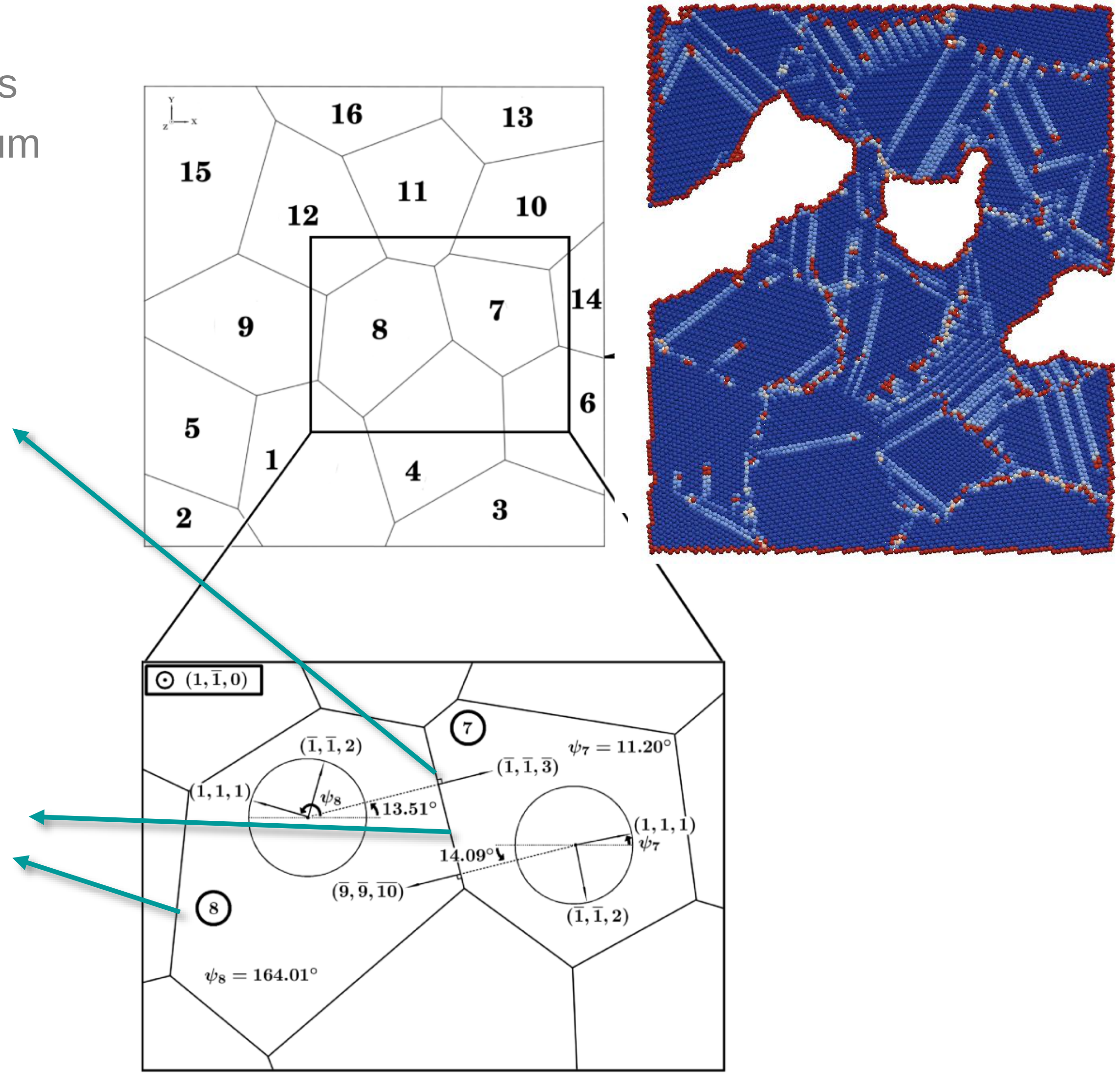

Multi-Scale Modeling of Nano-Crystal Grain Boundary Sliding

- Grain size effect
  - Competition between inter-intra granular

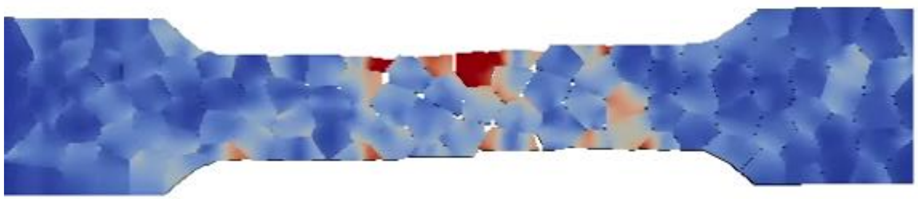

Grain size: 6.56 nm

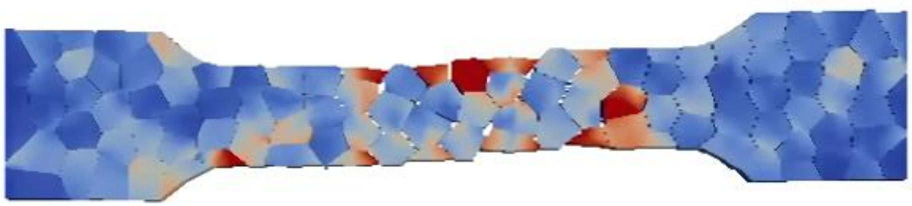

Grain size: 3.28 nm

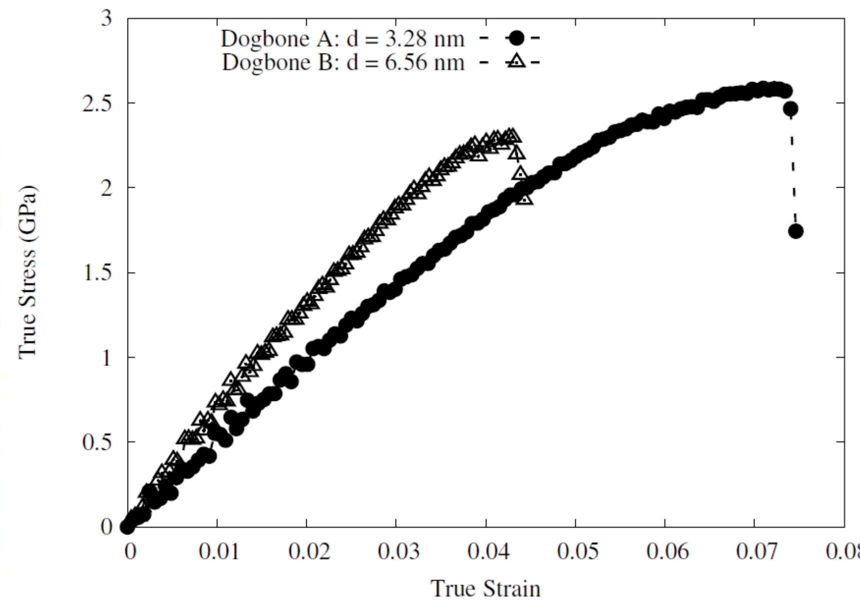

- Effect of nano-voids in the grain boundaries
  - Different deformation mechanism
  - Lower yield stress
- Collaboration
  - EC Nantes, Univ. of Vermont, Oxford
- Publications
  - 10.1016/j.commatsci.2014.03.070
  - 10.1016/j.actamat.2013.10.056
  - 10.1016/j.jmps.2013.04.009

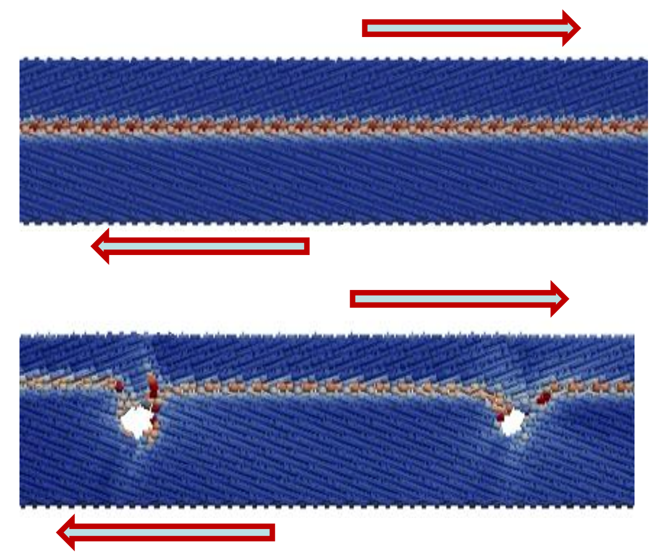

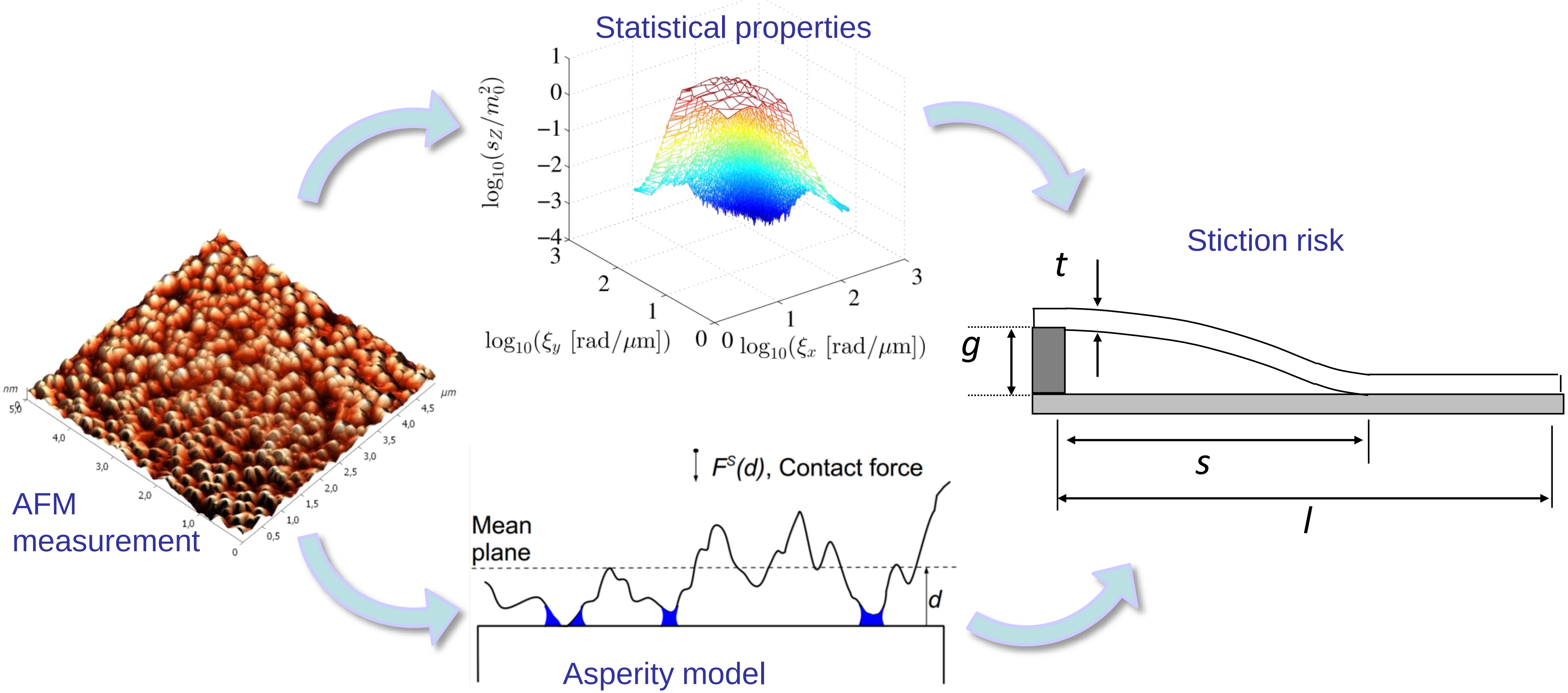

Stochastic Multi-Scale Model to Predict MEMS Stiction

3SMVIB: The research has been funded by the Walloon Region under the agreement no 1117477 (CT-INT 2011-11-14) in the context of the ERA-NET MNT framework.
The research has been funded by the Belgian National Fund for Education at the Research in Industry and Farming.

Stochastic Multi-Scale Model to Predict MEMS Stiction

- Stiction (adhesion of MEMS)
  - Different physics at the different scales
  - Elastic or Elasto-plastic behaviors
  - Due to van der Waals (dry environment) and/or capillary (humid environment) forces

- Requires surfaces topology knowledge (AFM measures)
  - Subject to uncertainties

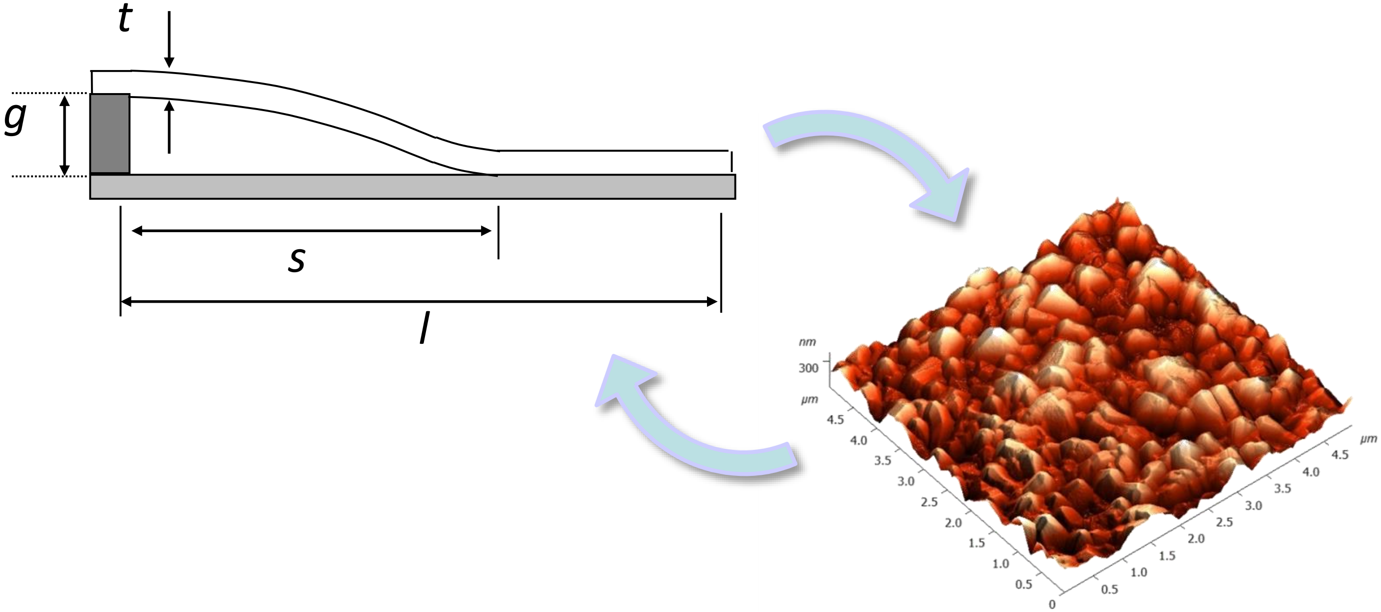

- Deterministic multi-scale models for van der Waals forces
  - Extraction of meso-scale adhesive-forces
  - Using statistical representations of the rough surface (average solution)
  - Account for induced elasto-plasticity (cyclic loading)

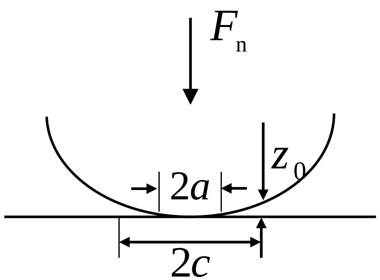

van der Waals/Hertz forces at the asperity level

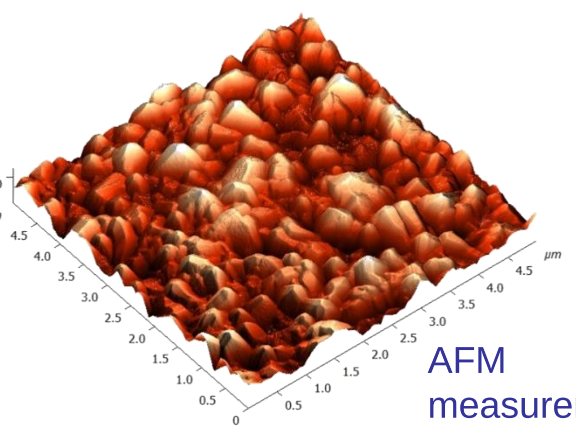

AFM measurement

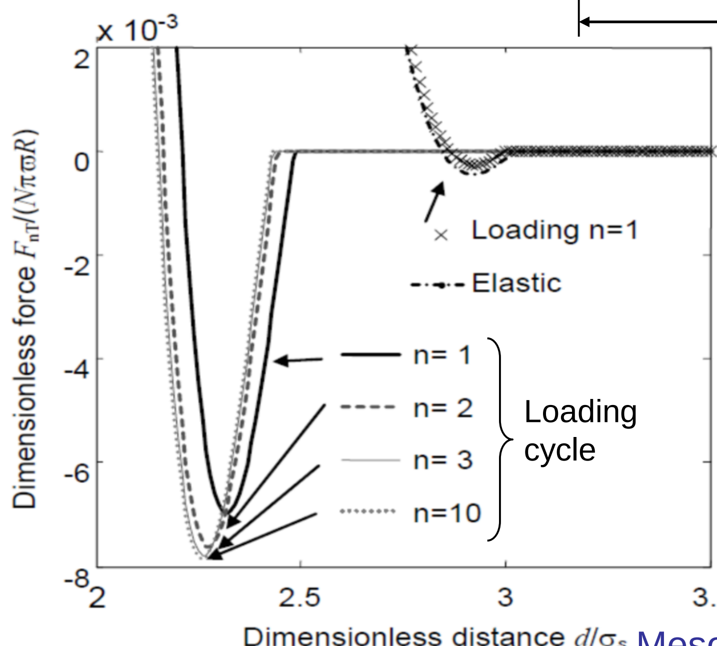

Meso-scale adhesive forces in terms of loading cycle

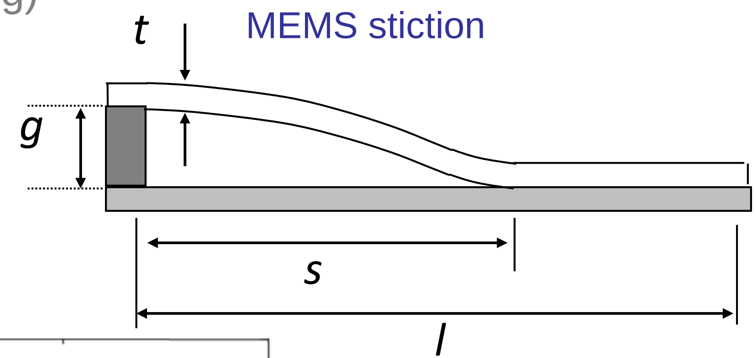

MEMS stiction

Beginning

- New multi-scale models with capillary effect
  - Extraction of meso-scale adhesive-forces from a single surface measurement
  - Depends on the surface sample measurement location
  - Motivates the development of a stochastic multi-scale method

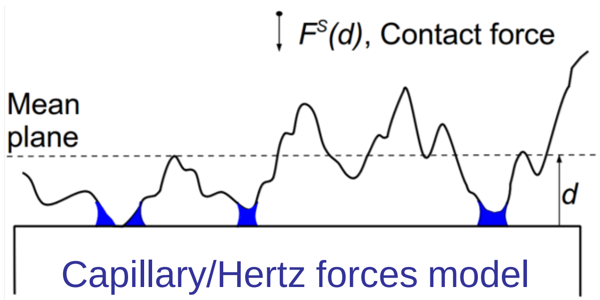

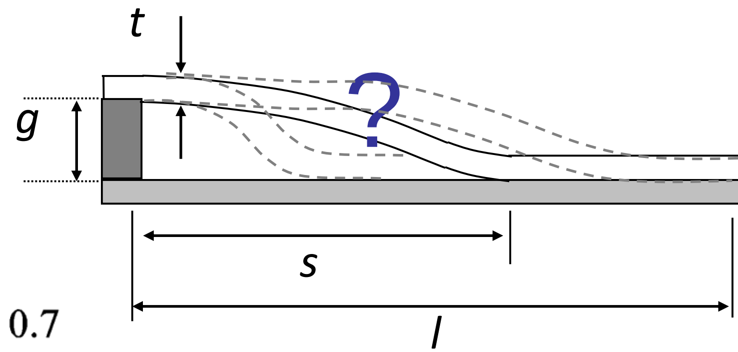

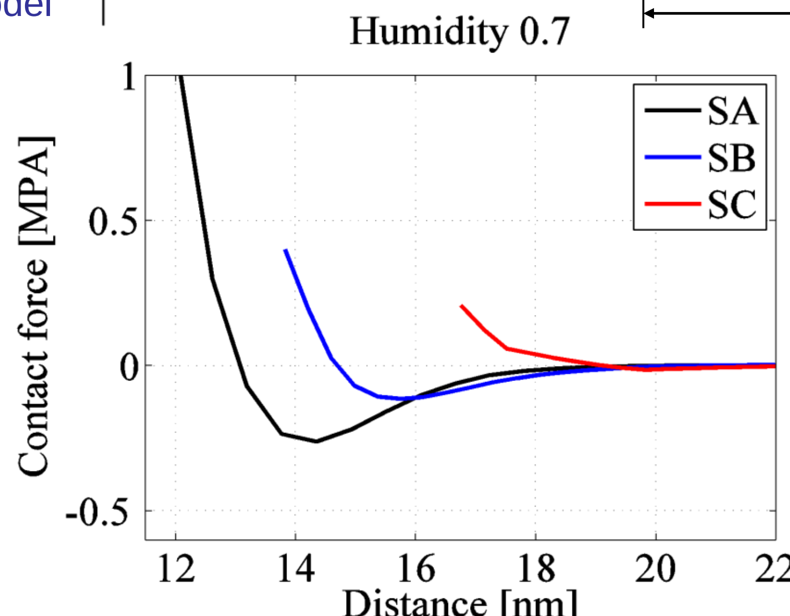

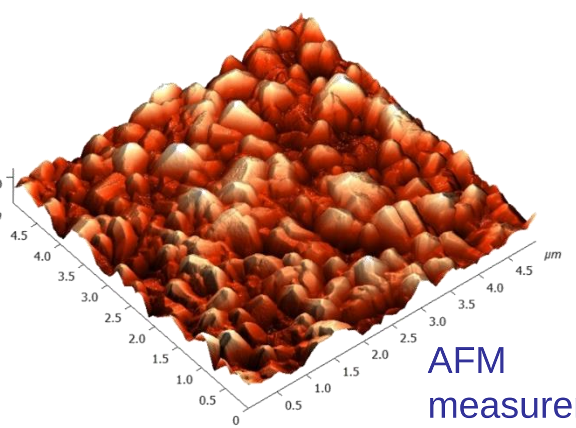

AFM measurement

Meso-scale adhesive forces in terms of surface sample

- Stochastic multi-scale model: From the AFM to virtual surfaces

Enforce statistical moments with maximum entropy method

$$m_i = \int_R z^i \mathrm{p}_Z(z)\, dz$$

$$\mathrm{p}_Z = \arg\max - \int_R \mathrm{p}_Z(z)\ \ln(\mathrm{p}_Z(z))\, dz$$

Evaluate PSD from covariance

$$\tilde{R}(\boldsymbol{\tau}) = \mathbb{E}[z(\boldsymbol{x}), z(\boldsymbol{x}+\boldsymbol{\tau})]$$

$$S_Z(\boldsymbol{\tau}) = \int_{R^2} \exp(-i\boldsymbol{\zeta}\cdot\boldsymbol{\tau})\tilde{R}_Z(\boldsymbol{\tau})d\boldsymbol{\zeta}$$

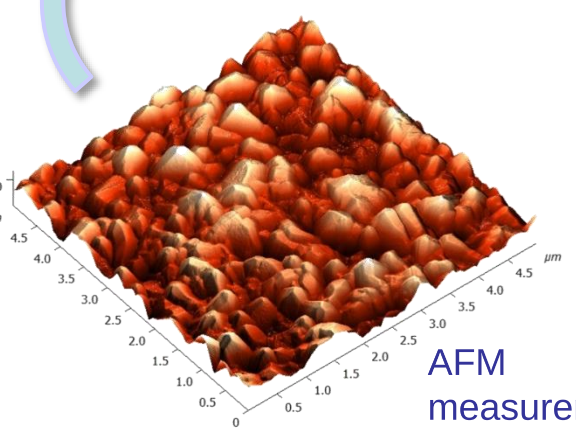

AFM measurement

Height Probability Density Function

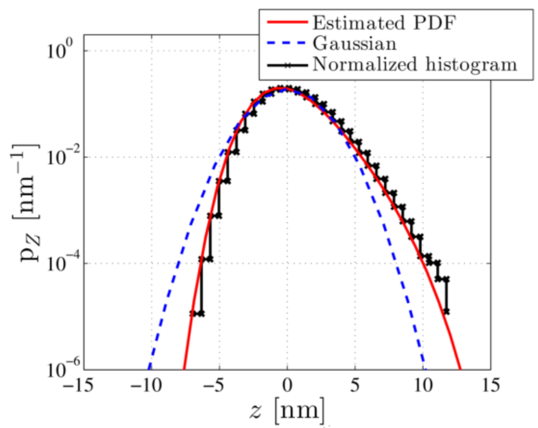

Power spectrum density

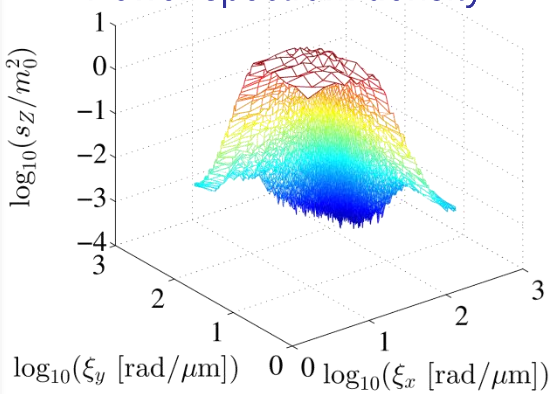

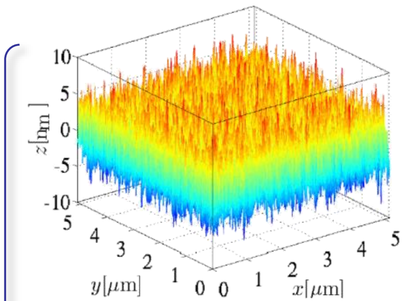

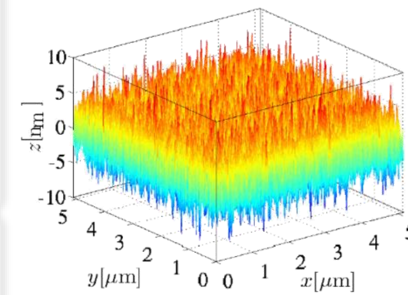

Generated non-Gaussian surface samples

- Stochastic multi-scale model: Evaluate meso-scale surface forces

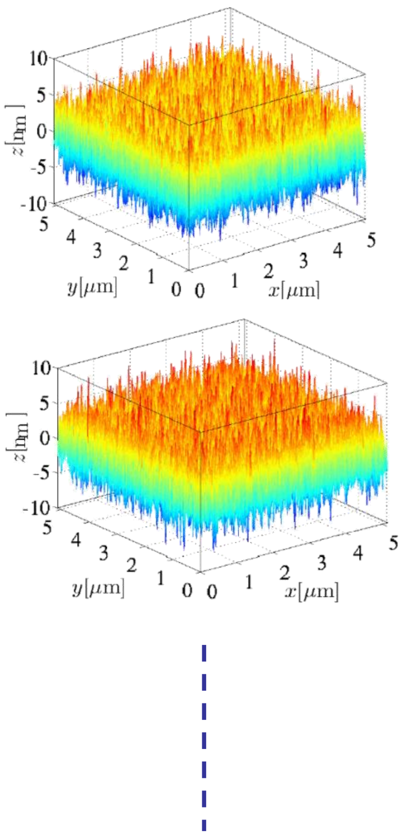

Generated non-Gaussian surface samples

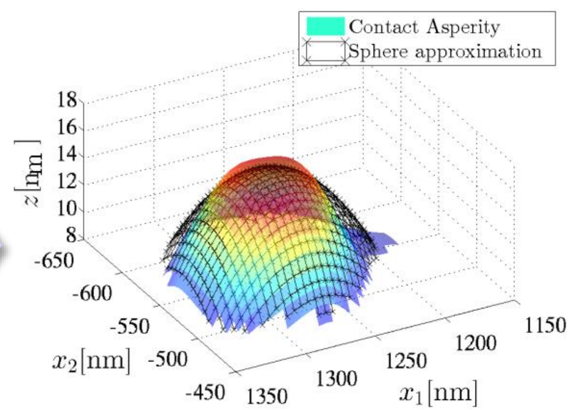

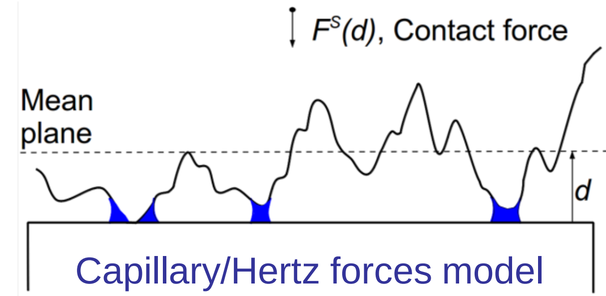

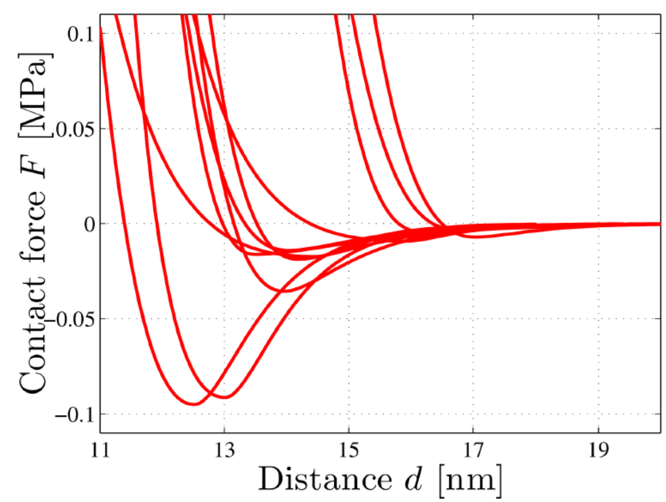

Computed meso-scale adhesive forces

- Stochastic multi-scale model: Stochastic model of meso-scale adhesion forces

Definition of parameter vector $\boldsymbol{v}$

$$\bar{f}(\bar{d}) = \Phi(\bar{d}, \boldsymbol{v})$$

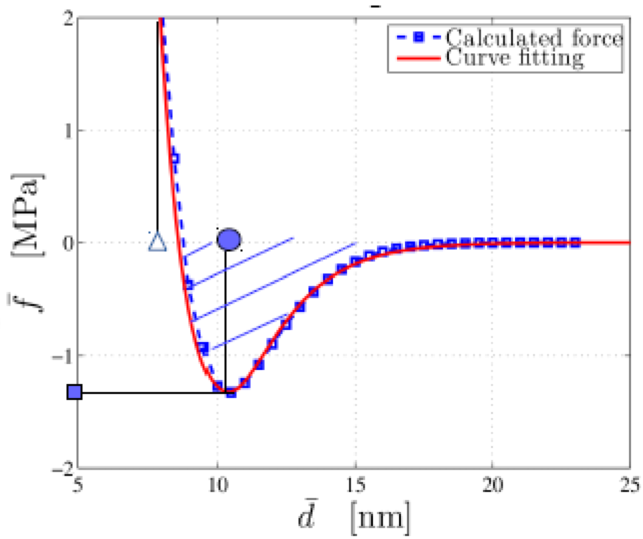

Enforce physical constraints

$$\boldsymbol{v}^{(i)} \rightarrow \boldsymbol{q}^{(i)}$$

Principal component analysis from covariance matrix $[\tilde{R}_Q]$ of vectors $\boldsymbol{q}^{(i)}$

$$\boldsymbol{\eta}^T = (\boldsymbol{q} - \bar{\boldsymbol{q}})^T [A][\lambda]^{-1/2}$$

Polynomial chaos expansion

$$\boldsymbol{\eta}^{\mathrm{PC}} = \sum c_\alpha \Psi_\alpha(\boldsymbol{\xi})$$

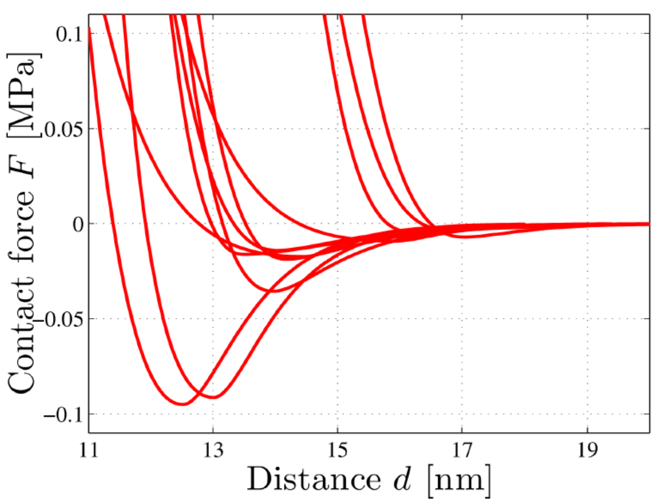

Computed meso-scale adhesive forces

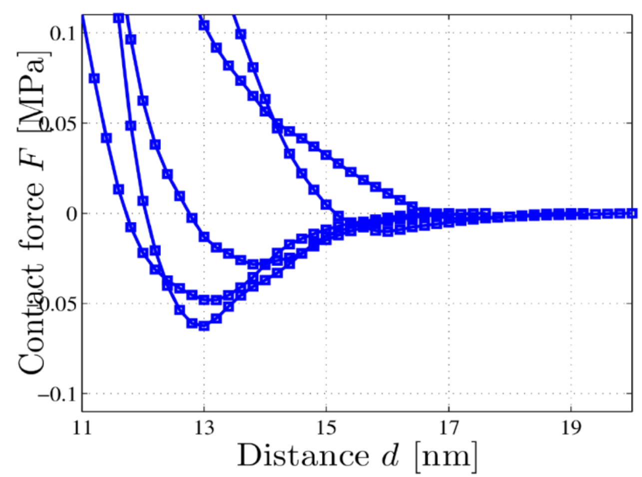

Generated adhesive forces

- Stochastic multi-scale model: Stochastic MEMS stiction analyzes

Stochastic finite elements (random contact law variable)

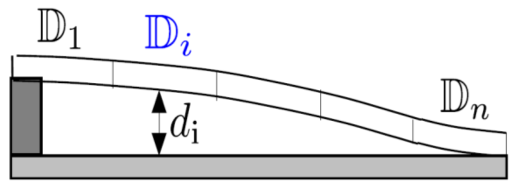

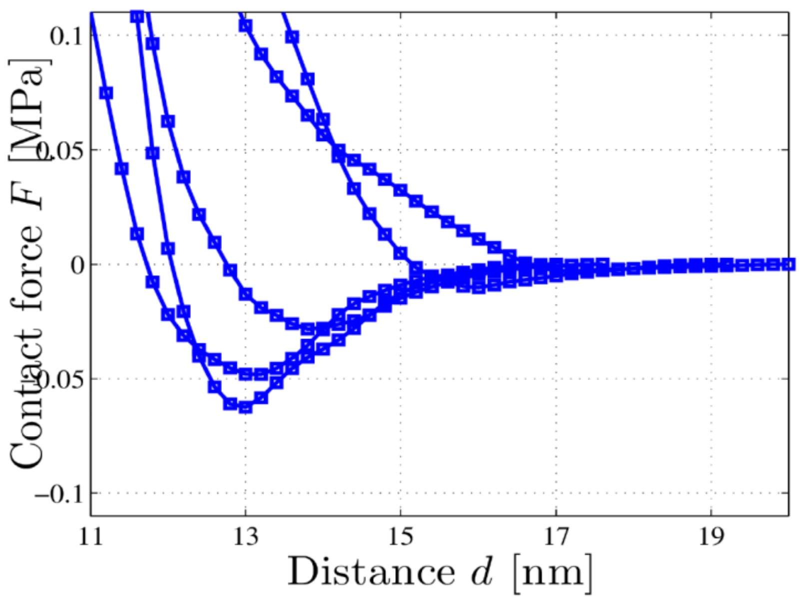

Generated meso-scale adhesive forces

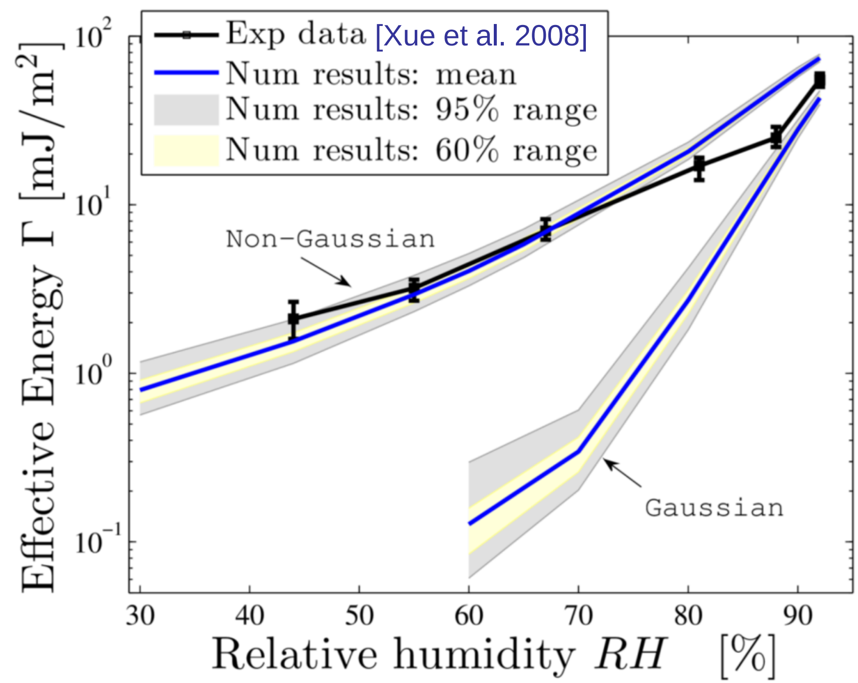

Stiction risk

Stochastic Multi-Scale Model to Predict MEMS Stiction

- Application to robust design
  - Determination of probabilistic meso-scale properties
  - Propagate uncertainties to higher scale
  - Vibro-meter sensors:
    - Uncertainties in stiction risk
- 3SMVIB MNT.ERA-NET project
  - Open-Engineering, V2i, ULiège (Belgium)
  - Polit. Warszawska (Poland)
  - IMT, Univ. Cluj-Napoca (Romania)
- FNRS-FRIA fellowship
- Publications (doi)
  - 10.1109/JMEMS.2018.2797133
  - 10.1016/j.triboint.2016.10.007
  - 10.1007/978-3-319-42228-2_1
  - 10.1016/j.cam.2015.02.022
  - 10.1016/j.triboint.2012.08.003
  - 10.1007/978-1-4614-4436-7_11
  - 10.1109/JMEMS.2011.2153823
  - 10.1063/1.3260248